JOINT TRANSPORTATION
RESEARCH PROGRAM
INDIANA DEPARTMENT OF TRANSPORTATION
AND PURDUE UNIVERSITY

Empowering the Indiana Bridge Inventory Database Toward Rapid Seismic Vulnerability Assessment

Leslie Bonthron, Corey Beck, Alana Lund,
Farida Mahmud, Xin Zhang, Rebeca Orellana Montano,
Shirley J. Dyke, Julio Ramirez, Yenan Cao, George P. Mavroeidis

SPR-4226 • Report Number: FHWA/IN/JTRP-2019/18 • DOI: 10.5703/1288284317282

RECOMMENDED CITATION

Bonthron, L., Beck, C., Lund, A., Mahmud, F., Zhang, X., Orellana Montano, R., Dyke, S. J., Ramirez, J., Cao, Y., & Mavroeidis, G. P. (2021). *Empowering the Indiana bridge inventory database toward rapid seismic vulnerability assessment* (Joint Transportation Research Program Publication No. FHWA/IN/JTRP-2021/03). West Lafayette, IN: Purdue University. https://doi.org/10.5703/1288284317282

AUTHORS

Leslie Bonthron
Corey Beck
Alana Lund
Farida Mahmud
Xin Zhang
Rebeca Orellana Montano
Graduate Research Assistants
Lyles School of Civil Engineering
Purdue University

Shirley J. Dyke, PhD
Professor of Mechanical and Civil Engineering
Lyles School of Civil Engineering
(765) 494-7434
sdyke@purdue.edu
Corresponding Author

Julio Ramirez, PhD
Kettelhut Professor of Civil Engineer and NHERI-NCO Center Director
Lyles School of Civil Engineering
(765) 494-2716
ramirez@purdue.edu
Corresponding Author

Farida Mahmud, PhD
Graduate Research Assistant
Lyles School of Civil Engineering
Purdue University

Yenan Cao
Graduate Research Assistant
Department of Civil & Environmental Engineering
& Earth Sciences
University of Notre Dame

George P. Mavroeidis, PhD
Assistant Professor
Department of Civil & Environmental Engineering
& Earth Sciences
University of Notre Dame
Principle Investigator

JOINT TRANSPORTATION RESEARCH PROGRAM

The Joint Transportation Research Program serves as a vehicle for INDOT collaboration with higher education institutions and industry in Indiana to facilitate innovation that results in continuous improvement in the planning, design, construction, operation, management and economic efficiency of the Indiana transportation infrastructure. https://engineering.purdue.edu/JTRP/index_html

Published reports of the Joint Transportation Research Program are available at http://docs.lib.purdue.edu/jtrp/.

NOTICE

TECHNICAL REPORT DOCUMENTATION PAGE

1. Report No. FHWA/IN/JTRP-2021/03	**2. Government Accession No.**	**3. Recipient's Catalog No.**
4. Title and Subtitle Empowering the Indiana Bridge Inventory Database Toward Rapid Seismic Vulnerability Assessment		**5. Report Date** December 2020 **6. Performing Organization Code**
7. Author(s) Leslie Bonthron, Corey Beck, Alana Lund, Farida Mahmud, Xin Zhang, Rebeca Orellana Montano, Shirley J. Dyke, Julio Ramirez, Yenan Cao, and George P. Mavroeidis		**8. Performing Organization Report No.** FHWA/IN/JTRP-2021/03
9. Performing Organization Name and Address Joint Transportation Research Program Hall for Discovery and Learning Research (DLR), Suite 204 207 S. Martin Jischke Drive West Lafayette, IN 47907		**10. Work Unit No.** **11. Contract or Grant No.** SPR-4222
12. Sponsoring Agency Name and Address Indiana Department of Transportation (SPR) State Office Building 100 North Senate Avenue Indianapolis, IN 46204		**13. Type of Report and Period Covered** Final Report **14. Sponsoring Agency Code**

15. Supplementary Notes

Conducted in cooperation with the U.S. Department of Transportation, Federal Highway Administration.

16. Abstract

With the recent identification of the Wabash Valley Seismic Zone in addition to the New Madrid Seismic Zone, Indiana's Department of Transportation (INDOT) has become concerned with ensuring the adequate seismic performance of their bridge network. While INDOT made an effort to reduce the seismic vulnerability of newly-constructed bridges, many less recent bridges still have the potential for vulnerability. Analyzing these bridges' seismic vulnerability is a vital task. However, developing a detailed dynamic model for every bridge in the state using information from structural drawings is rather tedious and time-consuming. In this study, we develop a simplified dynamic assessment procedure using readily-available information from INDOT's Bridge Asset Management Program (BIAS), to rapidly identify vulnerable bridges throughout the state. Eight additional data items are recommended to be added into BIAS to support the procedure. The procedure is applied in the Excel file to create a tool, which is able to automatically implement the simplified bridge seismic analysis procedure. The simplified dynamic assessment procedure and the Excel tool enable INDOT to perform seismic vulnerability assessment and identify bridges more frequently. INDOT can prioritize these bridges for seismic retrofits and efficiently ensure the adequate seismic performance of their assets.

17. Key Words seismic vulnerability, asset management, prioritization, screening, rapid vulnerability analysis, Indiana seismic assessment tool, seismic retrofit	**18. Distribution Statement** No restrictions. This document is available through the National Technical Information Service, Springfield, VA 22161.

19. Security Classif. (of this report) Unclassified	**20. Security Classif. (of this page)** Unclassified	**21. No. of Pages** 212 including appendices	**22. Price**

Form DOT F 1700.7 (8-72) Reproduction of completed page authorized

EXECUTIVE SUMMARY

Overview

With the recent identification of the Wabash Valley Seismic Zone in addition to the New Madrid Seismic Zone, Indiana's Department of Transportation (INDOT) has become concerned with ensuring the adequate seismic performance of their bridge network. While INDOT has steadily worked to reduce the seismic vulnerability of newly-constructed bridges via adequate seismic detailing, older bridges built without consideration for seismic effects still have the potential for vulnerability. Determining the extent of this seismic vulnerability requires developing dynamic models for each bridge and exposing these models to synthetic ground motions that are representative of the seismic hazard at the bridge site. However, the task of developing a detailed dynamic model for every bridge in the state using information from structural drawings is cumbersome and time-consuming.

In this study we develop a simplified dynamic assessment procedure (Simplified Assessment), using readily-available information from INDOT's Bridge Inspection Application System (BIAS), to rapidly identify vulnerable bridges throughout the state. Although BIAS houses information which enables rehabilitation, preservation, and preventative maintenance projects, the current BIAS data items are insufficient to estimate substructure stiffness and develop a simplified dynamic model. Therefore, we recommend eight additional data items be added to BIAS to ensure the accuracy and robustness of the Simplified Assessment. The procedure developed is implemented and automated through a macro-based Excel file named Indiana Seismic Assessment Tool (INSAT). By empowering BIAS with the capabilities to conduct a rapid seismic vulnerability assessment, INDOT can more frequently perform a seismic vulnerability assessment and identify bridges which are expected to be the most vulnerable based on their expected hazard level. Thus, INDOT can prioritize these bridges for seismic retrofits and efficiently ensure the adequate seismic performance of their assets.

This report was generated through the study SPR-4222, *Seismic Evaluation of Indiana Bridge Network and Current Bridge Database for Asset Management.*

Findings

- The results from the detailed seismic assessment on the 100-bridge sample set identified potentially vulnerable details typical of INDOT bridges. Some of the identified vulnerabilities include brittle failure of substructures with a low amount of longitudinal reinforcement, the formation of a plastic hinge in substructures with an adequate amount of longitudinal reinforcement, and the unseating of rocker bearings typical in steel bridges.
- The results from the detailed seismic assessment facilitated the identification of vulnerability trends for INDOT bridges. These trends, which relate displacement and drift thresholds to different levels of vulnerability, are leveraged in the Simplified Assessment.
- Potential retrofit options were identified to improve the seismic performance of bridges which have the potential to develop one of the identified vulnerable details. A few of these retrofit options include the following: isolating the superstructure, converting the abutment to an integral-type abutment (including semi-integral), adding restrainers between the superstructure and abutments, or jacketing the substructure.
- The Simplified Assessment procedure and a corresponding tool, INSAT, have been developed to rapidly assess the vulnerability of bridges across the state using information stored in BIAS.
- The Simplified Assessment was determined to agree with or yield a result which overestimates the vulnerability (e.g., a conservative result) of a given bridge when compared to the detailed assessment at approximately 90% accuracy.
- Eight additional data items have been identified and recommended to be incorporated into BIAS to empower INDOT to accurately perform rapid seismic vulnerability assessments. These eight data items include: substructure type, abutment type, deck thickness, number of elements, element length, element width, element height, and height ratio flag. Detailed descriptions of these data items are provided in Section 4.4.
- BIAS contains enough information in conjunction with INSAT to identify that, even without the eight data items, approximately 38% of the bridges in INDOT's bridge network can automatically be screened to *low vulnerability*, *moderate vulnerability*, or *detailed analysis required* due to superstructure indicators, such as single-span bridges, culverts, or bridges with expansion joints. Even with the inclusion of the eight additional data items, the 38% of the bridge network will always receive these classifications. Thus, the remaining 62% of bridges in the bridge network can be prioritized for data collection.
- Thousands of synthetic ground motion records were generated using stochastic simulation techniques for 100 sites across Indiana. This extensive, high-quality suite of ground motion records is valuable not only for design and analysis but also future research projects relevant to seismic hazards.

Implementation

A key contribution from this research is the development of a macro-based Excel file named INSAT which allows INDOT the ability to assess the vulnerability of the entire bridge network rapidly and automatically. Such a rapid assessment tool improves efficiency, saves personnel time, and can yield significant economic benefits to INDOT. In the current state, BIAS does not contain the eight additional data items required to ensure complete and accurate vulnerability assessments. The collection of these data items, specifically for the 62% of 5,000+ bridges in the INDOT inventory that cannot be classified without them, must be prioritized according to INDOT needs. The collection of these eight data items could occur during routine inspections, thus ensuring that INDOT can conduct a Simplified Assessment within 2 to 4 years.

With the recommended BIAS data enhancements, INDOT will be able to use INSAT to improve the seismic performance and safety of their bridge network throughout the entire life cycle of the bridges to better serve the public. New technology and innovation have been exploited to assist INDOT in collecting needed information. Methods such as artificial intelligence could be leveraged to collect data items like substructure type or abutment type using photos already stored in BIAS. Since 62% of INDOT's bridge network corresponds to approximately 3,650 bridges, additional prioritization filters can be applied so that information for bridges meeting certain criteria(s) is prioritized first. For example, the prioritization scheme could be focused on collecting information for bridges based on route carried, route crossed, hazard potential, soil class, or age.

CONTENTS

TABLE LIST

FIGURE LIST

1. INTRODUCTION

The seismic hazard for central and eastern United States (CEUS) has largely been associated with the New Madrid Seismic Zone (NMSZ). With the identification of a separate seismogenic source in the Wabash Valley—named the Wabash Valley Seismic Zone (WVSZ)—the Indiana Department of Transportation (INDOT) increased attention to the seismic vulnerability of bridge assets throughout the state.

As a responsible steward, INDOT is concerned with identifying structures throughout the state bridge network that may contain vulnerable details expected to respond poorly to the level of seismic excitation, as shown in Figure 1.1, that could be produced in the WVSZ. While completing a detailed analysis is plausible on a case-by-case basis, conducting such an intensive analysis for every bridge in the state would not be practical or even necessary. Rather, this study proposes and implements a simplified dynamic assessment of the bridge inventory to rapidly identify vulnerable bridges, using essential information beyond that which is already stored in INDOT's Bridge Inspection Application System (BIAS) database. The implementation of this assessment procedure is made possible through the Indiana Seismic Assessment Tool (INSAT), a macro-enabled Excel spreadsheet informed by BIAS.

***

The INSAT vulnerability estimate can assist INDOT in policy/guideline development to prioritize retrofit actions to reduce vulnerability of critical bridges and the overall bridge network.

***

Historically, the BIAS database has provided the data necessary for standard asset management tasks, such as the prioritization of bridge maintenance, rehabilitation, and replacement. As such, BIAS does not contain all of the information needed to implement a reliable seismic vulnerability assessment. Additional data items, such as substructure type and dimensions, are necessary to estimate the dynamic properties of the bridge and thereby infer its seismic vulnerability.

***

In agreement with INDOT, it is the goal of this project to not only develop a means for expediting the evaluation of the vulnerability of bridges throughout Indiana, but also to identify and recommend necessary data items to be added to BIAS in support of that vulnerability assessment.

***

The impact of adding these data items to BIAS, in terms of their improvement of the reliability of INSAT, is examined. Given the collection and curation of a relatively small set of data items beyond those already collected in BIAS, INDOT will have the ability to prioritize retrofit and maintenance decisions based on seismic vulnerability data of bridges throughout the state with respect to current understanding of local seismic hazards. In addition, as a result of the detailed assessment of a representative sample of 100 bridges (Section 3) throughout the state, a catalog of vulnerabilities found in some of these structures has been identified together with a suite of potential retrofit measures appropriate for the types of structures and hazard level in Indiana (Section 4).

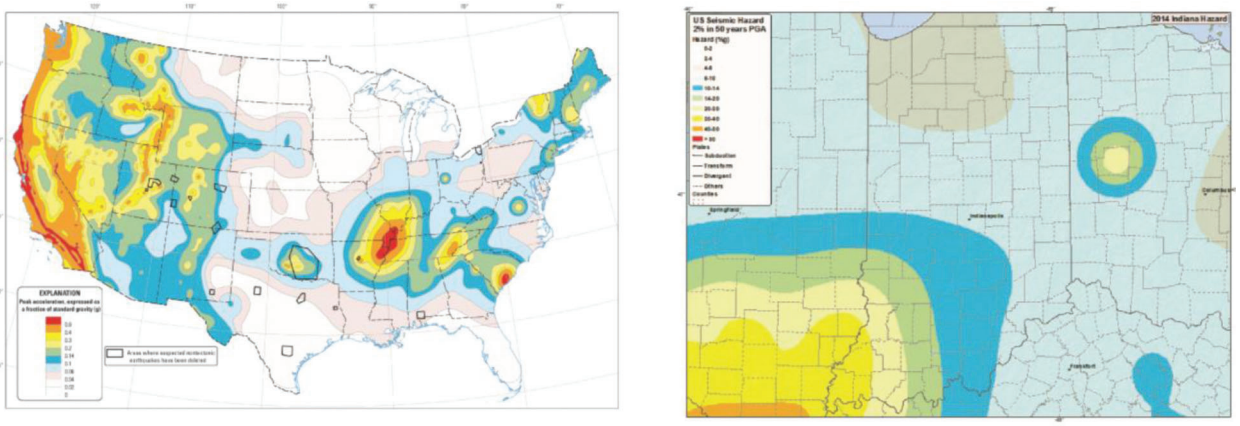

Figure 1.1 U.S. national (left) and state (right) seismic hazard map for 2% probability of exceedance in 50 years (Petersen et al., 2014).

2. SUMMARY OF ASSESSMENTS AND PURPOSE

To ensure a robust seismic assessment of INDOT's bridge network, the project is structured as three assessment components. The interdependencies among these components are discussed throughout this report and are briefly introduced below.

- *Level 2 Assessment:* a detailed, data-driven assessment procedure developed to evaluate the robustness of the Simplified Assessment procedure and to identify appropriate retrofit strategies for common vulnerabilities (Section 4).
- *Simplified Assessment:* a procedure conducted in two steps starting with the Level 0 assessment followed by the Level 1 assessment (Section 5).
- *Level 0 Assessment:* an initial classification performed based on trends identified for relatively common bridge types as an outcome of the Level 2 assessment. The process identifies both bridges of low or moderate vulnerability where a Level 1 assessment is not necessary, as well as those bridges that should go directly to a Level 2 assessment.
- *Level 1 Assessment:* a simplified dynamic modeling approach, developed using findings from the Level 2 assessment, and used to rapidly assess the vulnerability of bridges to which this simplified procedure can be applied.

3. DETERMINATION OF BRIDGE SAMPLE SET AND SEISMIC HAZARD FOR INDIANA

The identification of seismic vulnerability for bridges across Indiana begins with the selection of a representative sample of bridges to establish possible trends and test the Simplified Assessment procedure. A key factor in selecting this sample set is whether these bridges are located on INDOT critical routes. The estimation of the seismic response of these bridges is important as the critical routes provide key access corridors throughout the state during natural hazards and other emergencies (Ramirez et al., 2005). Of the representative bridges selected for this Level 2 assessment, 87% are on specified critical routes. Additional aspects considered when selecting this sample include the level of seismic hazard, availability of geotechnical information, geological and geographical diversity, type of route carried, type of route crossed, construction material, and superstructure components, such as number of spans. Currently, BIAS does not maintain information regarding substructure type, therefore no consideration is given to substructure type when selecting the sample set. A total of 100 bridges (51 prestressed concrete, 25 reinforced concrete, and 24 steel) throughout the state of Indiana are selected for the detailed analysis. Of the 100, 50 of the bridges are selected from the Vincennes District, which is assumed to have the highest level of seismic hazard due to its proximity to both WVSZ and NMSZ. Finally, 10 bridges are selected from each of the remaining five districts in the state.

A statistical analysis of the 100 sample bridges is conducted to verify that the sample set reflects the distribution of the 5,000+ state-owned bridges in terms of the superstructure characteristics that influence the dynamic response. As shown in Figure 3.1 and Appendix C, the selected sample set is representative of INDOT's bridges in terms of maximum span length, number of spans, total structure length, structure type (shown in Figure 3.1), out-to-out deck width, and skew. As Figure 3.1 shows, for the 22 categories of structure types (defined in *Recording and Coding Guide for the Structure Inventory and Appraisal of the Nation's Bridges* (Office of Engineering Bridge Division Bridge Management Branch, 1995)) across the three main construction materials (steel, reinforced concrete, prestressed concrete), the majority of structure types for each construction material are present in the sample.

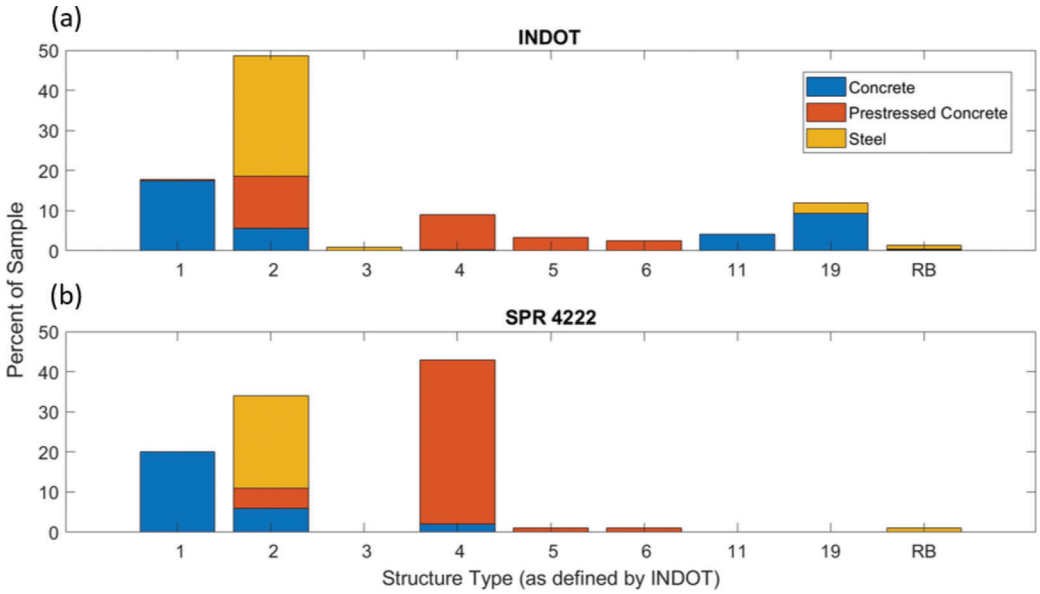

Figure 3.1 Distribution of structure type in (a) INDOT's bridge inventory and (b) 100 sample bridges selected for SPR-4222.

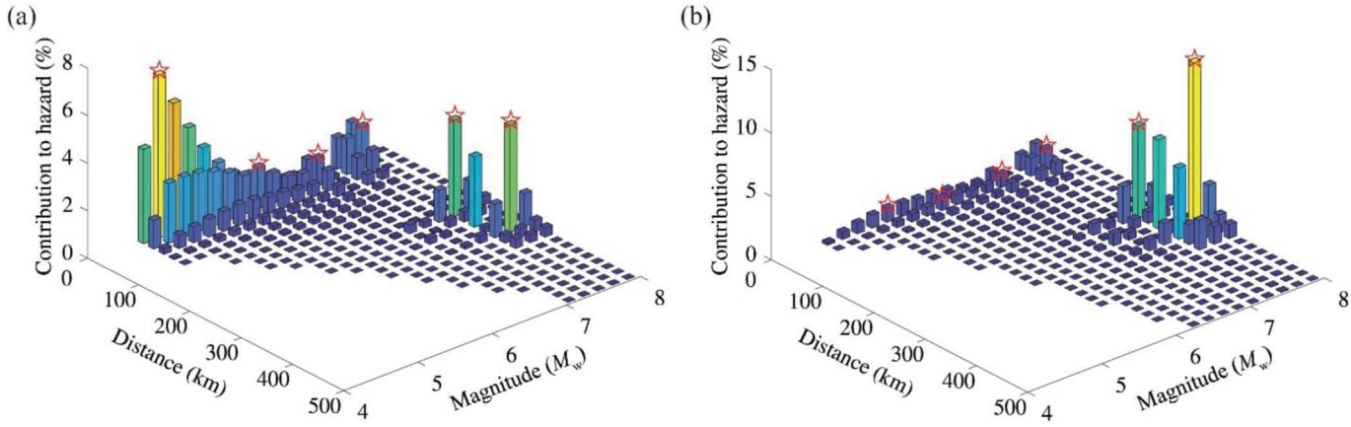

Figure 3.2 Deaggregation results for a bridge site in the Vincennes District and spectral acceleration at (a) 0.2 s and (b) 1.0 s.

The sample intentionally does not include culverts (structure type 19 in BIAS) as a buried structure does not have a surface independent of the ground movement, and thus are deemed as low-vulnerability. Note, RB is used here to capture the small percent of "Remaining Bridges" that did not fall into the detailed bins.

For states like Indiana where very few records of seismic ground motions exist, ground-motion time histories need to be simulated for scenario earthquakes to perform a seismic vulnerability assessment of the bridge network. These simulated ground motions consider the location of the bridge relative to the seismic source, the resulting attenuation of the seismic waves, and the local site condition at the bridge site. For each bridge in the sample, 100 ground-motion time histories are generated using stochastic and deterministic simulation techniques (Boore, 1983; Halldorsson & Papageorgiou, 2005; Mavroeidis, et al. 2020; Papageorgiou & Aki, 1983). These synthetic ground motions are generated from scenario earthquakes with magnitude and distance obtained from deaggregation analysis of the United States Geological Survey (USGS) uniform hazard spectrum (UHS). The deaggregation results, shown in Figure 3.2 for one sample bridge, allow us to identify the predominant seismic sources that contribute to the hazard at each bridge site, given the fundamental period of the structure. A comparison of Figure 3.2a and Figure 3.2b indicates that small nearby earthquakes form the main contribution to the seismic hazard for spectral accelerations at 0.2 s, whereas large distant earthquakes are the predominant sources of hazard for spectral accelerations at 1.0 s.

The simulation of ground motions requires either generic site amplification factors or detailed site response analysis to account for local site effects. For bridges having a soil profile with complete information on shear-wave velocity, thickness, plasticity index, and density, an equivalent-linear site response analysis is performed. As is typical throughout INDOT's bridge network, most bridges in the sample are not accompanied by sufficient geotechnical information to carry out a site response analysis. Instead, generic site amplification factors are developed for these sites using generic velocity profiles applicable to the CEUS. For structures where the precise soil class at the site is unknown, the soil class is estimated using the predicted response of the geological material map for Indiana (Hill, 2008).

***

All ground motions are generated for a return period of ~1,000 years (7% probability of exceedance in 75 years) consistent with current AASHTO (2017) design specifications. More information regarding the process for simulating ground motions can be found in Appendix C.

***

4. DETAILED ASSESSMENT (LEVEL 2) AND ASSOCIATED FINDINGS

The Level 2 assessment procedure is developed to ensure the accuracy and robustness of the Simplified Assessment procedure. A Level 2 assessment is conducted by an engineer and requires the interpretation of structural drawings and engineering judgement. As such, a Level 2 assessment is conducted for each bridge included in the 100-bridge representative sample discussed in Section 3. The Level 2 assessment has the following four main purposes:

1. identify common vulnerable details (Section 4.1) from which retrofit strategies specific to the local hazard level may be proposed (Section 4.3).
2. identify trends in vulnerability which can be leveraged to refine the Simplified Assessment (Section 4.2).
3. identify necessary database enhancements that ensure the robustness of INSAT (Section 4.4).
4. validate the results from the Simplified Assessment (Section 5.2).

To conduct the Level 2 assessment, a 2-D finite-element model for each of the 100 bridges is constructed for each direction of motion. The Level 2 assessment procedure, shown in Figure 4.1, contains the steps for determining the capacity (purple) and demand (green) of each bridge considered, allowing its vulnerability to

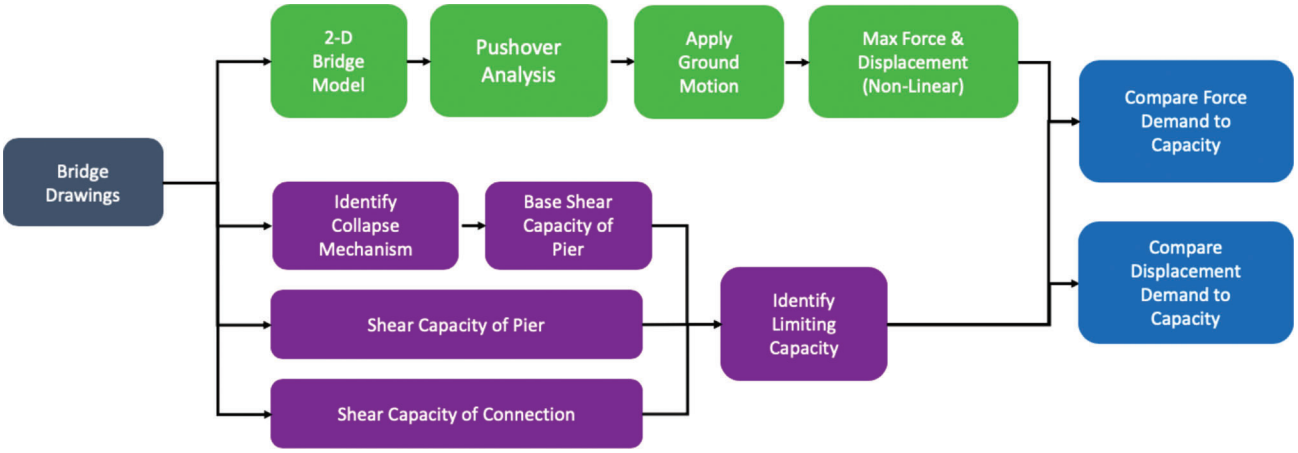

Figure 4.1 Detailed Level 2 assessment procedure.

TABLE 4.1
Summary of Capacity Thresholds Used for Level 1 Assessment

	Transverse Direction		Longitudinal Direction		
Level 2 vulnerability	Formation of plastic hinge	Exceedance of hinge rotational capacity	Formation of plastic hinge	Exceedance of hinge rotational capacity	Brittle failure
Level 1 threshold	Drift > 0.5%	Drift > 1.5%	Displacement > 1 in.	Displacement > 6 in.	Displacement > 0.1 in.
Additional identifiers	—	—	Substructure built after 1990	Substructure built after 1990	Substructure built before 1990[1]
Corresponding vulnerability classification	Moderate vulnerability	High vulnerability	Moderate vulnerability	High vulnerability	High vulnerability

[1]See footnote in Table 4.2.

be assessed (blue) for the expected level of earthquake excitation in Indiana. In Figure 4.1, base shear capacity of pier is the shear corresponding to the formation of the identified hinge mechanism, whereas shear capacity of pier corresponds to the pier's shear strength.

4.1 Identification of Vulnerability Trends

The results from the Level 2 assessment are also used to identify displacement-based trends from the response of the bridges to be used as capacity thresholds in the Level 1 assessment. These thresholds, originally taken from Ramirez et al. (2000), have been adapted to reflect the responses observed in the sample set and the capabilities of the Level 1 procedure. The most applicable capacity thresholds are summarized in Table 4.1. In this table, drift corresponds to the lateral displacement divided by the height of substructure between the fixed end(s) and point of zero moment or contraflexure. For walls in the transverse direction this corresponds to the element height (Section 4.4) whereas for frame bents this typically corresponds to half the element height. Additional capacity thresholds applicable to specific substructure-superstructure combinations are explained in Section 5.2.

4.2 Identification of Vulnerable Details

The results obtained using the dynamic models developed in the Level 2 assessment are leveraged to identify common vulnerable details across the state. These vulnerabilities influence the selection and design of applicable retrofits. Based on the results for the 100-bridge sample set, the identified vulnerabilities are summarized in Table 4.2. As Table 4.2 shows, most of the identified vulnerabilities are tied to substructure deficiencies. It is important to note that the dynamic modeling technique in this project emphasizes the response of the substructure, which allows these particular vulnerabilities to be identified more comprehensively. Although more complex modeling strategies, such as an energy-dissipation analysis of potential abutment pounding, could yield further insight into some specific vulnerabilities, the results in Table 4.2 are consistent with known vulnerabilities and can reasonably be taken as comprehensive of the common seismic vulnerabilities of the Indiana bridge inventory. More information regarding the Level 2 assessment, such as further discussion of the flowchart shown in Figure 4.1 and detailed descriptions and calculations for various substructure (column 2 of Table 4.2) and superstructure combinations, can be found in Appendix D.

TABLE 4.2
Summary of Identified Key Vulnerabilities

(1) Vulnerability Case	(2) Substructure Type	(3) Direction	(4) Additional Comments/ Criteria (When Applicable)	(5) Level of Vulnerability	(6) Reason for Classification
1	Walls	Longitudinal	Built before 1990 (grade 40 *ksi* steel)[1]	Highly vulnerable	Low flexural reinforcement ratio
2	Hammerhead walls	Longitudinal	Built before 1990 (grade 40 *ksi* steel)[1]	Highly vulnerable	Low flexural reinforcement ratio
3	Hammerhead walls	Longitudinal	Built After 1990 (grade 60 *ksi* steel)	Moderately vulnerable	Formation of plastic hinge
4	Hammerhead walls	Transverse	Prestressed concrete superstructure only	Moderately vulnerable	Formation of plastic hinge
5	Frame bents	Transverse	All types (H-Pile, CFT, reinforced concrete)	Moderately vulnerable	Formation of plastic hinge
6	Frame bents	Longitudinal	All types (H-Pile, CFT, reinforced concrete)	Moderately vulnerable	Formation of plastic hinge
7	—	—	Rocker bearings	Moderately vulnerable	Unseating

[1]In accordance with the *Manual for Bridge Evaluation* (2018) Table 6A.5.2.2-1, bridges built before 1990 are assumed to have reinforcing steel grade 40 ksi. If the bridge is identified as having grade 60 ksi steel and built before 1990, it could fall under vulnerability Case 3.

4.3 Retrofit Alternatives

For each of the vulnerabilities identified in column 6 of Table 4.2 a retrofit strategy is needed that can either eliminate a particular deficiency or reduce the damage associated with it. The retrofits discussed herein aim to fulfill this purpose either by reducing the seismic demand or by increasing the substructure capacity and are offered as possible alternatives for consideration by INDOT and its consultants. Table 4.3 relates each of the identified vulnerability cases (column 1) shown in Table 4.1 to applicable retrofit methods which have been proposed to improve the seismic performance of structures with similar deficiencies in the Central Southern United States (CSUS) (Choi, 2002; DesRoches et al., 2004a,b; Nielson & DesRoches, 2007; Wright et al., 2011). This table also shows the pros and cons of each retrofit strategy. A more thorough review of each retrofit strategy as well as a comprehensive retrofit selection guide is provided in Appendix E. It is possible that the vulnerability of the bridge detail can be improved by applying more than one of the recommended retrofits. In addition, it is possible that in a given bridge multiple retrofit schemes should be applied, as is the case for a bridge with steel rocker bearings (vulnerability case 7) supported by a deficient substructure (vulnerability cases 1–6 may apply).

4.4 Recommended Data Enhancements in BIAS

This project, through the Level 2 assessment of each bridge in the 100-bridge sample, has identified eight critical data items that BIAS does not contain but are necessary to conduct a robust Simplified Assessment. The impact of these data items on the overall capability to conduct a Simplified Assessment are explored in detail in Appendix F. Recommendations for how to collect the data as well as overall improvements to increase the efficiency of certain components of BIAS are also explored. The implementation of these data items in BIAS is discussed in Section 6.2. These eight data items, plus one indicator, briefly defined, are the following:

- *substructure type:* the most appropriate substructure type should be identified from these five: rectangular column frame bent, circular column frame bent, hammerhead wall, wall, and other. Bridges with more than one substructure types should also be classified as other. Note that a vulnerability assessment, other than Level 0 of the Simplified Assessment, is not possible without this data item.
- *abutment type:* the most appropriate abutment type should be added from these two—integral-type (including semi-integral) or non-integral-type.
- *deck thickness:* the thickness of the reinforced concrete deck (in).
- *number of elements:* typical number of columns in a single bent. For walls and hammerheads, this number is one.
- *element length:* out-to-out dimensions in the transverse direction for a single substructure element (ft). For example, this is the longer dimension for walls and hammerheads.
- *element width:* out-to-out dimension in the longitudinal direction for a single substructure element (ft).
- *element height:* either the clear height of the substructure or the unsupported height of the substructure (ft). Illustrations of this measurement are shown in Figure 6.1.
- *height ratio flag:* "yes" or "no" flag to identify if any piers in the bridge have a height ratio (H_{tall}/H_{short}) between the taller pier (H_{tall}) and shorter pier (H_{short}) greater than 1.1.
- *seismic retrofit:* a check box to indicate when a detailed seismic retrofit, which ensures a structural response resulting in low vulnerability, has been performed on a bridge.

TABLE 4.3
Options for Recommended Retrofits for Identified Vulnerabilities

Vulnerability Case (Table 4.1)	Potential Retrofits					
	Integral Abutments	Restrainers	Isolation	Additional Confinement	Post-Tension	Jacketing
1	×	×	×			×
2	×	×	×			×
3	×	×	×	×		×
4	×	×	×	×		
5	×	×	×	×	×	
6	×	×	×	×		
7	×	×	×	×		
Pros	1. Eliminate longitudinal vulnerability entirely	1. Simple design 2. Simple construction 3. Common design detail for INDOT bridges	1. Common retrofit 2. Reduce substructure demand significantly	1. Increases ductility 2. Simple design 3. Simple application	1. Changes to preferred failure mechanism (strong column–weak beam)[1]	1. Increases ductility and capacity 2. Identified as most beneficial for highly vulnerable bridges
Cons	1. Transverse direction check still requires vulnerability assessment 2. Extensive construction	1. May require another substructure retrofit (based on design constraints)	1. Potential for pounding unless appropriately designed or additional retrofit exist	1. Negligible increase in structural capacity 2. Not applicable post-damage (per INDOT)	1. Moderate design difficulty 2. May require additional retrofits	1. Jacketing options (steel, reinforced concrete) vary in implementation difficulty

[1]The post-tensioning is applied to the beam element of the frame bent to change the mechanism of hinge formation from strong column–weak beam (less favorable for rehabilitation) to weak column–strong beam (more favorable for rehabilitation).

5. SIMPLIFIED ASSESSMENT PROCEDURE (LEVEL 0 AND LEVEL 1)

The Simplified Assessment procedure, which includes the Level 0 and Level 1 assessments, serves as the basis for the INSAT tool's functionality. The Simplified Assessment procedure, shown in Figure 5.1, is used to determine the vulnerability of bridges in Indiana's bridge inventory for a given level of hazard. Using trends identified in the Level 2 assessment, certain bridges are immediately classified as low vulnerability, moderate vulnerability, or requiring a Level 2 assessment. This portion of the procedure is referred to as the Level 0 assessment, discussed in Section 5.1 The procedure for determining the vulnerability for each of the remaining bridges is the Level 1 assessment, discussed in Section 5.2.

5.1 Level 0 Assessment (Initial Classification)

The Simplified Assessment procedure begins with the Level 0 assessment, which immediately identifies bridges that can be classified as having low vulnerability, moderate vulnerability, or requiring a Level 2 assessment. This classification scheme is established using the trends identified in the Level 2 assessment. The bridge details that can be automatically screened as having low vulnerability are the following:

- bridges that have specifically been seismic retrofitted, due to the retrofit being designed for the level of hazard expected at the bridge site.
- short span single span bridges on rocker bearings (span length less than 60′–0″), due to the low probability of unseating.
- single span bridges not supported by rocker bearings, due to the low probability of unseating.
- buried structures, or culverts, as they are expected to move entirely with the ground.
- wall substructures in the transverse direction, due to their high rigidity resulting in low structure displacement and restoring force.
- bridges with integral abutments in the longitudinal direction, because of the low probability of any differential displacement between the substructure and the superstructure.

The bridge details that can automatically be screened to moderate vulnerability are the following:

- long span single span bridges on rocker bearings (span length greater than or equal to 60′–0″), due to the potential for overturning of the rocker bearings.

The bridge details that require a Level 2 assessment are the following:

- bridges with expansion joints, due to the modeling complexity.
- bridges with substructures classified as "other," due to their uniqueness and/or modeling complexity (see Section 6.2.1).
- bridges with piers having a height ratio between the tallest pier and the shortest pier greater than 1.1, due to their increased potential for non-simultaneous initiation

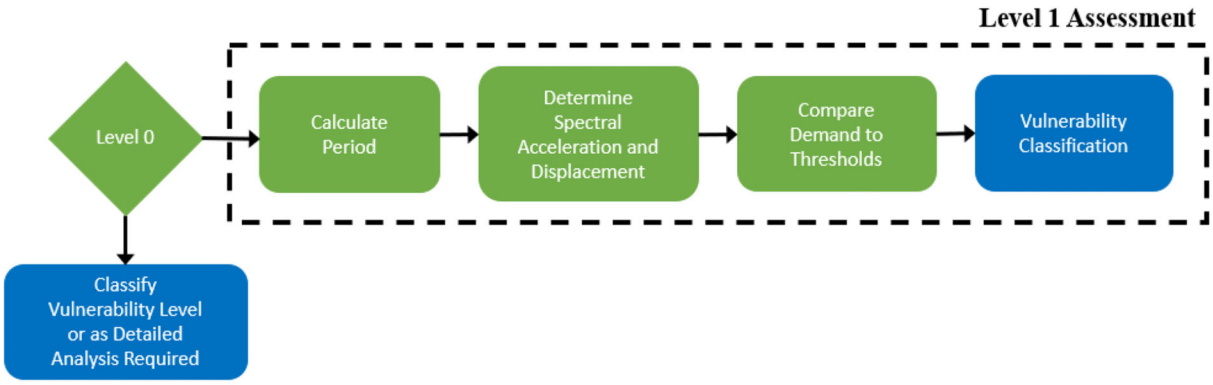

Figure 5.1 Simplified Assessment procedure.

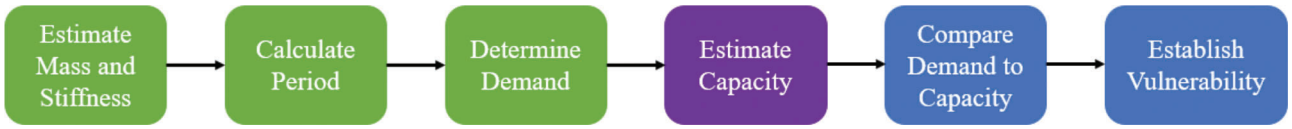

Figure 5.2 Level 1 assessment procedure.

of nonlinear behavior, which cannot be adequately identified in a Level 1 assessment.

- reinforced concrete superstructures with reinforced concrete column frame bents because detailed information regarding the reinforcement layout is required to determine the capacity of the substructure. Further rationale is explained in Section 5.2.
- frame bents with an aspect ratio (H/L) less than three, as there is a high likelihood that the substructure will not behave in flexure.

The full rationale for these classifications can be found in Appendix G. Of the 100 bridges selected for the detailed analysis, 69 of them fall into one of these three classifications. The remaining 31 bridges move on to a Level 1 assessment, which is described in Figure 5.2.

5.2 Level 1 Assessment

The Level 1 assessment is developed to rapidly evaluate the seismic vulnerability of Indiana's bridge network and is implemented through INSAT, which is described in more detail in Section 5.3. The Level 1 assessment leverages trends revealed through the Level 2 assessment, information that is currently available in BIAS, and additional critical data items, previously described, to develop simplified single degree-of-freedom (SDOF) bridge models. The Level 1 assessment procedure, shown in Figure 5.2, highlights the dynamic modeling procedure. A more detailed description is given in Appendix G, but a synopsis is provided here.

5.2.1 Modeling

The Level 1 assessment is applied to the 31 bridges that do not fall into one of the three categories characterized by the details described in Section 5.1. The mass calculation is superstructure dependent and is based on trends and averages seen in the Level 2 assessment. The stiffness calculation is substructure and superstructure dependent. The substructure determines which equation to use while the superstructure determines which piers add stiffness and the fixity of the connection between the substructure and the superstructure. While the stiffness of walls and hammerhead substructures can be determined using the same equations as the Level 2 assessment, the transverse direction stiffness calculations for frame bents cannot use these equations. Rather, the transverse stiffness for frame bents is calculated using a frame bent factor that relates the pre-condensed, pre-decoupled pure translation degree of freedom to the calculated stiffness of the frame bent. The longitudinal stiffness for frame bents is calculated using the same equation as the Level 2 assessment. The mass and stiffness determined by these procedures are then used to calculate the period of the structure in each direction. These calculations are presented in detail in Appendix G.

5.2.2 Assessment

Because each bridge is modeled as a SDOF system, a response spectrum is used to determine the spectral acceleration value for that bridge. This value, and the period of the structure, are used to estimate a linear displacement of the bridge in response to a level of hazard. To account for the nonlinear effects of RC substructures with adequate longitudinal reinforcement ratios, a multiplier of $\sqrt{2}$ is used to estimate an expected nonlinear displacement (Δ_{nl}) (Sozen, 2003). When applicable, this displacement is multiplied by the substructure stiffness to calculate the bridge's restoring force, or demand.

The exceedance of a bridge's capacity, and thus the resulting vulnerability level, is identified through the comparison of the resulting displacement or force with a corresponding threshold. For most structures, the displacement thresholds summarized in Table 4.2 are applicable. However, a few substructure and superstructure combinations require more detailed measures, such as the following:

- *pile-type substructures:* the vulnerability of concrete-filled tubes (CFT) and H-pile substructures supporting reinforced-concrete superstructures is determined using capacity-based thresholds. From the Level 2 assessment, it is determined that CFT and H-pile substructures solely support RC superstructure bridges over waterways. Due to the rigid connection between the substructure and superstructure, these bridges do not experience a displacement like prestressed concrete and steel bridges that do not have a rigid connection. Thus, the displacement thresholds outlined in Table 4.2 do not apply. However, from the Level 2 assessment, it is determined that a standard section for these substructure types is used in design. Thus, a standard base shear capacity exists, and this capacity is compared to the restoring force calculated using the Level 1 assessment.
- *reinforced concrete frame bent substructures supporting reinforced concrete slab deck bridges:* like pile-type substructures, these bridges are rigidly connected from the substructure to the superstructure. Thus, this bridge class does not experience a displacement like bridges without a rigid connection between the substructure and superstructure. However, unlike pile-type substructures, reinforced concrete substructures do not have a standard capacity. Thus, neither the displacement thresholds or capacity thresholds previously mentioned apply and these structures require a Level 2 assessment.
- *hammerhead substructures supporting prestressed concrete girder superstructures:* a small sample of prestressed concrete bridges are supported by hammerhead substructures with an aspect ratio greater than three. Thus, the formation of a plastic hinge is possible in the transverse direction. The capacity of the hinge is calculated as a function of the aspect ratio based on observations from the Level 2 assessment.

5.2.3 Verification and Validation

To validate the Level 1 procedure and defined thresholds, the suite of ground motions generated for each bridge site (Section 4) in the Level 2 assessment is used. The classification results for the Level 1 assessment are compared to the classification results from the Level 2 assessment. Figure 5.3 shows the comparison of the classification for all 31 bridges—a total of 3,400 ground motions, considering both applicable directions. If the classification from the Level 1 assessment matches the Level 2 classification, then the Level 1 assessment results are included in the bar chart as a "match." If the Level 1 assessment classifies the bridge as a higher level of vulnerability than the Level 2 assessment, the Level 1 assessment results "overestimate" the level of vulnerability of the bridge. If the Level 1 assessment classifies the bridge

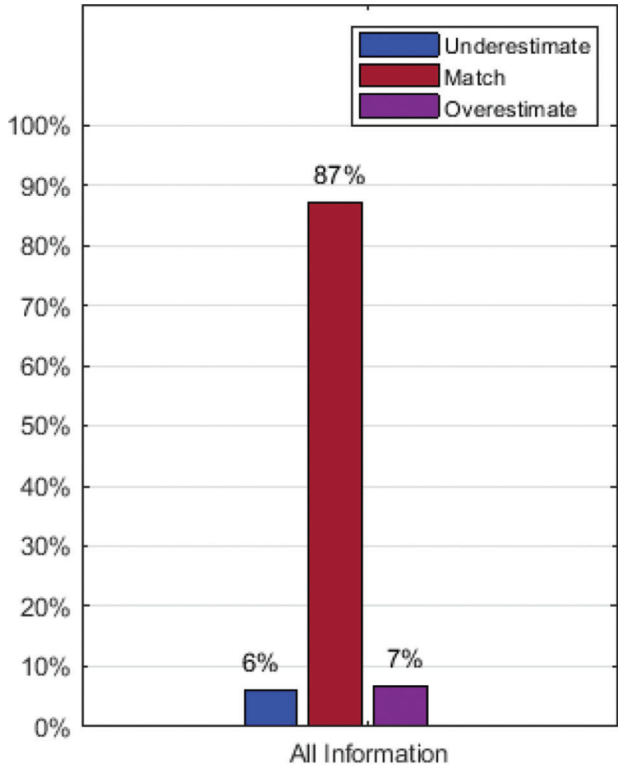

Figure 5.3 Comparison of the Level 1 classification to the Level 2 classification with all recommended information included for all 31 bridges.

at a lower level of vulnerability than the Level 2 assessment, the Level 1 assessment results "underestimate" the vulnerability of the bridge. The worse-case scenario is underestimating the vulnerability of the bridge.

More information regarding the Simplified Assessment process and results as well as a discussion of the importance of the recommended additional data items can be found in Appendix G.

5.3 Simplified Assessment in the Indiana Seismic Assessment Tool (INSAT)

The research team developed INSAT for INDOT to conduct a simplified seismic assessment to determine the vulnerability of the Indiana bridge inventory for a given level of hazard. The flow of data and the process used in the simplified assessment tool is shown in Figure 5.4. The functionality of the tool is described briefly below and in more detail in Appendix H.

INSAT contains the site class and uniform hazard spectra (UHS) data for each bridge in INDOT's bridge inventory as of January 27, 2020, where the UHS data is determined using USGS's nshmp-haz code (nshmp-haz, n.d.).

***

It is important to note that while the Level 1 assessment is validated using the simulated ground

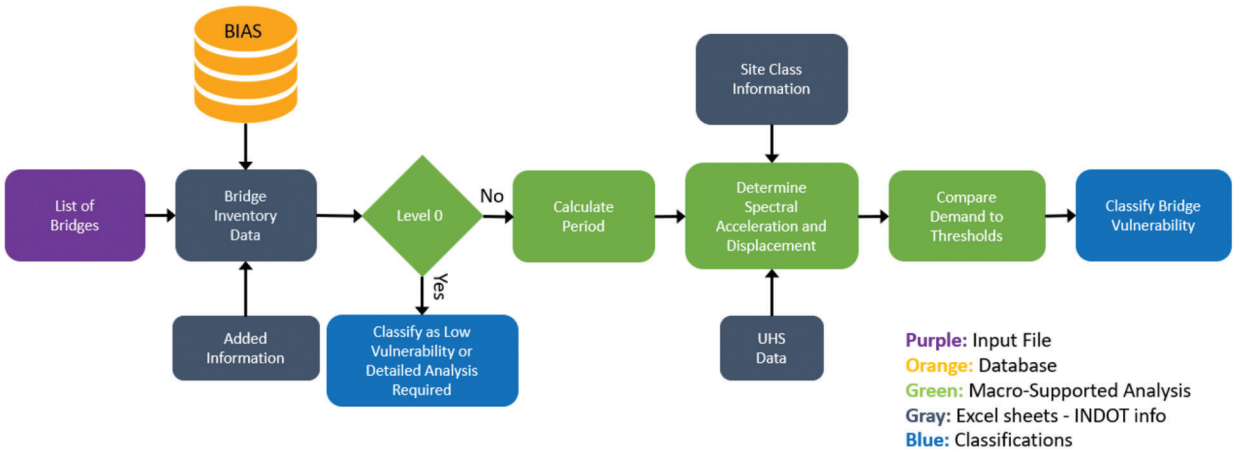

Figure 5.4 INSAT procedure.

motions for each site, the vulnerability of the bridge is determined in INSAT using the UHS.

***

The site class for each site is determined using the predicted response of the geological material map (Hill, 2008). The site class data and the UHS data are extracted from the Environmental Systems Research Institute (ESRI) Shapefile and USGS's tool, respectively, and are stored internally in the tool on the "Site Class" and the "UHS Information" sheets.

To run the Simplified Assessment, the most recent version of BIAS with, at a minimum, the National Bridge Inventory (NBI) data items shown in Table 5.1, are required. This data must be stored in a separate input file, referred to as "BIAS Data file" in Bonthron et al. (2020).

INSAT is designed to use information found in BIAS. However, in its current state, BIAS does not contain sufficient data items to perform the Simplified Assessment. In addition to the data items listed in Table 5.1, the tool also requires eight critical data items introduced earlier in Section 4.4. The importance of these data items and the impact they have on the accuracy of the Simplified Assessment is discussed in detail in Appendix G and Appendix F, respectively.

***

The necessary data items are substructure type, abutment type, element height, number of elements, element length, element width, deck thickness, a height ratio flag, and a seismic retrofit checkbox.

***

Because these data items are not currently included in BIAS, these data items can be stored in the BIAS Data file or in a separate input file, referred to as Additional Data file in INSAT's user guide (Bonthron et al., 2020), to run a vulnerability assessment. INSAT will prompt the user for an additional file if the data items are not in the BIAS Data file.

TABLE 5.1
Required Data Items from BIAS

NBI Data Item Number	Data Item Name
—	Asset name
08	Structure number
027	Year built
107	Year reconstructed
002	District
016	Latitude
017	Longitude
043A	Superstructure type (A)
043B	Superstructure type (B)
045	Number of spans in main unit
046	Number of approach spans
034	Skew
049	Structure length
052	Deck width, out-to-out
048	Length of maximum span
006	Feature intersected
007	Facility carried
054B	Minimum vertical under clearance

***

If these data items are not included or available, the tool will still execute, but the results will set all bridges that do not have the minimum level of data as requiring a Level 2 assessment.

***

INSAT allows the user to select a subset of bridges to analyze. It uses the entered information to first determine which level of assessment is applicable to each bridge. This step first determines which bridges can automatically be classified as low or moderate vulnerability through a "Level 0 Assessment" type. For the bridges that have details that require a Level 2 analysis, the assessment type is set to "Detailed Assessment." For the bridges that do not fall into either of these situations, the assessment type is set to a "Level 1 Assessment" and further assessment on those bridges is conducted within the tool. This outcome

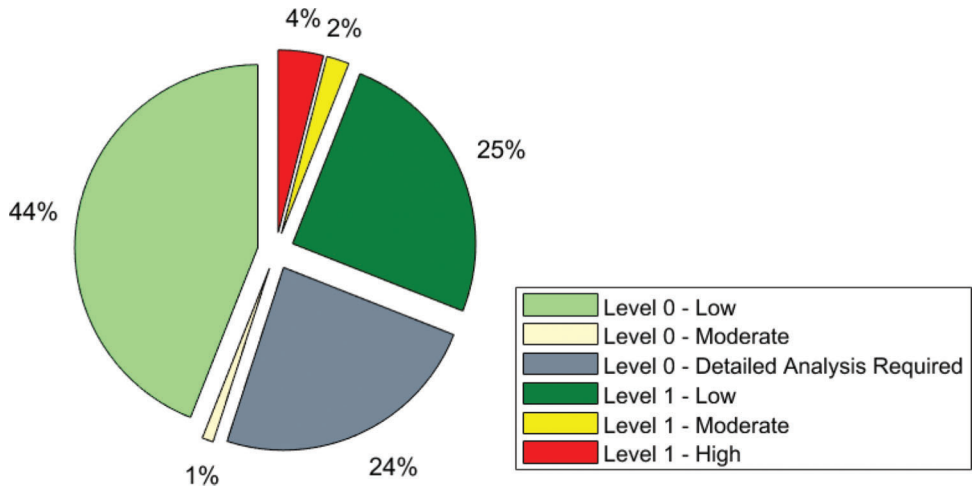

Figure 5.5 Vulnerability classification for the 100-bridge sample set.

means that the relevant bridges do not have unique details and the entered information for the bridges contains all the required information for a Level 1 assessment.

After performing the Level 0 classification, INSAT conducts a Level 1 assessment on the remaining bridges. The tool uses the equations, estimates and averages described briefly in Section 5.2 and in detail in Appendix G to calculate the mass, the stiffness, and the period. The calculated period is used with the UHS data stored internally in the tool to determine the spectral acceleration.

The UHS data used is specific to each bridge site, based on the longitude and latitude in BIAS, for a probability of exceedance of 7% in 75 years (AASHTO, 2017). The raw UHS data is for a site class B/C, however, most bridges sites in Indiana do not have a B/C site class. The tool uses site factors, found in AASHTO Section 3.10.3.2 (2017), to amplify or reduce the spectral acceleration provided by the UHS. More information regarding the version of the code and the process for generating the UHS data is explained in Appendix H.

The adjusted spectral acceleration is then used to determine a spectral displacement. A nonlinear displacement, using the $\sqrt{2}$ multiplier (Appendix G), is calculated for bridges which are likely to exhibit a ductile response. These bridges, unlike the bridges which are expected to exhibit a brittle mode of failure, experience amplified displacement once the bridge enters the nonlinear regime. When necessary, the stiffness of the bridge is used to calculate the restoring force. As mentioned previously, the displacement-based thresholds shown in Table 4.2 do not apply for these bridges. Rather, this force is compared to a standard capacity based on the assumed section-type. Based on the substructure type, the calculated displacement or restoring force is then compared to the corresponding capacity thresholds (full table of thresholds found in Appendix G) and the vulnerability classification is output to the "All Results" sheet. The overall vulnerability classification for the 100-bridge sample set, determined by the more vulnerable classification between the transverse and longitudinal directions, is shown in Figure 5.5.

It must be mentioned that even without any of the eight additional data items, the information within BIAS can still be leveraged to conduct a Simplified Assessment. This approach allows for INDOT to determine which bridges can automatically be classified using the Level 0 assessment given just the information currently housed in BIAS. As Figure 5.6 shows, 38% of Indiana's bridge inventory can still be classified without any additional information. These 38% fall into three categories: low vulnerability, moderate vulnerability, and detailed analysis required. The 8% of bridges that are categorized as "Level 0–Detailed Analysis Required" will always require a detailed analysis even with added information. This percent of the inventory corresponds to bridges which are expected to maintain expansion joints or internal hinges, thus requiring a more involved analysis. The remaining 62%, labeled as "Detailed Analysis Required" have the potential to be analyzed using the Simplified Assessment given the addition of the eight data items.

***

This insight into the current capabilities of INSAT reduces the number of bridges for which INDOT must collect information and results in an effective initial prioritization for data collection.

***

In addition to classifying the bridge inventory, INSAT is also set up to optionally apply a user-defined priority factor. Priority factors can be applied based on district, whether or not the bridge is on a critical route identified by INDOT (A. Post, personal communication, January 31, 2018), or for a user-defined list of NBI's with corresponding priority factors. When the user chooses to apply a priority factor, INSAT will sort the analysis results by both priority factor and by

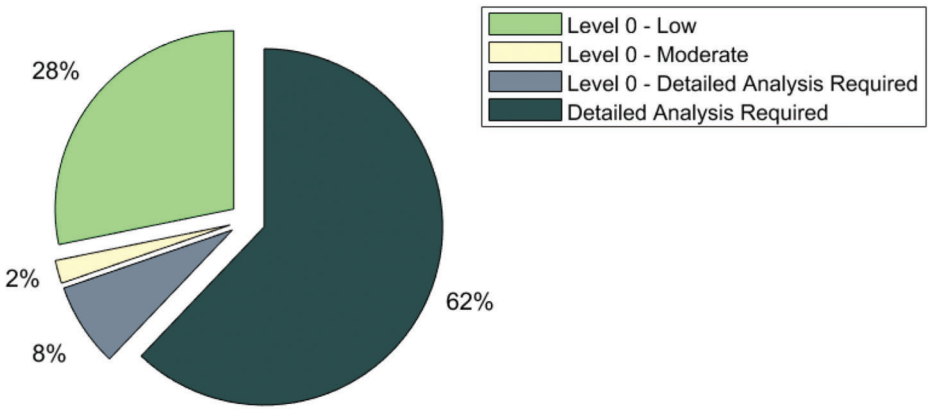

Figure 5.6 Vulnerability classification for INDOT's bridge inventory without additional eight data items in BIAS.

vulnerability classification, showing the bridges with the highest priority factor first within each vulnerability class.

These capabilities will support INDOT in narrowing down their entire bridge inventory to a smaller set of bridges that have a higher level of vulnerability. INDOT may then choose to prioritize and assess this much smaller set of bridges using a Level 2 assessment, and even identify a retrofit alternative that would be the most appropriate for each bridge. Alternatively, INDOT can leverage the functionality of INSAT to rapidly estimate the impact of implementing certain retrofits by adjusting bridge features such as abutment type, substructure type, or substructure dimensions. This overarching assessment and mitigation procedure (Level 1—Level 2—Retrofit Selection) will provide INDOT with the tools to improve the seismic response of their bridge network, thus yielding improved structural performance and hazard-mitigation.

6. IMPLEMENTATION RECOMMENDATIONS

The successful use of INSAT requires a statewide implementation procedure for the collection of additional data items either during routine inspections or through other methods, such as artificial intelligence, as discussed in Appendix F. In the sections below we discuss proposed recommendations for boring depth gathered during the generation of the ground motion histories, database improvements, how data items could be collected for inclusion in BIAS during routine inspections, and how to integrate INSAT into the existing bridge rehabilitation and replacement decision making process.

6.1 Geotechnical

Adequate geotechnical information, via a sufficient boring depth and shear wave velocity profile should be collected to evaluate liquefaction potential and enable site response analyses. It is recommended to extend both borings and shear-wave velocity profiles to greater depths to reach harder rock (i.e., those with shear-wave velocity preferably greater than 1,000 m/s (3,281 ft/s). Currently, boring depth is dictated by foundation requirements as opposed to seismic hazard potential. Refer to Appendix C for more information.

6.2 Database Items

The implementation of the Simplified Assessment requires the addition of the eight critical data items plus one indicator (seismic retrofit checkbox) defined in Section 4.4 and repeated here starting in Section 6.2.1. The incorporation of this information into BIAS is described in detail below. Their importance and the impact they have on the accuracy of the Simplified Assessment is discussed in detail in Appendix G and Appendix F, respectively. The following are a couple of key points regarding the data implementation:

- each time a bridge is rehabilitated, these data items should be updated to reflect the changes made.
- for single span bridges, the abutment type and deck thickness are the only data items that apply as the other six data items relate to the substructure. Thus, all other data items should be left blank in BIAS.

6.2.1 Substructure Type

Substructure type refers to the pier classification of the main spans. Five main substructure types were identified as typical in Indiana based on the 100-bridge sample set. These five substructure types are the following: circular frame bents, rectangular frame bents, hammerheads, walls, and other. The following points define each substructure type for easy reference.

- *frame bents, circular and rectangular:* a substructure with two or more unsupported columns that maintain an unsupported length greater than the column length. Additionally, the clear spacing between the columns is greater than the column length, and a bent cap (or beam-type element) is present connecting the columns. The columns could have a capital, as shown in Figure 6.1(c), but it is not required for this classification. The cross-section shape of a single column determines whether the

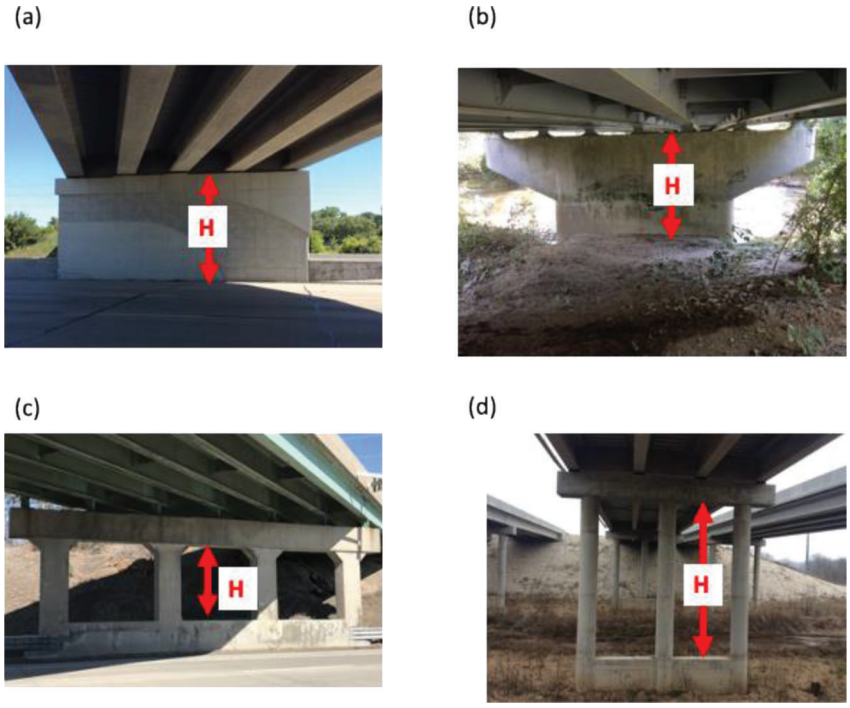

Figure 6.1 Elevation schematic showing height measurement for (a) wall substructures, (b) hammerhead substructures, (c) frame bent substructures with a capital, and (d) frame bent substructures without a capital.

substructure is identified as circular frame bent, shown in Figure 6.1(d), or a rectangular frame bent, shown in Figure 6.1(c).

- *hammerhead walls:* a concrete pier cap supported by a single reinforced concrete element. This element typically maintains a uniform width but experiences a definitive change in cross-sectional length along the height of the element, as shown in Figure 6.1(b).
- *walls:* a single reinforced concrete element, similar to hammerhead walls, that does not experience a definitive change in cross-sectional length along the height. Walls may experience a slight change in cross-sectional width due to the presence of a bent cap, as shown in Figure 6.1(a).
- *other:* substructures that do not definitely fit into one of the previously discussed substructure types should be classified as other. If multiple substructure types are used across a single bridge, the substructure type should be classified as other.

***

The incorporation of substructure type in BIAS should be a dropdown list that includes the five possible types. The bridge inspector, when filling out the rest of the inspection data, can easily select the most applicable substructure type. Once the substructure type is identified, it does not change unless the substructure is rehabilitated.

***

6.2.2 Abutment Type

Abutment type refers to the connection of the superstructure to the abutment. This project identified three abutment types typical to bridges in Indiana: integral, semi-integral, and non-integral. Integral abutments have no expansion joints and the beams are directly connected to the piles. This connection allows the superstructure to move entirely with the abutment. Semi-integral abutments also have no expansion joints in the deck but contain a shear key, unlike integral abutments. Like integral abutments, a portion of the superstructure is connected to the abutment to allow them to move together. Because both integral and semi-integral abutments allow for the superstructure to move entirely with the ground, both should be labeled as integral-type within BIAS. The presence of an expansion joint at the abutments is the distinguishing feature of non-integral abutments. This detail does not allow the superstructure to move with the abutment.

***

The incorporation of abutment type in BIAS should be a dropdown list that includes two categories: integral-type and non-integral-type. Once the abutment type is identified, it does not change unless the abutment type is changed during rehabilitation.

***

6.2.3 Number of Elements

Number of elements refers to the number of main substructure elements in one pier. For walls and hammerheads, this value is one as there is only one substructure element per pier. For frame bents, this number is the number of columns in one pier. If the piers have different numbers of columns, the minimum

number should be recorded and the length and width of the elements in that pier should be used for element length and element width.

***

The incorporation of the number of elements in BIAS should be implemented through a single, user-input box. The inspector can input the number of elements when filling out the rest of the inspection data.

***

6.2.4 Element Height

Element height refers to the clear height of the main substructure units recorded in feet. For wall and hammerhead type substructure this refers to the height from the ground to the top of the bent cap. For frame bents, this refers to the clear height of the column, measured from the ground or base of crash wall to the bottom of the bent cap, shown in Figure 6.1. For bridges over waterways, the height is measured from the bottom of the waterway to the top or bottom of the bent cap, depending on the substructure type. If the piers have varying heights, the largest is recorded since the associated tool is only capable of handling a single height. The reason for using the maximum height is discussed in more detail in Appendix G. Figure 6.1 shows the height on the three typical substructure types.

***

The incorporation of element height in BIAS should be implemented through a single user-input box. The inspector can input the largest element height, in feet, when filling out the rest of the inspection data. For bridges over waterways, the height should be gathered and updated with every inspection due to the high potential for change in element height due to scour.

***

6.2.5 Element Length

Element length refers to the dimension of the main substructure unit in the transverse direction to the deck, recorded in feet. For walls and hammerheads, this dimension is the longer dimension of the substructure measured at the base. For rectangular frame bents, this is the transverse dimension of a single column and for circular frame bents, this dimension is the diameter of a single column. If the length varies across a single pier, or pier to pier, the smallest dimension should be recorded.

***

The incorporation of the element length in BIAS should be implemented through a single user-input box for all substructure types. However, this data item would only need to be collected once.

***

6.2.6 Element Width

Element width refers to the dimension of the main substructure unit in the longitudinal direction, recorded in feet. For walls and hammerheads, this dimension is the shorter dimension of the substructure. For rectangular frame bents, this is the longitudinal dimension of the single column. This data item is the same as the element length for circular frame bents.

***

The incorporation of element width in BIAS should be implemented through a single user-input box for all substructure types. This data item would only need to be collected once.

***

6.2.7 Deck Thickness

Deck thickness refers to the depth of the reinforced concrete deck in the main spans, recorded in inches. As discussed in Appendix F and Appendix G, this data item is more critical for reinforced concrete slab deck bridges than for steel and prestressed girder bridges because of the variability in deck thickness for RC slab deck bridges in the sample set. However, in order to be consistent across all bridge types and inspections, the bridge deck thickness should be recorded for all bridges. Average deck thickness should be added if the deck thickness varies in the bridge.

***

The incorporation of deck thickness in BIAS should be implemented through a single user-input box for all superstructure types. This data item would need to be updated whenever a bridge deck replacement or rehabilitation is done.

***

6.2.8 Height Ratio Flag

Height ratio flag refers to a yes or no check box that signifies when there is a large variation in pier height across a single bridge. As shown in Appendix F and Appendix G, when a single bridge has largely varying pier heights, the Simplified Assessment is not applicable due to difficulties in modeling. This data item identifies these bridges based on a 1.1 ratio between the tallest and shortest pier. After the element height is gathered for each pier, the inspector can determine the height ratio for each bridge using the equation outlined in Section 4.4.

***

The incorporation of the height ratio flag in BIAS should be a check box that the inspector can check if there is a height ratio greater than 1.1 between the tallest and shortest pier. For all other bridges, the box should be left unchecked. For bridges over waterways, this data item must be recalculated every time heights are

measured to account for changes in clear height due to erosion or scour.

***

6.2.9 Seismic Retrofit Checkbox

Seismic retrofit checkbox refers to a checkbox that signifies when a detailed seismic retrofit has been designed and applied to a bridge. When an engineer designs the seismic retrofit, the design must meet all current code requirements and be designed to perform well, resulting in a classification of low vulnerability for the expected level of hazard.

***

The incorporation of the seismic retrofit checkbox in BIAS is simply an indicator that the engineer can check if a detailed seismic retrofit, such as steel jacketing of the column or seismic isolation, has been applied to the bridge. This box should only be checked when an engineer does detailed calculations to confirm the design meets all current code requirements. ***This should not be checked if other types of retrofits that do not affect seismic vulnerability are applied to the bridge, such as geometric changes like bridge deck widening or changes to abutment type (assuming abutment type is added as a data item).***

***

6.3 Tool Implementation

The generalized implementation of the associated seismic evaluation tool requires the addition of the data items discussed above. Once the data items are included in BIAS, INSAT can be used to identify bridges with a higher vulnerability classification and thus prioritize bridges in need of retrofits or replacements. A user guide for INSAT is provided in Bonthron et al. (2020).

6.4 Data Collection

With the identification of the eight data items necessary for implementing a robust Simplified Assessment comes the need for developing a prioritization scheme through which the critical information can be collected most efficiently. As noted in Section 5.3, INSAT can be executed with BIAS as is to help prioritize the process to collect data by identifying the 62%, bridges labeled as "Detailed Analysis Required," which have the potential to be analyzed using the Simplified Assessment given the addition of the eight data items.

The prioritization scheme for data collection could be further focused in a variety of ways, based on either single or multiple criteria. For instance, four focuses of the prioritization scheme could be the following:

1. *key-access corridors:* prioritization of data collection for bridges along major key-access corridors. These corridors can be further prioritized based on daily traffic counts where bridges along highly-traveled corridors are investigated before bridges that are less traveled.
2. *hazard potential:* prioritization of data collection for bridges in regions with higher seismic potential. Based on the seismic hazard map shown in Figure 1.1, this scheme would focus on collecting data for bridges in the Vincennes District first.
3. *soil class:* prioritization of data collection for bridges with a predicted soil class that is unfavorable. Based on the predicted response of the geological material map for Indiana (Hill, 2008), this scheme would focus on collecting data for bridges with soil class "D" or worse.
4. *age:* prioritization of data collection for bridges expected to be built without proper seismic detailing. Based on the age and rehabilitation information for the bridges, this scheme would focus on collecting data for bridges built before 1990 and no substructure rehabilitations.

7. SUMMARY

In this project, the seismic vulnerability of bridges in Indiana subjected to a suite of synthetic ground motions consistent with a hazard level of 7% probability of exceedance in 75 years was examined using detailed dynamic models for a sample set of 100 representative bridges across the state. In addition, the BIAS database was evaluated to serve as the basis to enable seismic vulnerability assessment of the bridges under the oversight of INDOT. The INSAT tool was developed and enhancements to the database were recommended to facilitate implementation of the findings.

7.1 Benefits, Deliverables, Implementation, and Cost Savings

We anticipate that the findings from this study will have direct impact on the Indiana Department of Transportation policies, processes, and procedures. The work conducted in this project has resulted in several deliverables including the suite of ground motions, the vulnerabilities of bridges in Indiana, the BIAS database gap analysis, recommended retrofit options, and the INSAT tool that yield the following significant benefits:

Benefit 1. The results from the dynamic models have already facilitated the identification of typical potentially vulnerable details and vulnerability trends in the INDOT bridges. These trends are directly employed in the execution of the Simplified Assessment. Some of the identified vulnerabilities include the brittle failure of substructures with a low amount of longitudinal reinforcement, the formation of a plastic hinge in substructures with an adequate amount of longitudinal reinforcement and unseating of rocker bearings typical to steel bridges.

Benefit 2. Potential retrofit options for these vulnerabilities are recommended and include isolating the mass, converting the abutment to an integral-type abutment, adding additional confinement to the substructure, and jacketing the substructure.

Benefit 3. A Simplified Assessment procedure and a corresponding tool, INSAT, have been developed to autonomously

assess bridges across the state based on information stored in BIAS.

Benefit 4. Through the identification of eight key data items to be incorporated in BIAS, this project empowered INDOT, if those data are collected, to quickly perform the Simplified Assessment, a robust evaluation of the seismic vulnerability of bridges throughout the state.

Benefits 5. Even without the addition of eight data items, BIAS contains enough information in conjunction with INSAT to show that using the Simplified Assessment developed in this project, 38% of the bridges can be screened using the Level 0 Assessment. The remaining 62% are identified as requiring a Level 2 assessment, but this is due to a lack of information that is essential for conducting a Level 1 Assessment. This 62% are the bridges that could be prioritized for data collection. The 38% corresponds to the following:

- *28% low vulnerability:* short span single span bridges supported by rocker bearings, single span bridges not supported by rocker bearings, and culverts.
- *2% moderate vulnerability: long span single span bridges supported* by rocker bearings.
- *8% detailed analysis required:* bridges which are expected to maintain expansion joint(s) or internal hinge(s).

Benefit 6. INSAT is intended to rapidly identify bridges in the state that have higher levels of vulnerability to assist INDOT in the development of guidelines for retrofitting. With INSAT and BIAS data enhancements, INDOT will have the ability to improve the seismic performance and safety of their bridge network to better serve the public.

Benefit 7. As a result of this project, thousands of synthetic ground motion records consistent with a hazard level of 7% probability of exceedance in 75 years were also generated using stochastic and deterministic simulation techniques for specific sites across Indiana. This extensive and high-quality suite of ground motion records is quite a valuable tool both for design/analysis work conducted at INDOT and for future research projects relevant to seismic hazards.

This research culminated in the development of a macro-based Excel file named INSAT which integrates all of the findings and assessment methods, and thus *provides INDOT with the tools* they need to rapidly assess the vulnerability of their entire bridge network. The *innovative tool* can be used right now to automatically and rapidly assess and classify 38% of the bridges in the state according to their vulnerability level. With implementation of the recommended BIAS database improvements the remainder of the bridges in the state can be classified according to their vulnerability. Furthermore, with the retrofit recommendations provided, bridges across the state and especially those along emergency routes can be identified and prioritized, making them less vulnerable in the case of a seismic event. Regular access to this information will serve to *increase both public safety and mobility* in the case of a hazard event.

Using this more comprehensive and risk-based strategy for asset management across the state has strong potential to *reduce the financial burden on the state*, as the lifetime of bridges in the network may be extended. With more complete and accessible information in the database, decisions regarding maintenance, repair, and replacement can be streamlined, and in some cases automated. Such use of the database will result in financial savings and enhanced asset management by the Indiana Department of Transportation.

Together, the deliverables and findings resulting from this project will enable the Indiana Department of Transportation to *maintain the portfolio of aging assets in a more comprehensive and sustainable* manner and be more cost effective in prioritizing bridge maintenance, rehabilitation, and replacement.

REFERENCES

AASHTO. (2017). *AASHTO LRFD bridge design specifications* (8th ed.). American Association of State Highway and Transportation Officials.

Office of Engineering Bridge Division Bridge Management Branch. (1995, December). *Recording and coding guide for the structure inventory and appraisal of the nation's bridges* (Report No. FHWA-PD-96-001). Federal Highway Administration. https://www.fhwa.dot.gov/bridge/mtguide.pdf

Bonthron, L., Beck, C., Lund, A., Zhang, X., Cao, Y., Dyke, S. J., Ramirez, J., Mavroeidis, G., Baah, P., & Hunter, J. (2020). *A rapid seismic vulnerability assessment tool for bridges in Indiana–INSAT*. DesignSafe-CI Repository. https://doi.org/10.17603/ds2-b5s1-6686

Boore, D. M. (1983, December). Stochastic simulation of high-frequency ground motions based on seismological models of the radiated spectra. *Bulletin of the Seismological Society of America*, *73*(6), 1865–1894. http://w.daveboore.com/pubs_online/1983bssa_stochastic_sims.pdf

Choi, E. (2002). *Seismic analysis and retrofit of mid-America bridges* [Doctoral dissertation, Georgia Institute of Technology]. Georgia Tech Library. http://hdl.handle.net/1853/21538

DesRoches, R., Choi, E., Leon, R. T., Dyke, S. J., & Aschheim, M. (2004a). Seismic response of multiple span steel bridges in central and southeastern United States. I: As built. *Journal of Bridge Engineering*, *9*(5), 464–472. https://doi.org/10.1061/(ASCE)1084-0702(2004)9:5(464)

DesRoches, R., Choi, E., Leon, R. T., & Pfeifer, T. A. (2004b). Seismic response of multiple span steel bridges in central and southeastern United States. II: Retrofitted. *Journal of Bridge Engineering*, *9*(5), 473–479. https://doi.org/10.1061/(asce)1084-0702(2004)9:5(473)

Halldorsson, B., & Papageorgiou, A. S. (2005). Calibration of the specific barrier model to earthquakes of different tectonic regions. *Bulletin of the Seismological Society of America*, *95*(4), 1276–1300. https://doi.org/10.1785/0120040157

Hill, J. R., & Foshee, B. D. (2008). *A preliminary guide to the responses of geologic materials in Indiana to seismically induced ground shaking*, Indiana Geological Survey Report of Progress 35. https://igws.indiana.edu/bookstore/details.cfm?Pub_Num=RP35

Mavroeidis, G., Cao, Y., Beck, C., Bonthron, L., Lund, A., Zhang, X., Dyke, S., Ramirez, J., Baah, P., & Hunter. J. (2020). *Synthetic ground-motion records for 100 bridge sites in Indiana*. DesignSafe-CI Data Repository. https://doi.org/10.17603/ds2-n5b6-4051

Nielson, B. G., & DesRoches, R. (2007). Analytical seismic fragility curves for typical bridges in the central and southeastern United States. *Earthquake Spectra*, *23*(3), 615–633. http://dx.doi.org/10.1193/1.2756815

nshmp-haz. (n.d.). *National seismic hazard mapping project (NSHMP) code*. Retrieved June 20, 2018, from https://github.com/usgs/nshmp-haz

Papageorgiou, A. S., & Aki, K. (1983, June 1). A specific barrier model for the quantitative description of inhomogeneous faulting and the prediction of strong ground motion. I. Description of the model. *Bulletin of the Seismological Society of America*, *73*(3), 693–722.

Petersen, M. D., Moschetti, M. P., Power, P. M., Mueller, C. S., Haller, K. M., Frankel, A. D., Zeng, Y., Rezaeian, S., Harmsen, S. C., Boyd, O. S., Field, E. H., Chen, R., Rukstales, K. S., Luco, N., Wheeler, R. L., Williams, R. A., & Olsen, A. H. (2014). *Documentation for the 2014 update of the United States national seismic hazard maps* (USGS Open-File Report 2014-1091). U.S. Geological Survey. https://dx.doi.org/10.3133/ofr20141091

Ramirez, J. A., Frosch, R. J., Sozen, M. A., & Turk, A. M. (2000). *Handbook for the post-earthquake safety evaluation of bridges and roads* (Joint Transportation Research Program, Publication No. FHWA/IN/JTRP-2000/30). West Lafayette, Indiana: Purdue University. https://doi.org/10.5703/1288284315557

Ramirez, J., Peeta, S., Sozen, M., Garcia, L., & Viswanath, K. (2005). *Emergency earthquake routes; Part I, Criteria for selection of primary routes*; and Part II: *Route seismic vulnerability aspects* (Joint Transportation Research Program, Publication No. FHWA/IN/JTRP-2003/22). West Lafayette, Indiana: Purdue University. https://doi.org/10.5703/1288284313203

Sozen, M. A. (2003). The velocity of displacement. In S. T. Wasti & G. Ozcebe (Eds.), *Seismic Assessment and Rehabilitation of Existing Buildings*. NATO Science Series (Series IV: Earth and Environmental Sciences), vol 29, 11–28. Springer, Dordrecht. https://doi.org/10.1007/978-94-010-0021-5_2

Wright, T., DesRoches, R., & Padgett, J. E. (2011). Bridge seismic retrofitting practices in the central and southeastern United States. *Journal of Bridge Engineering*, *16*(1), 82–92. https://doi.org/10.1061/(ASCE)BE.1943-5592.0000128

APPENDICES

Appendix A. Nomenclature

Appendix B. Summary of Bridges in Sample Set

Appendix C. Procedure for Simulation of Ground Motion at Bridge Sites in Sample Set

Appendix D. Development of Level 2 Procedure and Determination of Capacity Thresholds for Identification of Vulnerability Levels in INSAT

Appendix E. Application of Recommended Retrofits for Improved Seismic Performance of Indiana Bridge Network

Appendix F. Identification of Bias Database Enhancements to Enable Simplified (Level 1) Seismic Vulnerability Assessment

Appendix G. Development of Simplified Assessment Procedure for Rapid Identification of Vulnerable Bridges

Appendix H. Development of Indiana Seismic Assessment Tool (INSAT Tool)

APPENDIX A. NOMENCLATURE

Note: To reduce the number of total variables used throughout the report, some variables can be applied to the analysis in both the longitudinal and transverse direction. For example, K_{sub} is used to represent the stiffness of the substructure in both the transverse and longitudinal direction.

A_b	Area of beam (ft^2)
A_c	Area of column core (in^2)
A_g	Gross shear area (in^2)
A_{isol}	Cross-sectional area of isolator–for shear resistance (in^2)
A_R	Area of concrete in the railing (ft^2)
A_{rest}	Cross-sectional area of restrainers for single beam (in^2)
A_s	Area of longitudinal steel (in^2)
A_{sh}	Total cross-section area of tie reinforcement (in^2)
A_{cv}	Area of concrete in shear
A_v	Area of shear reinforcement (in)
b_{pg}	Width of plate girder (in)
b_v	Width of the section (in)
$\mathbf{C_{dc}}$	Decoupled damping matrix [($kips{\cdot}s$)/in]
c_{isol}	Inherent viscous damping rate of isolator [($kips{\cdot}s$)/in]
C_{limit}	Limiting capacity of substructure ($kips$)
c_{sub}	Inherent viscous damping rate of pier [($kips{\cdot}s$)/in]
$c_{N.A.}$	Depth to the Neutral Axis (in)
d_{isol}	Displacement of isolator (in)
d_y	Displacement of isolator at yield (in)
d_v	Equivalent moment arm between resulting tension and compressive forces (in)
E_c	Modulus of elasticity of concrete (ksi)
E_d	Modulus of elasticity of concrete in deck (ksi)
E_{rest}	Modulus of elasticity, restrainer material (ksi)
E_s	Modulus of elasticity for steel (ksi)
f_c	Assumed stress profile for concrete (ksi)
f_c'	Compressive strength of concrete (psi)
F_{dem}	Force demand on structure ($kips$)
F_{cap}	Force capacity of substructure ($kips$)
F_{con}	Connectivity factor based on superstructure material type
F_{conc}	Total force in the concrete ($kips$)
F_{FB}	Frame bent factor
F_{isol}	Shear force of isolator ($kips$)
F_l	Linear force for a given time history ($kips$)
F_{Length}	Hammerhead length factor
F_{RCFB}	Deck stiffness factor for RC slab deck bridges
F_{s_c}	Force in compression steel ($kips$)
F_{s_t}	Force in tension steel ($kips$)
f_y	Yield stress in reinforcement (ksi)
F_y	Shear force of isolator at yield ($kips$)
f_s	Yield stress of reinforcement (ksi)
G	Shear modulus of concrete (ksi)
G_{isol}	Shear modulus of isolator (ksi)
g	Gravitational constant (in/s^2)

H	Clear height of pier (*ft*)
H_{ratio}	Height ratio of the tallest pier to the shortest pier
H_{tall}	Height of the tallest pier (*ft)*
H_{short}	Height of the shortest pier (*ft)*
h_b	Height of beam (*ft*)
h_c	Core dimension of tied column in the direction under consideration (*in*)
h_{isol}	Height of isolator (*in*)
h_{pg}	Height of plate girder (*in*)
I_b	Moment of inertia of beam (in^4)
I_c	Moment of inertia of column (in^4)
I_{CFT}	Moment of inertia of standard CFT pile (in^4)
I_d	Moment of inertia of deck (in^4)
I_{dir}	Moment of inertia of substructure element (in^4)
I_g	Gross moment of inertia (in^4)
I_{HP}	Moment of inertia of standard H-pile shape (in^4)
$\mathbf{K}$	Stiffness matrix (*kip/in*)
$\mathbf{K_{dc}}$	Decoupled stiffness matrix (*kip/in*)
K_{bend}	Bending stiffness of walls (*kip/in*)
k_d	Post-elastic stiffness of isolator (*kips/in*)
K_{isol}	Effective linear stiffness of isolator (*kips/in*)
K_{pier}	Stiffness of individual pier (*kip/in*)
K_{rest}	Stiffness of restrainers for single beam (*kips/in*))
K_{sub}	Total stiffness of substructure (*kip/in*)
K_{sys}	Stiffness of restrainer system and substructure system (*kips/in*)
K_u	Loading and unloading elastic stiffness (*kips/in*)
K_v	Shear stiffness of walls (*kip/in*)
L_{ele}	Length of the substructure element (*ft*)
L_{pg}	Length of plate girder section (*in*)
L_{bridge}	Length of bridge (*in*)
L_{rest}	Length of activated (taut) restrainer (*in*)
l_D	Cross-sectional width of diaphragm
l_{pier}	Length of superstructure supported by each pier (*ft*)
L_{pier}	Length of the top of the substructure (*ft*)
L_p	Length of plastic hinge in substructure (*in*)
L_y	Length of yielding in substructure (*in*)
$\mathbf{M}$	Lumped mass matrix (*kips/g*)
M_{cr}	Cracking moment (*kips·ft*)
m_D	Mass of diaphragm (*kips/g*)
m_{pier}	Mass of superstructure over each pier (*kips/g*)
m_R	Mass of railing (*kips/g*)
m_{SS}	Mass of primary structural system (*kips/g*)
m_{sub}	Mass of substructure (*kips/g*)
m_{sup}	Activated mass of superstructure (*kips/g*)
M_u	Ultimate moment (*kips*ft*)
M_y	Yield moment (*kips*in*)
N_b	Number of beams
N_{bars_c}	Number of bars in compression
N_{bars_t}	Number of bars in tension

N_c	Number of columns in each bent
N_{pier}	Number of piers participating in seismic response
Q_u	Characteristic strength of isolator (*kips*)
r_{rb}	Radius of rocker bearing (*in*)
s	Spacing of shear reinforcement (*in*)
s_a	Spectral acceleration (g)
s_b	Spacing of beams (*ft*)
s_{clear}	Clear spacing of columns (*ft*)
t	Thickness of substructure element (*ft*)
t_{deck}	Thickness of the deck (*in*)
t_{steel}	Thickness of steel (*in*)
T	Period of Structure (s)
u_i	Translational degree of freedom
u_b	Relative displacement between the bottom of isolator and the ground (*in*)
$\dot{u_b}$	Relative velocity between the bottom of isolator and the ground (*in/s*)
$\ddot{u_b}$	Relative acceleration between the bottom of isolator and the ground (*in/s*^{2})
u_s	Relative displacement between the superstructure and the ground (*in*)
$\dot{u_s}$	Relative velocity between the superstructure and the ground (*in/s*)
$\ddot{u_s}$	Relative acceleration between the superstructure and the ground (*in/s*^{2})
V_{bs}	Base shear strength of pier (*kips*)
V_c	Shear strength of concrete (*kips*)
V_{cfr}	Frictional resistance provided by the deck (*kips*)
V_{cr}	Cracking shear resultant (*kips*)
V_{conn}	Shear capacity of connection (*kips*)
V_d	Direct shear capacity (*kips*)
V_p	Pier capacity (*kips*)–for failure mechanisms other than typical types
V_n	Shear capacity (*kips*)
$V_{n_{lft}}$	Shear capacity of substructure per linear foot (*kips/lft*)
V_{pg}	Volume per linear foot of plate girder (*in*^{3}*/lft*)
V_s	Shear strength of transverse reinforcement (*kips*)
V_{sf}	Shear strength of reinforcement (*kips*)
w	Width of substructure element (*ft*)
w_{bridge}	Width of the bridge deck (out-to-out) (*ft*)
W_b	Weight of beam (*lb/lft*)
w_{rb}	Width of rocker bearing (*in*)
w_{oto}	Out-to-out width of the deck (*ft*)
W_s	Weight of steel in the railing (*lbs/lft*)
x_b	Displacement at the top of the substructure/bottom of isolator (*in*)
x_g	Ground displacement (*in*)
$\ddot{x}_g$	Ground acceleration (*in/s*^{2})
x_s	Displacement (*in*)
$\dot{x_s}$	Velocity (*in/s*)
$\ddot{x_s}$	Acceleration (*in/s*^{2})
α_c	Constant associated with the shear capacity of walls
Δ_{rb}	Allowable displacement of rocker bearing (*in*)
Δ_l	Linear displacement (*in*)
Δ_{nl}	Nonlinear displacement (*in*)
Δ_p	Plastic displacement (*in*)
γ_c	Density of concrete (*150 pcf*)

ε_c	Strain in concrete
$\varepsilon_{N.A.}$	Strain in extreme fiber for given neutral axis
ε_s	Strain in reinforcement
ε_y	Yield strain in reinforcement
ε_0	Maximum nominal concrete strain
λ	Light-weight concrete multiplier
λ_R	Aspect ratio
ρ	Reinforcement ratio of longitudinal (flexural) steel to concrete
ρ_s	Reinforcement ratio of transverse (shear) steel to concrete
μ	Shear term
μ_s	Coefficient of static friction
θ_i	Rotational degree of freedom
$\mathbf{\Phi}$	Mode shape of MDOF systems
$\varphi(x)$	Total curvature equation
φ_{cr}	Curvature at cracking (*rad/in*)
φ_u	Curvature at ultimate moment (*rad/in*)
φ_y	Curvature at yield (*rad/in*)
$\varphi_y(x)$	Liner curvature equation
ν	Poisson's ratio (assumed to be 0.15)
ζ_{isol}	Viscous damping coefficient of isolator (%)
ζ_{pier}	Viscous damping coefficient of pier (%)

APPENDIX B. SUMMARY OF BRIDGES IN SAMPLE SET

The 100-bridge sample set referenced throughout the main document and supporting appendices are summarized here, for convenience. The rationale for selecting these bridges is provided in Appendix C. As a note, the SS used in the District column corresponds to bridges which site-specific amplification factors are used to generate the ground motions (see Appendix C for further details).

Table B.1 Bridges in Sample Set

Asset Name	NBI Number	District	Material
024-56-00899 B	5880*	La Porte	Concrete
064-63-03590 A	22950	Vincennes	Concrete
067-28-00938 A	23770	Vincennes	Concrete
I69-030-09187 NB	80114	Vincennes SS	Concrete
018-05-06573 B	4880	Fort Wayne	Concrete Continuous
028-79-07672	7640	Crawfordsville	Concrete Continuous
(35)22-27-04724 B	11170	Fort Wayne	Concrete Continuous
(237)37-13-07277	11840	Vincennes	Concrete Continuous
041-42-05080 BNBL	14650	Vincennes	Concrete Continuous
041-56-03828 BSBL	15440*	La Porte	Concrete Continuous
044-55-06793	16310	Seymour	Concrete Continuous
055-45-07366	19880	La Porte	Concrete Continuous
056-63-07286	19933	Vincennes	Concrete Continuous
057-14-06739	20690	Vincennes	Concrete Continuous
063-86-05970 BNBL	22810	Crawfordsville	Concrete Continuous
064-19-03723 A	22960	Vincennes	Concrete Continuous
066-13-05443 A	23670	Vincennes	Concrete Continuous
067-42-07298	23760	Vincennes	Concrete Continuous
067-55-03831 ANBL	24100	Crawfordsville	Concrete Continuous
075-06-04958 A	24860	Crawfordsville	Concrete Continuous
252-55-08713	30721	Seymour	Concrete Continuous
252-24-06934 A	30780	Seymour	Concrete Continuous
327-17-06419 A	31350	Fort Wayne	Concrete Continuous

I69-334-04590 BNB	40720	Fort Wayne	Concrete Continuous
I70-112-05137 DEBL	42960	Greenfield	Concrete Continuous
018-04-09861	4591	Crawfordsville	Prestressed Concrete
064-26-06591	22850	Vincennes	Prestressed Concrete
006-20-09858	51480	Fort Wayne	Prestressed Concrete
(37)145-13-08531	76728	Vincennes	Prestressed Concrete
031-50-09771 SB	79822	La Porte	Prestressed Concrete
031-50-02753 SB	79834	La Porte	Prestressed Concrete
I69-029-09183 SB	80106	Vincennes SS	Prestressed Concrete
I69-037-09460 SB	80136	Vincennes	Prestressed Concrete
I69-038-09462 NB	80140	Vincennes SS	Prestressed Concrete
I69-049-09492 NB	80175	Vincennes SS	Prestressed Concrete
I69-061-09527 DRN	80242	Vincennes SS	Prestressed Concrete
I69-062-02793 DR	80246	Vincennes SS	Prestressed Concrete
I69-064-09401 NB	80266	Vincennes SS	Prestressed Concrete
I69-069-09531 NB	80306	Vincennes SS	Prestressed Concrete
I69-077-02797 NB	80316	Vincennes SS	Prestressed Concrete
I69-083-09446 NB	80338	Vincennes SS	Prestressed Concrete
231-28-09532	80380	Vincennes SS	Prestressed Concrete
(50)750-40-02771	80488	Seymour	Prestressed Concrete
024-91-08973	5941	La Porte	Prestressed Concrete Continuous
231-19-08231	16711	Vincennes	Prestressed Concrete Continuous
050-15-00210 BEBL	18790	Seymour	Prestressed Concrete Continuous
105-35-05447 A	25280	Fort Wayne	Prestressed Concrete Continuous
152-45-02730	27661	La Porte	Prestressed Concrete Continuous
I69-317-09800	40441	Fort Wayne	Prestressed Concrete Continuous
I70-004-04612 BEBL	41070	Crawfordsville	Prestressed Concrete Continuous
I465-149-08854 JSBL	50795	Greenfield	Prestressed Concrete Continuous
I69-112-09708 SB	51350	Seymour	Prestressed Concrete Continuous
I69-106-09739 SB	51385	Seymour	Prestressed Concrete Continuous

I69-095-09674 SB	60622	Vincennes	Prestressed Concrete Continuous
(52)231-79-07531 AEBL	76430	Crawfordsville	Prestressed Concrete Continuous
I465-129-08708	76442	Greenfield	Prestressed Concrete Continuous
I465-128-09119 EBL	76636	Greenfield	Prestressed Concrete Continuous
024-02-09089 A	76840	Fort Wayne	Prestressed Concrete Continuous
031-71-08917	79844	La Porte	Prestressed Concrete Continuous
031-71-08916	79846	La Porte	Prestressed Concrete Continuous
I69-100-09683 SB	79944	Vincennes	Prestressed Concrete Continuous
I69-040-09473 NB	80150	Vincennes SS	Prestressed Concrete Continuous
(56)61-63-09488	80168	Vincennes SS	Prestressed Concrete Continuous
I69-050-09496	80180	Vincennes	Prestressed Concrete Continuous
I69-051-09504	80186	Vincennes SS	Prestressed Concrete Continuous
I69-065-09405 NB	80274	Vincennes SS	Prestressed Concrete Continuous
I69-066-09409 NB	80278	Vincennes SS	Prestressed Concrete Continuous
I69-074-09423 NB	80302	Vincennes SS	Prestressed Concrete Continuous
I69-079-09437 NB	80326	Vincennes SS	Prestressed Concrete Continuous
I69-087-09551 NB	80356	Vincennes SS	Prestressed Concrete Continuous
064-26-09191	80372	Vincennes SS	Prestressed Concrete Continuous
356-63-09491	80374	Vincennes SS	Prestressed Concrete Continuous
058-14-09425	80376	Vincennes SS	Prestressed Concrete Continuous
045-28-09679	80438	Vincennes	Prestressed Concrete Continuous
(265)I265-11-09604	80482	Seymour	Prestressed Concrete Continuous
031-34-09790 SBL	80602	Greenfield	Prestressed Concrete Continuous
038-89-04111 B	13000	Greenfield	Steel Continuous
052-24-06649	19430	Seymour	Steel Continuous
062-74-06621	22190	Vincennes	Steel Continuous
067-18-05459 D	24210	Greenfield	Steel Continuous
I64-05-05201 CEBL	33240	Vincennes	Steel Continuous
041-82-05415 CSBL	14280	Vincennes SS	Steel Continuous

062-82-02589 WBL	21985	Vincennes	Steel Continuous
062-13-07329	22240	Vincennes	Steel Continuous
I469-12-06947 AEB	32841	Fort Wayne	Steel Continuous
I64-07-02367 BEBL	33280	Vincennes	Steel Continuous
I69-309-04548 B	40300	Fort Wayne	Steel Continuous
037-55-03632 JASBL	12250	Seymour	Steel
057-26-03322 A	20530	Vincennes	Steel
154-77-01976 B	27720	Vincennes	Steel
(421)39-12-01792 B	32200	Crawfordsville	Steel
041-77-03864 JBNB	14840	Vincennes	Steel Continuous
I65-118-02313 JCSB	36890	Greenfield	Steel Continuous
I70-006-04712 BEBL	41130	Crawfordsville	Steel Continuous
I70-008-02344 BEBL	41230	Crawfordsville	Steel Continuous
I70-074-05231 A	42020	Greenfield	Steel Continuous
I94-29-04469 CEB	49120	La Porte	Steel Continuous
I465-127-05274 DEBL	50340	Greenfield	Steel Continuous
I69-050-09497 NB	80182	Vincennes	Steel Continuous
I69-057-09506	80226	Vincennes SS	Steel Continuous

[*] *Bridges have been replaced during the duration of the project. The notated NBI no longer exists within BIAS.*

APPENDIX C. PROCEDURE FOR SIMULATION OF GROUND MOTION AT BRIDGE SITES IN SAMPLE SET

Introduction

The implementation of a detailed seismic assessment (Level 2) requires quantifying the seismic hazard specific to each bridge in the sample set. This seismic hazard, specifically for Indiana, is primarily associated with the seismicity of the New Madrid Seismic Zone (NMSZ) and the Wabash Valley Seismic Zone (WVSZ)—two areas of seismicity in the central and eastern United States (CEUS) that can generate major intraplate earthquakes. The NMSZ, stretching from northeastern Arkansas to southern Illinois, is the most seismically active area in the CEUS. This zone is responsible for a sequence of powerful earthquakes with estimated moment magnitudes (M_w) of 7.0–8.0 which occurred during the winter of 1811 and 1812, causing strong ground shaking throughout the region (e.g., Johnston & Schweig, 1996). A repeat of such an earthquake today has the potential to cause severe damage to the built environment in the CEUS. On the other hand, the WVSZ is located along the southern border of Illinois and Indiana, where several small-to-moderate earthquakes have occurred since the 19th century (Herrmann et al., 2008). Previous research studies have also shown paleoliquefaction evidence, thus pointing to the occurrence of large prehistoric earthquakes ($M_w > 7.0$) in the WVSZ over the past few thousand years (e.g., Obermeier, 1998).

Potential large earthquakes from the NMSZ and the WVSZ pose a significant seismic risk to the bridge network in Indiana. However, the vulnerability assessment of the Indiana bridge network has been hindered by the lack of strong-motion recordings in the area. In addition, synthetic ground-motion time histories have not been generated for scenario earthquakes in Indiana. In this study, seismic hazard assessment is performed for Indiana using the U.S. National Seismic Hazard Maps generated by the U.S. Geological Survey (USGS). Deaggregation analysis is first conducted to identify the predominant seismic sources that contribute to the seismic hazard for the representative 100-bridge sample set. Synthetic ground motions compatible with the deaggregation results are then generated using stochastic and deterministic simulation techniques along with generic site amplification factors or site response analysis.

Selection of Representative Bridge Sites

The determination of seismic vulnerability for bridges in the state of Indiana requires seismic response analysis of representative bridges with respect to local ground motions. As few ground-motion records have been recorded in Indiana, it is necessary to generate synthetic ground motions compatible with the geotechnical conditions at the desired analysis sites. Therefore, representative sites along specified emergency routes are selected with respect to the level of seismic hazard, the amount of available geotechnical information, and geological and geographical diversity. A representative 100-bridge sample set is selected from the state bridge inventory with respect to the type of route, service under the bridge, construction material, and structure length. Among these 100 candidate bridges 50 correspond to the Vincennes District, which is expected to have the highest seismic hazard, while the other 50 correspond to the remaining five districts (with 10 bridges per district).

The selection of bridges in the Vincennes district is subject to additional constraints because of its higher seismic hazard. Candidate bridges in the Vincennes district are further filtered based on the availability of comprehensive geotechnical information. This information is required for performing site response analysis. Qualifying geotechnical reports contain:

- Boring data with a depth of at least 15 *m* (50 *ft*).
- Shear-wave velocity profile presented in a tabular format.
- A contract number that is assigned to a state bridge within the BIAS database.

Using these criteria, 24 bridges in the Vincennes District are selected. The other 76 bridges in the sample leverage generic amplification factors. The final 100 bridge sites selected for all districts are shown in Figure C.1, using a Google Earth map. Appendix B provides a summary of the selected bridges along with additional relevant information.

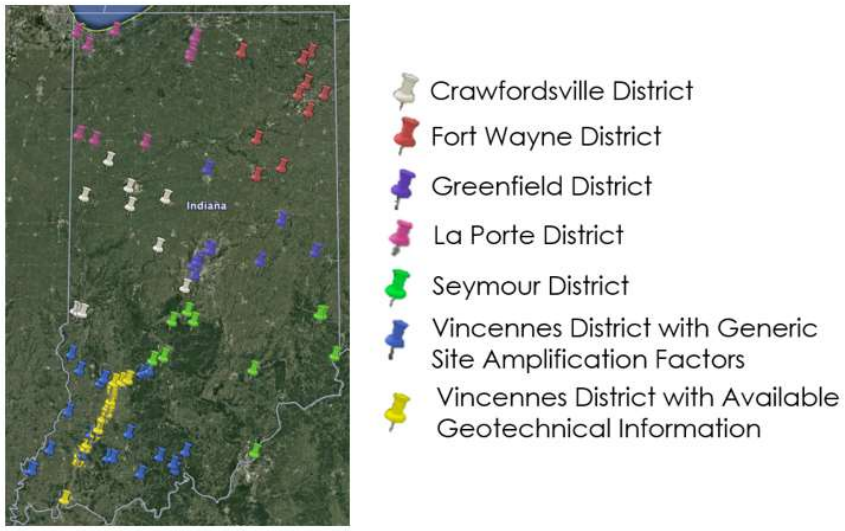

Figure C.1 Selected Candidate Bridges for the State of Indiana

A statistical analysis is conducted to verify that the 100-bridge sample set reflects all 5,891 state-owned bridges for certain superstructure configurations, which influences the dynamic analysis. These superstructure characteristics include max span length (*ft*), number of spans, total structure length (*ft*), structure type, out-to-out deck width (*ft*), and skew. These six characteristics are selected as they span the geometrical variations relevant for mass estimation and contribute to the stiffness of the system in some cases.

For the 22 categories of structure types across the three main construction materials (steel, concrete, and prestressed concrete), the majority of the structure types for each construction material are present in the sample, as shown in Figure C.2. The sample intentionally does not include culverts (structure type 19) as a buried structure does not have a surface independent of the ground movement. Note, RB is designated in the figures to signify the percent of "Remaining Bridges" that did not fall into the detailed bins. Across the sample, skew values between 0 to 43 degrees are well represented. Skew is found to have little impact on superstructure stiffness for bridges with a skew ranging from 0 to 30 degrees. Therefore, while the sample is representative, this characteristic has less impact on the dynamic analysis than other characteristics. To ensure that the dynamic variability induced by expansion joints and multi-span interactions is incorporated into the Level 1 and 2 analysis, the bridge sample includes bridges with multiple spans, ranging from single- to thirty-span bridges as shown in Figure C.3. This is particularly important in the transverse direction as the number of spans and piers is related to the number of degrees of freedom and dynamic modes for the system (specifically reinforced-concrete slab deck bridges). Lastly, the geometric variations in max span length, total structure length, and out-to-out deck width are representative. While these characteristics are well-represented, they are not shown graphically as they contribute to the total mass of the deck, given the density of concrete, in a straightforward manner. Overall, the selection is representative of the bridges in Indiana, which will provide a robust sample set for the development and validation of a Simplified Assessment

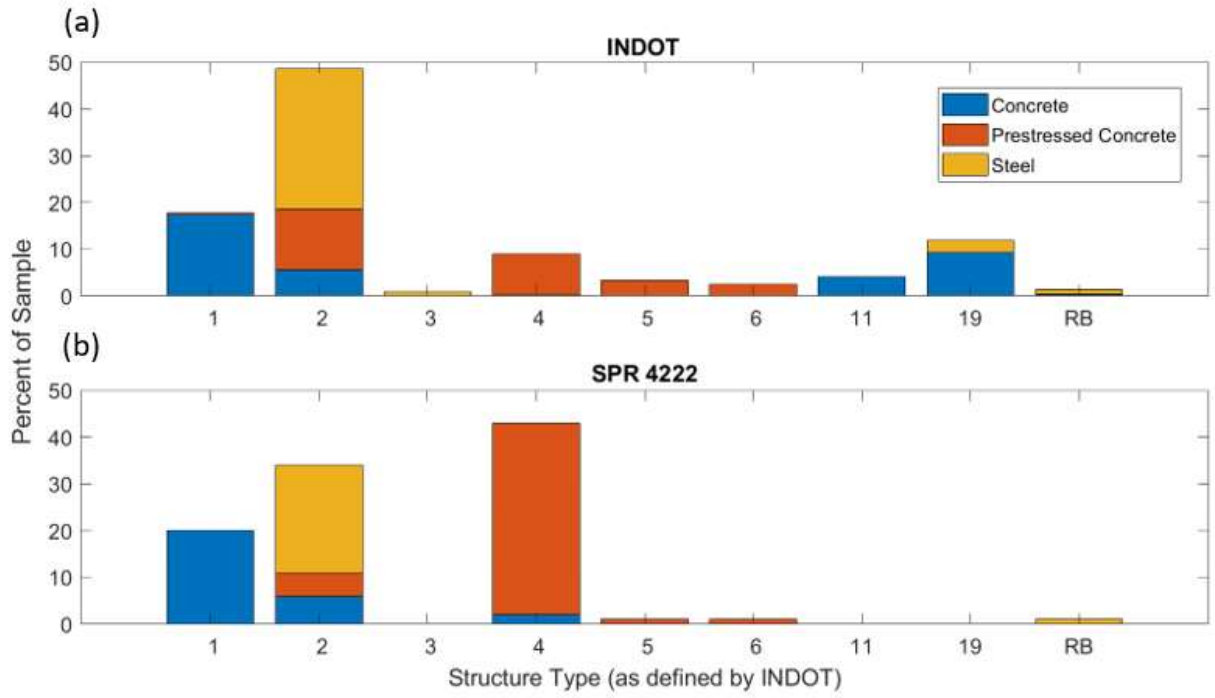

Figure C.2 Distribution of Structure Type in: (a) INDOT's Bridge Inventory (b) 100 Sample Bridges Selected for SPR-4222

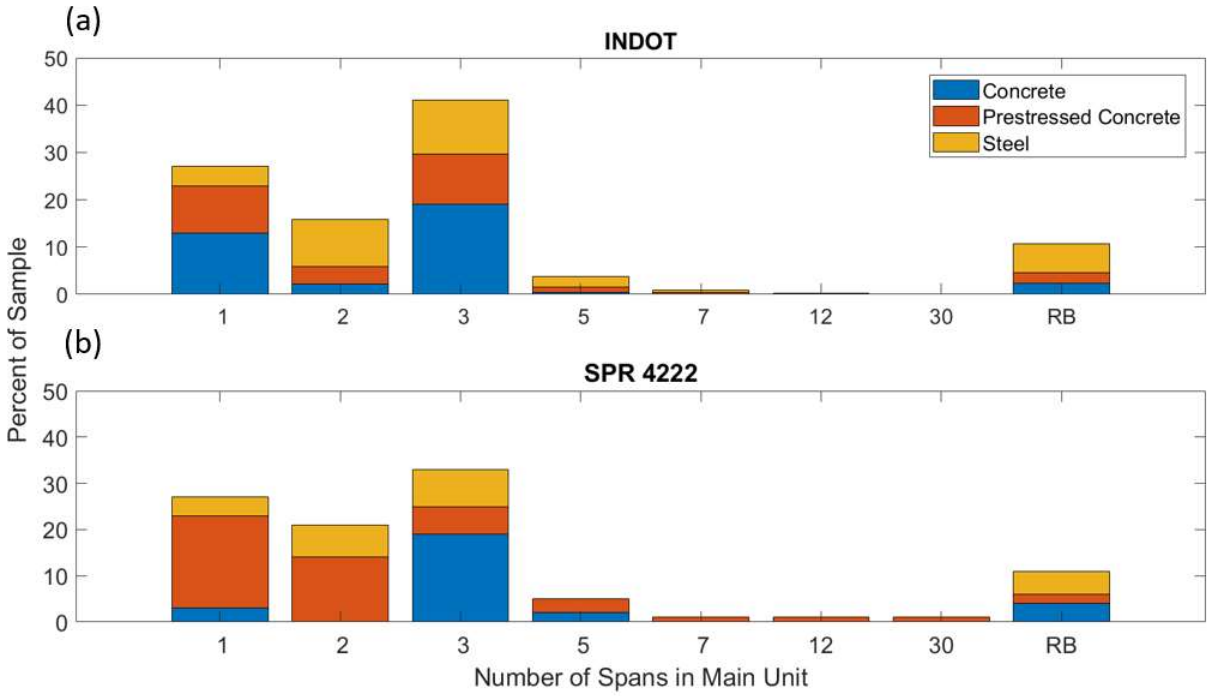

Figure C.3 Distribution of Number of Spans in: (a) INDOT's Bridge Inventory (b) 100 Sample Bridges Selected for SPR-4222

Seismic Hazard Assessment

U.S. National Seismic Hazard Maps

The U.S. National Seismic Hazard Maps generated by the USGS display the ground motions (i.e., peak ground acceleration and spectral acceleration at different structural periods) across the U.S. for various probability levels. These seismic hazard maps form the basis of seismic design provisions for buildings, bridges, highways, railways, and other structures. In the *AASHTO LRFD Bridge Design Specifications* (AASHTO, 2017), the seismic hazard at a bridge site is defined by the design response spectrum, which is constructed based on seismic hazard maps provided by the USGS.

The USGS generated the seismic hazard maps by performing a probabilistic seismic hazard analysis. The analysis accounts for all possible seismic sources, each assigned with a probability of occurrence. These seismic sources include the regional background seismicity and characteristic earthquakes from known faults. The ground motions expected at a site are calculated using a suite of attenuation models. The hazards from all seismic sources are then combined to generate the hazard curve, from which the ground motion intensity measures corresponding to a prescribed probability of exceedance are used to construct the seismic hazard maps. The latest U.S. National Seismic Hazard Maps were generated by the USGS in 2014. The seismic sources and attenuation models used to describe the hazard in the CEUS were documented in detail in Petersen et al. (2014). Figure C.4a shows the 2014 seismic hazard map of peak ground acceleration (PGA) with 2% probability of exceedance in 50 years (a return period of ~2,500 years), whereas Figure C.4b presents a zoom-in view of Indiana. Because of the close proximity to the NMSZ and the WVSZ, southwestern Indiana exhibits larger PGA values than other parts of the state (Figure C.4). Finally, the USGS has also generated seismic hazard maps for spectral acceleration at different structural periods (e.g., 0.2 and 1.0 s) and return periods (e.g., ~500 and ~1,000 years) (Petersen et al., 2014). All these maps show high seismic hazard in southwestern Indiana.

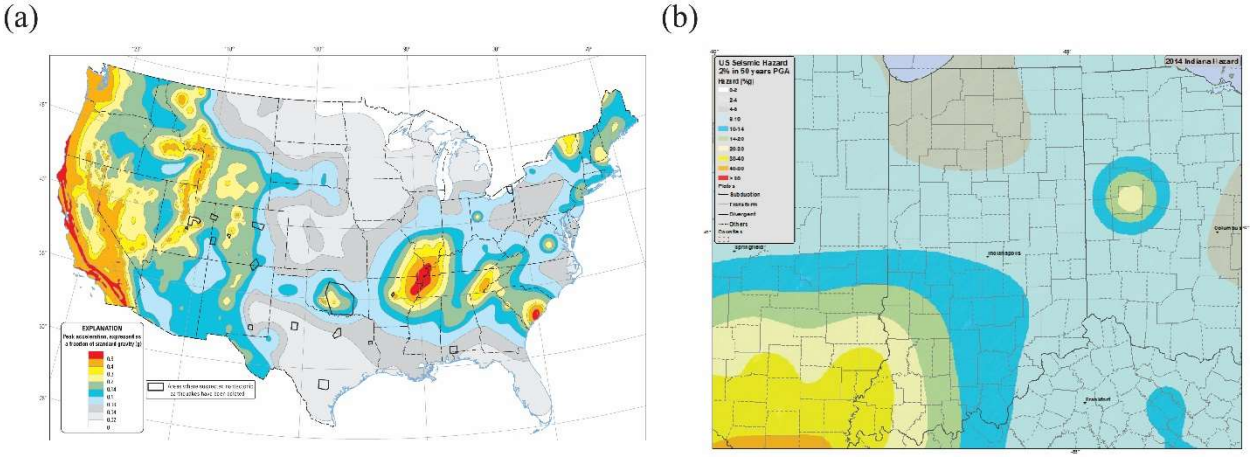

Figure C.4 (a) 2014 U.S. National Seismic Hazard Map (Petersen et al., 2014), Showing PGA with 2% Probability of Exceedance in 50 years, and (b) Zoom-in View of Indiana

Deaggregation of Seismic Hazard

Deaggregation of seismic hazard allows us to identify the predominant seismic sources (magnitude M_w and rupture distance R) that contribute to the hazard at a site. The deaggregation analysis is performed for 100 selected bridge sites and for spectral acceleration at five structural periods (0.1, 0.2, 0.3, 0.5, 1.0 *s*) using the nshmp-haz software (nshmp-haz, n.d.). The analysis is based on the 2014 version of U.S. National

Seismic Hazard Maps. Consistent with the current AASHTO design specifications (AASHTO, 2017), a return period of ~1,000 years (corresponding to 7% probability of exceedance in 75 years) is considered. As an example, Figure C.5 shows the deaggregation results (i.e., magnitude-distance bins and their contribution to seismic hazard) for a bridge site in the Vincennes District and spectral acceleration at 0.2 and 1.0 *s*. In Figure C.5 the magnitude ranges from 4.7 to 7.9 with an increment of 0.2, whereas the distance ranges from 10 to 490 *km* (6 to 304 *mi*) with an increment of 20 *km* (12 *mi*). From Figure C.5, three main types of seismic sources are identified: small nearby earthquakes associated with background seismicity (e.g., $4.7 \leq M_w \leq 5.7$, 10 *km* $\leq R \leq$ 50 *km* (6 *mi* $\leq R \leq$ 31 *mi*)), large nearby earthquakes from the WVSZ (e.g., $6.7 \leq M_w \leq 7.5$, 10 *km* $\leq R \leq$ 50 *km* (6 *mi* $\leq R \leq$ 31 *mi*)), and large distant earthquakes from the NMSZ (e.g., $6.7 \leq M_w \leq 7.9$, 200 *km* $\leq R \leq$ 350 *km* (124 *mi* $\leq R \leq$ 217 *mi*)). A comparison of Figures 5a and 5b indicates that small nearby earthquakes form the main contribution to the seismic hazard for spectral accelerations at 0.2 *s*, whereas large distant earthquakes are the predominant sources of hazard for spectral accelerations at 1.0 *s*.

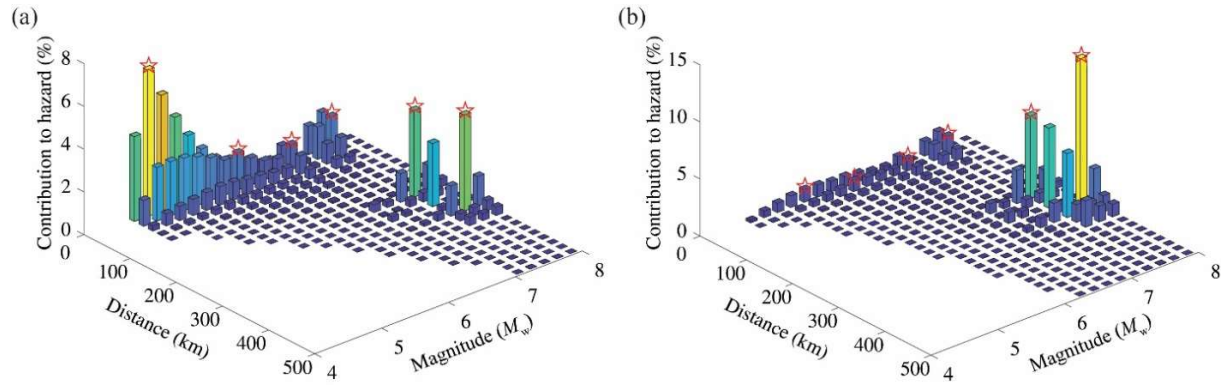

Figure C.5 Deaggregation Results for Bridge Site in the Vincennes District and Spectral Acceleration at (a) 0.2 s and (b) 1.0 s. Red Stars Indicate the Selected Scenario Events

Scenario events are selected based on the magnitude-distance bins and their contribution to seismic hazard obtained from deaggregation analysis. Table C.1 illustrates the selection of scenario events based on the deaggregation results shown in Figure C.5a. Six groups with distinct ranges of magnitude and distance are considered for clustering the magnitude-distance bins. The contribution to seismic hazard of each group is calculated by summing up the contribution of all magnitude-distance bins within the group. It is noted that the total contribution to seismic hazard of the six groups is 98.7%, indicating that almost all magnitude-distance bins that contribute to the hazard have been included in the analysis. A scenario event is selected for each group, which corresponds to the magnitude-distance bin within the group that has the largest contribution to seismic hazard (Table C.1, see also Figure C.5a). A total of 50 realizations are considered for all scenario events shown in Table C.1, and the number of realizations for each scenario event is proportional to the contribution to seismic hazard of the corresponding group. It is noted that a similar procedure is used to determine the scenario events and their number of realizations for each bridge site and structural period of interest.

Table C.1 Scenario Events Selected Based on Deaggregation Results Shown in Figure C.5a

Group No.	M_w and R (km) Ranges	Contribution	Scenario Event	Number of Realizations
1	$4.7 \leq M_w \leq 5.7$, $10 \leq R \leq 110$	43.8%	$M_w = 4.9$, $R = 10$ km	22
2	$5.9 \leq M_w \leq 6.5$, $10 \leq R \leq 110$	15.2%	$M_w = 6.1$, $R = 30$ km	8
3	$6.7 \leq M_w \leq 7.1$, $10 \leq R \leq 110$	7.1%	$M_w = 6.9$, $R = 30$ km	4
4	$7.3 \leq M_w \leq 7.9$, $10 \leq R \leq 110$	9.5%	$M_w = 7.5$, $R = 30$ km	5
5	$6.7 \leq M_w \leq 7.9$, $190 \leq R \leq 250$	12.6%	$M_w = 7.5$, $R = 210$ km	6
6	$6.7 \leq M_w \leq 7.9$, $270 \leq R \leq 350$	10.5%	$M_w = 7.7$, $R = 290$ km	5
Total		98.7%		50

Simulation of Ground Motion without Site Response Analysis

Simulation Procedure

For the 76 bridge sites where information on site conditions is not available, synthetic ground motions are generated for the selected scenario events using generic site amplification factors. Figure C.6 illustrates the procedure of simulating ground-motion time histories for distant (e.g., $R > 60$ *km* (37 *mi*)) and nearby (e.g., $R < 60$ *km* (37 *mi*)) scenario events, respectively. For distant scenario events, synthetic ground motions at the surface are generated using the stochastic simulation method and a point-source representation (Fig. 6a). For nearby scenario events, the point-source assumption is no longer valid, and an extended-source representation is adopted. Synthetic ground motions from nearby scenario events are generated using a hybrid deterministic-stochastic method (Fig. 6b). Namely, the high-frequency components of ground motion are generated using the stochastic simulation method and an extended-source model, whereas the low-frequency components of ground motion are generated using finite-fault simulations. The broadband synthetic ground motions at the surface are obtained by combining the high- and low-frequency components of ground motion. For both distant and nearby scenario events, frequency-dependent site amplification factors compatible with the National Earthquake Hazards Reduction Program (NEHRP) site classes are used in stochastic simulations to account for site effects. It is noted that a distance of 60 *km* (37 *mi*) is considered to distinguish distant and nearby scenario events, whereas all scenario events with $M_w < 5.0$ are regarded as distant ones.

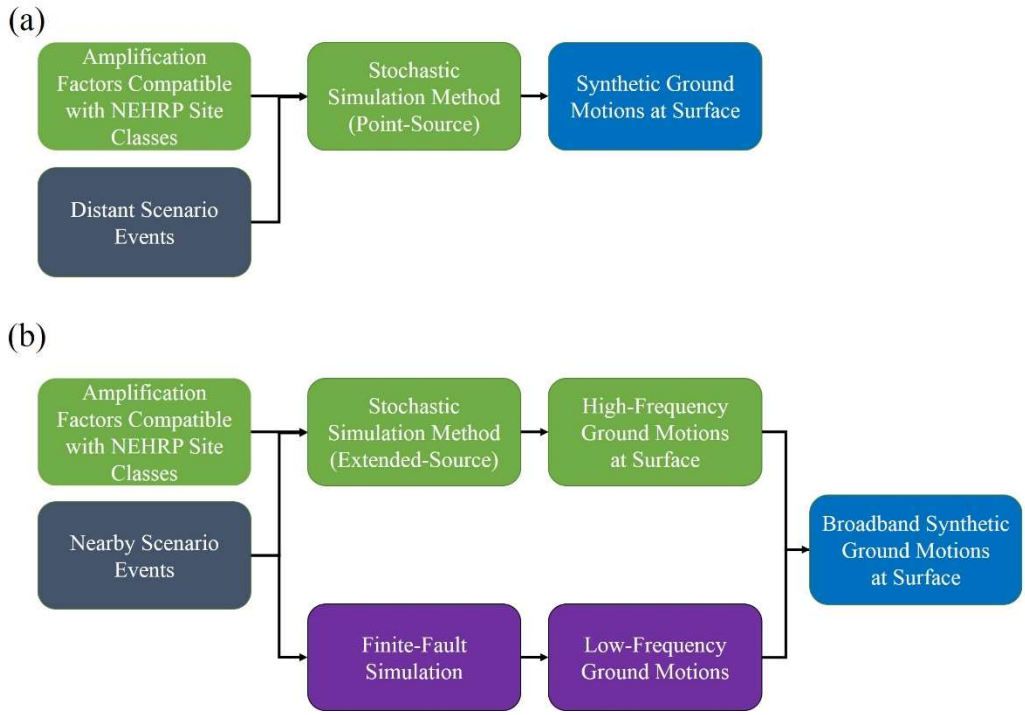

Figure C.6 Ground-Motion Simulation Procedure for Bridge Sites Without Information on Site Conditions and for (a) Distant and (b) Nearby Scenario Events

Stochastic Simulations

The specific barrier model (SBM) (Papageorgiou & Aki, 1983) is adopted for stochastic ground-motion simulations in the context of the stochastic modeling approach (Boore, 1983). The SBM is a physical model of the seismic source that applies both in the far-field (point-source) and near-fault (extended-source) regions, allowing for consistent ground-motion simulations over a wide frequency range and for all distances of engineering interest. The SBM has been calibrated to shallow crustal earthquakes of three different tectonic regions: interplate, intraplate, and extensional regimes (Halldorsson & Papageorgiou, 2005). In this study, model parameters of the SBM that were either selected or obtained in the calibration of the SBM to strong-motion data of intraplate earthquakes are used (see Table C.8 of Halldorsson & Papageorgiou, 2005).

The SBM has adopted the NEHRP site classes as indicators of site response based on the average shear-wave velocity in the uppermost 30 *m* (98 *ft*) (V_{S30}). This is accomplished by applying a frequency-dependent amplification factor (obtained from a generic shear-wave velocity profile) for each site class. It is noted that such amplification factors have been proposed in the literature for soil and rock sites in the western United States, but only a few are available for soil sites in the CEUS. Figure C.7a shows the generic shear-wave velocity profiles down to 35 *km* (22 *mi*) for NEHRP A (V_{S30} = 2,032 *m/s* (6,667 *ft/s*)), B (V_{S30} = 1,170 *m/s* (3,839 *ft/s*), C (V_{S30} = 560 *m/s* (1,837 *ft/s*)), and D (V_{S30} = 270 *m/s* (886 *ft/s*)) sites in the CEUS (W. Silva, personal communication, April 18, 2018). These velocity profiles were generated by placing shallow velocity profiles on top of a crustal model applicable to the CEUS. Figure C.7b shows the frequency-dependent amplification factors computed for the velocity profiles of Figure C.7a using the square-root-impedance method (Boore, 2013). In this study, generic site amplification factors presented in Figure C.7b for NEHRP A, B, C, and D sites and those proposed by Boore and Campbell (2017) for an NEHRP B/C site (V_{S30} = 760 *m/s* (2,493 *ft/s*)) are incorporated into the SBM to account for the site effects in the CEUS. The spectral decay parameter κ that describes the high-frequency diminution of acceleration spectra is

considered to be 0.006, 0.01, 0.02, 0.02, and 0.02 for NEHRP A, B, B/C, C, and D sites in the CEUS, respectively. These values are consistent with those reported in the literature (e.g., Atkinson & Boore, 2006; Boore & Campbell, 2016; Silva et al., 2000). Since no information on the site conditions for the 76 bridge sites is available, synthetic ground motions are generated for NEHRP A, B, B/C, C, and D site classes.

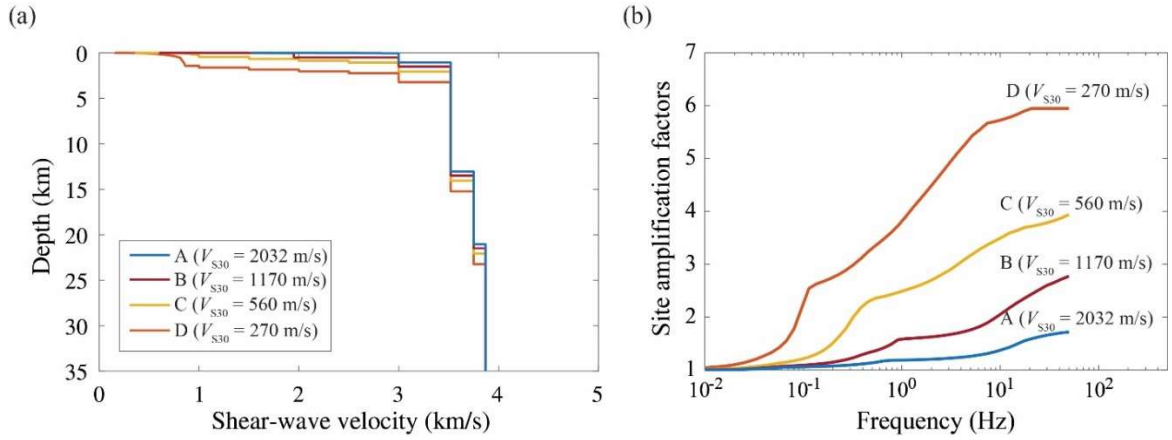

Figure C.7 (a) Generic Shear-Wave Velocity Profiles Down to 35 *km* for NEHRP A (V_{S30} = 2,032 *m/s* (6,667 *ft/s*)), B (V_{S30} = 1,170 *m/s* (3,839 *ft/s*), C (V_{S30} = 560 *m/s* (1,837 *ft/s*)), and D (V_{S30} = 270 *m/s* (886 *ft/s*)) Sites in the CEUS (W. Silva, personal communication, April 18, 2018). (b) Generic Site Amplification Factors Computed for the Shear-Wave Velocity Profiles Shown in (a)

Figure C.8 presents the synthetic acceleration time histories (obtained from a single realization of the stochastic simulations) for the selected scenario events shown in Table C.1. An NEHRP B/C site is considered in the simulations. It is noted that the low-frequency components of ground motion are not included in the time histories in Figure C.8, which shows that small nearby earthquakes associated with background seismicity (e.g., M_w = 4.9, R = 10 *km* (6 *mi*)) generate acceleration time histories of short duration. Large nearby earthquakes from the WVSZ (e.g., M_w = 7.5, R = 30 *km* (19 *mi*)) and large distant earthquakes from the NMSZ (e.g., M_w = 7.7, R = 290 *km* (180 *mi*)) produce acceleration time histories of long duration, whereas ground motions from distant earthquakes show significantly smaller amplitude than those from nearby earthquakes.

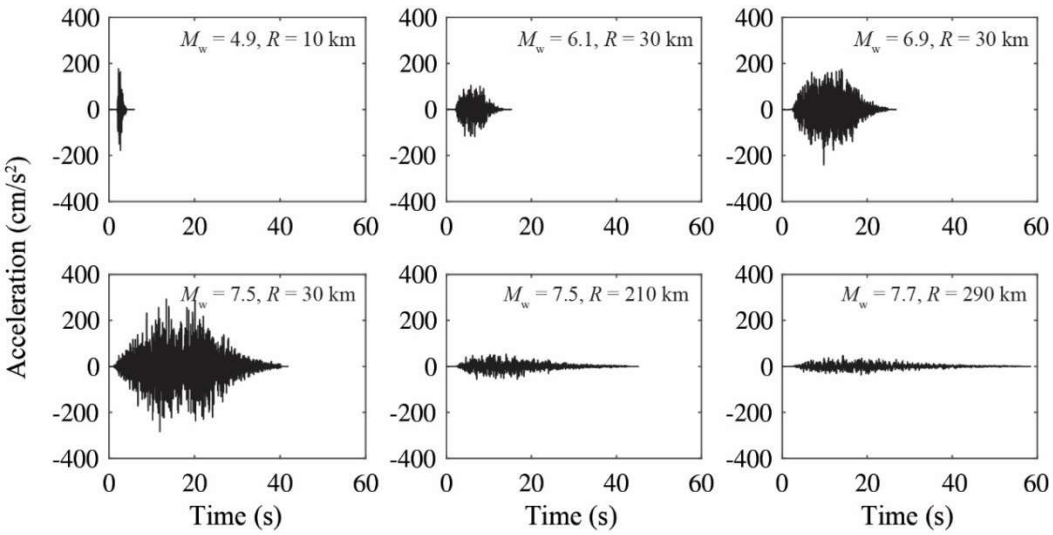

Figure C.8 Synthetic Acceleration Time Histories (Obtained from a Single Realization of the Stochastic Simulations) for the Selected Scenario Events shown in Table C.1. NEHRP B/C Site is Considered in the Simulation

Finite-Fault Simulations

For nearby scenario events, finite-fault simulations based on kinematic source models are performed to generate the low-frequency components of ground motion. Consistent with the focal mechanisms of past earthquakes in Indiana and neighboring states (Coppersmith et al., 2012), a vertical strike-slip fault and a reverse fault with a 50˚ dip angle are considered (Figure C.9). For each nearby scenario event, two-thirds of the realizations correspond to the strike-slip fault and one-third corresponds to the reverse fault (Coppersmith et al., 2012). The length (*L)* and width (*W)* of the causative fault, which depend on the fault type and earthquake magnitude, are calculated using the empirical equations proposed by Wells and Coppersmith (1994). The burial depth of the causative fault is 2 *km* (1.2 *mi*). The 1D crustal model proposed by Wang and Herrmann (1980) for the central United States is considered. A uniform slip amplitude is calculated based on the earthquake magnitude, the fault dimensions, and the rigidity of the elastic medium. The time dependence of slip at a given point on the fault is represented by a ramp function whose rise time is inferred from the slip amplitude and a slip velocity value of 1.0 *m/s* (3 *ft/s*). The hypocenter is located at 0.2*L* along strike and 0.6*W* down-dip (see Figure C.9). Finally, a circular rupture front propagating across the fault at a constant rupture velocity of 3.0 *km/s* (1.9 *mi/s*) (80% of local shear-wave velocity) is assumed. It is noted that the values of source parameters (e.g., rupture velocity, slip velocity, hypocenter location, burial depth) considered in this study are within the typical range of values obtained from kinematic source inversions of past earthquakes (e.g., Mai, et al., 2005; Somerville et al., 1999). The low-frequency components of ground motion are generated at three stations with rupture distances of 10, 30, and 50 *km* (6, 19, and 31 *mi*), respectively (Figure C.9). These distances are consistent with the magnitude-distance bins obtained from the deaggregation analysis. The computation of the low-frequency components of ground motion is performed using the discrete wavenumber representation method (Bouchon, 1979; Bouchon & Aki, 1977). The generalized transmission and reflection coefficient technique (Luco & Apsel, 1983) is utilized for the propagation of the seismic wavefield through the 1D crustal model. As an example, Figure C.10 presents the low-frequency acceleration, velocity, and displacement time histories simulated at stations S1, S2, and S3 for an M_w 7.5 strike-slip earthquake. The frequency range considered in the simulations is 0 *Hz* (static) to 1.0 *Hz*. It is observed from Figure C.10 that the low-frequency components of ground motion attenuate rapidly with distance from the fault.

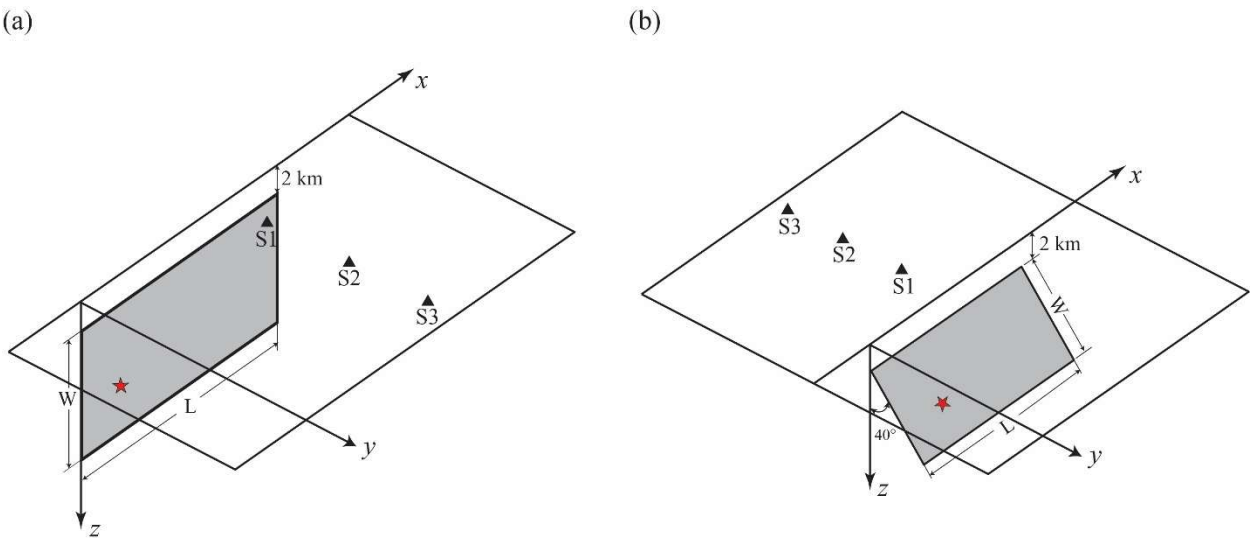

Figure C.9 Fault-Station Geometry for (a) Strike-Slip and (b) Reverse Earthquakes, showing the Rectangular Fault with a Uniform Slip Distribution (Gray Area), the Hypocenter Location (Star), and the Locations of 3 Stations (Triangles) with Rupture Distances of 10, 30, and 50 *km* (6, 19, and 31 *mi*), Respectively

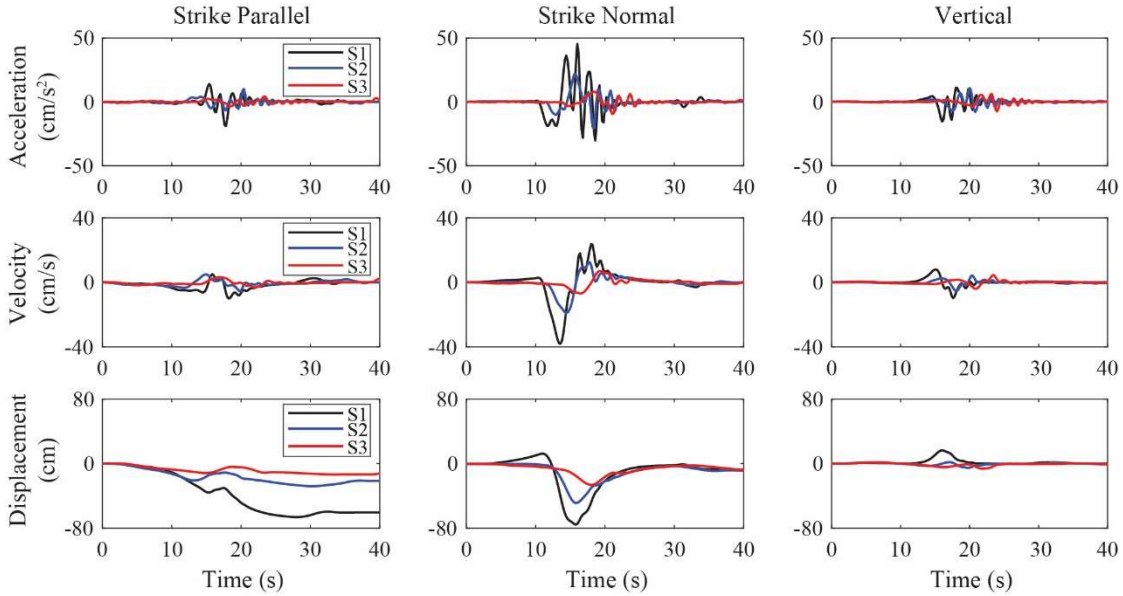

Figure C.10 Low-frequency Acceleration, Velocity, and Displacement Time Histories Simulated at Stations S1, S2, and S3 for an M_w 7.5 Strike-Slip Earthquake

Broadband Ground Motions

For nearby scenario events, the independently derived high- and low-frequency components of ground motion are combined using matched filtering at a crossover frequency of 1.0 *Hz* to generate broadband ground-motion time histories. As an example, Figure C.11 shows the broadband acceleration, velocity, and displacement time histories simulated for a scenario event with $M_w = 7.5$ and $R = 30$ *km* (19 *mi*). An NEHRP

B/C site is considered in the simulations, and a strike-slip fault is assumed to generate the low-frequency components of ground motion.

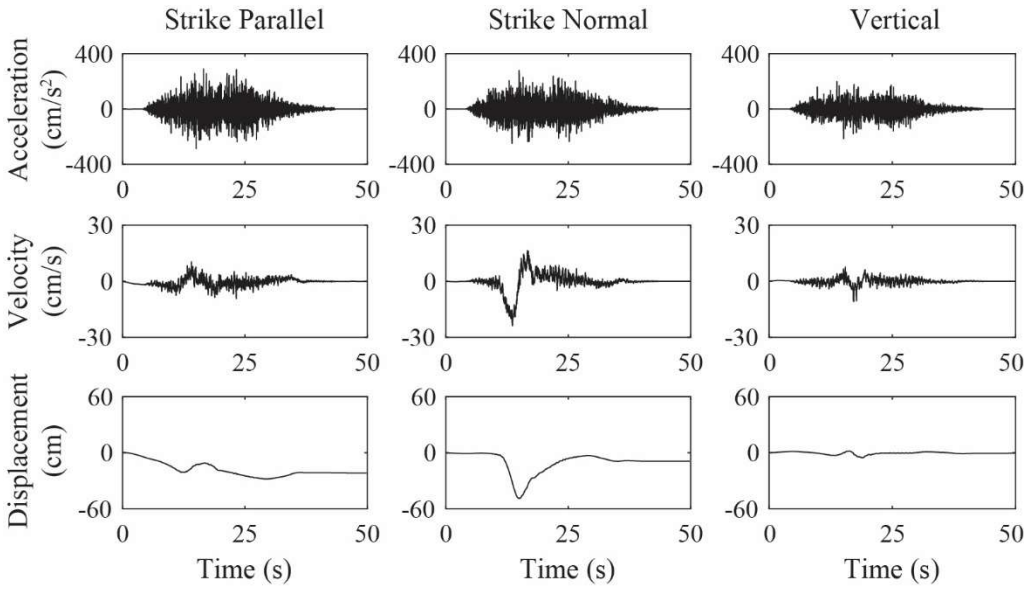

Figure C.11 Broadband Acceleration, Velocity, and Displacement Time Histories Simulated for a Scenario Event with M_w = 7.5, R = 30 *km* (19 *mi*). NEHRP B/C Site is Considered in the Simulation, and a Strike-Slip Fault is Assumed for Generating the Low-Frequency Components of Ground Motion

Simulation of Ground Motion with Site Response Analysis

Simulation Procedure

Figure C.12 shows the procedure of simulating ground-motion time histories with site response analysis for the 24 bridge sites in the Vincennes District with soil profiles that include complete information on shear-wave velocity, thickness, plasticity index, and density. The simulation procedure consists of three main steps. First, a soil profile is constructed based on the shear-wave velocity profile and boring log provided in the geotechnical engineering reports. Second, synthetic motions at the engineering bedrock level (i.e., shear-wave velocity of 400 to 800 *m/s* (1,312 to 2,625 *ft/s*)) are generated using approaches similar to those presented in the *Simulation of Ground Motion without Site Response Analysis section*. Specifically, a generic site amplification factor compatible with the shear-wave velocity at the engineering bedrock level is used in the stochastic simulations to account for the amplification of ground motions from the seismic source to the soil-bedrock interface. Third, a 1D equivalent-linear site response analysis is performed to generate synthetic ground motions at the surface.

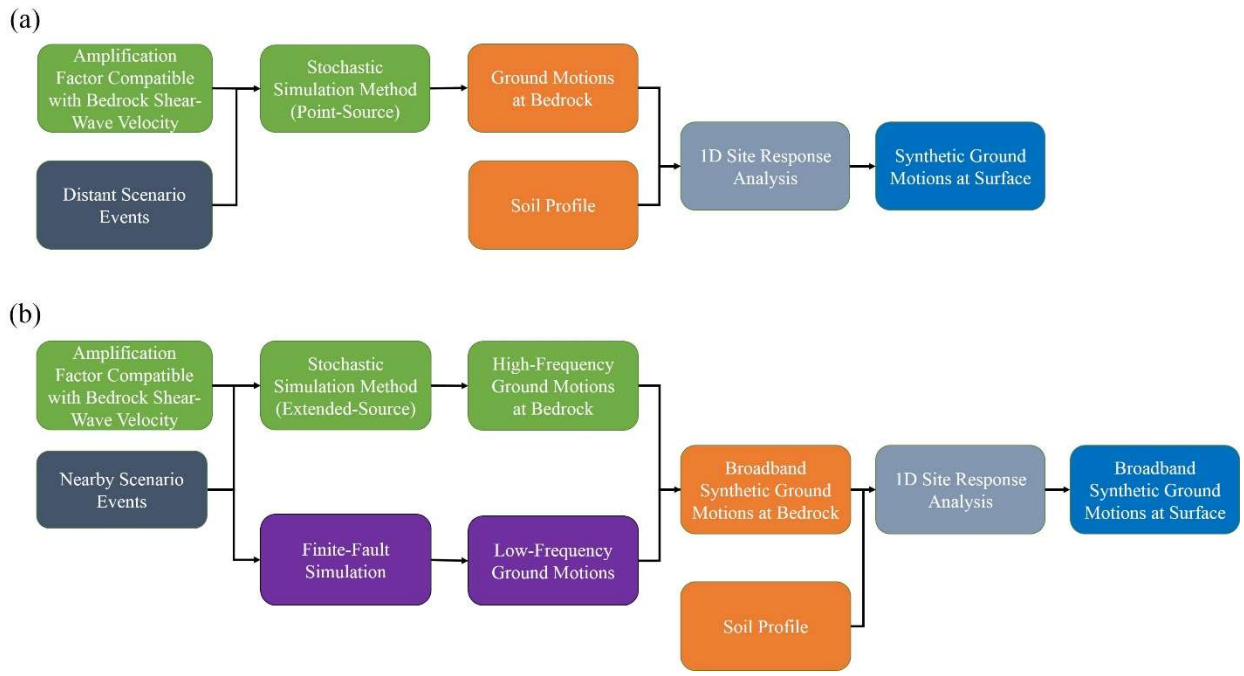

Figure C.12 Ground-Motion Simulation Procedure for Bridge Sites with Complete Information on Soil Profiles and for (a) Distant and (b) Nearby Scenario Events

Equivalent-Linear Site Response Analysis

A bridge site shown in Figure C.13a is selected herein as an example to demonstrate the simulation of ground motions at the surface with site response analysis. Table C.2 presents the boring log down to 31.4 *m* (103 *ft*) obtained from the geotechnical engineering report of the bridge site. The boring log indicates multiple soil layers classified as silty loam, silt, and sandy loam down to 26.9 *m* (88 *ft*), a depth where sandstone (a sedimentary rock) is reached. The geotechnical engineering report also provides the layered shear-wave velocity profile down to 33.3 *m* (109 *ft*) (Figure C.13b). It is observed from Figure C.13b that the shear-wave velocity significantly increases from 364.7 *m/s* (1,197 *ft/s*) to 628.3 *m/s* (2,061 *ft/s*) at a depth of 24.4 *m* (80 *ft*), indicating that soft rock is reached. Such velocity contrast is consistent with the findings from the boring log. Therefore, the depth to the engineering bedrock level for this bridge site is considered to be ~26.9 *m* (88 *ft*), and the shear-wave velocity at the engineering bedrock level is 628.3 *m/s* (2,061 *ft/s*) (corresponding to NEHRP Site Class C). Following the steps illustrated in Figure C.12, synthetic ground motions are first generated at a depth of 26.9 *m* (88 *ft*) using a generic site amplification factor compatible with NEHRP Site Class C (see Figure C.7). These motions are then used as input motions at the soil-bedrock interface for the site response analysis.

An equivalent-linear site response analysis is performed by propagating the input motions through the upper 26.9 *m* (88 *ft*) of the soil profile, for which the layered shear-wave velocity profile is shown in Figure C.13b. The density of each layer is estimated from the shear-wave velocity using the empirical equations proposed by Boore (2016). The variations of the normalized shear modulus and damping ratio with cyclic shear strain are obtained for each layer using the generic curves proposed by Vucetic and Dobry (1991) along with the plasticity index provided in the geotechnical engineering report. The equivalent-linear site response analysis is performed in the frequency domain using the computer program DEEPSOIL (Hashash et al., 2016) to generate the ground motions at the surface.

(a) (b)

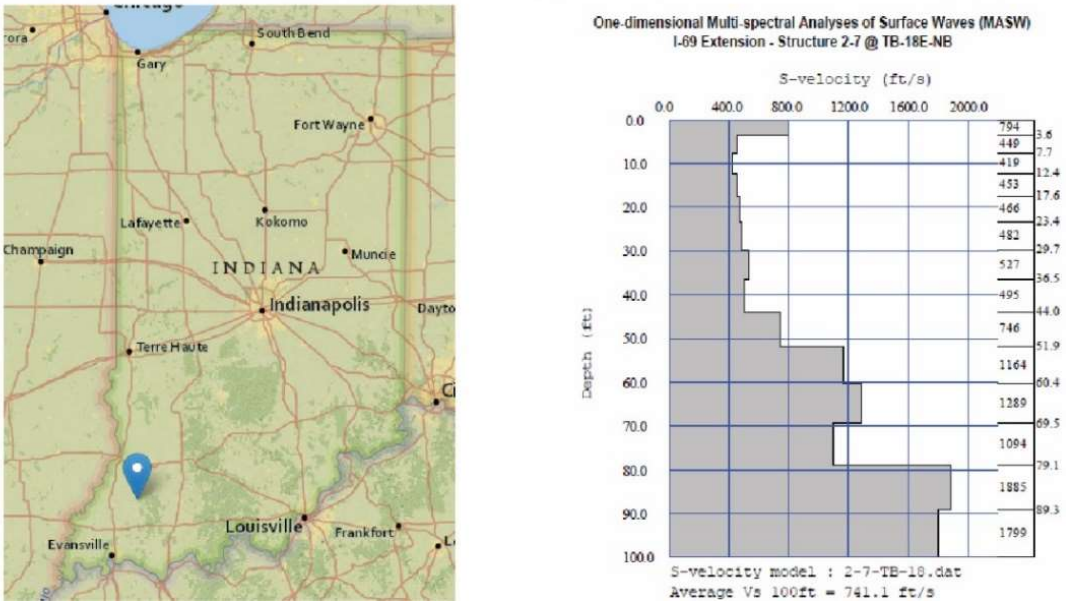

Figure C.13 (a) Location of a Bridge Site in the Vincennes District with a Complete Soil Profile, and (b) Shear-Wave Velocity Profile at the Bridge Site Obtained from the Geotechnical Engineering Report

Table C.2 Boring Log for the Bridge Site shown in Figure C.13a

Boring No.	Soil/Material Description	Soil Lab No.	Top Depth (ft)	Bottom Depth (ft)
2-7-TB-18E-NB	Topsoil	Visual	0.00	0.50
2-7-TB-18E-NB	Silty Loam A-6	ATC101	0.50	23.00
2-7-TB-18E-NB	Silty Loam A-6	ATC109	23.00	53.00
2-7-TB-18E-NB	Silt A-4	ATC104	53.00	54.50
2-7-TB-18E-NB	Sandy Loam A-2-4	ATC111	54.50	63.00
2-7-TB-18E-NB	Silt A-4	ATC104	63.00	68.00
2-7-TB-18E-NB	Sandy Loam A-2-4	ATC111	68.00	73.00
2-7-TB-18E-NB	Silty Loam A-6	ATC109	73.00	78.00
2-7-TB-18E-NB	Sandy Loam A-2-4	ATC111	78.00	88.30
2-7-TB-18E-NB	Sandstone	Visual	88.30	89.30
2-7-TB-18E-NB	Siltstone	Visual	89.30	103.00

Comparison with Simulation Results using Generic Site Amplification Factors

For comparison purposes, synthetic ground motions at the surface are also generated for the 24 bridge sites using generic site amplification factors (without performing site response analysis). Namely, the simulation procedure presented in Figure C.6 is adopted to simulate ground motions, while a generic site amplification factor compatible with the V_{S30} determined from the shear-wave velocity profile is used. For the bridge site shown in Figure C.13a, the V_{S30} inferred from Figure C.13b is 224.8 *m/s* (738 *ft/s*) (NEHRP Site Class D). Figure C.14 compares spectral accelerations at 0.2, 0.5, and 1.0 *s* for ground motions simulated with site response analysis (i.e., following the procedure of Figure C.12) with those simulated using a generic site amplification factor (i.e., following the procedure in Figure C.6). It is noted that the 50 realizations differ for the three structural periods because of their distinct deaggregation results. Figure C.14 indicates that the

seismic demands computed for ground motions simulated using a generic site amplification factor can be similar, larger, or smaller than those computed for ground motions simulated with site response analysis, depending on the structural period and scenario event. It should be pointed out that generic site amplification factors take into account site effects in an "average" sense and do not capture the site-to-site variability. For sites with a complete soil profile, the site response analysis accounts for site-specific characteristics more accurately than the generic site amplification factor. However, these two methods have their own limitations. Generic site amplification factors are obtained from generic soil profiles assuming linear response (without taking into account nonlinear soil behavior) and may overestimate amplification in the high-frequency range when the effect of soil nonlinearity is significant. On the other hand, the equivalent-linear site response analysis has been reported to under-predict the high-frequency content for soft soil sites subjected to high-intensity ground motions (e.g., Bolisetti et al., 2014; Griffiths et al., 2016).

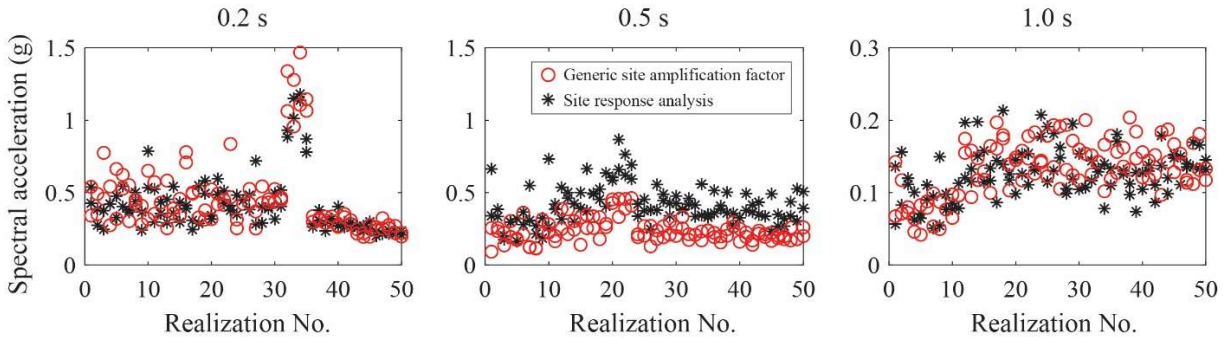

Figure C.14 Comparison of Spectral Accelerations at 0.2, 0.5, and 1.0 *s* for Ground Motions Simulated with Site Response Analysis and Using a Generic Site Amplification Factor

Summary and Recommendations

In this study, seismic hazard assessment was conducted for the state of Indiana based on the U.S. National Seismic Hazard Maps. Deaggregation of seismic hazard was performed for 100 selected bridge sites to obtain the magnitude-distance bins and their contribution to seismic hazard, from which the scenario events were selected. Synthetic ground motions compatible with the deaggregation results were then generated using stochastic and deterministic simulation techniques along with generic site amplification factors or equivalent-linear site response analysis.

For bridge sites without complete soil profiles (26 sites in the Vincennes District and 50 sites in other districts), synthetic ground motions were generated for five structural periods (0.1, 0.2, 0.3, 0.5, and 1.0 *s*) and five site conditions (NHERP A, B, B/C, C, and D) using generic site amplification factors. For bridge sites with complete soil profiles (24 sites in the Vincennes District), synthetic ground motions were generated for five structural periods (0.1, 0.2, 0.3, 0.5, and 1.0 *s*) by performing equivalent-linear site response analyses. For these 24 bridge sites, synthetic ground motions were also generated using generic site amplification factors compatible with the NEHRP site class determined from soil profiles.

To conduct a more comprehensive assessment of the seismic vulnerability of the Indiana bridge network, it is recommended to collect adequate geotechnical information in areas of high seismic hazard. Based on the available boring data and shear-wave velocity profiles seen to date, rocks at around 15 *m* (50 *ft*) are relatively soft with shear-wave velocities in the range of 400–800 *m/s* (1,312–2,625 *ft/s*) (engineering bedrock). It is recommended that borings and shear-wave velocity profiles be extended to greater depths in order to reach harder rocks (i.e., those with shear-wave velocity preferably greater than 1,000 *m/s* (3,281 *ft/s*)) when 1D site response analysis using site specific characteristics is desired by INDOT.

APPENDIX D. DEVELOPMENT OF LEVEL 2 PROCEDURE AND DETERMINATION OF CAPACITY THRESHOLDS FOR IDENTIFICATION OF VULNERABILITY LEVELS IN INSAT

Introduction

The successful implementation of the Simplified Assessment requires the development of a detailed assessment procedure (Level 2) for validation. To perform this validation, we develop a detailed finite-element model for the 100-bridge sample set selected in Appendix B to identify trends in demand, capacity, and vulnerable bridge details. The Level 2 assessment utilizes structural drawings, material properties, and engineering judgement. The results of the Level 2 assessment will be leveraged to identify vulnerable structural details present throughout INDOT's bridge network. These vulnerable details will serve as a basis for the identification of retrofits (see Appendix E) that can improve the seismic performance of INDOT's bridge network.

Level 2 Assessment Procedure

The procedure for the Level 2 assessment, shown in Figure D.1, is intended to perform a detailed assessment to determine bridge vulnerability. Performing a detailed assessment is essential for validating the Simplified Assessment and for identifying trends to help determine the capacity thresholds for the Level 1 assessment. Furthermore, this analysis identifies those structures that either require no analysis (Level 0) or require a Level 2 because they are not within the scope of the Simplified Assessment. These criteria are implemented in the Level 1 assessment and associated tool named INSAT. The Level 2 assessment shown in Figure D.1 is composed of capacity (purple) and demand (green) steps that will be used to establish the vulnerability (blue) of the bridge.

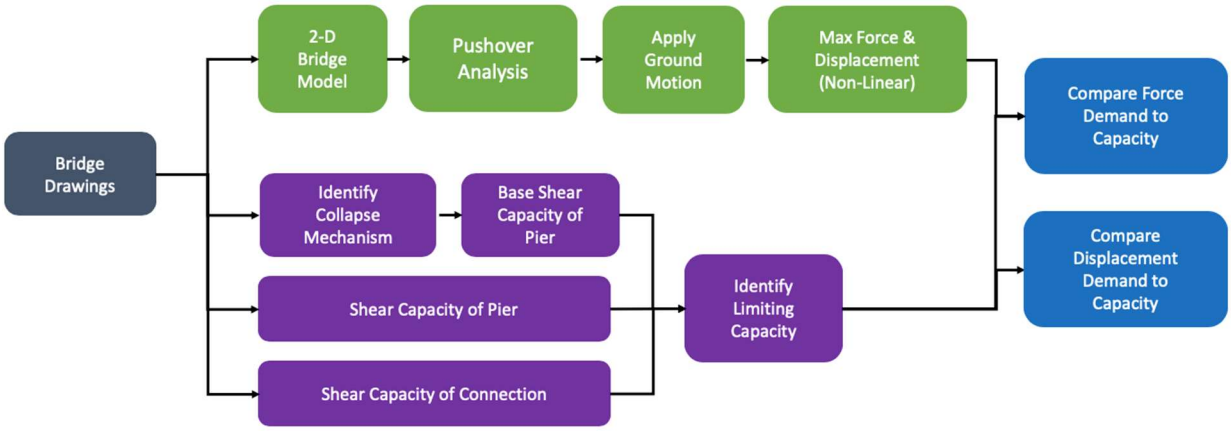

Figure D.1 Detailed Level 2 Assessment Procedure

The Level 2 assessment requires the support of a structural engineer to interpret the structural drawings, develop a mechanical model, identify potential vulnerabilities, and determine relevant capacity measures. First, we describe the Level 2 assessment procedure and assumptions. Then the subsequent case studies provide detailed sample calculations for the four substructure categories: walls, hammerhead walls, frame

bents, and other. These sample calculations span all three superstructure types identified (reinforced concrete, prestressed concrete, and steel).

Bridge Information

Bridge Drawings

The first step in the Level 2 assessment is to identify all relevant information that will impact the dynamic model of the bridge using all available bridge drawings, including rehabilitation plans. This information includes superstructure and substructure geometry as well as abutment details.

Capacity

Identify Mechanism of Hinge Formation

Each substructure's mechanism of hinge formation depends on the structure's ability to resist moment(s) at fixed end(s). To conduct a pushover analysis, based on the flexural mechanism of hinge formation, and estimate the bridge displacement when one or more piers enters the nonlinear region, the moment-curvature relationship for cracking, yielding, and ultimate must be calculated. On the other hand, the ability of the structure to achieve the flexure mechanism depends on the structure having enough shear capacity, avoiding anchorage failure, and other potential modes of failure that are described in the following sections and illustrated in the examples in this deliverable. The capability of the substructure to exhibit this mode of failure is based on the aspect ratio. The aspect ratio is defined as the cross-sectional height to depth ratio in the plane of bending. This ratio, hereafter referred to as λ_R, primarily applies to wall-type substructures in the transverse direction. For a substructure with λ_R less than 2.5, the response is a combination of flexure and shear as shown in Figure D.2 (Fares, 2018). This research and guidance from AASHTO (2017) show that a RC substructure with λ_R less than 2.5 cannot exhibit a response dominated by flexure and form a plastic hinge.

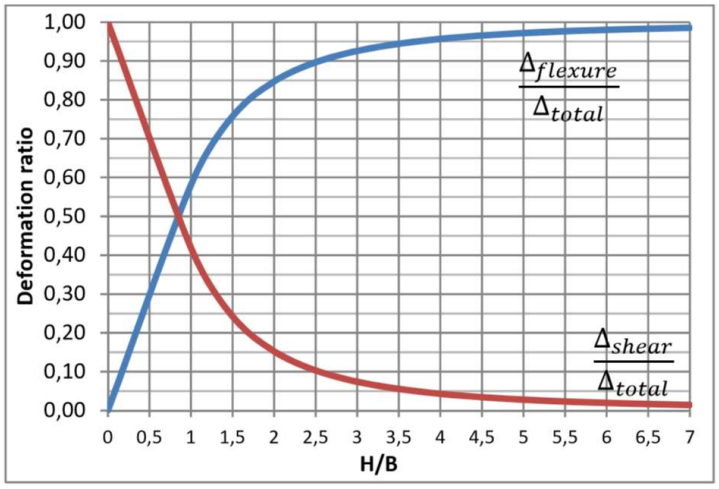

Figure D.2 Shear & Bending Stiffness Based on Aspect Ratio (Fares, 2018)

The moment associated with cracking is calculated using the gross moment of inertia and a centroid assumed to be half of the section depth. The following equation for cracking moment (M_{cr}) and the corresponding curvature is used:

$$M_{cr} = 7.5\sqrt{f'_c} * \frac{2I_g}{H} \tag{1}$$

$$\varphi_{cr} = \frac{M_{cr}}{I_g * E_c}. \tag{2}$$

The yielding moment (M_y) is calculated assuming that the strain in the layer of tension steel closest to the member end first yields. The solution for M_y is obtained when force equilibrium of the cross-section is met for this strain condition. The yield strain of the extreme fiber and resulting curvature can be calculated as:

$$\varepsilon_y = \frac{f_y}{E_s} \tag{3}$$

$$\varphi_y = \frac{\varepsilon_c}{c_{N.A.}}. \tag{4}$$

The moment associated with ultimate curvature (M_u), or the point when the substructure fully develops the mechanism of hinge formation, is calculated assuming strain hardening of outer steel layer in tension ($\varepsilon_s = .01$) or a compressive concrete strain (ε_c) of .003 has occurred—whichever occurs first. The solution for the ultimate moment is achieved by determining a neutral axis that leads to force equilibrium. The resulting curvature can be calculated using the same equation for yielding, but with a $c_{N.A.}$, depth of the neutral axis (N.A.) value, that reflects equilibrium of the ultimate moment section.

Base Shear

Using the identified mechanism of hinge formation and information from the moment capacity of the substructure, the base shear (*kips*) in each pier is calculated. Additional design considerations like rotational capacity are also considered.

Shear Capacity of the Pier

The shear capacity of each substructure type is calculated in accordance with guidance outlined by AASHTO (2017). For structures where shear reinforcement is not present on the structural drawings (e.g., older walls, specifically in the bridge longitudinal direction), the shear capacity of the substructure is derived solely from the strength provided by the concrete.

Horizontal Shear Capacity of the Connection

The Level 2 assessment assumes continuity between the superstructure and substructure displacement. This leads to a well-defined relationship for the restoring force drawn to each pier. The restoring force is the amount of force carried by each pier. This assumption is valid if and only if the horizontal shear connection between the superstructure and substructure holds. The shear capacity of the connection is calculated using accepted friction coefficients and common values for direct shear (both concrete and steel).

Identify Limiting Capacity

The limiting capacity (base shear, shear capacity of the substructure, or horizontal shear capacity of the connection) is identified to determine the corresponding vulnerability criterion. A limit mechanism based on the formation of plastic hinges is the desired mechanism of failure as this mode is rather ductile and the total collapse of the structure is dictated by a limiting rotation of the substructure. This assumes the gravity load capacity can be maintained considering P-delta effects and that the substructure still provides enough bearing seat length. However, in bridges where the shear capacity of the substructure or the horizontal shear strength of the connection between the superstructure and substructure exceeds the calculated base shear, the substructure is unable to form plastic hinges which can result in brittle failure.

Demand

2-D Bridge Model

To calculate the lateral flexure and shear demand on a bridge, the dynamic properties of the structure must be determined. The traditional approach in the design of reinforced and prestressed concrete structures has been to design each of the two orthogonal directions independently. Thus, a 2-D finite element modeling procedure is adopted to determine the fundamental dynamic characteristics of each bridge to form the equations-of-motion for both the transverse and longitudinal directions (Garcia, 1998; Metzger, 2004). The transverse and longitudinal directions are defined as shown in Figure D.3.

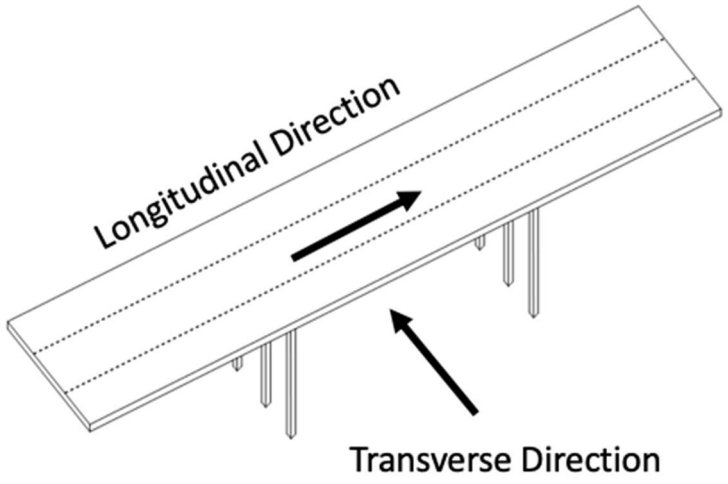

Figure D.3 Bridge Directions

Transverse Stiffness

The lateral stiffness of prestressed concrete or steel girder bridges depends primarily on the substructure. Specifically, it depends on the single piers, column bents, or walls with connections capable of transferring force from the superstructure to the substructure. Information is required to calculate the stiffness of each

pier, including, but not limited to, the unsupported height, cross-section dimensions, material properties, and the degree of fixity both at the base of the substructure and between the substructure and superstructure.

The lateral stiffness of reinforced-concrete superstructures with the deck rigidly connected to the substructure, depends primarily on the deck because it adds stiffness. The bridge deck is modeled as a deep girder where the depth of the girder corresponds to the deck width and the breadth of the girder corresponds to the deck thickness. To model the deck, rotation and translation are allowed at the intermediate bents, and only rotation is allowed at the abutments, as shown in Figure D.4. The deck is assumed to be simply-supported at the abutments. Overall, the structure behaves as a multi-degree-of-freedom (MDOF) system.

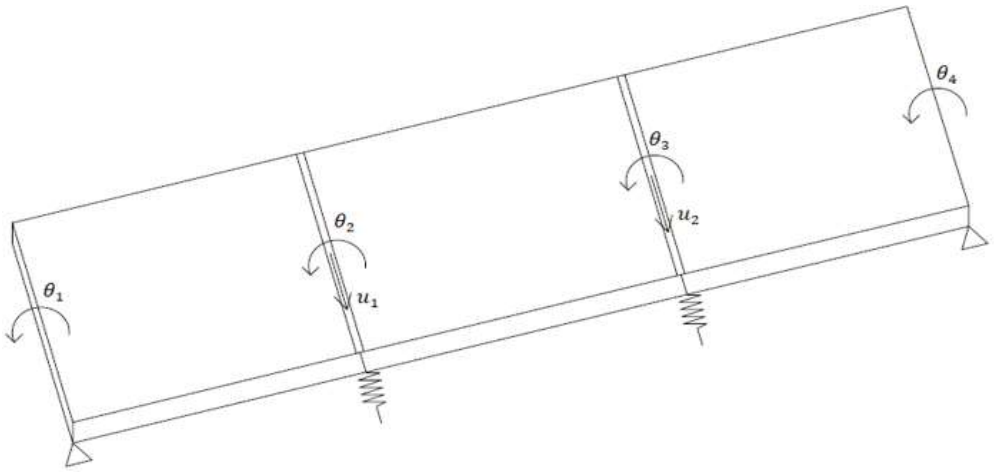

Figure D.4 Plan View of 3-Span Bridge Deck Showing Degrees-of-Freedom

For prestressed concrete and steel superstructures, the deep beam action described above is not as significant and it can be neglected. However, the deck is assumed to be sufficiently rigid such that the intermediate piers act as springs in parallel, but not so rigid as to inhibit the inertial effects of the mass. For these superstructure types, the bridge is modeled as a single-degree-of-freedom (SDOF) system with a singular displacement to represent the motion of the continuous sections of the bridge in each direction.

Longitudinal Stiffness

In the longitudinal direction, all types of bridge superstructures are modeled as a SDOF system with the intermediate piers acting as springs in parallel, as shown in Figure D.5. At each pier, the base of the substructure is assumed to be fixed while the top of the substructure has a degree of fixity related to the superstructure type. The connection between the substructure and superstructure is taken as fixed, semi-fixed, or free for reinforced-concrete, prestressed concrete, and steel, respectively. The bridge stiffness is then modeled as the summation of the individual pier stiffnesses.

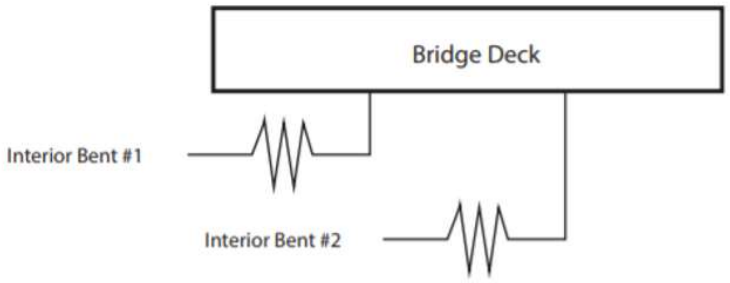

Figure D.5 SDOF Model of 3-Span Bridge in the Longitudinal Direction

Transverse Mass

The mass of the bridge is calculated using the superstructure geometry, barrier dimensions, concrete diaphragms, and the material properties of concrete and steel. In the transverse direction, the activated mass is determined using the tributary mass supported by each pier (lumped mass model).

Longitudinal Mass

The mass of the bridge is calculated using the superstructure geometry, barrier dimensions, concrete diaphragms, and the material properties of concrete and steel. The entire mass of the bridge superstructure is used in the longitudinal direction.

Equation-of-Motion

With the mass and stiffness known, vicious damping matrix can be computed. Damping, while difficult to predict, is inherent to all structural systems. Here we assume a viscous damping ratio (ζ_{pier}) for this analysis of 5%. The damping is computed using

$$c_{sub} = 2\zeta_{pier}\sqrt{K_{sub}m_{sup}}. \tag{5}$$

Now, the equations-of-motions of the bridge (for a SDOF) subjected to a ground motion input, $\ddot{x}_g$, can be written, for each direction, as

$$m_{sup}\ddot{x}_s + c_{sub}\dot{x}_s + K_{sub}x_s = -m_{sup}\ddot{x}_g. \tag{6}$$

As is necessary for reinforced-concrete superstructures in the transverse direction, Equation (6) can easily be vectorized to account for a MDOF system.

Nonlinear Pushover Analysis

A non-linear pushover analysis is conducted herein for bridges that have multiple piers of different heights and stiffnesses. This is necessary because individual piers may exhibit non-simultaneous nonlinear response. The pushover analysis allows us to understand and quantify the expected redistribution of lateral forces between the piers due to structural softening which occurs when a given pier enters the nonlinear region.

To perform a nonlinear pushover analysis, we incrementally apply a displacement to the structure. At each increment, the force drawn to the pier is controlled by the assumption that the deck and piers will equally displace. Using the moment-area theorem, Equation (10), the force that would result due to the displacement is calculated. The percent of the total force drawn to each pier (force ratio) is then computed. This pushover analysis is conducted for a displacement ranging from the first yield of the stiffest pier through the formation of plastic hinges in all piers. This analysis requires adequate ductility such that the pier can form the identified mechanism of hinge formation. Thus, it is not conducted for bridges with a substructure that is expected to form a brittle mechanism of failure.

SAP2000 is used to verify the pushover analysis procedure. In SAP2000, a finite element model of a 2-span, continuous steel girder bridge with circular reinforced-concrete frame bents (NBI 33280) is developed to verify the pushover analysis results. Using the assumptions as applied in generating the MATLAB model, and appropriately defining the moment-curvature relationship within SAP2000, a displacement-controlled non-linear pushover analysis is repeated using SAP2000. The results of the SAP2000 model are then used to verify the MATLAB results. Figure D.6 shows a comparison of the SAP2000 results and MATLAB results. The comparison shows that the results are quite similar.

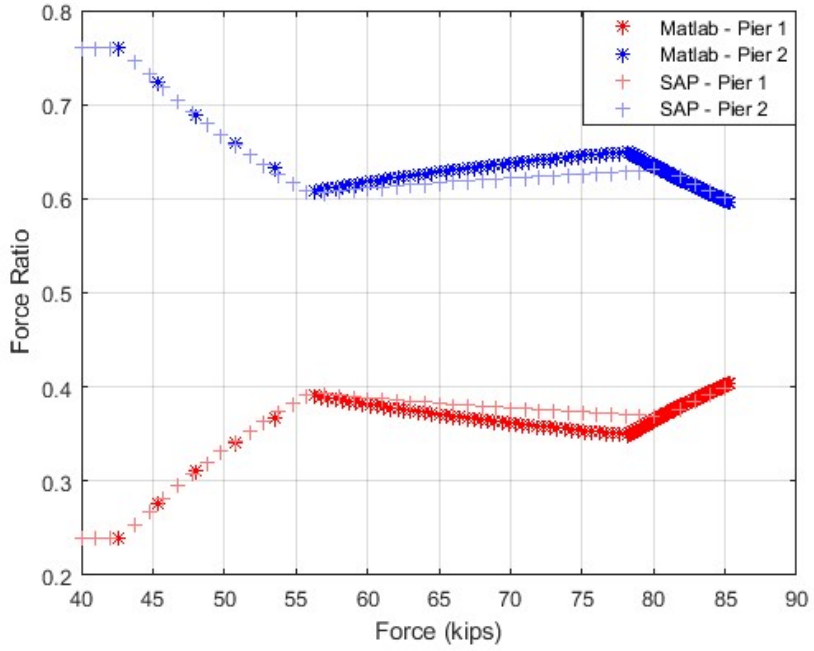

Figure D.6 Pushover Analysis Comparison

Apply Ground Motion

The Level 2 assessment utilizes the time histories developed using the approaches outlined in Appendix B along with a time-domain analysis using a 4th order Runge-Kutta integration scheme to determine the displacement-response of the structure.

Maximum Force & Displacement

The displacement of each pier is calculated using the moment-area theorem and equations shown in Figure D.7.

$$\Delta_p = \int_0^{L_y} \left(\varphi(x) - \varphi_y(x)\right) * \left(\frac{H}{2} - x\right) dx \quad (7)$$

$$\Delta_l = \frac{\frac{2M_y}{H}}{K_{pier}} \quad (8)$$

$$\Delta_{nl} = \Delta_l + \Delta_p \quad (9)$$

The plastic displacement is calculated using the change in curvature times the distance to the inflection point over the length of the yielded section of the substructure. The linear displacement is taken as the displacement associated with the yield moment. The overall displacement of the pier is the sum of the plastic and linear displacement as shown in Figure D.7.

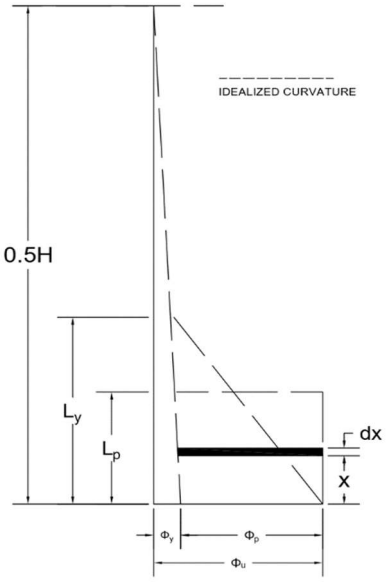

Figure D.7 Moment-Curvature Diagram for Frame Bents with Both Ends Fixed

The Level 2 procedure assumes the total force drawn to the structure remains the same for both the linear and nonlinear approach. Using the total force calculated with the linear model, the forces are redistributed (when applicable) using results from the displacement-controlled pushover analysis. Using the maximum displacement from the ground motion application, the linear response of the structure can be calculated as

$$F_l = K_{pier} * \Delta_l. \quad (10)$$

From the displacement-controlled pushover analysis, the redistribution ratio and displacement are known for all loads. The SAP2000 model is used to evaluate the MATLAB results for total force versus bridge displacement, shown in Figure D.8.

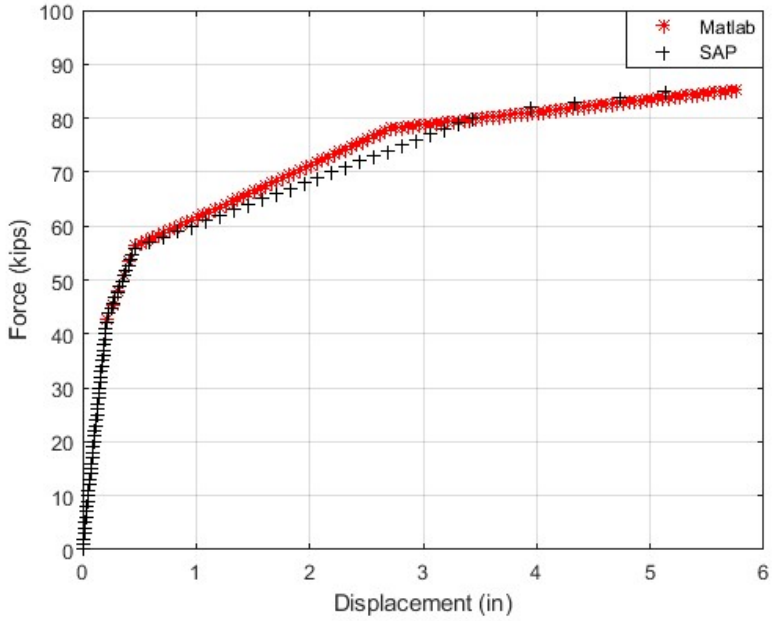

Figure D.8 Force vs. Bridge Displacement Comparison and Validation

Compare Force Demand to Capacity

The overall vulnerability of the structure, for each time history, is defined in terms of a comparison between capacity and demand. Generally, a force demand which exceeds the controlling force capacity results in a structure that is either moderately vulnerable or highly vulnerable depending on the failure mechanism.

Compare Displacement Demand to Allowable Displacement

Additional displacement checks must also be considered when applicable. For bridges with expansion joints, the exceedance of the expansion joint size should be checked as an indicator of abutment pounding. Additionally, the allowable displacement of rocker bearings for steel bridges, when present, should be checked as an indicator for overturning. Lastly, for bridges with a low flexural reinforcement ratio (see Table D.1. Synopsis of Vulnerabilities in INDOT Bridge Network), the allowable displacement is likely the substructure displacement associated with the cracking moment.

Synopsis of Vulnerabilities in INDOT

From the Level 2 assessment of the 100-bridge sample set, certain common vulnerabilities have been identified. These vulnerabilities, primarily focused on deficient substructures, are summarized in Table D.1.

Table D.1 Summary of Key Vulnerabilities Identified in INDOT Bride Network

Vulnerability Case	Substructure Type	Direction	Additional Comments/Criteria (When Applicable)	Level of Vulnerability	Reason for Classification
1	Walls	Longitudinal	Built Before 1990 (Grade 40 ksi steel)*	Highly Vulnerable	Low Flexural Reinforcement Ratio
2	Hammerhead Walls	Longitudinal	Built Before 1990 (Grade 40 ksi steel)*	Highly Vulnerable	Low Flexural Reinforcement Ratio
3	Hammerhead Walls	Longitudinal	Built After 1990 (Grade 60 ksi steel)	Moderately Vulnerable	Formation of Plastic Hinge
4	Hammerhead Walls	Transverse	Prestressed Concrete Superstructure Only	Moderately Vulnerable	Formation of Plastic Hinge
5	Frame Bents	Transverse	All types (H-Pile, CFT, Reinforced Concrete)	Moderately Vulnerable	Formation of Plastic Hinge
6	Frame Bents	Longitudinal	All types (H-Pile, CFT, Reinforced Concrete)	Moderately Vulnerable	Formation of Plastic Hinge
7	-	-	Rocker Bearings	Moderately Vulnerable	Unseating

*In accordance with the *Manual for Bridge Evaluation* (AASHTO, 2018) Table 6A.5.2.2-1, bridges built before 1990 are assumed to have Grade 40 *ksi* steel. If a given bridge is identified as having Grade 60 *ksi* steel and was built before 1990, it may instead fall under vulnerability case 3.

Identification of Capacity Thresholds for Application to Simplified Assessment & Tool

Each of the vulnerabilities shown in Table D.1 can be mapped to a capacity threshold, the exceedance of which will allow for the identification of distinct vulnerability levels in the Simplified Assessment. These thresholds, originally identified by Ramirez et al. (2000), have been extrapolated to account for additional vulnerabilities identified in the detailed assessment. These additional vulnerabilities primarily correspond to the brittle failure of substructures due to the low flexural reinforcement ratio. These updated thresholds plus original thresholds are shown in Table D.2.

Table D.2 Summary of Capacity Thresholds for Simplified Assessment

	Transverse Direction		**Longitudinal Direction**		
Level 2 Vulnerability	Formation of Plastic Hinge	Exceedance of Hinge Rotational Capacity	Formation of Plastic Hinge	Exceedance of Hinge Rotational Capacity	Brittle Failure
Level 1 Threshold	Drift > 0.5%	Drift > 1.5%	Displacement > 1 in.	Displacement > 6 in.	Displacement > 0.1 in.
Additional Identifiers	-	-	Substructure Built After 1990	Substructure Built After 1990	Substructure Built Before 1990*

Most of the vulnerabilities identified in Table D.1 can be linked to a vulnerability threshold shown in Table D.2, but a few exceptions do exist. These exceptions apply to unique substructure and superstructure combinations that are better modeled using capacity-based thresholds rather than displacement-based thresholds. For example, concrete-filled tubes (CFT) frame bents supporting reinforced-concrete superstructures are modeled in the Level 1 using the capacity of the CFT section. Unlike reinforced-concrete substructures, this capacity is consistent across almost all bridges with this substructure type. Additionally, this structure does not displace as much as typical RC substructures because the rigid connection between the reinforced-concrete slab deck and the substructure allows the participation of the superstructure which significantly increases the transverse stiffness. Thus, the accurate modeling of this structure requires comparing the restoring force to the moment capacity. This substructure type, as well as hammerhead substructures supporting prestressed concrete superstructures and H-Pile frame bent substructures supporting RC superstructures are modeled in a similar manner. More explicit details regarding these exceptions to the capacity thresholds shown in Table D.2 are detailed in Appendix G.

Sample Applications of the Level 2 Assessment Procedure

For easy reference, the Level 2 assessment procedure shown again in Figure D.9. The Level 2 assessment will now be applied to three case studies representing the superstructure-substructure combinations identified previously.

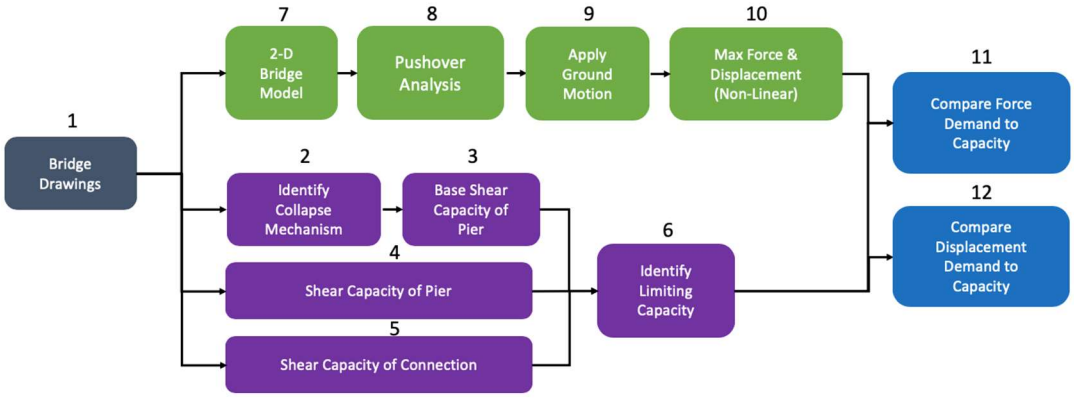

Figure D.9 Level 2 Assessment Procedure

Case Study 1: Prestressed Concrete Bulb-Tee Beams with Supporting Walls at Interior Supports

1. Bridge Information

Structure Number 024-91-08973 (NBI 5941) is a five-span, prestressed concrete bridge located in White County, which is in the La Porte District. Originally constructed in 2014, the bridge has not undergone any rehabilitation work. The superstructure is composed of six Bulb-Tee 66 × 48 beams with an 8 *in* (20.32 *cm*) reinforced concrete deck. The bridge is skewed at 13-*degrees*, is 64′–6″ (19.66 *m*) wide, and has span lengths (from west to east) of 94′–0″ (28.65 *m*), 102′–0″ (31.09 *m*), 102′–0″ (31.09 *m*), 102′–0″ (31.09 *m*), and 76′–0″ (23.16 *m*) as shown in Figure D.10 and Figure D.11.

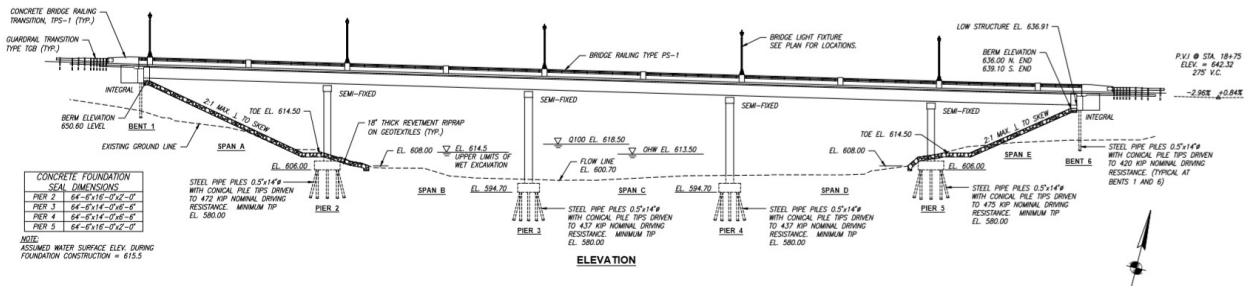

Figure D.10 Elevation View of Bridge NBI 5941 (2014)

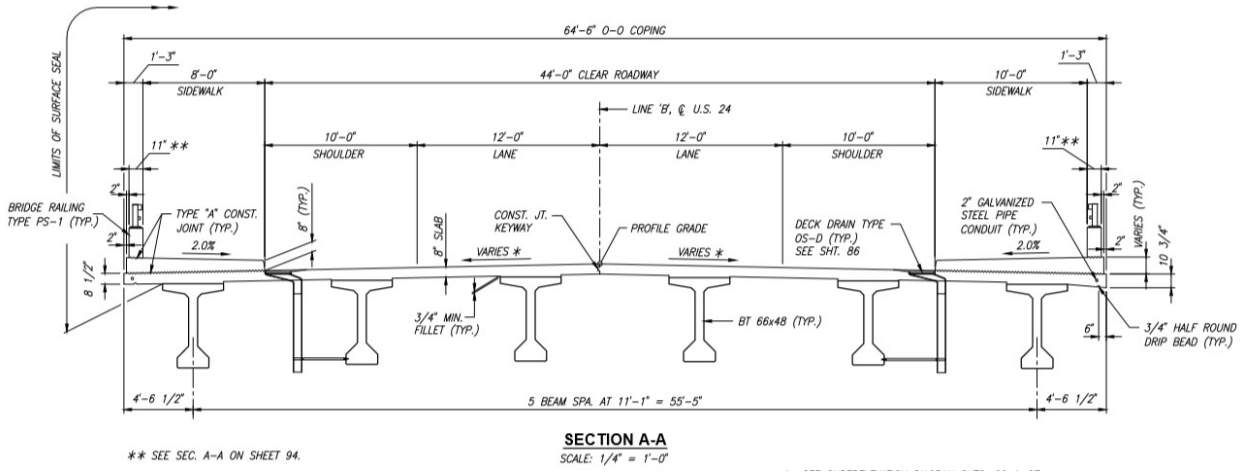

Figure D.11 Typical Section of Bridge (NBI 5941) (2014)

The bridge is supported by two integral end bents and four interior walls, as shown in Figure D.10. Due to the presence of integral end bents, we can assume that the bridge will not be vulnerable to seismic hazards in the longitudinal direction of motion. Therefore, we only present the calculations for the transverse direction here.

For this substructure type, the geometries relevant to these calculations are wall thickness, length, and height. Each wall has a uniform thickness of 3′–6″ (1.06 *m*) and an equivalent rectangular base length of 58′–3″ (17.75 *m*). The wall height varies and for the four walls from left to right, is taken as 37′–7″ (11.45 *m*), 45′–10″ (13.97 *m*), 42′–10″ (13.05 *m*), and 29′–0″ (8.84 *m*). The height of each wall is measured from the top of the footing to the top of the bent cap. However, the additional width of the bent cap is ignored when determining the stiffness.

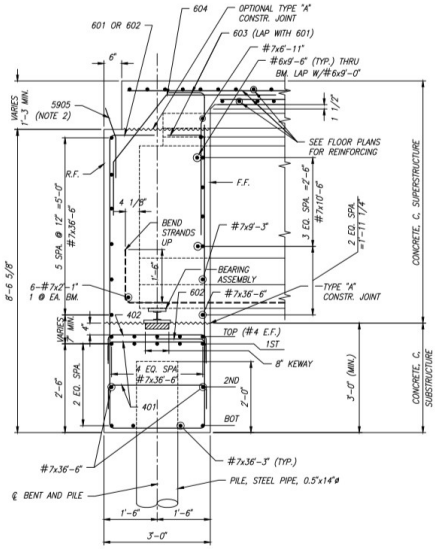

Figure D.12 Abutment Detail of Bridge (NBI 5941) (2014)

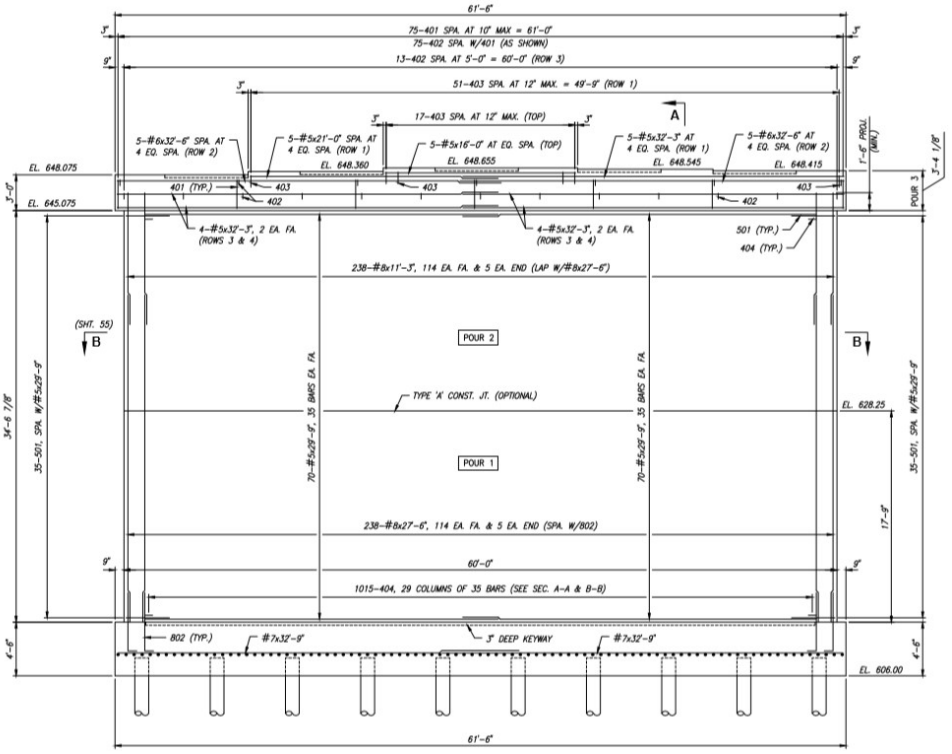

Figure D.13 Transverse Elevation of an Interior Pier of Bridge (NBI 5941) (2014)

Capacity

2. Identify Mechanism of Hinge Formation

The controlling mechanism of hinge formation for all fixed-free or fixed-semi-fixed walls is identified as the formation of a plastic hinge at the base of the wall. The ultimate force the wall can take, in either direction, is calculated as

$$V_{bs} = \frac{M_u}{H}. \tag{11}$$

3. Base Shear of Pier

The aspect ratio of the wall in the transverse direction is calculated as

$$\lambda_R = \frac{H}{w} = \frac{37.6\ \text{ft}}{60\ \text{ft}} = 0.62. \tag{12}$$

As discussed previously, a substructure with an aspect ratio less than 2.5 has a structural response that is not dominated by flexure. Therefore, the bridge will not develop a hinge in the transverse direction.

While the bridge will not experience this failure mechanism, in-detail calculations are provided for purposes of completeness as this moment-curvature methodology and assumptions are applicable to all cross-sections.

To determine the nonlinear behavior of the substructure, the moment and corresponding curvature for cracking, yielding, and ultimate is calculated. The cross-section at the base of the wall is shown in Figure D.14.

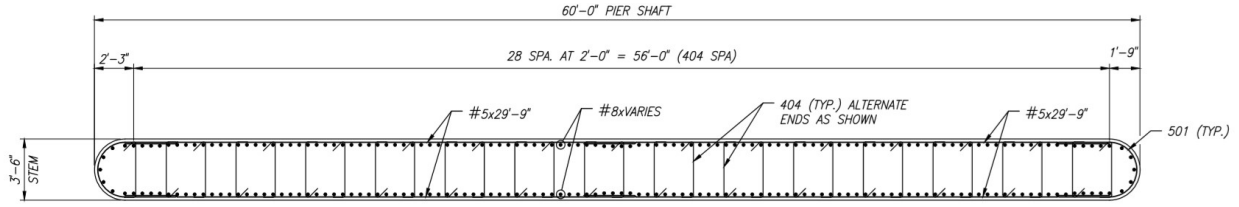

Figure D.14 Cross-section of Typical Interior Pier of Bridge (NBI 5941) (2014)

The elongated oval shape is modeled as an equivalent rectangular section with a total reinforcement ratio of 0.65% or 3.22 in^2/ft (68.15 cm^2/m). In the transverse direction, the entire section of the wall is considered when calculating the base shear capacity.

The moment associated with cracking is calculated using the gross moment of inertia and a centroid equivalent to half the cross-section, as given by Equation (1). The gross moment of inertia in the transverse direction is found as

$$I_g = \frac{tw^3}{12} = \frac{(3.5 * 58.25^3)ft^4}{12} * (12\ in)^4 = 1.2 * 10^9\ in^4. \tag{13}$$

The cracking moment is computed as

$$M_{cr} = 7.5\sqrt{3500\ psi} * \frac{2 * 1.2 * 10^9 in^4}{58.25ft} = 1.26 * 10^5\ kip * ft. \tag{14}$$

The curvature equation (Equation (2)) utilizes the assumption that plane sections remain plane after deformation. With this assumption, coupled with the linear strain profile assumption, the curvature associated with the cracking moment is found as

$$\varphi_{cr} = \frac{(1.26 * 10^5)\ kip * ft}{(1.2 * 10^9 in^4) * 3410\ \text{ksi}} = 3.7 * 10^{-7} \frac{rad}{in}. \tag{15}$$

The moment associated with yielding is calculated assuming the extreme tension fiber has just yielded. Sample calculations are presented for the transverse direction. For a neutral axis value ($c_{N.A.}$) of 134.3 in (341.12 cm), force-equilibrium is achieved. Taking the maximum nominal concrete strain as $\varepsilon_o = \frac{2 * f'_c}{E_c}$, the assumed stress profile for concrete is

$$f_c = \begin{pmatrix} f'_c * (2\frac{\varepsilon_c}{\varepsilon_o} - \left(\frac{\varepsilon_c}{\varepsilon_o}\right)^2 & \varepsilon_c \leq \varepsilon_o \\ f'_c\left(1 - \frac{0.15(\varepsilon_c - \varepsilon_o)}{.003 - \varepsilon_o}\right) & \varepsilon_c > \varepsilon_o \end{pmatrix}. \tag{16}$$

Using numerical integration (e.g., Simpson's rule), the total force in the concrete is found as

$$F_{conc} = \int_0^{\varepsilon_{N.A.}=.0005} f(x) * t * dx = 4418.6\ kips\,. \tag{17}$$

Using the material's yield strain ($\varepsilon_y = \frac{f_y}{E_s} = \frac{60\ ksi}{29000\ ksi}$) and a linear strain profile, the stress profile for steel is

$$f_s = \begin{pmatrix} f_y * \left(\frac{\varepsilon_s}{\varepsilon_y}\right) & \varepsilon_s \leq \varepsilon_y \\ f_y & \varepsilon_s > \varepsilon_y \end{pmatrix}. \tag{18}$$

Summing the force in each layer of steel, the total force in compression and tension, respectively, are

$$F_{s_c} = \sum_{i=1}^{N_{bars_c}} f_{s_i}(x) * A_{s_i} = 155.8\ kips \tag{19}$$

$$F_{s_t} = \sum_{i=1}^{N_{bars_t}} f_{s_i}(x) * A_{s_i} = 4570.4\ kips. \tag{20}$$

Summing forces, the force-equilibrium of the section for the given N.A. depth is confirmed to be within the acceptable threshold of 5 *kips* as

$$F_{conc} + F_{s_c} + F_{s_t} = 4418.6\ kips + 155.8\ kips - 4570.4\ kips < 5\ kips. \tag{21}$$

The above calculations are used to obtain the yield force. The yield moment, taken about the N.A., in the transverse direction is

$$M_y = 1.61 * 10^5\ kip * ft \tag{22}$$

and the resulting curvature is

$$\varphi_y = 3.72 * 10^{-6} \frac{rad}{in}. \tag{23}$$

The same approach (using Equations (17–21)) is applied to the cross-section to determine the ultimate moment. However, the accepted solution occurs when either the strain of the ultimate tensile fiber reaches strain hardening ($\varepsilon_s = 0.01$) or the ultimate compressive fiber of the concrete reaches a strain of 0.003. For this pier, the steel strain controls in both directions. The resulting ultimate moment for a N.A. depth of 96.4 *in* (244.86 *cm*) and a concrete strain of .0016 in the transverse direction is

$$M_u = 2.64 * 10^5\ kip * ft. \tag{24}$$

The corresponding curvature is

$$\varphi_u = .165 * 10^{-4} \frac{rad}{in}. \tag{25}$$

Figure D.15 shows the resulting moment-curvature plot in the transverse direction of Pier 2.

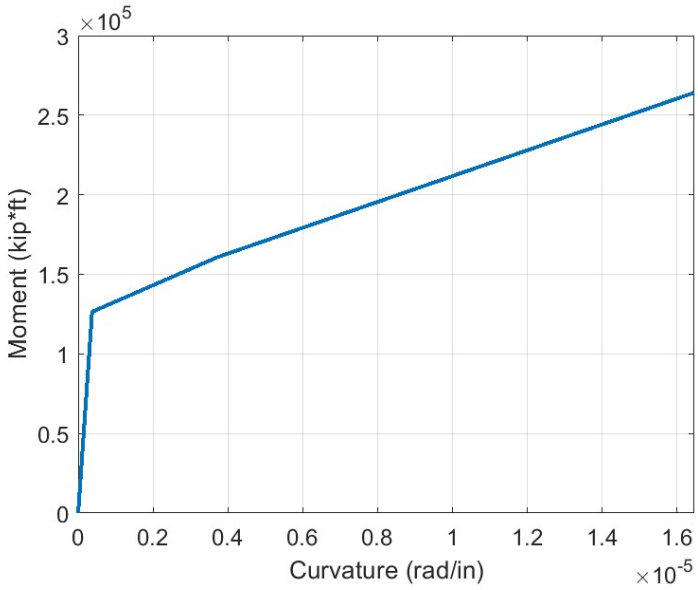

Figure D.15 Transverse Moment-Curvature Diagram for Pier 2 of Bridge (NBI 5941)

Typically, the moment-curvature relationship will remain rather consistent among all piers for a specific bridge. However, due to the varying pier height, the corresponding base shear resultant (Equation (11)) for this structure will change. The resulting base shear capacity of the four piers in the transverse direction is

$$V_{bs} = [7031 \quad 5827 \quad 6238 \quad 9109]\, kips. \tag{26}$$

Again, it is important to note that while the calculation for base shear capacity is feasible for walls in the transverse direction, the substructure will not actually behave in flexure due to a small aspect ratio.

4. Shear Capacity of Pier

In the transverse direction, the shear capacity of the pier is calculated in accordance with AASHTO 5.8.3. An α_c value is determined to account for the difference between the expected occurrence of flexure-shear cracking for slender walls in comparison to web-shear cracking in shorter walls. This value is

$$\alpha_c = \begin{pmatrix} 2 & \frac{H}{w} \geq 2 \\ 3 & \frac{H}{w} \leq 1.5 \\ 0.5 * \left(\frac{H}{w}\right) & 1.5 < \frac{H}{w} < 2 \end{pmatrix}. \tag{27}$$

Assuming normal-weight concrete ($\lambda = 1$), the shear capacity of the wall in the transverse direction is

$$V_n = tw\left(\alpha_c \lambda \sqrt{f_c'} + \rho f_y\right) = (3.5ft) * (58.25ft) * \left(3\sqrt{3500psi} + .0025 * 60ksi\right) = 9544\, kips. \tag{28}$$

The resulting shear capacity of the four piers in the transverse direction is

$$V_n = [9544 \quad 10289 \quad 10377 \quad 9544]\, kips. \tag{29}$$

5. Shear Capacity of Connection

Using the interior pier diaphragm detail, shown in Figure D.17, the shear capacity of the connection is taken as the direct shear capacity of the concrete key. Using a friction factor, μ_s, of 0.4, the shear capacity of the connection is found as

$$V_{conn} = \mu_s f_c' A_{cv}(N_b - 1) = 0.4 * 3.5ksi * (133in - 48in) * 12in * 5 = 8160\ kips. \quad (30)$$

The presence of the interior pier diaphragms is essential for transferring force from the superstructure to the substructure. With this detail, the piers can restore the bridge mass to its original position, when the structure is excited.

6. Identify Limiting Capacity

With values for the two failure mechanisms considered (transverse shear, horizontal shear connection), the limiting capacity is identified as the minimum of these values. Thus, for Pier 2, the limiting capacity in the transverse direction is

$$C_{limit} = \min(9544, 8160)\ kips = 8160\ kips. \quad (31)$$

Thus, Pier 2 is controlled by the horizontal shear connection between the superstructure and substructure. The controlling capacity and corresponding mechanism of failure for all piers in the transverse direction are summarized in Table D.3.

Table D.3 Limiting Capacity of Substructure in Transverse Direction of Bridge NBI 5941

Pier No.	Capacity–Trans.	Mechanism
2	8160 $kips$	Shear Connection
3	8160 $kips$	Shear Connection
4	8160 $kips$	Shear Connection
5	8160 $kips$	Shear Connection

Demand

7. 2-D Bridge Model

7.1a Transverse Stiffness

The stiffness in both the transverse and longitudinal directions is derived solely from the substructure stiffness. As mentioned previously, the deck is assumed to be sufficiently rigid to allow the intermediate piers to act as springs in parallel.

The stiffness of the walls in the transverse direction considers both bending and shear because the aspect ratio, λ_R, deviates significantly from the assumptions of beam theory (Fares, 2018). For a bridge with an aspect ratio greater than 2.5, it is clearly shown in Figure D.2 that the response is dominated by flexure whereas for a substructure with an aspect ratio less than 2.5, the response is the combination of flexure and shear. This supporting research and plot are provided as additional justification for using a controlling

aspect ratio of 2.5 for determining whether a flexural response, and the formation of a plastic hinge, is feasible.

For prestressed concrete superstructures, the substructure is assumed to be fixed-free, and the resulting bending stiffness and shear stiffness is then

$$K_{bend} = \frac{3E_c I}{H^3} = \frac{3E_c\left(\frac{tw^3}{12}\right)}{H^3} = \frac{3 * 3410ksi * \left(\frac{3.5 * 58.25^3}{12}\right)ft^4}{(37.6ft)^3} = 133127\frac{kip}{in} \quad (32)$$

$$K_v = \frac{Gtw}{1.2H} = \frac{1482.5\ ksi * 58.25ft * 3.5ft}{1.2 * 37.6ft} = 80384\frac{kip}{in}, \quad (33)$$

respectively, where the shear modulus, G, is

$$G = \frac{E_c}{2(1+\nu)} = \frac{3410\ ksi}{2 * 1.15} = 1482.5\ ksi. \quad (34)$$

The resulting stiffness for all four piers in the transverse direction is

$$K_{pier} = [213511 \quad 159212 \quad 186929 \quad 394390]\frac{kip}{in}. \quad (35)$$

7.2b Transverse Mass

The activated mass of the bridge in the transverse direction is calculated using the superstructure geometry, barrier dimensions, and concrete stiffeners. The weight of the beams (W_b) is taken as 1,015 *lb/ft* (140.33 *kg/m*) from *INDOT's Design Manual* Figure D.406-14I (Revised June 2018). The mass attributed to each pier is calculated using the tributary area calculated as half of each span length adjacent to the pier. Using 150 *lb/ft*^{3} (2,402.77 *kg/m*^{3}) (as the density of concrete (γ_c), the mass of the primary structural system (SS) over each pier is

$$m_{SS} = \frac{l_{pier} * (w_{oto} * t_{deck} * \gamma_c + W_b * N_b)}{g}$$

$$= \frac{98ft * \left(64.5ft * 8in * 150pcf + 1011\frac{lb}{lft} * 6\right)}{386.4\frac{in}{s^2}} = 3.17\frac{kips}{g} \quad (36)$$

The mass of the concrete bridge railing type PS-1, calculated using INDOT standard drawing E 706-BRPP-03, is

$$m_R = 2 * \frac{l_{pier} * (\gamma_c * A_R + W_s)}{g} = \frac{98ft * \left(150pcf * 2.3ft^2 + 19.6\frac{lbs}{lft}\right)}{\frac{386.4in}{s^2}} = 0.19\frac{kips}{g}. \quad (37)$$

The presence of lateral stiffeners between the beams over each pier allows for the transfer of forces from the substructure to superstructure, but also contributes to the mass of the system. The total mass of the stiffener is a function of the beam spacing, beam height, and width of bent cap. Figure D.16 and Figure D.17 show the detail for the lateral stiffener for this case.

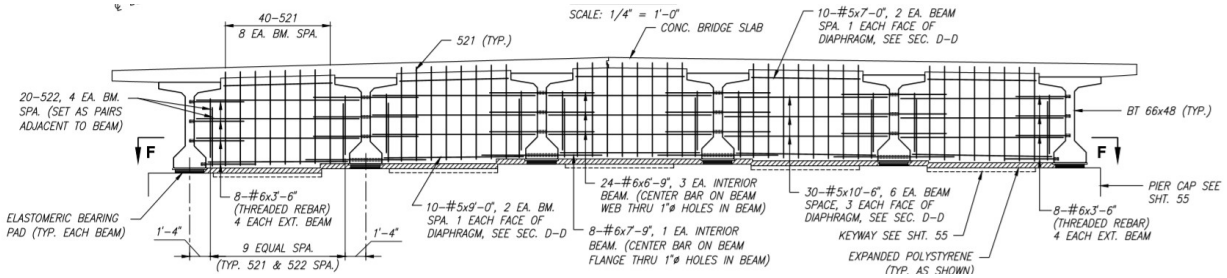

Figure D.16 Transverse Elevation of Pier 2 Diaphragms (NBI 5941) (2014)

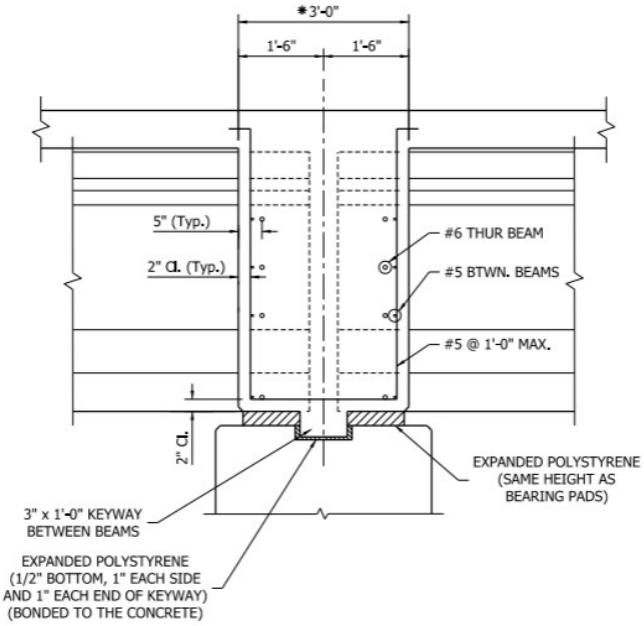

Figure D.17 Elevation Detail of Typical Interior Diaphragm of Bridge (NBI 5941) (2014)

The mass of the diaphragms over each pier is

$$m_D = \gamma_c * \frac{l_D * (h_b s_b - A_b) * (N_b - 1)}{g}$$

$$= 150pcf * \frac{3ft * (11.08ft * 5.5ft - 1118in^2) * 5}{\frac{386.4in}{s^2}} = 0.28\frac{kips}{g}. \quad (38)$$

Summing these values, the total mass of the superstructure over Pier 2 is

$$m_{pier} = m_{SS} + m_R + m_D = (2.99 + 0.089 + 0.37)\frac{kips}{g} = 3.65\frac{kips}{g}. \quad (39)$$

Thus, the mass of the superstructure over each of the piers is computed as

$$m_{pier} = [3.65 \quad 3.81 \quad 3.81 \quad 3.37]\frac{kip}{g}. \quad (40)$$

7.3 Equation-of-Motion

Because the rigidity of the deck ensures uniform movement in both directions, the total stiffness and mass are calculated as the summation of all the individual pier components. The total stiffness in the transverse direction is

$$K_{\text{sub}} = \sum_{i=1}^{N_{pier}} K_{pier_i} = 954042 \frac{kip}{in}. \tag{41}$$

The total mass in the transverse direction is

$$m_{\text{sup}} = \sum_{i=1}^{N_{pier}} m_{pier_i} = 14.7 \frac{kips}{g}. \tag{42}$$

With the mass and stiffness calculated, the equation-of-motion is written. The form of the equation-of-motion is given in Equation (6).

As mentioned previously, we assume a viscous damping ratio (ζ_{pier}) for this analysis of 5%. Using Equation 5 damping is computed as

$$c_{sub} = 2 * 0.05 \sqrt{954042 \frac{kip}{in} * 14.7 \frac{kips}{g}}. \tag{43}$$

Thus, the equation-of-motion in the transverse direction to be used for dynamic analysis is

$$14.7 \frac{kips}{g} \ddot{x} + \left(374.5 \frac{kips * s}{in}\right) \dot{x} + \left(954042 \frac{kips}{in}\right) x = -14.7 \frac{kips}{g} \ddot{x}_g. \tag{44}$$

8. Displacement-Controlled Pushover Analysis

As the structure is not expected to respond in flexure in the transverse direction, a displacement-controlled pushover analysis is not required. Because the controlling mechanism is the shear connection, the forces drawn to pier are not expected to redistribute or vary from a linear model.

9. Apply Ground Motion

Generic site amplification factors were used to generate 100 stochastically-simulated earthquakes representative of the expected earthquake excitation for this site (see Deliverable 1). Using a 4th order Runge-Kutta integration scheme, the bridge's linear response to each earthquake is evaluated using Equation (44). The maximum displacement is recorded and used in Section 10 to determine the response of the structure for each earthquake.

10. Maximum Force and Displacement

The linear displacement and stiffness are used to calculate the total force applied to the bridge. Using the results of the displacement-controlled pushover analysis, the redistribution of forces (if applicable) is applied to account for the nonlinearity of the pier(s). If the pier remains linear (e.g., no yielding of the longitudinal steel), the displacement is calculated using the linear spring relationship ($F_{lin} = K_{lin} u$). If any

of the piers behave nonlinear, the force-displacement relationship (Displacement-controlled pushover analysis) is used to determine the displacement of the bridge.

11. Compare Force Demand to Capacity

In the transverse direction, the maximum force resulting from the application of each of the 100 seismic ground motions is compared to the capacity to assess if the capacity is exceeded. The maximum resulting force from 100 ground motions never exceeds the capacity in the transverse direction controlled by the shear connection between the substructure and superstructure.

Vulnerability Assessment of Detail

In the transverse direction, wall substructures have low vulnerability. This is seen across all superstructure types. Thus, this detail is classified as low vulnerability using the Level 0 assessment.

Case Study 2: Continuous Steel Girder Bridge with Hammerhead Piers

1. Bridge Information

Structure Number 052-24-06649 (NBI 19430) is a four-span, continuous steel girder bridge located in Franklin County which is in the Seymour District. The bridge was originally constructed in 1983 and has no additional rehabilitation work done at this time. The superstructure is composed of 8 plate girders with an 8 *in* (20.32 *cm*) reinforced concrete deck. The bridge is skewed at 27-*degrees*, is 53′–6″ (16.03 *m*) wide, and has span lengths (from left to right) of 65′–0″ (19.81 *m*), 81′–4″ (24.79 *m*), 81′–4″ (24.79 *m*), and 65′–0″ (19.81 *m*) as shown in Figure D.19.

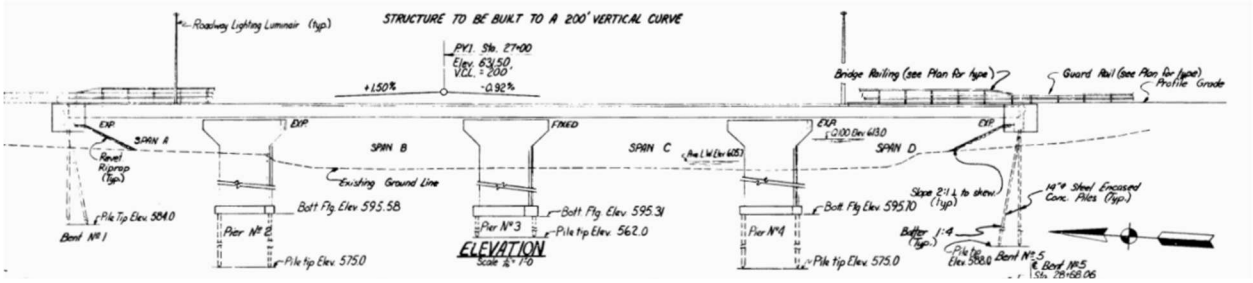

Figure D.18 Elevation View of Bridge (NBI 19430) (1982)

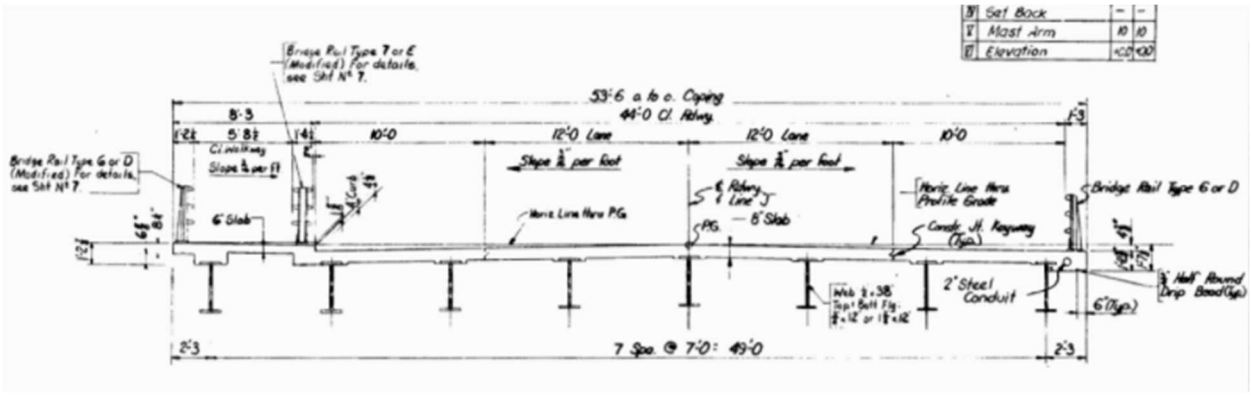

Figure D.19 Typical Section of Bridge (NBI 19430) (1982)

The bridge is supported by two abutments and three interior hammerhead piers, shown in Figure D.18. At each abutment and the two outermost piers, the superstructure is supported by eight expansion shoes (Figure D.20). At the middle pier (Pier 3), the superstructure is supported by eight fixed shoes (Figure D.21). The dimensions for the fixed bearing and the expansion bearing assembly can be found in INDOT standard drawings E 711-BSTS-01 and E 711-BSTS-02, respectively.

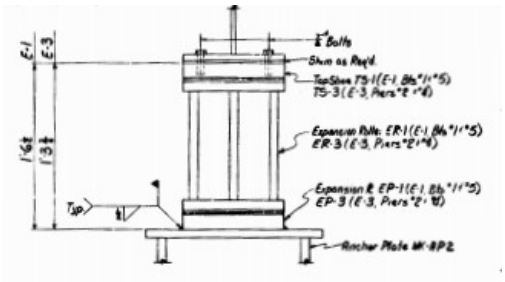

Figure D.20 Expansion Shoe at Abutments and Piers 2 and 4 for Bridge (NBI 19430) (1982)

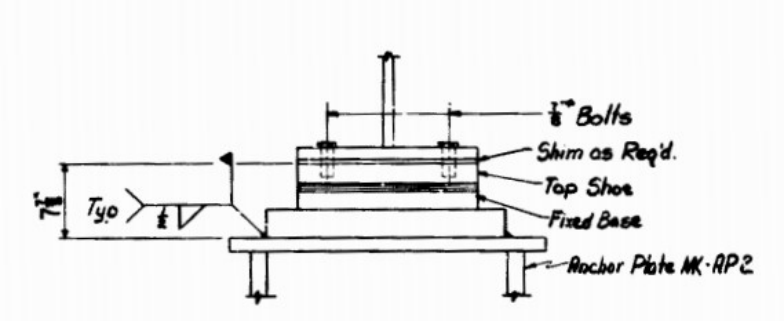

Figure D.21 Fixed Shoe at Pier 3 for Bridge (NBI 19430) (1982)

For this substructure type, the geometries relevant to the calculations are wall length at the base, wall thickness, and wall height. Each pier has a uniform thickness of 2′–6″ (76.2 *cm*), and an equivalent

rectangular base length of 42′–0″ (12.80 *m*). The typical pier elevation is shown in Figure D.22. The base length is used in the following calculations, rather than the length at the top, because the base of the pier is where yielding will occur. The additional length of the top of the pier is ignored when determining the stiffness. The total heights of Pier 2, 3, and 4 are 26′–6″ (8.08 *m*), 27′–6″ (8.38 *m*), and 26′–6″ (8.08 *m*), respectively.

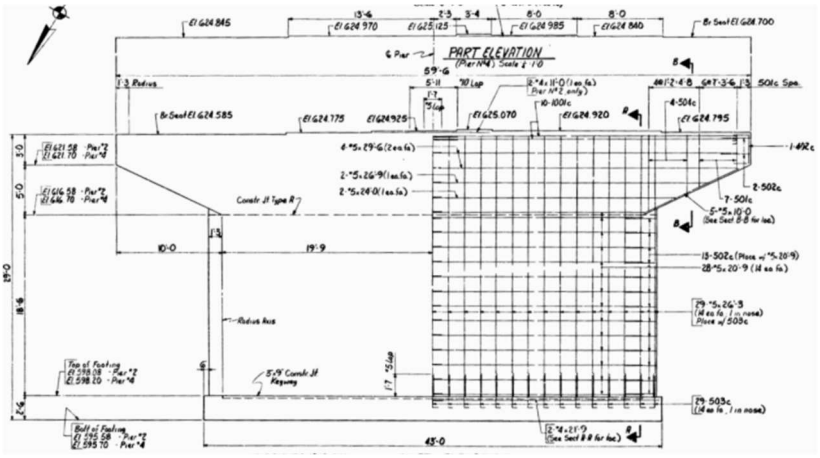

Figure D.22 Transverse Elevation of an Interior Pier of Bridge (NBI 19430) (1982)

Capacity

2. Identify Mechanism of Hinge Formation

The controlling mechanism of hinge formation for all fixed-free or fixed semi-free hammerheads is identified as the formation of a plastic hinge at the base of the pier. On this basis, the ultimate force the pier can take, in either direction, is calculated using Equation (11). This force (Base Shear Capacity) is then compared to the available transverse shear capacity, and horizontal shear capacity of connections between the pier and the superstructure in order to determine the controlling mechanism in terms of force.

3. Base Shear

As described in Case Study 1, walls in the transverse direction with aspect ratios less than 2.5 are controlled by shear. The aspect ratio for this bridge is calculated using Equation (12) and is

$$\lambda_R = \frac{H}{w} = \frac{26.5\ ft}{42\ ft} = 0.63. \tag{45}$$

This means that the bridge will not develop a hinge in the transverse direction.

In the longitudinal direction, the base shear, controlled by the flexure mechanism, of each pier is calculated using the reinforcement layout shown in Figure D.23 and the procedure described in the detailed calculations for the prestressed concrete bridge (Equations (13–25)). The elongated oval shape is modeled as an equivalent rectangular section with a total reinforcement ratio of 0.11% or 0.41 in^2/ft (8.68 cm^2/m). A

12 *in* (30.48 *cm*) section of the wall is used for the longitudinal direction calculations and then multiplied by the total length to get the total base shear. Table D.4 shows the results of the moment-curvature analysis of each pier in the longitudinal direction.

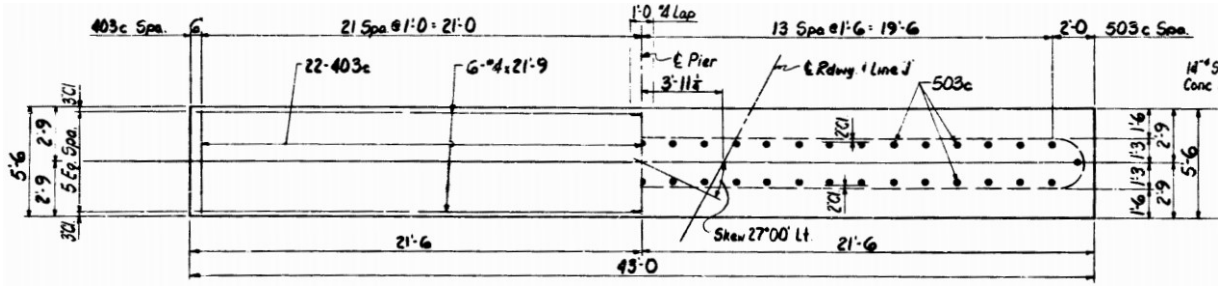

Figure D.23 Cross-section of Typical Interior Pier of Bridge (NBI 19430) (1982)

Table D.4 Moment-Curvature Results for the Longitudinal Direction for Bridge NBI 19430

	Pier 2		Pier 3		Pier 4	
	Moment (kip*ft)	φ	**Moment (kip*ft)**	φ	**Moment (kip*ft)**	φ
Cracking	2588	8.70E-06	2588	8.70E-06	2588	8.70E-06
Yield	768	5.96E-05	768	5.96E-05	768	5.96E-05
Ultimate	819	3.77E-04	819	3.77E-04	819	3.77E-04

The cracking moment is larger than the yield moment and the ultimate moment for every pier because of low flexural reinforcement ratio, 0.11%. If the cracking moment is ever exceeded, brittle failure may occur unless an alternate load path can be established. The cracking moment is therefore conservatively taken as the controlling moment for this case study and a linear response of the bridge is used in all further calculations.

The shear force that causes cracking is calculated as

$$V_{cr} = \frac{M_{cr}}{H}. \tag{46}$$

The shear force, over the entire length of the wall, that causes cracking of the three piers in the longitudinal direction is

$$V_{cr} = [97.7 \quad 94.1 \quad 97.1]\ kips. \tag{47}$$

4. Shear Capacity of Pier

In the transverse direction, the shear capacity of each pier is calculated using Equation (28). An α_c value of 3 is used based on the height to length ratio and a lambda (λ) value of 1 is used for normal-weight concrete. The reinforcement ratio for each pier is 0.11%. The yield strength of the longitudinal reinforcement is assumed to be 40 *ksi* (27.58 kN/cm^2) because the bridge was built during or after 1945

(*Manual for Bridge Evaluation* Table 6A.5.2.2-1 (AASHTO, 2018)). The shear capacity of the Pier 2 in the transverse direction is

$$V_n = (2.5ft) * (42ft) * \left(3\sqrt{3000psi} + .0011 * 40ksi\right) = 3178.9\ kips. \quad (48)$$

The resulting shear capacity of the three piers in the transverse direction is

$$V_n = [3178.9 \quad 3178.9 \quad 3178.9]\ kips. \quad (49)$$

The shear capacity of each pier in the longitudinal direction is calculated in accordance with AASHTO 5.8.3.3. The minimum value of Equation (50) and (51) is taken as the controlling shear capacity.

$$V_n = 0.25 * f'_c * b_v * d_v \quad (50)$$

$$V_n = V_c + V_s, \quad (51)$$

where V_c and V_s are calculated as

$$V_c = 0.0316 * 2 * \sqrt{f'_c} * b_v * d_v \quad (52)$$

$$V_s = \frac{A_v * f_y * d_v}{s}. \quad (53)$$

The value b_v corresponds to the width of the section considered, so for walls and hammerhead piers, this value is 12 *in* (30.48 *cm*). The value of d_v corresponds to the equivalent moment arm between the resulting tensile and compressive forces. For the three piers in this bridge, the value for V_c, per linear foot, is

$$V_c = 0.0316 * 2 * \sqrt{3ksi} * 12in * 22.1in = 34.31\frac{kips}{lft}. \quad (54)$$

The area of steel, A_v, is the area of shear ties connecting the two faces of longitudinal steel. However, for this bridge, there are no shear ties and therefore, the value of V_s is 0. The value of V_n, per linear foot, is calculated as the minimum of

$$V_{n_{lft}} = 0.25 * 3ksi * 12in * 22.1in = 135\frac{kips}{lft} \quad (55)$$

$$V_{n_{lft}} = 34.31\frac{kips}{lft} + 0\frac{kips}{lft} = 34.31\frac{kips}{lft} \quad (56)$$

$$V_{n_{lft}} = 34.31\frac{kips}{lft}. \quad (57)$$

The resulting shear capacity of the three piers in the longitudinal direction is

$$V_n = w * V_{n_{lft}} = 42ft * 34.31\frac{kip}{lft} = 1441.2\ kips \quad (58)$$

$$V_n = [1441.2 \quad 1441.2 \quad 1441.2]\ kips. \quad (59)$$

5. Shear Capacity of Connection

The shear connection capacity between the substructure and the superstructure for steel bridges is the capacity of the connection of the bearing to the substructure. For steel bridges on expansion and fixed shoes,

the bottom plates are connected to anchor plates using a 2 *in* (5.08 *cm*) long, ½ *in* (1.27 *cm*) fillet weld (shown in Figure D.20 and Figure D.21). Because these welds were not designed to transfer shear forces and because of the age of the bridges with these bearings, theses welds cannot be expected to perform reliably during earthquakes. Therefore, the shear capacity of the connection is conservatively taken as the frictional force between the substructure and the superstructure. A value of 0.57 is used for the coefficient of static friction (μ_s) (Rabbat & Russell, 1985) and the weight is taken as the tributary weight supported by each pier. Detailed calculations for the weight can be seen in Equations (69) through (72). The shear capacity of the connection found as

$$V_{conn} = \mu_s * m_{pier} * g = \ 0.57 * 1.27 \frac{kips}{g} * 386.4 \frac{in}{s^2} = 279\ kips. \tag{60}$$

Because the shear capacity of the connection is based only on the mass supported by each pier, it is the same in the transverse and the longitudinal direction. Therefore, the shear capacity of the connections of Piers 2, 3, and 4 are

$$V_{conn} = [279 \quad 310 \quad 279]\ kips. \tag{61}$$

6. Identify Limiting Capacity

With values for the two failure mechanisms considered (shear failure, and shear connection failure) the limiting capacity is identified as the minimum of these values. Thus, for Pier 2, the limiting capacity in the transverse direction is

$$C_{limit} = \min(3178.9, 279) = 279\ kips. \tag{62}$$

Thus, Pier 2 is controlled by the shear connection of the capacity. The controlling capacity and corresponding failure mechanism for all piers in the transverse and longitudinal direction are summarized in Table D.5 and Table D.6, respectively.

Table D.5 Limiting Capacity of Substructure in Transverse Direction for Bridge (NBI 19430)

Pier No.	Capacity–Trans.	Mechanism
2	279 kips	Shear Connection Failure
3	310 kips	Shear Connection Failure
4	279 kips	Shear Connection Failure

Table D.6 Limiting Capacity of Substructure in Longitudinal Direction for Bridge (NBI 19430)

Pier No.	Capacity–Long.	Mechanism
2	97.7 kips	Brittle Failure of Pier
3	94.1 kips	Brittle Failure of Pier
4	97.7 kips	Brittle Failure of Pier

6.1. Additional Longitudinal Displacement Capacity

In the longitudinal direction, when expansion shoe bearings are present, the allowable displacement of the expansion shoe bearing is an additional displacement threshold.

The allowable displacement of the bridge is limited by the rotation of the expansion shoe-type bearings as they have the potential to overturn. The allowable displacement is taken as one-half of the arc length of the bearing. For this bridge, the expansion shoe-type bearing is an E1-type at the abutments and an E3-type at Piers 2 and 4. E1-type bearings have a height of 12 *in* (30.84 *cm*) and a width of 8 *in* (20.32 *cm*). E3-type bearings have a height 12 *in* (30.84 *cm*) and a width of 6 *in* (15.24 *cm*). The bearing with the smaller width will govern. The allowable displacement of the rocker bearing is

$$\Delta_{rb}= \frac{w_{rb} * 2 * \sin^{-1}\left(\frac{0.5 * w_{rb}}{r_{rb}}\right)}{2} = \frac{6\ in * 2 * \sin^{-1}\left(\frac{3}{6} in\right)}{2} = 3.1in. \quad (63)$$

Demand

7. 2-D Bridge Model

The stiffness in both the transverse and longitudinal direction derives solely from the substructure stiffness. As mentioned previously, the deck is assumed to be rigid enough to allow the intermediate piers to act as springs in parallel.

7.1a Transverse Stiffness

The stiffness of hammerhead piers in the transverse direction is calculated using the same equations as a wall (Equations (32) through (34)). The transverse length is taken as the length of the wall at the bottom of the pier. For steel superstructures, the substructure is assumed to be fixed-free. The resulting bending stiffness and the shear stiffness of Pier 2 in the transverse direction is then

$$K_{bend} = \frac{3 * 3155ksi * \left(\frac{2.5 * 42^3}{12}\right) ft^4}{(26.5\ ft)^3} = 94204.3 \frac{kip}{in}. \quad (64)$$

$$K_v = \frac{Gtw}{1.2H} = \frac{1371.7\ ksi * 42ft * 2.5ft}{1.2 * 26.5ft} = 54351.9 \frac{kip}{in}, \quad (65)$$

Respectively, where the shear coefficient, G, is calculated using Equation (34) and is

$$G = \frac{3155\ ksi}{2 * 1.15} = 1371.7\ ksi. \quad (66)$$

The resulting stiffness of each pier in the transverse direction is

$$K_{pier} = [148556 \quad 136672.2 \quad 148556] \frac{kip}{in}. \quad (67)$$

7.1b Longitudinal Stiffness

The stiffness of hammerhead piers in the longitudinal direction is derived solely from bending and is assumed to behave as a fixed-free column. For steel bridges, the type of bearing on each pier determines if

the pier adds stiffness. Piers with expansion shoe bearings do not contribute to the stiffness of the bridge in the longitudinal direction because of the behavior of the expansion shoes. Expansion shoes are used to allow thermal expansion and contraction and do not allow lateral forces to be transferred from the superstructure to the substructure in the longitudinal direction. Fixed shoes allow the transfer of lateral forces from the superstructure to the substructure and are considered to add stiffness to the bridge model in the longitudinal direction.

Because Pier 3 is the only pier that has fixed shoes, the longitudinal stiffness is solely the longitudinal stiffness of Pier 3. The stiffness of Pier 3 is found as

$$K_{pier} = \frac{3E_cI}{H^3} = \frac{3E_c\left(\frac{wt^3}{12}\right)}{H^3} = \frac{3 * 3155ksi * \left(\frac{42 * 2.5^3}{12}\right)ft^4}{(27.5\ ft)^3} = 298.7\frac{kip}{in}. \quad (68)$$

7.2a Transverse Mass

The activated mass of the bridge in the transverse direction is calculated using the superstructure geometry. For rolled shapes, the weight per linear foot of each beam is given in the beam designation. For built-up plate girders, the weight per linear foot is calculated using the density of steel and the volume of the plates. The density of steel is assumed to be 0.284 lb/in^3 (7.75 g/cm^3). The average volume per linear foot of the plate girder is

$$V_{pg} = \frac{\sum_{i=1}^{n} L_{pg} * b_{pg} * h_{pg}}{L_{bridge}}. \quad (69)$$

The plate girder is symmetric about the centerline of the bridge, shown in Figure D.24.

Table D.7 shows the dimensions and the calculated volume for each plate.

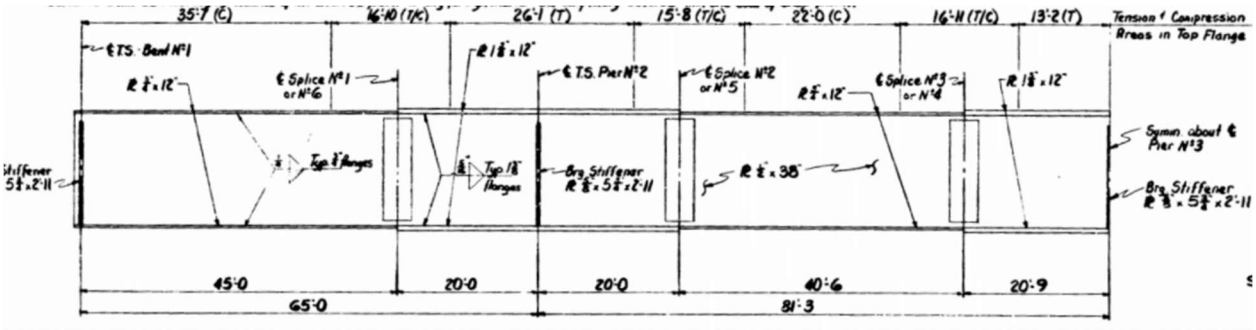

Figure D.24 Typical Plate Girder Elevation for Bridge (NBI 19430) (1982)

Table D.7 Plate Girder Volume for Bridge (NBI 19430)

	Length (ft)	Width (in)	Height (in)	Volume (in^3)
Top Plate A	45	12	0.5	3240
Web Plate A	45	0.5	38	10260
Bottom Plate A	45	12	0.5	3240
Top Plate B	40	12	1.375	7920
Web Plate B	40	0.5	38	9120
Bottom Plate B	40	12	1.375	7920
Top Plate C	40.5	12	0.75	4374
Web Plate C	40.5	0.5	38	9234
Bottom Plate C	40.5	12	0.75	4374
Top Plate D	20.75	12	1.375	4108.5
Web Plate D	20.75	0.5	38	4731
Bottom Plate D	20.75	12	1.375	4108.5
			Total	72630

A 15% increase in mass is applied to all steel bridges to account for the mass of the diaphragms, cross-bracing, connections. Because the railings are steel and aluminum, the 15% increase in beam mass is assumed to account for their mass as well. The weight per linear foot of each beam is found as

$$W_b = 1.15 * 0.284\frac{lb}{in^3} * V_{pg} = 1.15 * 0.284\frac{lb}{in^3} * \frac{2 * 72630in^3}{295ft} = 0.16\frac{kips}{lf}. \quad (70)$$

The mass of the primary structural systems (SS) over Pier 2 is

$$m_{SS} = \frac{l_{pier} * (w_{oto} * t_{deck} * \gamma_c + W_b * N_b)}{g}$$
$$= \frac{73.12ft * (53.5ft * 8in * 150pcf + 0.16klf * 8)}{g} = 1.27\frac{kips}{g}. \quad (71)$$

The mass of the superstructure over each pier is

$$m_{pier} = [1.27 \quad 1.41 \quad 1.27]\frac{kip}{g}. \quad (72)$$

7.2b Longitudinal Mass

The entire superstructure mass is activated in the longitudinal direction. This mass is calculated using Equations (69) through (72), but uses the entire length of the bridge. The longitudinal mass is

$$m_{sup} = 5.07\frac{kip}{g}. \quad (73)$$

7.3 Equation-of-Motion

Because the rigidity of the deck ensures uniform movement, the total stiffness and mass in the transverse direction are calculated as the sum of the individual pier stiffnesses and masses, respectively. The total stiffness in the transverse direction is

$$K_{sub} = \sum_{i=1}^{N_{pier}} K_{pier_i} = 433784 \frac{kip}{in}. \quad (74)$$

The total mass in the transverse direction is

$$m_{sup} = \sum_{i=1}^{N_{pier}} M_{pier_i} = 3.95 \frac{kips}{g}. \quad (75)$$

As mentioned previously, the total stiffness in the longitudinal direction is calculated as the sum of the individual pier stiffnesses whose bearings allow them to participate. The longitudinal stiffness is

$$K_{sub} = 298.7 \frac{kip}{in}. \quad (76)$$

The mass in the longitudinal direction is the entire mass of the bridge (5.07 *kips/g*) (22.55 *kN/g*).

With the mass and stiffness calculated in both directions, the equation-of-motion can be written. The basic equation-of-motion is given in Equation (6). For all bridges in this study, the viscous damping ratio (ζ_{pier}) is taken as 5%. The damping is calculated for each direction using Equation (43). The equation-of-motion in the transverse direction to be used for dynamic analysis is

$$3.95 \frac{kips}{g} \ddot{x}_s + \left(130.89 \frac{kips * s}{in}\right) \dot{x}_s + \left(433784 \frac{kips}{in}\right) x_s = -3.95 \frac{kips}{g} \ddot{x}_g. \quad (77)$$

The equation-of-motion in the longitudinal direction to be used for dynamic analysis is

$$5.07 \frac{kips}{g} \ddot{x}_s + \left(3.89 \frac{kips * s}{in}\right) \dot{x}_s + \left(298.7 \frac{kips}{in}\right) x_s = -5.07 \frac{kips}{g} \ddot{x}_g. \quad (78)$$

8. Pushover analysis

As mentioned earlier, because the cracking moment of each pier is larger than the yield moment, the bridge will remain in the linear region until brittle failure. Because of this, no pushover analysis is needed.

9. Apply Ground Motions

The same process for developing and applying ground motions used in Case Study 1 is used to develop 100 stochastically-simulated ground motions using generic site amplification factors.

10. Maximum Force and Displacement Demand

The linear displacement and the linear stiffness are used to calculate the total force applied to the bridge. Since the pushover analysis is not applicable to this bridge, the force is distributed to each pier based on the relative stiffness of the piers. With the force, the corresponding displacement is calculated. As mentioned earlier, because of the moment-curvature relationship, the total displacement is the linear displacement.

11. Compare Force Demand to Capacity

In each direction, the maximum force resulting from the application of each of the seismic ground motions is compared to the capacity to assess if the capacity is exceeded. For Structure Number 052-24-06649 (NBI 19430), the maximum force resulting from 100 ground motions never exceeds the capacity in the transverse direction, controlled be the shear connection between the substructure and superstructure. In the longitudinal direction, the maximum force resulting from 100 ground motions exceeds the capacity, controlled by brittle failure of the pier, 99% of the time.

12. Compare Displacement Demand to Allowable Displacement

In the longitudinal direction, the allowable displacement of the bridge is determined by the substructure (due to the low flexural reinforcement ratio) rather than the expansion joint size or allowable bearing rotation. Like the force demand, 99% of the ground motions result in an exceedance of the allowable substructure displacement.

Vulnerability Assessment of Detail

In the transverse direction, hammerhead walls supporting steel superstructures have low vulnerability. In the longitudinal direction, hammerhead walls (specifically older walls built before 1990) have the potential for high vulnerability due to the low flexural reinforcement ratio. This vulnerability is expected to be brittle.

Case Study 3: Reinforced Concrete Bridge with Rectangular Frame Bents

1. Bridge Information

Structure Number 041-42-05080 BNBL (NBI 014650) is a three-span reinforced concrete slab-deck bridge located in Knox County in the Vincennes District. The bridge was originally constructed in 1967 and has had two rehabilitations. In 1991, the bridge was widened, and an additional column was added to each pier and in 2009, the bridge deck overlay was placed. The superstructure is a 25.5 *in* (64.77 *cm*) thick reinforced-concrete slab deck, as seen in Figure D.26. The bridge is skewed at 8-*degrees*, is 55′–5″ (16.89 *m*) wide and has span lengths of 38′–6″ (11.73 *m*), 43′–0″ (13.10 *m*), and 38′–6″ (11.73 *m*).

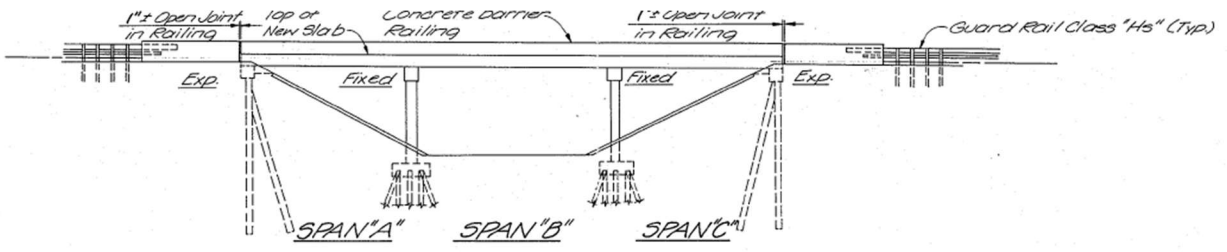

Figure D.25 Elevation View of Bridge (NBI 14650) (1991)

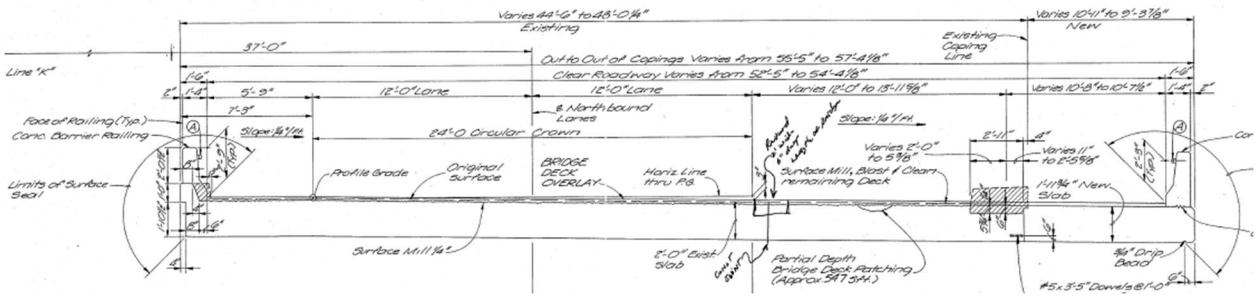

Figure D.26 Typical Section of Bridge (NBI 14650) (1991)

The bridge is supported by two abutments and two interior rectangular column frame-bent piers, shown in Figure D.25. There are two abutment details for this bridge. The connection of the original bridge deck to the abutment is shown in Figure D.27. Due to the presence of a joint, and no reinforcement extending from the abutment into the bridge deck, the abutment is classified as non-integral.

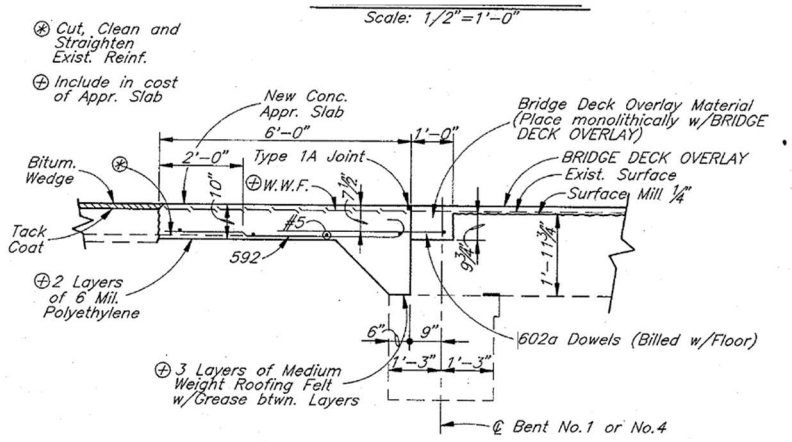

Figure D.27 Abutment Detail of Bridge at Original Bridge Deck (NBI 14650) (1991)

When the bridge was widened in 1991, the bridge width was increased by 21%. At the additional column, the abutment detail, shown in Figure D.28, is integral. Because the portion of the abutment connection that is integral is minimal (18% of the total bridge width), we assume that the portion of the abutment that is integral will not be able to resist the movement of the mass. Therefore, the bridge is non-integral and there is potential for vulnerability in the longitudinal direction

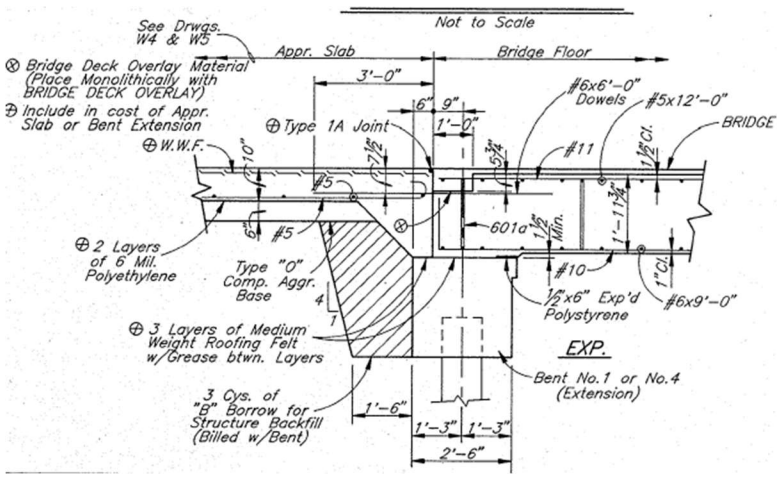

Figure D.28 Abutment Detail of Bridge at Added Column (NBI 14650) (1991)

At the interior piers, longitudinal bars extend from the bent cap to the deck. This connection is assumed to be rigid enough to allow moment transfer and allows the deck to add stiffness. Each frame bent is composed of six, 36″ × 24″ (19.44 *cm* × 60.96 *cm*) rectangular reinforced-concrete columns and a 30″ × 24″ (76.2 *cm* × 60.96 *cm*) bent cap. The columns in Pier 2 have a clear height of 11′–3″ (3.43 *m*) and a clear span of 6′–3″ (1.90 *m*), except for the outermost column, which has a clear span of 7′–1 ½″ (2.17 *m*). The columns in Pier 3 have a clear height of 11′–0″ (3.35 *m*) and a clear span of 6′–6″ (1.98 *m*), except for the outermost column, which has a clear span of 7′–3″ (2.21 *m*). The clear height is measured from the top of the crash wall to the base of the bent cap. Figure D.29 and Figure D.30 show the original elevation view for the pier and the addition pier, respectively.

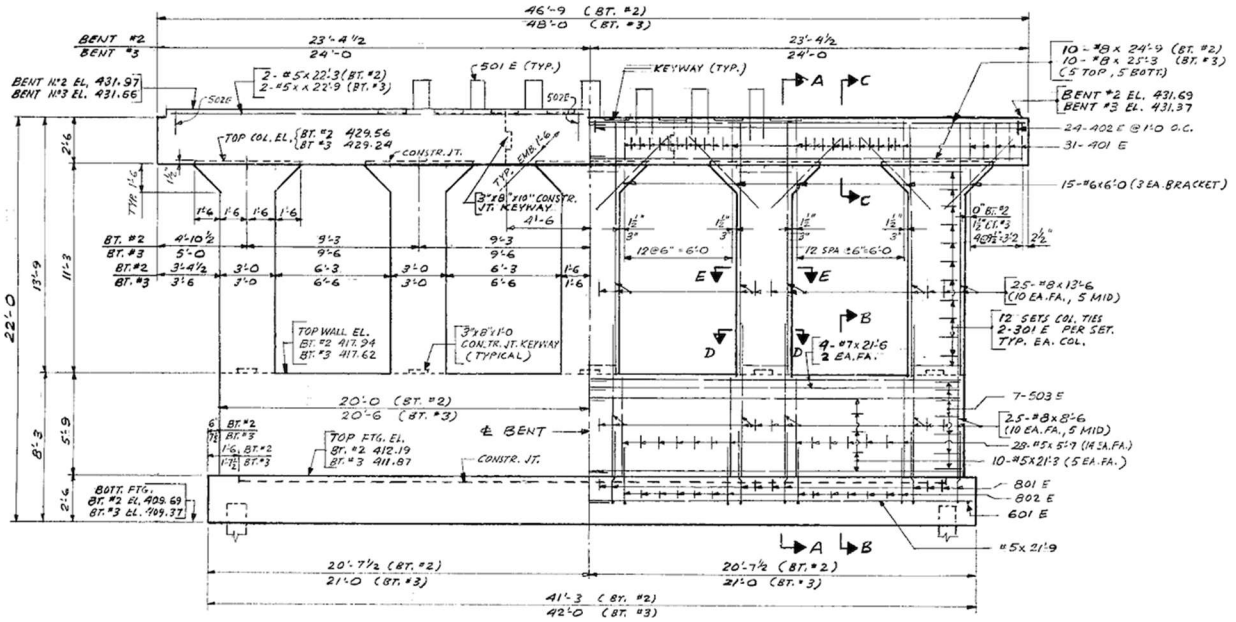

Figure D.29 Transverse Elevation of an Interior Pier of Bridge (NBI 14650) (1964).

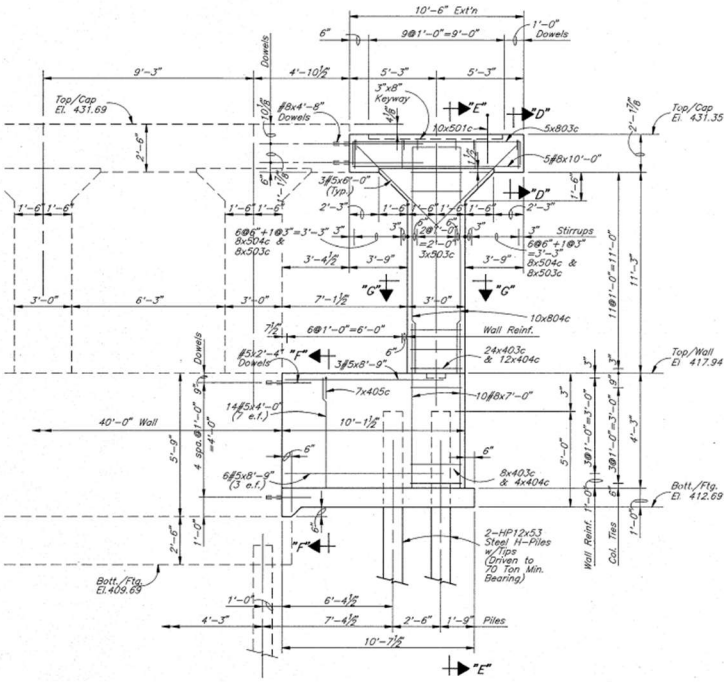

Figure D.30 Transverse Elevation of Interior Pier Column Addition of Bridge (NBI 14650) (1991).

Capacity

2. Identify Mechanism of Hinge Formation

A limit analysis is used to determine the controlling mechanism of hinge formation of the frame bent in the transverse direction. Two mechanisms of hinge formation are considered: one where plastic hinges form at the base and the top of every column, and another where plastic hinges form at the base of the columns and at either end of each beam, shown in Figure D.31 and Figure D.32, respectively.

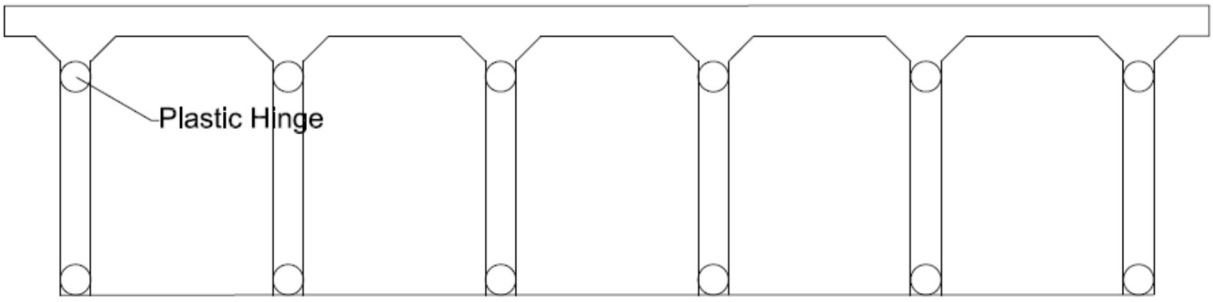

Figure D.31 The First Mechanism of Hinge Formation: Plastic Hinges Formed at Base and Top of Columns

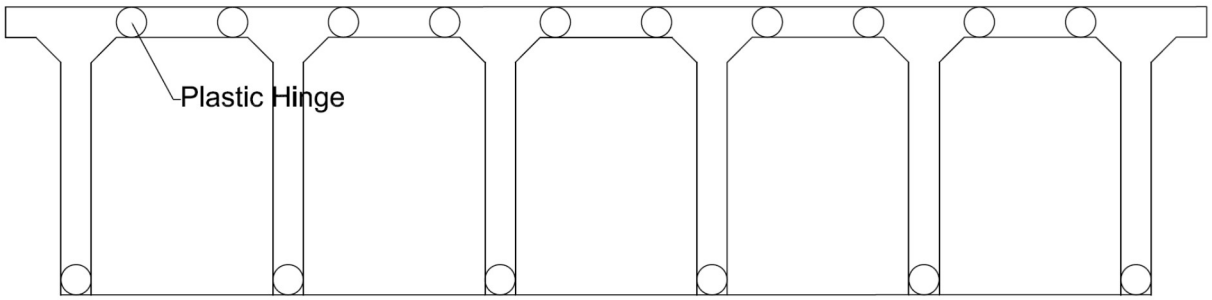

Figure D.32 The Second Mechanism of Hinge Formation: Plastic Hinges Formed at Base of Columns and End of Beams

The controlling mechanism of hinge formation is the mechanism that results in the smallest base shear, calculated as

$$V_{bs} = \frac{\sum M_u}{H}, \tag{79}$$

where M_u is the ultimate moment calculated using the moment-curvature procedure described in Equations (13) through (25). The reinforcement layouts used to calculate the cracking, yield, and ultimate moments of the column and the beams are shown in Figure D.33 and Figure D.34, respectively. The columns have a reinforcement ratio of 0.91% and the beams have a reinforcement ratio of 1.1%. The moment-curvature relationship is calculated for a single column and beam. Table D.8 and Table D.9 show the moment-curvature results for the columns and the beams in the transverse direction, respectively.

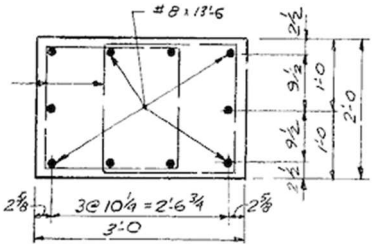

Figure D.33 Typical Cross-section of Column for Bridge (NBI 14650) (1964)

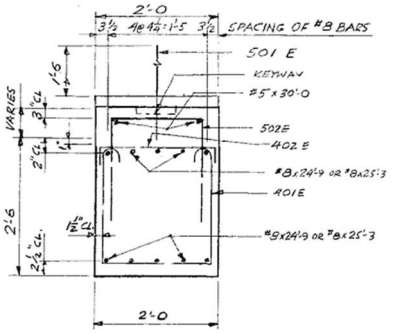

Figure D.34 Typical Cross-section of Beam for Bridge (NBI 14650) (1964)

Table D.8 Column Moment-Curvature Results for the Transverse Direction of Bridge (NBI 14650)

	Pier 2		Pier 3	
	Moment (kip*ft)	**φ**	**Moment (kip*ft)**	**φ**
Cracking	177.5	7.20E-06	177.5	7.20E-06
Yield	278.8	5.68E-05	278.8	5.68E-05
Ultimate	390.6	3.47E-04	390.6	3.47E-04

Table D.9 Beam Moment-Curvature Results for the Transverse Direction of Bridge (NBI 14650)

	Pier 2		Pier 3	
	Moment (kip*ft)	**φ**	**Moment (kip*ft)**	**φ**
Cracking	123.2	8.70E-06	123.2	8.70E-06
Yield	307.1	6.90E-05	307.1	6.90E-05
Ultimate	335.5	4.00E-04	335.5	4.00E-04

Using the ultimate moment and the number of hinges formed, the shear resultant of Pier 2 for the first mechanism of hinge formation is

$$V_{bs,1} = \frac{12 * 390.6\ kip * ft}{11.25\ ft} = 416.64\ kips. \tag{80}$$

The shear resultant of Pier 2 for the second mechanism of hinge formation is

$$V_{bs,2} = \frac{6 * 390.6\ kip * ft + 10 * 335.5\ kip * ft}{11.25\ ft} = 506.54\ kips. \tag{81}$$

The shear resultants of Pier 2 for the first and section mechanisms are 426.1 *kips* (1895.39 *kN*) and 518.1 *kips* (2304.62 *kN*), respectively. For both piers, the first mechanism of hinge formation governs, meaning that plastic hinges will form only in the columns.

The controlling mechanism of hinge formation for frame bents in the longitudinal direction is the formation of a plastic hinge at the base of each column. The ultimate force the pier can take in the longitudinal direction is calculated using Equation (11).

3. Base Shear

The base shear for the controlling flexure mechanism in the transverse direction is for the two interior piers is

$$V_{bs} = [416.6 \quad 426.1] kips. \tag{82}$$

In the longitudinal direction, the bents are modeled as being fixed at the base. The moment-curvature relationship in the longitudinal direction was developed using the procedure described in Equations (13) through (25) and the results are shown in Table D.10.

Table D.10 Column Moment-Curvature Results for the Longitudinal Direction of Bridge (NBI 14650)

	Pier 2		**Pier 3**	
	Moment (kip*ft)	***φ***	**Moment (kip*ft)**	***φ***
Cracking	118.3	1.09E-05	118.3	1.09E-05
Yield	203.6	8.62E-05	203.6	8.62E-05
Ultimate	254.9	5.23E-04	254.9	5.23E-04

The base shear in the longitudinal direction is calculated using H as the total height of the bent, including the bent cap

$$V_{bs} = \frac{\sum M_u}{H} = \frac{6 * 254.9\ kip * ft}{12.75\ ft} = 120\ kips. \tag{83}$$

The base shear in the two piers in the longitudinal direction is

$$V_{bs} = [120 \quad 122.4]\ kips. \tag{84}$$

4. Shear Capacity of Pier

The shear capacity of the piers in the transverse direction is calculated using Equations (50) and (51) and multiplied by the number of columns in each pier. Each column has #3 ties spaced at 12 *in* (30.48 *cm*) on center. The shear capacity of Pier 2 in the transverse direction is the minimum of

$$V_n = 6 * (0.25 * 3000\ psi * 24in * 23.4in) = \ 2527.2\ kips \tag{85}$$

$$V_n = 6 * \left(0.0316 * 2 * \sqrt{3\ ksi} * 24 * 23.4\ in + \frac{0.22\ in^2 * 40ksi * 23.4in}{12\ in}\right) = 471.3\ kips. \tag{86}$$

The shear capacity of each pier in the transverse direction is found as

$$V_n = [473.1 \quad 473.1] kips. \tag{87}$$

The shear capacity in the longitudinal direction is calculated using the same equations. The shear capacity of Pier 2 in the longitudinal direction is the minimum of

$$V_n = 6 * (0.25 * 3000\ psi * 36in * 16.5in) = \ 2673\ kips \tag{88}$$

$$V_n = 6 * \left(0.0316 * 2 * \sqrt{3\ ksi} * 36 * 16.5\ in + \frac{0.22\ in^2 * 40ksi * 16.5in}{12\ in}\right) = 462.7\ kips. \tag{89}$$

The shear capacity of the two piers in the longitudinal direction is

$$V_n = [462.7 \quad 462.7] kips. \tag{90}$$

5. Horizontal Shear Capacity of Connection

The horizontal shear capacity of the connection comes from the strength of the reinforcement extending from the bent cap into the deck and the frictional resistance of the weight of the deck supported by each pier, with an assumed frictional coefficient (μ_s) of 0.6 (Metzger, 2004). There are 7-#5 bars extending from the bent cap to the deck, shown in Figure D.29. The calculations for $m_{pier}$is shown in the demand section. The shear capacity of the connection for Pier 2 is

$$V_{conn} = V_{sf} + V_{cfr}, \tag{91}$$

where

$$V_{sf} = \ \mu_s * A_v * f_y = 0.6 * 7 * 0.31in^2 * 40ksi = 52.1\ kips \tag{92}$$

$$V_{cfr} = \ \mu_s * m_{pier} * g = 0.6 * 1.98\frac{kip}{g} * g = 459.2\ kips \tag{93}$$

$$V_{conn} = 52.1\ kips + 477.6\ kips = 511.3\ kips. \tag{94}$$

The horizontal shear capacity of the connection of each pier is

$$V_{conn} = [511.3 \quad 511.3]\ kips. \tag{95}$$

6. Identify Limiting Capacity

With the values for the three potential failure mechanisms considered (base shear based on flexure mechanism, transverse shear, and shear connection capacity), the limiting lateral force is identified as the minimum value. Thus, for Pier 2, the limiting capacity in the transverse direction is

$$C_{limit} = \min(416.6, 473.1, 511.3)\ kips = 416.6\ kips. \tag{96}$$

Thus, Pier 2 is controlled by the base shear from the flexure mechanism 1 in the transverse direction. The controlling capacity and corresponding mechanism of failure for all piers in the transverse and longitudinal direction is summarized in Table D.11 and Table D.12.

Table D.11 Limiting Capacity of Substructure in Transverse Direction of Bridge (NBI 14650)

Pier No.	Capacity–Trans.	Mechanism
2	416. 6 kips	Base Shear (1)
3	426.2 kips	Base Shear (1)

Table D.12 Limiting Capacity of Substructure in Longitudinal Direction of Bridge (NBI 14650)

Pier No.	Capacity–Long.	Mechanism
2	120 kips	Base Shear
3	122.4 kips	Base Shear

Demand

7. 2-D Bridge Model

The stiffness in the transverse direction, for reinforced concrete superstructures, is derived from the stiffness of the substructure as well as the stiffness of the deck. In contrast, the stiffness in the longitudinal direction is derived solely from the stiffness of the substructure.

7.1a Transverse Stiffness

Each pier is modeled as a planar moment resisting frame with translation allowed at top of the pier and rotation allowed at each node, shown in Figure D.35.

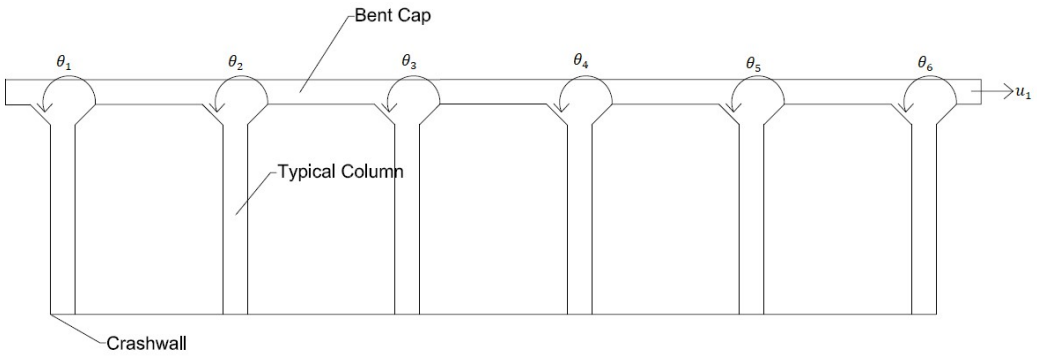

Figure D.35 Transverse Elevation of Interior Bent with Degrees of Freedom Shown (NBI 14650)

The stiffness matrix for each bent is assembled using the stiffness matrix of a single bay frame as the elemental matrix. The assembled pier stiffness matrix is shown in Table D.13. The pier stiffness matrix is then condensed to obtain the stiffness for the translational degree-of-freedom. The stiffness of each pier is

$$K_{pier} = [6644.6 \quad 7030.2]\frac{kips}{in}. \tag{97}$$

As described earlier, the bridge deck is modeled as a deep girder with rotation and translation allowed at each intermediate bent and only rotation allowed at the abutments. A beam element matrix that includes shear effect is used as the elemental matrix and the stiffness of each pier is added to the corresponding translational degree of freedom. The matrix is condensed down to the translational degrees of freedom and the resulting matrix is the stiffness matrix in the transverse direction. Table D.14 shows the pre-condensed deck stiffness matrix where the shear term is

$$\mu = \frac{12E_d I_d}{GA_v l_{pier}^2}. \tag{98}$$

The condensed form of the transverse deck stiffness is

$$\boldsymbol{K} = \begin{bmatrix} 63277 & -40662 \\ -40662 & 63662 \end{bmatrix}\frac{kip}{in}. \tag{99}$$

Table D.13 Interior Pier Stiffness Matrix in the Transverse Direction (NBI 14650)

Degree of freedoms	u_1	θ_1	θ_2	θ_3	θ_4	θ_5	θ_6
u_1	$N_c \frac{12A}{H^3}$	$\frac{6A}{H^2}$	$\frac{6A}{H^2}$	$\frac{6A}{H^2}$	$\frac{6A}{H^2}$	$\frac{6A}{H^2}$	$\frac{6A}{H^2}$
θ_1	$\frac{6A}{H^2}$	$\frac{4A}{H}+\frac{4B}{s_{clear}}$	$\frac{2B}{s_{clear}}$	0	0	0	0
θ_2	$\frac{6A}{H^2}$	$\frac{2B}{s_{clear}}$	$\frac{4A}{H}+2\frac{4B}{s_{clear}}$	$\frac{2B}{s_{clear}}$	0	0	0
θ_3	$\frac{6A}{H^2}$	0	$\frac{2B}{s_{clear}}$	$\frac{4A}{H}+2\frac{4B}{s_{clear}}$	$\frac{2B}{s_{clear}}$	0	0
θ_4	$\frac{6A}{H^2}$	0	0	$\frac{2B}{s_{clear}}$	$\frac{4A}{H}+2\frac{4B}{s_{clear}}$	$\frac{2B}{s_{clear}}$	0
θ_5	$\frac{6A}{H^2}$	0	0	0	$\frac{2B}{s_{clear}}$	$\frac{4A}{H}+2\frac{4B}{s_{clear}}$	$\frac{2B}{s_{clear}}$
θ_6	$\frac{6A}{H^2}$	0	0	0	0	$\frac{2B}{s_{clear}}$	$\frac{4A}{H}+\frac{4B}{s_{clear}}$

Where: $A = E_c I_c \quad B = E_c I_b$

Table D.14 Deck Stiffness Matrix in the Transverse Direction (NBI 14650)

Degree of freedoms	u_1	u_2	θ_1	θ_2	θ_3	θ_4
u_1	$\frac{12E_dI_d}{(1+\mu)l_1^3} + \frac{12E_dI_d}{(1+\mu)l_2^3} + K_{pier}$	$-\frac{12E_dI_d}{(1+\mu)l_2^3}$	$-\frac{6E_dI_d}{(1+\mu)l_1^2}$	$-\frac{6E_dI_d}{(1+\mu)l_1^2} + \frac{6E_dI_d}{(1+\mu)l_2^2}$	$\frac{6E_dI_d}{(1+\mu)l_2^2}$	0
u_2	$-\frac{12E_dI_d}{(1+\mu)l_2^3}$	$\frac{12E_dI_d}{(1+\mu)l_2^3} + \frac{12E_dI_d}{(1+\mu)l_2^3} + K_{pier}$	0	$-\frac{6E_dI_d}{(1+\mu)l_2^2}$	$-\frac{6E_dI_d}{(1+\mu)l_2^2} + \frac{6E_dI_d}{(1+\mu)l_3^2}$	$\frac{6E_dI_d}{(1+\mu)l_3^2}$
θ_1	$-\frac{6E_dI_d}{(1+\mu)l_1^2}$	0	$\frac{(4+\mu)E_dI_d}{(1+\mu)l_1}$	$\frac{(2-\mu)E_dI_d}{(1+\mu)l_1}$	0	0
θ_2	$-\frac{6E_dI_d}{(1+\mu)l_1^2} + \frac{6E_dI_d}{(1+\mu)l_2^2}$	$-\frac{6E_dI_d}{(1+\mu)l_2^2}$	$\frac{(2-\mu)E_dI_d}{(1+\mu)l_1}$	$\frac{(4+\mu)E_dI_d}{(1+\mu)l_1} + \frac{(4+\mu)E_dI_d}{(1+\mu)l_2}$	$\frac{(2-\mu)E_dI_d}{(1+\mu)l_2}$	0
θ_3	$\frac{6E_dI_d}{(1+\mu)l_2^2}$	$-\frac{6E_dI_d}{(1+\mu)l_2^2} + \frac{6E_dI_d}{(1+\mu)l_3^2}$	0	$\frac{(2-\mu)E_dI_d}{(1+\mu)l_2}$	$\frac{(4+\mu)E_dI_d}{(1+\mu)l_2} + \frac{(4+\mu)E_dI_d}{(1+\mu)l_3}$	$\frac{(2-\mu)E_dI_d}{(1+\mu)l_3}$
θ_4	0	$\frac{6E_dI_d}{(1+\mu)l_3^2}$	0	0	$\frac{(2-\mu)E_dI_d}{(1+\mu)l_3}$	$\frac{(4+\mu)E_dI_d}{(1+\mu)l_3}$

7.1b Longitudinal Stiffness

In the longitudinal direction, the bridge is modeled as a SDOF system with the piers behaving as springs in parallel. Each column is assumed to be fixed at the base and the top. The stiffness of Pier 2 in the longitudinal direction is

$$K_{pier} = N_c * \frac{12E_cI}{H^3} = 6 * \frac{12 * 3155\ ksi * \frac{36in * (24in)^3}{12}}{(12.75ft)^3} = 2630.3\frac{kip}{in}. \quad (100)$$

The longitudinal stiffness of each pier is

$$K_{pier} = [2630.3 \quad 2791.3]\frac{kips}{in}. \quad (101)$$

7.2a Transverse Mass

The activated mass of the bridge in the transverse direction is calculated using superstructure geometry and barrier dimensions. Since the bridge is a slab-deck bridge, most of the mass comes from the deck. The mass of the primary structural system over Pier 2 is calculated using Equation (36) and is

$$m_{SS} = \frac{40.75\ ft * (55.4\ ft * 25.5\ in * 150\ pcf)}{386.4\frac{in}{s^2}} = 1.89\frac{kips}{g}. \quad (102)$$

The mass of the concrete barrier railing type BR-5, calculated using Equation (37) is

$$m_R = \frac{40.75ft * (150pcf * 2.58ft^3 + 26.3lbs)}{386.4\frac{in}{s^2}} = 0.08\frac{kip}{g}. \quad (103)$$

The mass of the superstructure over each pier is

$$m_{pier} = [1.98 \quad 1.98]\frac{kip}{g}. \quad (104)$$

7.2b Longitudinal Mass

In the longitudinal direction, the bridge is modeled as a SDOF system where the mass is the total mass of the bridge

$$m_{sup} = 5.83\frac{kip}{g}. \quad (105)$$

7.3 Equation-of-Motion

Because the deck is assumed to add stiffness in the transverse direction, the bridge is modeled as a MDOF system with the number of degrees-of-freedom corresponding to the number of intermediate piers and the mass, stiffness and damping terms written as matrices. The mass matrix for the transverse direction is

$$\boldsymbol{M} = \begin{bmatrix} 1.98 & 0 \\ 0 & 1.98 \end{bmatrix}\frac{kip}{g}. \quad (106)$$

The decoupled stiffness matrix is calculated as

$$\boldsymbol{\Phi}^{\boldsymbol{T}}\boldsymbol{K}\boldsymbol{\Phi}, \tag{107}$$

where Φ is the mode shape of the structure, found by solving the eigen-value problem and is

$$\boldsymbol{\Phi} = \begin{bmatrix} -0.71 & -0.71 \\ -0.71 & 0.71 \end{bmatrix}. \tag{108}$$

Here the fundamental mode shape is shown in column 1, and additional modes are in the corresponding columns. Using this, the decoupled stiffness matrix in the transverse direction is

$$\boldsymbol{K_{dc}} = \begin{bmatrix} 22810 & 0 \\ 0 & 104130 \end{bmatrix} \frac{kip}{in}. \tag{109}$$

Using the assumption and Equation (43), previously defined for damping, the decoupled damping matrix for this bridge is taken as

$$\boldsymbol{C_{dc}} = \begin{bmatrix} 21.25 & 0 \\ 0 & 45.41 \end{bmatrix} \frac{kip * s}{in}. \tag{110}$$

The equation-of-motion in the transverse direction is

$$\begin{bmatrix} 1.98 & 0 \\ 0 & 1.98 \end{bmatrix} \frac{kip}{g} \ddot{x}_{sup} + \begin{bmatrix} 21.25 & 0 \\ 0 & 45.41 \end{bmatrix} \frac{kip * s}{in} \dot{x}_{sup} + \begin{bmatrix} 22810 & 0 \\ 0 & 104130 \end{bmatrix} \frac{kip}{in} * x_{sup} = -\begin{bmatrix} 1.98 & 0 \\ 0 & 1.98 \end{bmatrix} \frac{kips}{g} \ddot{x}_g \tag{111}$$

and the stiffness in the longitudinal direction is the sum of the stiffnesses of each pier, and is

$$\mathrm{K}_{sub} = 5421.6 \frac{kip}{in}. \tag{112}$$

The damping in the longitudinal direction is

$$c_{sub} = 17.77 \frac{kips * s}{in} \tag{113}$$

The equation-of-motion in the longitudinal direction is

$$5.83 \frac{kips}{g} \ddot{x}_s + \left(17.77 \frac{kips * s}{in}\right) \dot{x}_s + \left(5421.6 \frac{kips}{in}\right) x_s = -5.83 \frac{kips}{g} \ddot{x}_g. \tag{114}$$

8. Pushover analysis

A displacement-controlled pushover analysis is performed to better understand the redistribution of forces as piers progressively exhibit nonlinear behavior. By incrementally applying a displacement to the structure beginning with the first yield of the stiffest pier through the formation of plastic hinges in all piers, the force redistribution is quantified. The results of the pushover analysis in the transverse direction and the longitudinal direction is shown in Figure D.36 and Figure D.37, respectively.

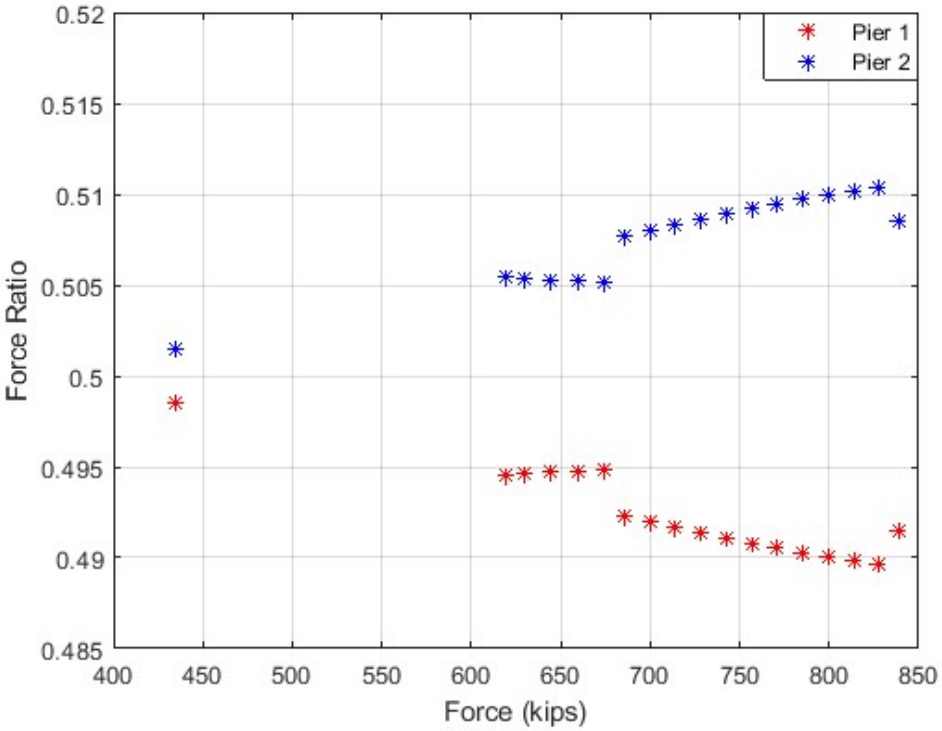

Figure D.36 Pushover Analysis Results in the Transverse Direction (NBI 14650)

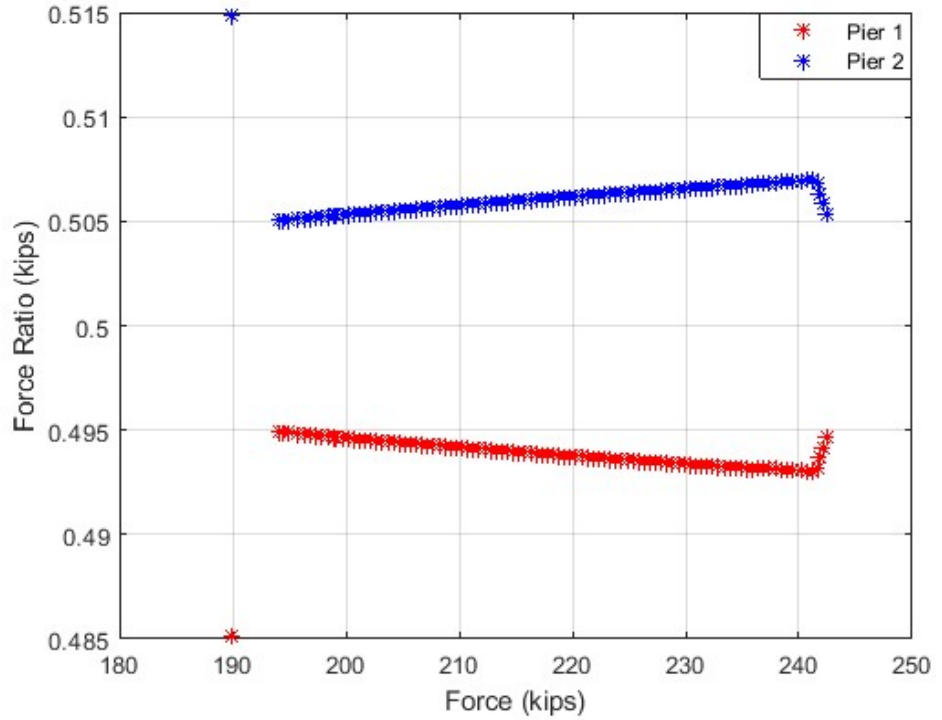

Figure D.37 Pushover Analysis Results in the Longitudinal Direction (NBI 14650)

9. Apply Ground Motions

The same process for developing and applying ground motions used in Case Study 1 and 2 is used to develop 100 stochastically-simulated ground motions using generic site amplification factors.

10. Maximum Force and Displacement

The process described in Case Study 1 is used to calculate the maximum displacement of the bridge and the force transferred to each pier in both directions.

11. Compare Force to Capacity

In each direction, the maximum force resulting from the application of each of the seismic ground motions is compared to the capacity to assess if the capacity is exceeded. For Structure Number 041-42-05080 BNBL (NBI 14650), the maximum force resulting from 100 ground motions exceeds the capacity in the transverse direction, controlled by the base shear from the flexure mechanism 1, 71% of the time. In the longitudinal direction, the maximum force exceeds the capacity, controlled be the base shear, 100% of the time.

Vulnerability Assessment of Detail

Frame bent substructures in both the longitudinal and transverse direction have the potential for moderate vulnerability due to the formation of the identified hinge mechanism for the given level of seismic excitation. The precipitation of the hinge mechanism is expected to be ductile.

Case Study 4: Prestressed Concrete Bridge with Two-Story Rectangular Frame Bents

1. Bridge Information

Structure Number 050-15-00210 BEBL (NBI 18790) is a five-span prestressed concrete bridge located in Dearborn County of the Seymour District. Originally constructed in 1938, the bridge has had two rehabilitations. In 1976, the bridge underwent general rehabilitation and in 2016, the superstructure was replaced (steel to prestressed) and both the superstructure and substructure were widened. With this rehab, an additional column was added to each pier. The superstructure is composed of seven Bulb-Tee 66 × 60 Beams with an 8-*inch* (20.3 *cm*) reinforced-concrete deck. The bridge is skewed at 20-*degrees*, has span lengths of approximately 82′–2″ (25 *m*), 105′–7.5″ (32 *m*), 113′–9″ (34.4 *m*), 105′–7.5″ (32 *m*), and 81′–3″ (24.7 *m*), and is 72′–2″ (21.9 *m*) wide.

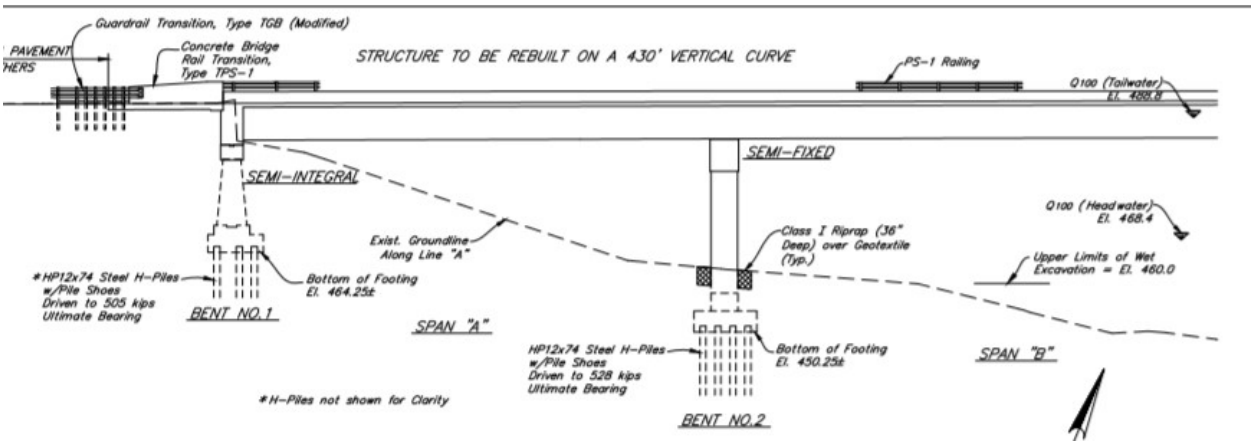

Figure D.38 Elevation View of the Bridge—Span 1 and 2 (NBI 18790) (2014)

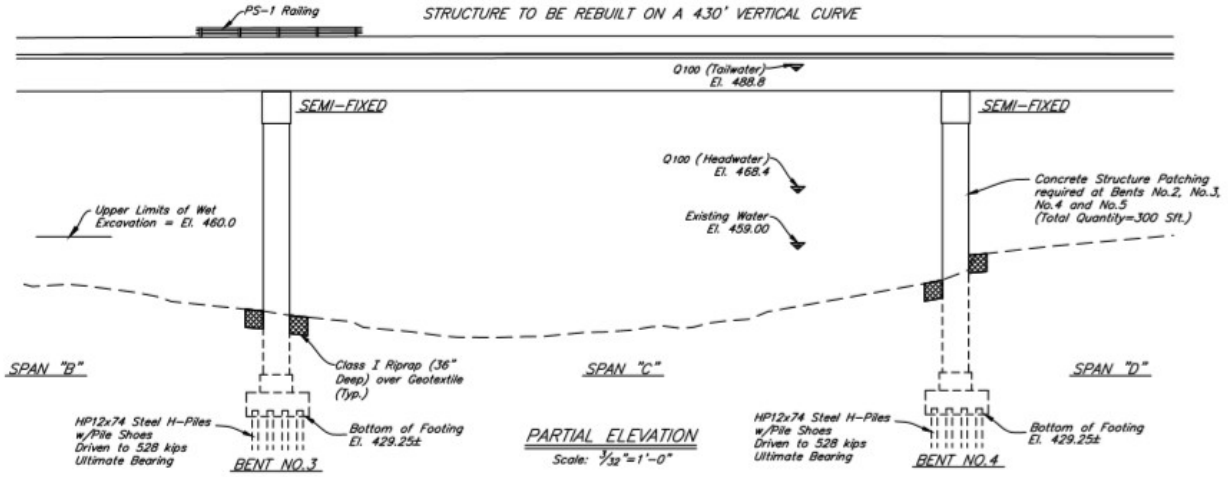

Figure D.39 Elevation View of the Bridge—Span 2, 3, and 4 (NBI 18790) (2014)

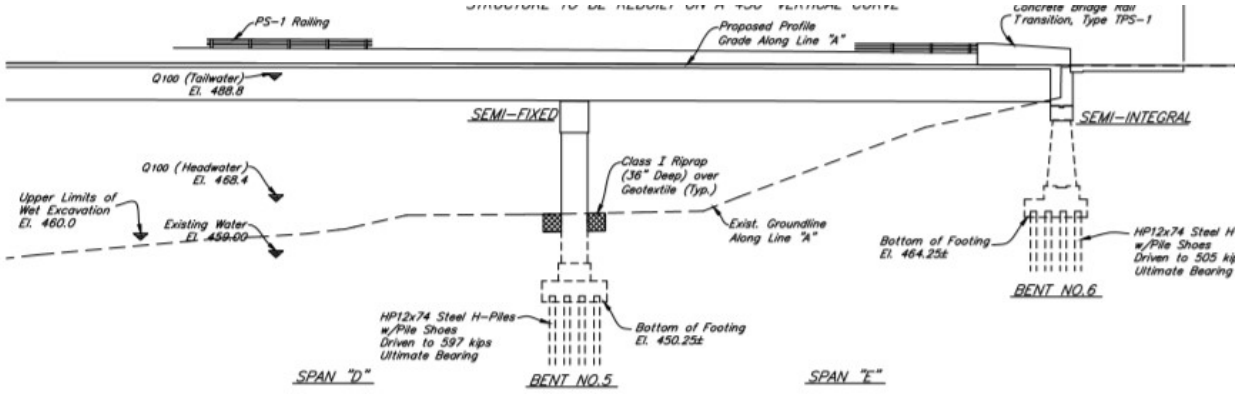

Figure D.40 Elevation View of the Bridge—Span 4 and 5 (NBI 18790) (2014)

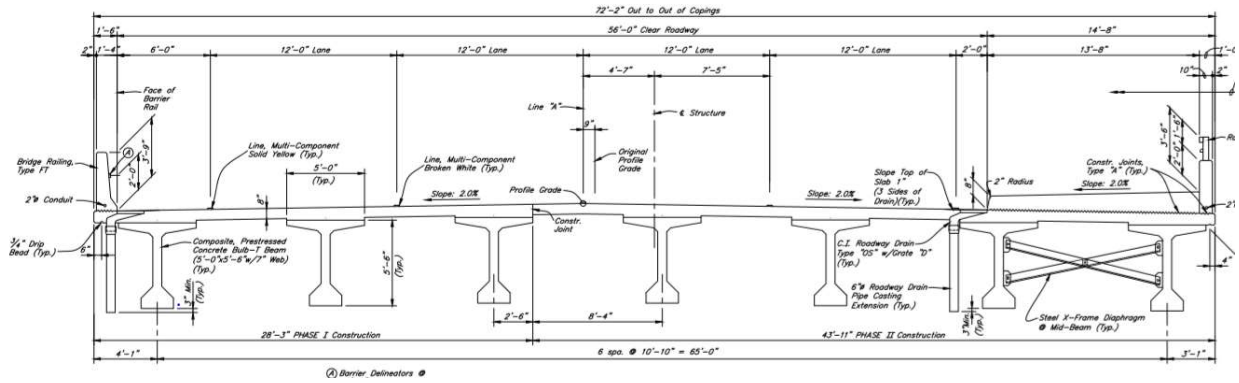

Figure D.41 Typical Section of the Bridge (NBI 18790) (2014)

The bridge is supported by two integral-type abutments and four interior rectangular column frame-bent piers, as shown in Figure D.38 through Figure D.40. From left to right, the piers are classified as one-story, two-story, two-story, and one-story frame bents. Due to the presence of semi-integral type abutments, as shown in Figures D.41 through Figure D.44, we can assume that the bridge will not be vulnerable to seismic hazards in the longitudinal direction of motion. Therefore, only the calculations for the transverse direction are presented.

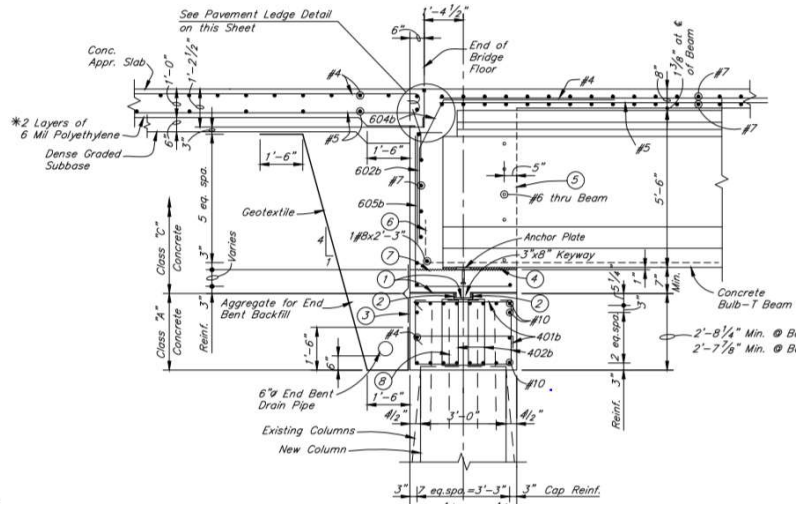

Figure D.42 Abutment Detail of the Bridge (NBI 18790) (2014)

Pier 2 and 5 are composed of four, 48″ × 48″ (122 *cm* × 122 *cm*) rectangular-type reinforced-concrete (RC) columns and a 54″ × 54″ (137 *cm* × 137 *cm*) bent cap. The columns have a clear height of 21′–0″ (6.4 *m*) and a clear span of 21′–0″ (6.4 *m*), except for the outermost column, which has a clear span of 7′–1/2″ (2.15 *m*). Pier 3 and 4 is a two-story frame bent. The bottom story is composed of four, 54″ × 54″ (137 *cm* × 137 *cm*) rectangular-type RC columns whereas the top story is composed of four, 48″ × 48″ (122 *cm* × 122 *cm*) rectangular-type RC columns and a 54″ × 54″ (137 *cm* × 137 *cm*) bent cap. The bottom-story columns have a conservative modeling height of 23′–6″ (7.16 *m*) and a clear span of 20′–6″ (6.24 *m*), except for the outermost column, which has a clear span of 7′ (2.13 *m*). Naturally, the spacing of the top columns remains

the same as the bottom. The modeling height of the top columns is taken as 18′–3″ (5.5 *m*). The modeling height is defined by the change in cross-sectional area of the column.

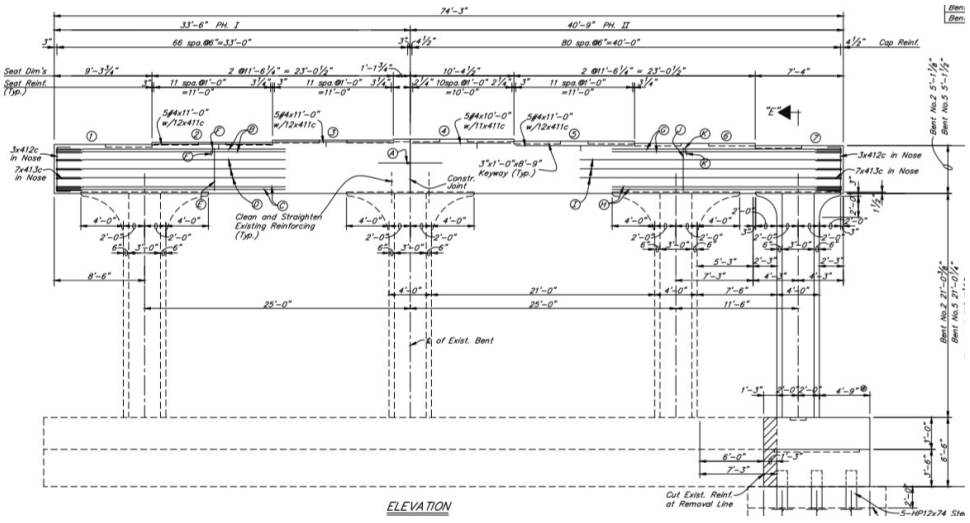

Figure D.43 Transverse Elevation of Interior Pier 2 (NBI 18790) (2014)

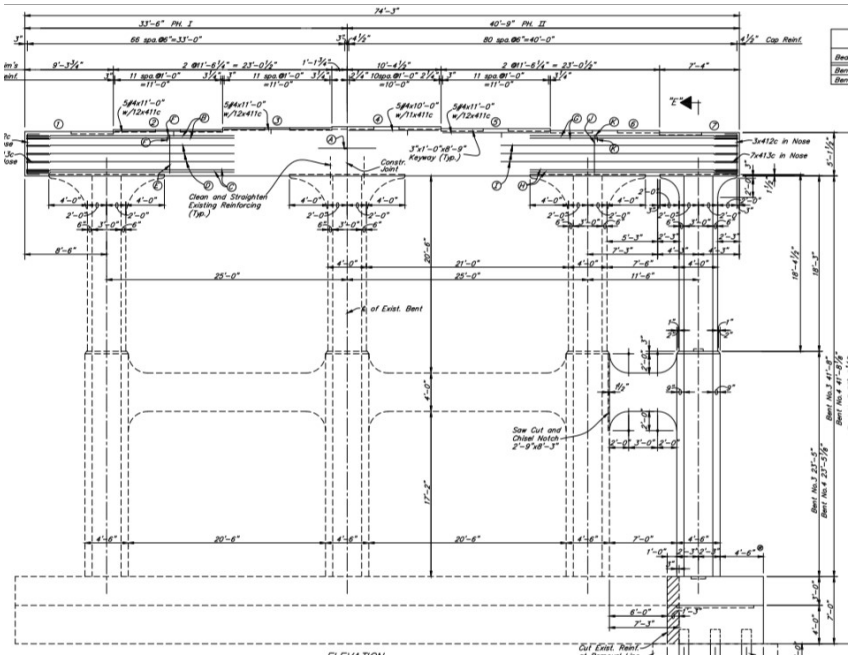

Figure D.44 Transverse Elevation of Interior Pier 3 (NBI 18790) (2014)

Capacity

2. Identify Mechanism of Hinge formation

A limit analysis is used to determine the controlling mechanism of hinge formation of the frame bents. For Pier 2 and 5, the same two mechanism of hinge formations identified for the previous RC example are considered, shown in Figure D.31, Figure D.32. For Pier 3 and 4, three different mechanism of hinge formations are considered: formation of two plastic hinges in first-story columns (the first mechanism of hinge formation), formation of a plastic hinge in the column at the base and bent cap and two hinges in each intermediate beam (the second mechanism of hinge formation), and the formation of a plastic hinges in the column at the base and two plastic hinges in each intermediate beam and bent cap (the third mechanism of hinge formation). The mechanism of hinge formations for Piers 3 and 4 are shown in Figure D.45, Figure D.46, and Figure D.47, respectively.

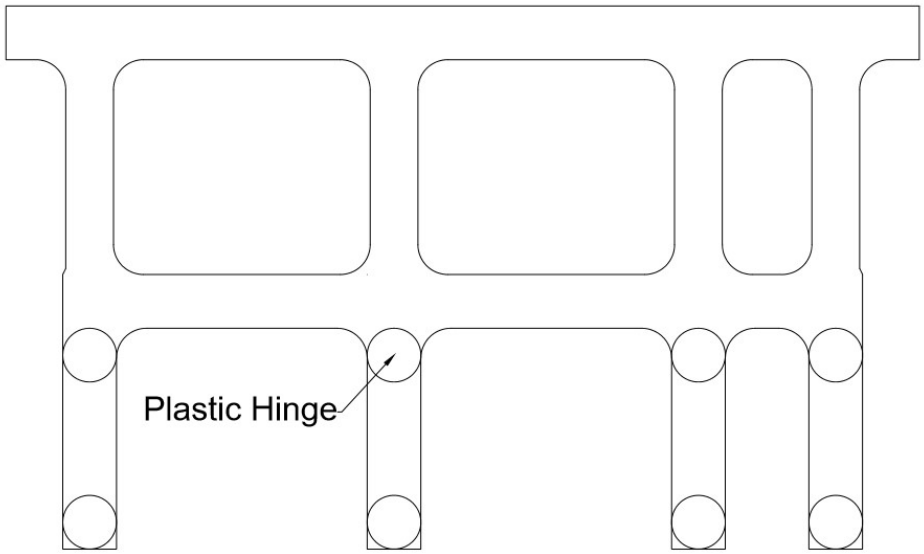

Figure D.45 The First Mechanism of Hinge Formation

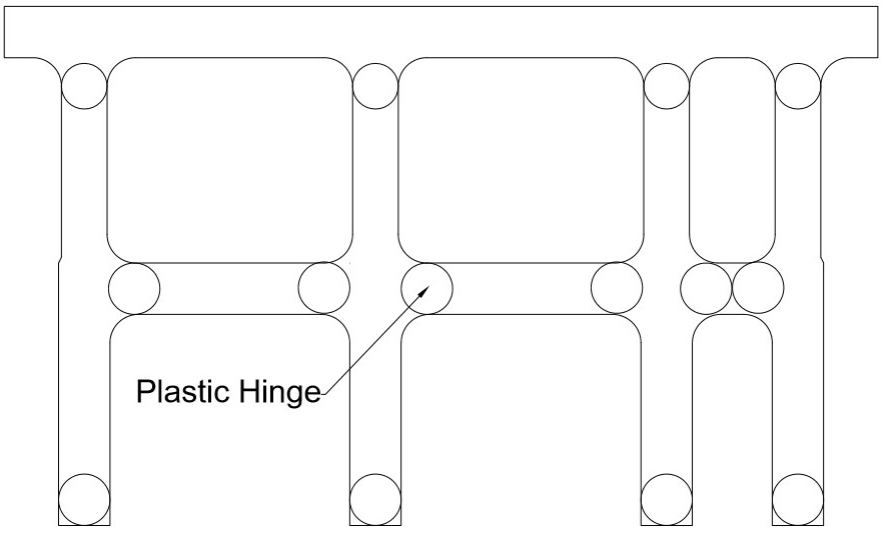

Figure D.46 The Second Mechanism of Hinge Formation

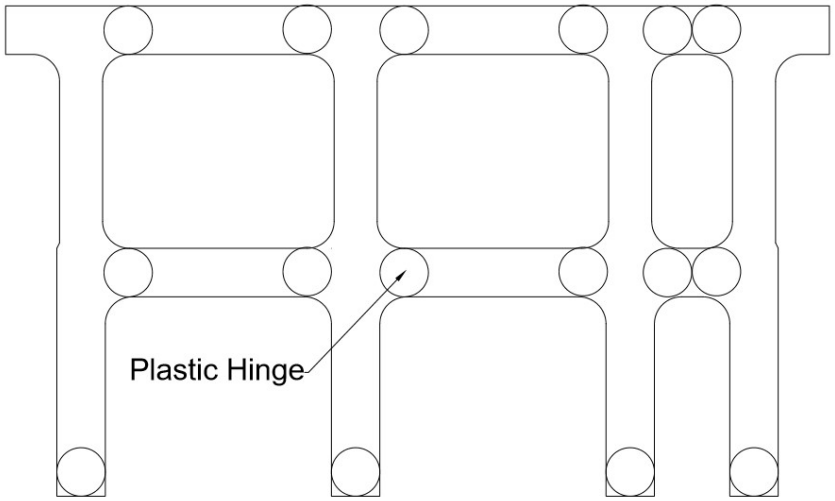

Figure D.47 The Third Mechanism of Hinge Formation

The reinforcement layouts are group based on design similarities are defined as the following: the columns in Pier 2, Pier 5, and the top story of Pier 3 and 4 (column type 1), the columns in the bottom story of Pier 3 and 4 (column type 2), the bent caps of all piers (beam type 1), and the intermediate beams for Pier 3 and 4, are shown in Figure D.48 and Figure D.49, respectively.

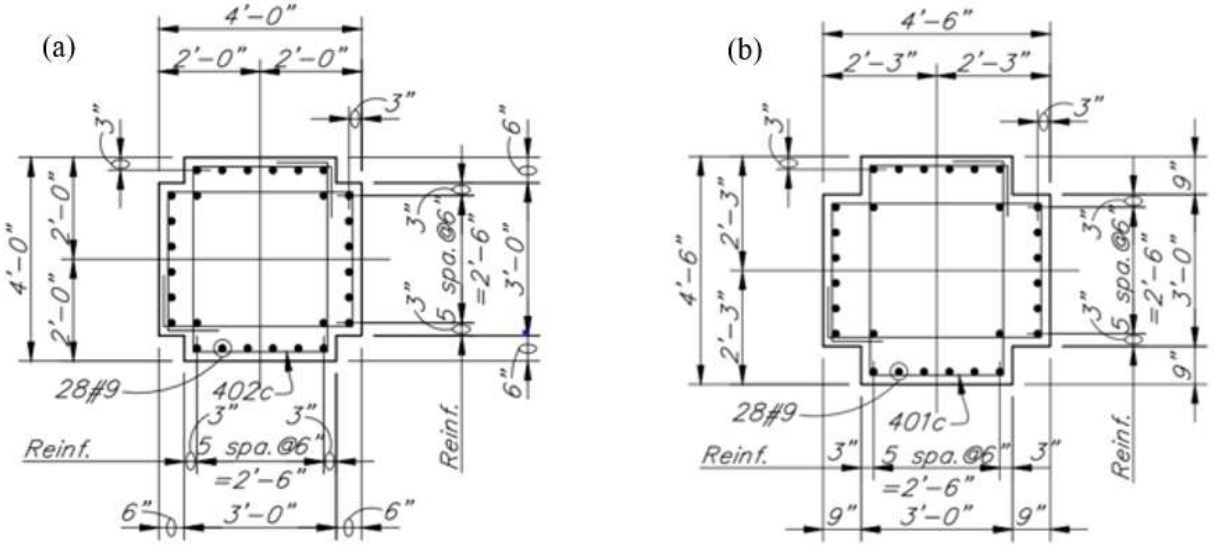

Figure D.48 Typical Cross-Section of Column Type 1 (a) and Column Type 2 (b) (NBI 18790) (2014)

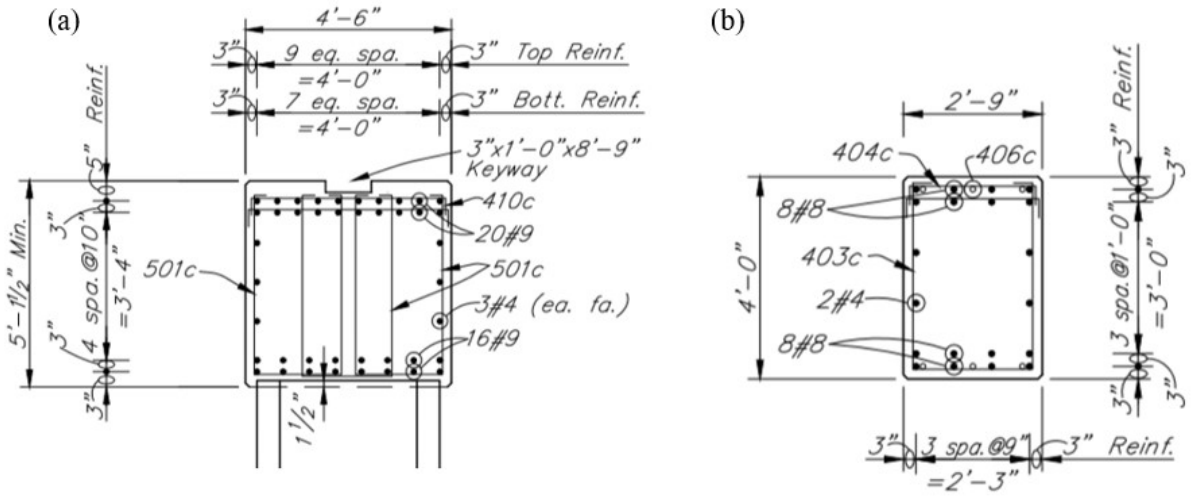

Figure D.49 Typical Cross-Section of the Beam Type 1 (a) and Beam Type 2 (b) (NBI 18790) (2014)

Table D.15 shows the moment-curvature results for the columns and the beams in the transverse direction, respectively.

Table D.15 Column Moment Curvature Results for the Transverse Direction

	Column Type 1		**Column Type 2**		**Beam Type 1**		**Beam Type 2**	
	Moment (kip*ft)	Phi	Moment (kip*ft)	Phi	Moment (kip*ft)	Phi	Moment (kip*ft)	Phi
Cracking	401.5	5.4E-06	571.6	4.8E-06	1198	4.3E-06	468.6	5.4E-06
Yield	1429.3	4.6E-05	1584.1	3.9E-05	2735.4	4.1E-05	769.7	4.2E-05
Ultimate	2063.9	2.8E-04	2365.4	2.4E-04	3398.2	2.4E-04	903.8	2.5E-04

3. Base Shear

Using the ultimate moment and the number of hinges formed, the base shear capacity of Pier 3 for the first mechanism of hinge formation is

$$V_{bs,1} = \frac{2\frac{hinge}{col} * 2361.8\ kip * ft}{23.5\ ft} * 4\frac{col}{pier} = 805\ kips. \quad (115)$$

The base shear capacity of Pier 3 for the second mechanism of hinge formation is

$$V_{bs,2} = \frac{(2361.8 + 2061.6)\frac{kip * ft}{col} * 4\frac{col}{pier}}{0.5 * (23.5 + 18.5)ft} + \frac{2\frac{hinge}{beam} * 902\ kip * ft * 3\frac{beams}{pier}}{\left(\frac{1}{3}\right) * (2 * 20.5\ ft + 7\ ft)} = 1180\ kips. \quad (116)$$

The base shear capacity of Pier 3 for the third mechanism of hinge formation is

$$V_{bs,3} = \frac{2361.8\ \frac{kip*ft}{col} * 4\frac{col}{pier}}{23.5ft} + \frac{2\frac{hinge}{beam} * (902 + 3394.9)\frac{kip*ft}{col} * 3\frac{beams}{pier}}{\left(\frac{1}{3}\right) * (2 * 20.5\ ft + 7\ ft)} = 2013\ kips. \quad (117)$$

The controlling mechanism of hinge formation for Pier 3 and 4 is identified as the first mechanism of hinge formation, weak column–strong beam. The controlling mechanism of hinge formation for Pier 2 and 5 are calculated using the method outlined in Equations (79) to (81). The controlling mechanism are weak column–strong beam and strong column–weak beam, respectively, are 784 and 1,362 *kips*. The mechanism of hinge formation for Pier 2 and 5 is identified as weak column–strong beam.

4. Shear Capacity of Pier

The shear capacity of the pier at the critical locations (defined by the mechanism of hinge formation) are calculated using Equation (85) to (90).

5. Horizontal Shear Capacity of Connection

The shear force is transferred from the superstructure to the substructure using the typical interior pier diaphragm shown in Figure D.17. The capacity of the connection is calculating using Equation (30). The resulting capacities are shown in the table below.

Table D.16 Shear Capacity of Substructure and Connection (NBI 18790)

Pier No.	Shear Capacity–Pier (kips)	Shear Capacity–Connection (kips)
1	1078.4	8064
2	1308.7	8064
3	1308.7	8064
4	1078.4	8064

6. Identify Limiting Capacity

The limiting capacity is identified as the minimum among base shear capacity, substructure shear capacity and shear connection. The controlling capacity and corresponding mechanism of failure for all piers in the transverse direction is summarized in Table D.17.

Table D.1 Limiting Capacity of Substructure in Transverse Direction (NBI 18790)

Pier No.	Capacity–Trans.	Mechanism
2	784 kips	Base Shear (1)
3	804 kips	Base Shear (1)
4	804 kips	Base Shear (1)
5	784 kips	Base Shear (1)

Demand

1. 2-D Bridge Model

The stiffness in the transverse direction is derived solely from the stiffness of the substructure. As mentioned previously, the deck is assumed to be rigid enough to allow the intermediate piers to act as springs in parallel.

7.1a Transverse Stiffness

Piers 2 and 5 are modeled using the frame bent modeling procedure identified in the main document (Case Study 3 through Section 7.1a). Piers 3 and 4 are modeled as a planar moment resisting frame with translation allowed at the top of the pier and intermediate beams and rotation allowed at each node, shown in Figure D.50. Like the single-story modeling procedure, the stiffness matrix for each bent is assembled using the stiffness matrix of a single bay frame as the originating matrix. Only the translational degree of freedom for the bent cap is associated with mass. Therefore, the pier stiffness matrix is then condensed to obtain the stiffness of this translational degree of freedom. The stiffness of all four piers

$$K_{pier} = [3830 \quad 2259 \quad 2520 \quad 3661]\frac{kips}{in}. \tag{1}$$

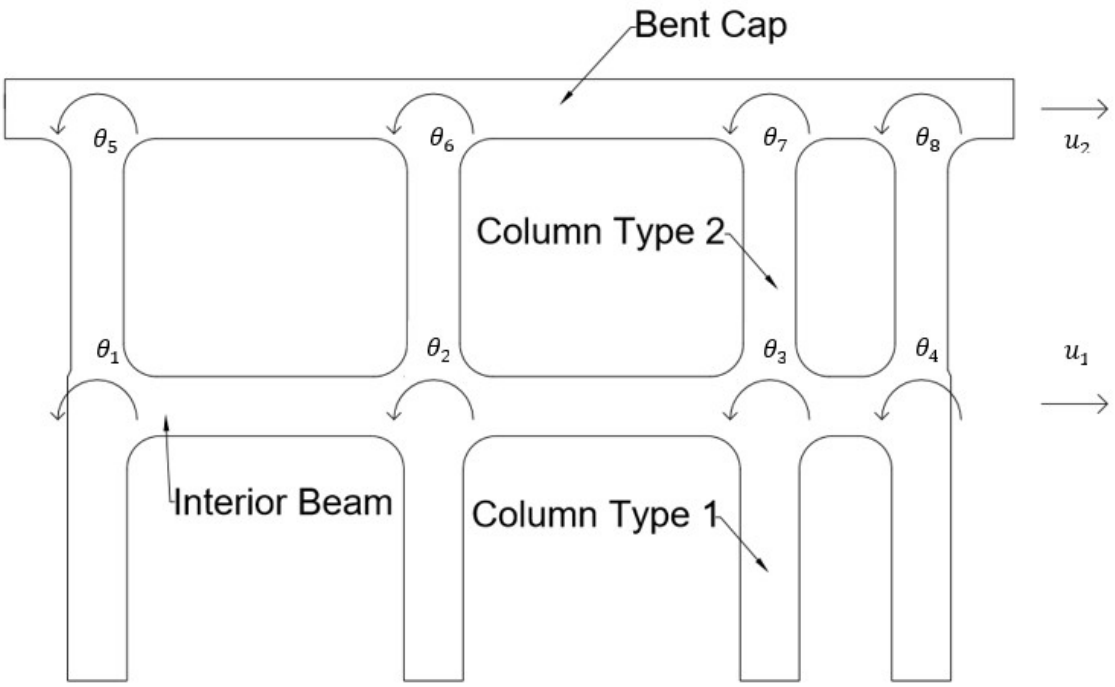

Figure D.50 Transverse Elevation of Interior Bent with Degrees of Freedom Shown

7.2a Transverse Mass

The activated mass of the bridge in the transverse direction is calculated using superstructure geometry and barrier dimensions. Equation (36) to (40) show the details for calculating the mass of each element where the total mass of the superstructure over each pier is calculated using the tributary length of each adjacent span. The total mass is

$$m_{pier} = [4.36 \quad 5.03 \quad 5.03 \quad 4.35]\frac{kip}{g}. \tag{119}$$

7.3 Equation of Motion

Because the rigidity of the deck ensures uniform movement, the total stiffness and mass in the transverse direction is calculated as the summation of the individual pier components. Using the 5% assumption for viscous damping, the components for the equation of motion are calculated as

$$K_{sub} = 12270\frac{kip}{in}, \tag{120}$$

$$m_{sup} = 18.7\frac{kip}{g}, \tag{121}$$

$$c_{sub} = 47\frac{kip * s}{in}. \tag{122}$$

The equation of motion in the longitudinal direction is

$$18.7\,\frac{kips}{g}\ddot{x}_s + \left(47\,\frac{kips * s}{in}\right)\dot{x}_s + (12270\,kips * in)x_s = -18.7\frac{kips}{g}\ddot{x}_g. \quad (123)$$

8. Displacement-Controlled Pushover Analysis

A displacement-controlled pushover analysis is required to better understand the redistribution of forces as piers progressively exhibit nonlinear behavior. The results of the pushover analysis in the transverse direction can be seen in Figure D.51.

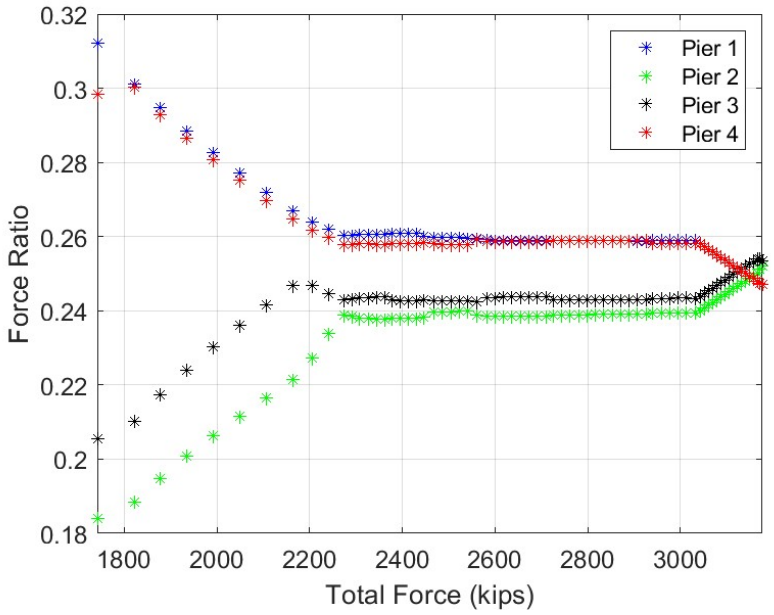

Figure D.51 Displacement-Controlled Pushover Analysis in Transverse Direction for Bridge (NBI 18790)

9. Apply Ground Motions

The same process for developing and applying ground motions is used to develop 100 stochastically-simulated ground motions using generic site amplification factors.

10. Maximum Force and Displacement

The process described in Equation (7) to (10) is used to calculate the maximum displacement of the bridge and the force transferred to each pier.

11. Compare Force Demand to Capacity

In the transverse direction, the maximum force resulting from the application of each of the 100 seismic ground motions is compared to the capacity to assess if the capacity is exceeded. For Structure Number 050-15-00210 B (NBI 18790) the maximum resulting force from 100 ground motions never exceeds the capacity in the transverse direction controlled by the base shear capacity.

Vulnerability Assessment of Detail

Two-story frame bents have the potential for low vulnerability. However, given the uniqueness of the substructure, the vulnerability of every substructures labeled other must be evaluated on a case-by-case basis. Thus, the Level 1 tool does not accommodate the analysis of this substructure, rather recommends a Level 2 assessment.

Case Study 5: Prestressed Concrete Bridge with Frame Bent Substructure with Infill Walls

1. Bridge Information

Structure Number I465-149-08854 JSBL (NBI 50795) is a three-span prestressed concrete bridge located in Marion County of the Greenfield District. Originally built in 2012 as a new bridge replacement, no additional rehabs have occurred. The superstructure is composed of ten Bulb-Tee 78 × 48 Beams with an 8.5 *in* (21.59 *cm*) reinforced-concrete deck. The bridge is skewed at 17-*degrees*, has span lengths of 97′–6″ (29.72 *m*), 148′–6″ (45.26 *m*), and 109′–0″ (33.22 *m*), and is 94′–10.5″ (28.92 *m*) wide.

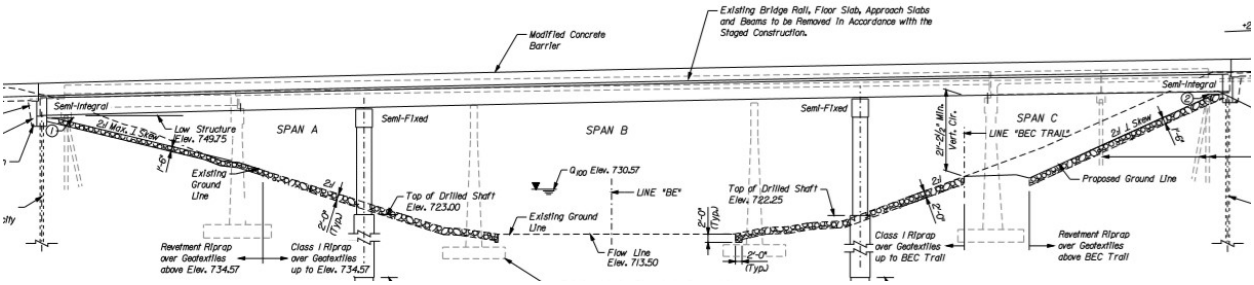

Figure D.52 Elevation View of the Bridge (NBI 50795) (2009)

It is important to note that no plans showing the typical section or details for the prestressed concrete bridge exists. Most of the information for this case study is taken from the steel alternative, with beam information taken from shop drawings provided by INDOT.

The bridge is supported by two integral-type abutments and two interior frame bents with infill walls, as shown in Figure D.52. Due to the presence of semi-integral type abutments, we can assume that the bridge will not be vulnerable to seismic hazards in the longitudinal direction of motion. Therefore, only the calculations for the transverse direction are presented.

Both Pier 2 and 3 are composed of five, 54″ (137.16 *cm*) diameter circular RC columns and a 60″ × 60″ (152.4 *cm* × 152.4 *cm*) minimum depth bent cap. The bridge maintains a superelevation along the profile of the structure; therefore, the columns maintain different clear heights within each pier. Using the drawings shown in Figure D.53, the clear height is taken from the top of the drilled shaft to the base of the bent cap. Additionally, the clear spacing between the columns varies between the bays. As an example, the modeling height for column 1 (left-most column), Pier 2 is taken as 27′–2.5″ (8.29 *m*) with a clear spacing between column 1 and 2 of 17′–6″ (5.33 *m*). Additionally, each bay of the frame bent has a 1–6″ (0.46 *m*) thick infill

wall that extends nearly the entire height of the column. However, as Figure D.53 shows, the height of the wall stops approximately 1′–0″ (0.305 *m*) or less from the base of the bent cap creating an exposed column length significantly less than the diameter of the column. An inspection photo, shown in Figure D.54, depicts this phenomenon more clearly.

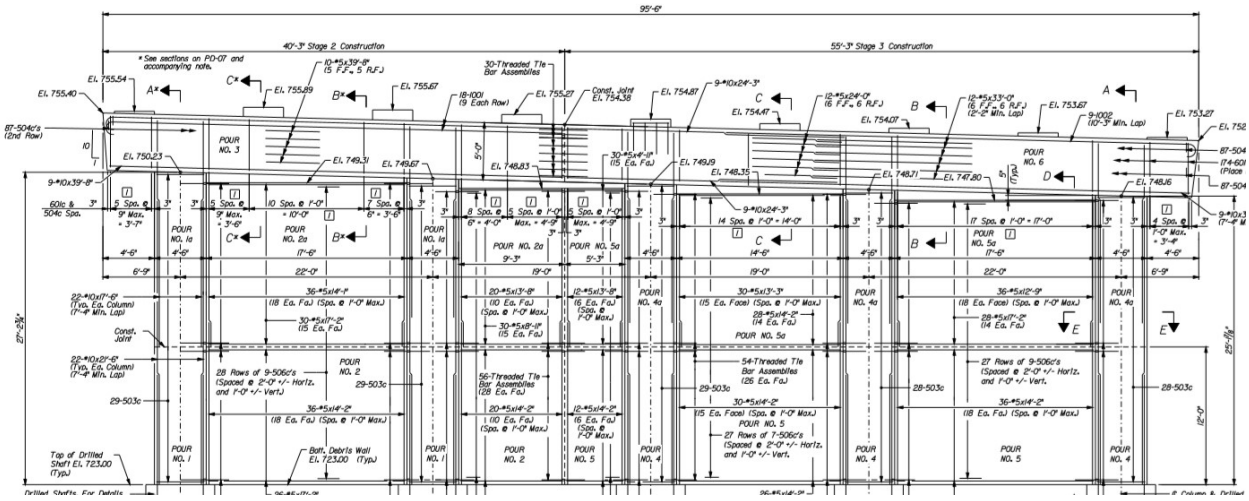

Figure D.53 Transverse Elevation of Interior Pier 2 (NBI 50795) (2009)

Figure D.54 Pier Detail from Inspection Photos (NBI 50795) (BIAS)

Capacity

2. Identify Mechanism of Hinge Formation

The detailing of the pier creates a failure mechanism different than the ductile mechanisms of hinge formation previously explored for frame bent substructures. Because of the minimal exposed column length, it is assumed that this section is incapable of responding in flexure. Rather, the controlling mechanism of hinge formation is controlled by the formation of two plastic hinges in the exterior column and direct shear failure of all other columns. As the earthquake progresses, both exterior columns will have

the potential for developing plastic hinges depending on the motion of the mass at each time step. The exterior column that moves in the direction of the mass is not confined by the interior infill walls and will develop plastic hinges. The reinforcement layout for the columns is shown in Figure D.55. Table D.18 shows the moment-curvature results for the column in the transverse direction.

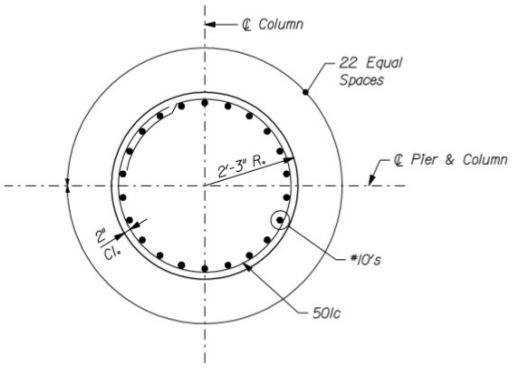

Figure D.55 Typical Cross-Section of Column (NBI 50795) (2009)

Table D.18 Column Moment-Curvature Result (NBI 50795)

	Moment (kip*ft)	$\boldsymbol{\varphi}$
Cracking	571.6	4.8E-06
Yield	1923.3	5.9E-05
Ultimate	2865.7	2.6E-04

3. Base Shear

Using the moment-curvature results and the identified mechanism of hinge formation, the capacity of the structure is calculated using Equations (13) through (25).

The formation of the plastic hinges in the controlling external column is

$$V_{bs} = \frac{2M_u}{H} = 2 * \frac{2865.7\ kip * ft}{27.2\ ft} = 210.7\ kips. \tag{124}$$

The direct shear capacity of each circular column is calculated using AASHTO Section 5.13.2.4.2. The direct shear capacity of each column is taken as

$$V_d = \min\left(\frac{0.2 f_c' A_g}{2}, \frac{0.8 f_c' A_g}{2}\right) = 0.2 * (3.5\ ksi) * \frac{\pi(54\ in)^2}{8} = 801.6\ kips \tag{125}$$

where A_g is applicable if and only if the longitudinal reinforcement is symmetrical about the middle of the column. Otherwise, the area should be calculated using parameters specifically defined in AASHTO 5.13.2.4.2-1/2.

The total capacity of the pier is calculated as

$$V_p = V_u + (N_c - 1)V_d = \ 3417\ kips. \tag{126}$$

4. Shear Capacity of Pier

The shear capacity of the pier at the critical locations (defined by the mechanism of hinge formation) is calculated using Equation (85) through (90).

5. Horizontal Shear Capacity of Connection

The shear force is transferred from the superstructure to the substructure using the typical interior pier diaphragm shown in Figure D.17. The capacity of the connection is calculating using Equation (30). The resulting capacities are shown in the table below.

Table D.19 Shear Capacity of Piers and Connection (NBI 50795)

Pier No.	Shear Capacity–Pier (kips)	Shear Capacity–Connection (kips)
1	1605.4	13824
2	1605.4	13824

6. Identify Limiting Capacity

The limiting capacity is identified as the minimum among base shear capacity, substructure shear capacity and shear connection. The controlling capacity and corresponding mechanism of failure for all piers in the transverse direction is summarized in Table D.20.

Table D.20 Limiting Capacity of Substructure in Transverse Direction (NBI 50795)

Pier No.	Capacity–Transverse (kips)	Mechanism
2	1605.4	Shear Failure of Pier
3	1605.4	Shear Failure of Pier

Demand

7. 2-D Bridge Model

The stiffness in the transverse direction is derived solely from the stiffness of the substructure. As mentioned previously, the deck is assumed to be rigid enough to allow the intermediate piers to act as springs in parallel.

7.1a Transverse Stiffness

The overall stiffness of Piers 2 and 3 is modeled by assuming the frame bent and infill wall stiffnesses act in parallel. Therefore, the total stiffness is the sum of the individual components. The stiffness of the frame bent is modeling using the procedure identified in Case Study 3 Section 7. The walls are modeled like the procedure outlined in Equation (32) to (33), but without the added stiffness due to shear. For continuity purposes, one portion of the substructure is incapable of deforming in flexure and shear while the other portion deforms solely in flexure. For the case of frame bents with infill walls, it is assumed the response of the frame bents will dominate therefore stiffness in derived only from flexure. The stiffness of each pier is

$$K_{pier} = [18040.5 \quad 12010.3]\frac{kips}{in}. \tag{127}$$

7.2a Transverse Mass

The activated mass of the bridge in the transverse direction is calculated using superstructure geometry and barrier dimensions. The procedure outlined in Case Study 1 is used to calculate the mass of each superstructure element over each pier using the tributary length of the adjacent spans. The total mass is

$$m_{pier} = [7.9 \quad 8.24]\frac{kips}{g}. \tag{128}$$

7.3 Equation of Motion

Because the rigidity of the deck ensures uniform movement, the total stiffness and mass in the transverse direction is calculated as the summation of the individual pier components. Using the 5% assumption for viscous damping, the components for the equation of motion are calculate as

$$K_{su} \ = 30{,}050\frac{kips}{in}, \tag{129}$$

$$m_{sup} = 16.1\frac{kips}{g}, \tag{130}$$

$$c_{sub} = 69.6\frac{kips * s}{in}. \tag{131}$$

The equation of motion in the transverse direction is

$$16.1\frac{kips}{g}\ \ddot{x}_s + \left(69.6\frac{kips * s}{in}\right)\dot{x}_s + (30050\ kips * in)x_s = \ -16.1\frac{kips}{g}\ \ddot{x}_g. \tag{129}$$

8. Displacement-Controlled Pushover Analysis

Because the limiting capacity of the structure is shear failure of the columns, a displacement-controlled pushover analysis is not required since non-linear redistribution is not expected.

9. Apply Ground Motions

The same process for developing and applying ground motions is used to develop 100 stochastically-simulated ground motions using generic site amplification factors.

10. Maximum Force and Displacement

The process described in Equation (7) to (10) is used to calculate the maximum displacement of the bridge and the force transferred to each pier.

11. Compare Force Demand to Capacity

In the transverse direction, the maximum force resulting from the application of each of the 100 seismic ground motions is compared to the capacity to assess if the capacity is exceeded. For Structure Number I465-149-08854 JSBL (NBI 50795) the maximum resulting force from 100 ground motions exceeds the capacity 13% in the traverse direction controlled by the shear capacity of the pier.

Vulnerability Assessment of Detail

In the transverse direction, frame bent substructures with infill walls have the potential to be highly vulnerable. Given the uniqueness of the substructure, the vulnerability of every substructures labeled other must be evaluated on a case-by-case basis. Thus, the Level 1 tool does not accommodate the analysis of this substructure, rather recommends a Level 2 assessment.

Case Study 6: Steel Bridge with Expansion Joints

1. Bridge Information

Structure Number I64-05-05201 CEBL (NBI 033240) is a thirteen-span steel girder bridge located in the Posey county of the Vincennes District. Originally constructed in 1966, the bridge has had three rehabilitations. In 1984, the bridge deck overlay was replaced. In 2003, the bridge deck was patched and repaired and in 2016, a sealer was applied, and other general bridge rehabilitations were done. The super structure for spans 1–4 and 8–13 is composed of six W36×135 beams with a 7¾ *in* (19.87 *cm*) reinforced concrete deck (Figure D.58). The superstructure for spans 5–7 is composed of four plate girders with a 7 ¾ *in* (19.87 *cm*) reinforced concrete deck (Figure D.59). The bridge is skewed at 15-*degrees*, has span lengths of 60′–0″ (18.29 *m*), 75′–0″ (22.86 *m*), 75′–0″ (22.86 *m*), 60′–0″ (18.29 *m*), 120′–0″ (36.57 *m*), 160′–0″ (48.77 *m*), 120″-0″ (36.57 *m*), 60′–0″ (18.29 *m*), 75′–0″ (22.86 *m*), 75′–0″ (22.86 *m*), 75′–0″ (22.86 *m*), 75′–0″ (22.86 *m*), and 60′–0″ (18.29 *m*), and is 33′–6″ (10.21 *m*) wide.

The bridge is supported by two abutments and twelve interior piers shown in Figure D.56 and Figure D.57. Piers 2–4, and 9–13 are hammerhead piers. Piers 5–8 are wall piers. At each abutment and Piers 3–6, and 8–12, the superstructure is supported by expansion shoes (Figure D.60). At Piers 2, 7, and 13, the superstructure is supported by fixed shoes (Figure D.61).

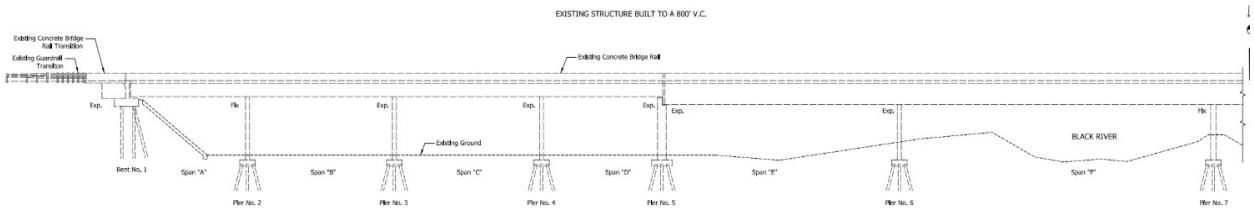

Figure D.56 Elevation View of Spans 1-6 of the Bridge (NBI 33240) (2015)

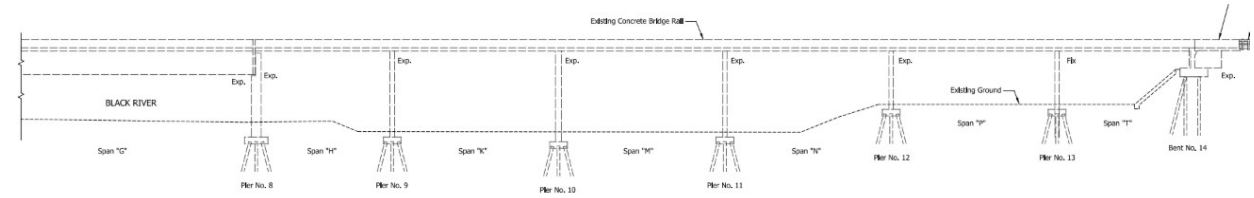

Figure D.57 Elevation View of Spans 7-13 of the Bridge (NBI 33240) (2015)

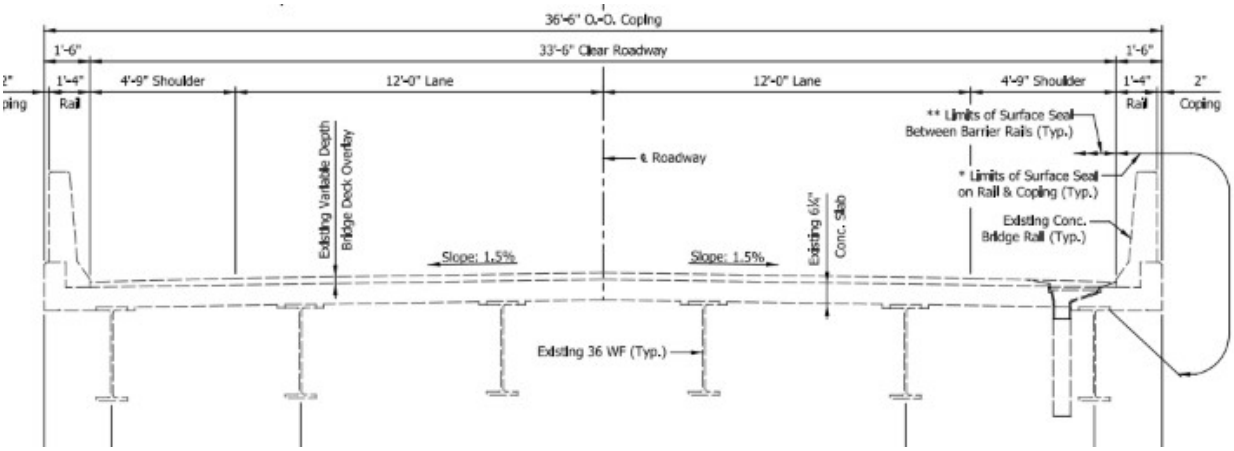

Figure D.58 Typical Section of Spans 1-4 and 8-13 of the Bridge (NBI 33240) (2014)

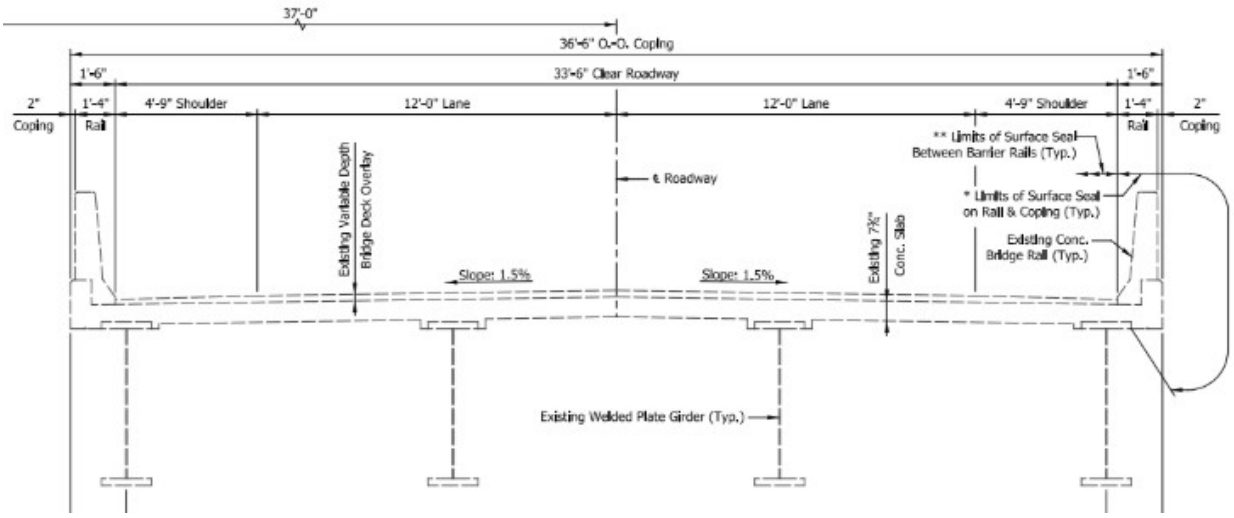

Figure D.59 Typical Section of Spans 5-7 of the Bridge (NBI 33240) (2014)

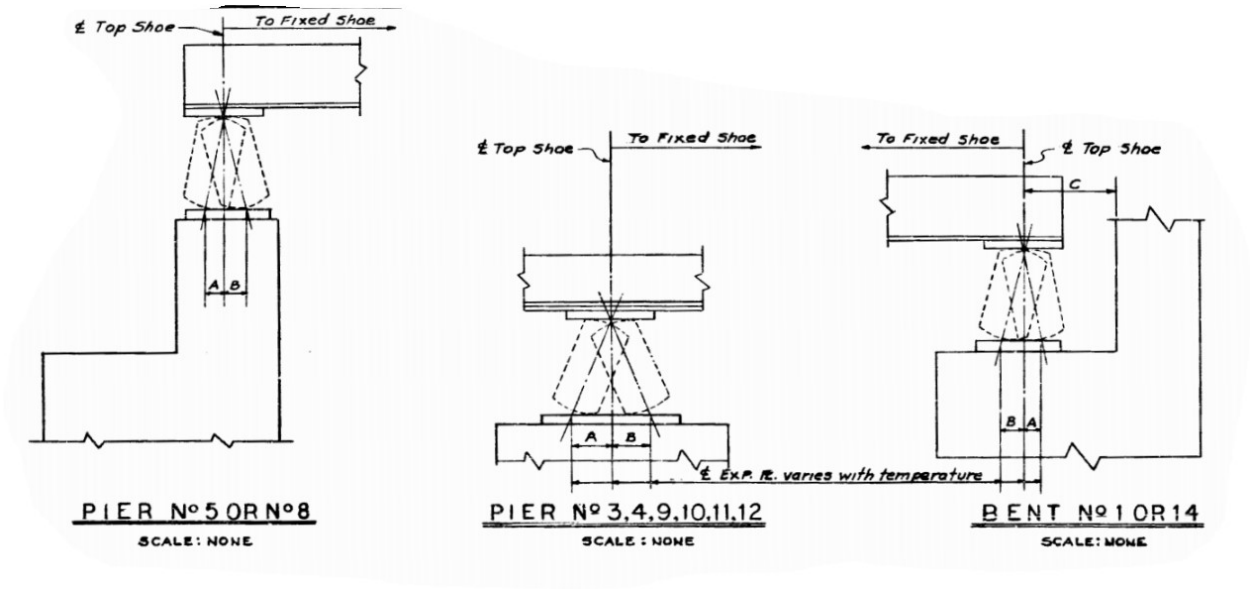

Figure D.60 Expansion Shoes for the Bridge (NBI 33240) (1966)

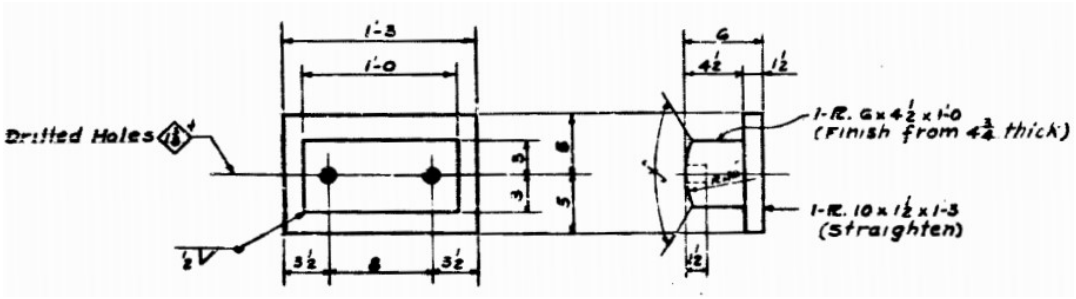

Figure D.61 Fixed Shoes for the Bridge (NBI 33240) (1966)

Over Piers 5 and 8, the bridge deck is broken up by expansion joints, shown in Figure D.62. The presence of the expansion joints allows the bridge deck to move as three separate bodies and therefore the bridge is modeled as three separate systems. System A includes spans 1–4 and Piers 2–4. Pier 5 is not included due to the expansion shoe connecting the superstructure to the substructure. System B includes spans 5–7 and Piers 6 and 7. Like in System A, Pier 5 and Pier 8 are not included in the model because of the expansion shoe. System C includes spans 8–13 and Piers 9–13, again, Pier 8 is not included because of the expansion shoe.

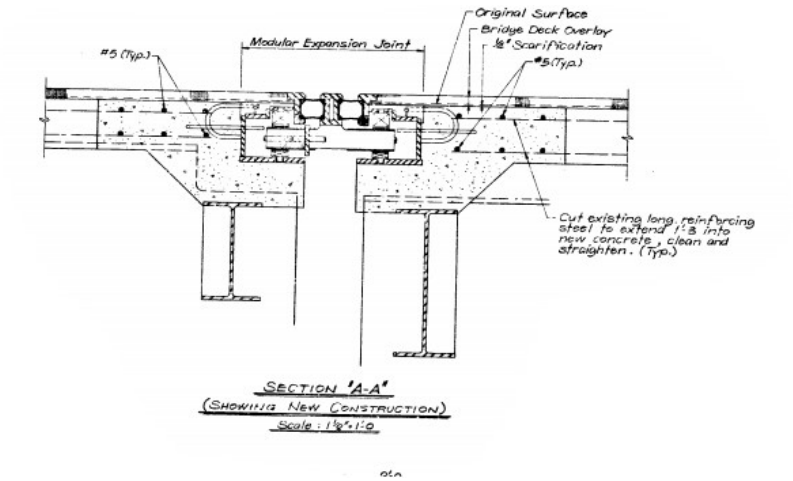

Figure D.62 Expansion Joints over Piers 5 and 8 for the Bridge (NBI 33240) (1978)

System A:

The substructure for System A is a hammerhead wall. For this substructure type, the geometries relevant to the calculations are wall length at the base, wall thickness, and wall height. Each pier has a uniform thickness of 2′–0″ (0.61 *m*), and an equivalent rectangular base length of 21′–6″ (6.55 *m*). The typical pier elevation is shown in Figure D.63. The heights of Piers 2, 3, and 4 are 22′–0″ (6.7 *m*), 21′–3″ (6.47 *m*), and 21′–3″ (6.47 *m*).

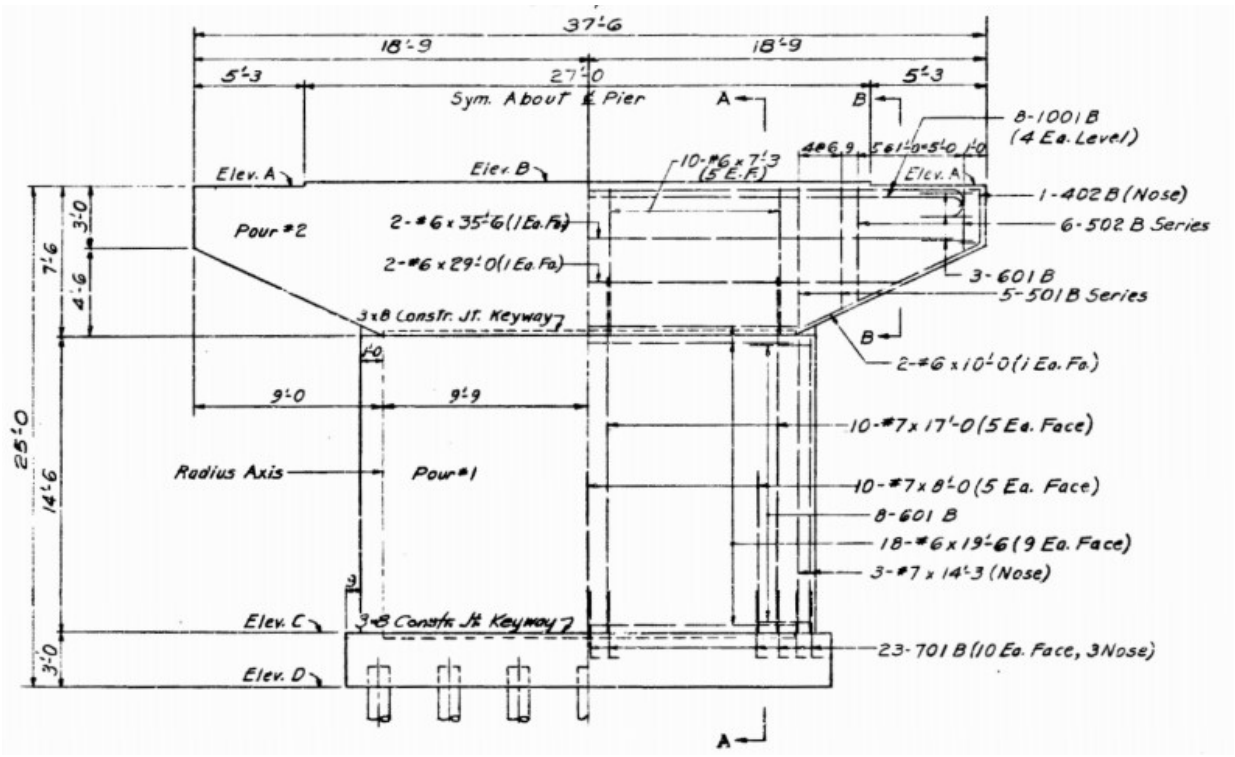

Figure D.63 System A: Transverse Elevation of an Interior Pier the Bridge (NBI 33240) (1978)

Capacity

2. Identify Mechanism of Hinge Formation

As mentioned in Case Study 2, the controlling mechanism of hinge formation for all fixed-free or fixed semi-free hammerheads is identified as the formation of a plastic hinge at the base of the pier.

3. Base Shear

As described in the Case Study 1, walls in the transverse direction with aspect ratios less than 2.5 are controlled by shear. The aspect ratio for this bridge is calculated using Equation (12) and is

$$\lambda_R = \frac{22\ ft}{21.5\ ft} = 1.02. \tag{132}$$

This means that the bridge will not develop a hinge in the transverse direction.

In the longitudinal direction, the base shear, controlled by the flexure mechanism, of each pier is calculated using the reinforcement layout shown in Figure D.64 and the moment-curvature procedure described in Case Study 1. The elongated oval shape is modeled as an equivalent rectangular section with a total reinforcement ratio of 0.20% or 0.6 in^2/ft (12.7 cm^2/m). A 12 *in* (30.48 *cm*) section of the wall is used for the longitudinal direction calculations and then multiplied by the total length to get the total base shear. Table D.21 shows the results of the moment-curvature analysis of each pier in the longitudinal direction.

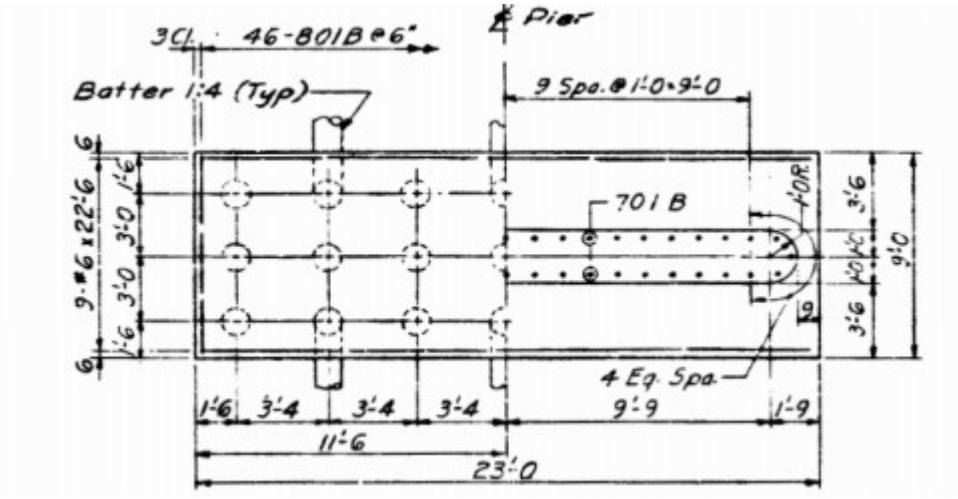

Figure D.64 System A: Cross Section of Typical Interior Pier of the Bridge (NBI 33420) (1986)

Table D.21. System A: Moment-Curvature Results for the Longitudinal Direction for Bridge (NBI 19430)

	Pier 2		Pier 3		Pier 4	
	Moment (kip*ft)	φ	**Moment (kip*ft)**	φ	**Moment (kip*ft)**	φ
Cracking	847.87	1.09E-5	847.87	1.09E-5	847.87	1.09E-5
Yield	831.64	7.68E-5	319.40	7.13E-5	319.40	7.13E-5
Ultimate	898.03	4.95E-4	340.34	4.79E-4	340.34	4.79E-4

Like in Case Study 2, the cracking moment exceeds the yield moment and the ultimate moment for Pier 3 and 4 and brittle failure my occur unless an alternate load path can be established. The cracking moment is therefore conservatively taken as the controlling moment for Piers 3 and 4. For Pier 2, the moment is larger than the cracking moment and therefore it is controlled by the base shear resulting from flexure. Using Equation (11), the shear force, over the entire length of the wall, that causes cracking or yielding (for Pier 2) of the three piers in the longitudinal direction is

$$V_{cr} = [61.93 \quad 61.66 \quad 61.66]\ kips. \tag{133}$$

4. Shear Capacity of Pier

In the transverse direction, the shear capacity of each pier is calculated using Equation (28). An α_c value of 3 is used based on the height to length ratio and a lambda (λ) value of 1 is used for normal-weight concrete. The reinforcement ratio for each pier is 0.20%. The yield strength of the longitudinal reinforcement is assumed to be 40 *ksi* (27.58 kN/cm^2) because the bridge was built during or after 1945 (*Manual for Bridge Evaluation* Table 6A.5.2.2-1 (AASHTO, 2018)). The shear capacity of each pier in the transverse direction is calculated as

$$V_n = [1275.4 \quad 1206.6 \quad 1206.6]\ kips. \tag{134}$$

The shear capacity of the piers in the longitudinal direction is calculated using Equations (50) through (53) and
is

$$V_n = [546.2 \quad 572.1 \quad 572.1]\ kips. \tag{135}$$

5. Shear Capacity of Connection

As mentioned in Case Study 2, the shear capacity of the connection is conservatively taken as the frictional force between the substructure and the superstructure and it is the same in the transverse and the longitudinal direction. The shear capacity of the connections of Piers 2, 3, and 4 are calculated using Equation (60) are

$$V_{conn} = [171.9 \quad 191.0 \quad 171.9]\ kips. \tag{136}$$

6. Identify Limiting Capacity

Table D.22 and Table D.23 show the controlling capacity and the corresponding failure mechanism for all the piers in the transverse and longitudinal direction, respectively.

Table D.22 System A: Limiting Capacity of Substructure in Transverse Direction for Bridge NBI 19430

Pier No.	Capacity–Trans.	Mechanism
2	171.9 kips	Shear Connection Failure
3	191.0 kips	Shear Connection Failure
4	171.9 kips	Shear Connection Failure

Table D.23 System A: Limiting Capacity of Substructure in Longitudinal Direction for Bridge NBI 19430

Pier No.	Capacity–Long.	Mechanism
2	61.93 kips	Base Shear
3	61.66 kips	Brittle Failure of Pier
4	61.66 kips	Brittle Failure of Pier

6.1. Additional Longitudinal Displacement Capacity

In the longitudinal direction, when expansion shoe bearings are present, we consider the allowable displacement of the expansion shoe bearing as an additional displacement threshold. This threshold is calculated using Equation (63) and is

$$\Delta_{rb} = 5.42 \text{ in.}$$

Demand

7. 2-D Bridge Model

The stiffness in both the transverse and longitudinal direction derives solely from the substructure stiffness. As mentioned previously, the deck is assumed to be rigid enough to allow the intermediate piers to act as springs in parallel.

7.1a Transverse Stiffness

The stiffness of hammerhead piers in the transverse direction is calculated using Equations (32) through (34). The resulting stiffness of each pier in the transverse direction is

$$K_{pier} = [44479.7 \quad 47363.6 \quad 47363.6]\frac{kip}{in}. \tag{137}$$

7.1b Longitudinal Stiffness

As described in Case Study 2, piers with expansion shoes connecting the superstructure to the substructure do not add stiffness in the longitudinal direction. Because of this, Pier 2 is the only pier that contributes to the longitudinal stiffness. The value is calculated using Equation (68) and is

$$K_{pier} = 152.9\frac{kip}{in}. \tag{138}$$

7.2a Transverse Mass

The activated mass of the bridge in the transverse direction is calculated using the superstructure geometry. Since the superstructure of System A consists of rolled shapes, the weight per linear foot of each beam, given in the beam designation is used as the weight of the beams. Using Equation (71) the mass of the superstructure over each pier is calculated as

$$m_{pier} = [.78 \quad .87 \quad .78]\frac{kip}{g}. \tag{139}$$

7.2b Longitudinal Mass

The entire superstructure mass is activated in the longitudinal direction as is

$$m_{sup} = 3.12\frac{kip}{g}. \tag{140}$$

7.3 Equation-of-Motion

The equation-of-motion for the transverse direction is written as

$$2.43\frac{kips}{g}\ddot{x}_s + \left(58.16\frac{kips * s}{in}\right)\dot{x}_s + \left(139206.9\frac{kips}{in}\right)x_s = -2.43\frac{kips}{g}\ddot{x}_g. \tag{141}$$

The equation-of-motion for the longitudinal direction is written as

$$3.12\frac{kips}{g}\ddot{x}_s + \left(2.19\frac{kips * s}{in}\right)\dot{x}_s + \left(152.9\frac{kips}{in}\right)x_s = -3.12\frac{kips}{g}\ddot{x}_g. \tag{142}$$

8. Pushover analysis

As mentioned earlier, because the cracking moment of each pier is larger than the yield moment, the bridge will remain in the linear region until brittle failure. Because of this, no pushover analysis is needed.

9. Apply Ground Motions

The same process for developing and applying ground motions used in Case Study 1 is used to develop 100 stochastically-simulated ground motions using generic site amplification factors.

10. Maximum Force and Displacement Demand

The linear displacement and the linear stiffness are used to calculate the total force applied to the bridge. Since the pushover analysis is not applicable to this bridge, the force is distributed to each pier based on the relative stiffness of the piers. With the force, the corresponding displacement is calculated. As mentioned earlier, because of the moment-curvature relationship, the total displacement is the linear displacement.

11. Compare Force Demand to Capacity

In each direction, the maximum force resulting from the application of each of the seismic ground motions is compared to the capacity to assess if the capacity is exceeded. For Structure Number 052-24-06649 (NBI 19430), the maximum force resulting from 100 ground motions exceeds the capacity in the transverse direction, controlled be the shear connection between the substructure and superstructure, 9% of the time. In the longitudinal direction, the maximum force resulting from 100 ground motions exceeds the capacity, controlled by brittle failure of the pier, 100% of the time.

System B:

The substructure for System B is a wall. For this substructure type, the geometries relevant to the calculations are wall length, wall thickness, and wall height. Each pier has a uniform thickness of 2′–6 (0.76 *m*) and an equivalent rectangular base length of 40′–6″ (12.34 *m*). The typical pier elevation is shown in Figure D.65. The heights of Piers 6 and 7 are 30′–6″ (9.30 *m*) and 30′–6″ (9.30 *m*), respectively.

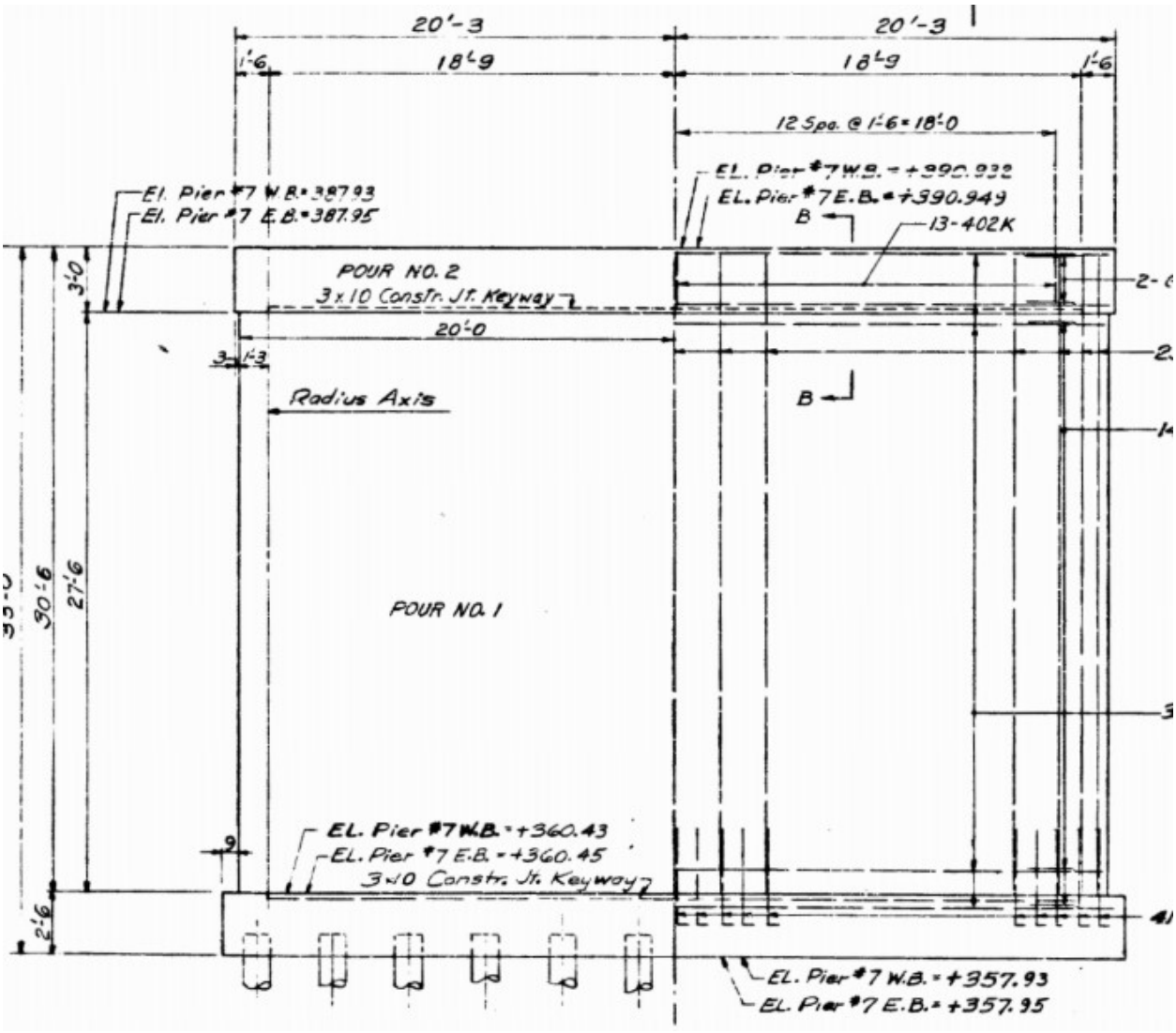

Figure D.65 System B: Transverse Elevation of an Interior Pier the Bridge (NBI 33240) (1978)

Capacity

2. Identify Mechanism of Hinge Formation

As mentioned in Case Study 2, the controlling mechanism of hinge formation for all fixed-free or fixed semi-free hammerheads is identified as the formation of a plastic hinge at the base of the pier.

3. Base Shear

As described in the Case Study 1, walls in the transverse direction with aspect ratios less than 2.5 are controlled by shear. The aspect ratio for this bridge is calculated using Equation (12) and is

$$\lambda_R = \frac{30.5\ ft}{40.5\ ft} = 0.75. \tag{143}$$

This means that the bridge will not develop a hinge in the transverse direction.

In the longitudinal direction, the base shear, controlled by the flexure mechanism, of each pier is calculated using the reinforcement layout shown in Figure D.66 and the procedure described in the detailed calculations for the prestressed concrete bridge (Equations (13) through (25)). The elongated oval shape is modeled as an equivalent rectangular section with a total reinforcement ratio of 0.12% or 0.44 in^2/ft (9.31 cm^2/m). A 12 *in* (30.48 *cm*) section of the wall is used for the longitudinal direction calculations and then multiplied by the total length to get the total base shear. Table D.24 shows the results of the moment-curvature analysis of each pier in the longitudinal direction.

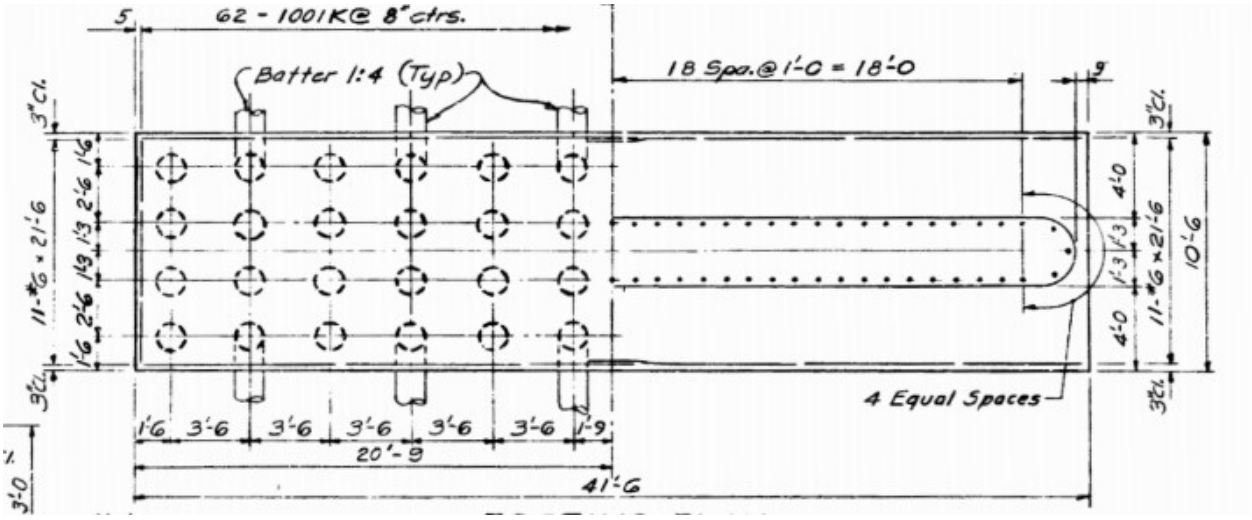

Figure D.66 System B: Cross Section of Typical Interior Pier of the Bridge (NBI 33420) (1986)

Table D.24 System B: Moment-Curvature Results for the Longitudinal Direction for Bridge NBI 19430

	Pier 6		Pier 7	
	Moment (kip*ft)	**φ**	**Moment (kip*ft)**	**φ**
Cracking	2695.5	8.7E-6	2695.5	8.7E-6
Yield	1925.8	1.01E-4	1925.8	1.01E-4
Ultimate	2033.1	4.51E-4	2033.1	4.51E-4

Like in Case Study 2, the cracking moment exceeds the yield moment and the ultimate moment for every pier and brittle failure my occur unless an alternate load path can be established. The cracking moment is therefore conservatively taken as the controlling moment for this bridge and a linear response of the bridge

is used in all further calculations. Using Equation (11), the shear force shear force, over the entire length of the wall, that causes cracking of the three piers in the longitudinal direction is

$$V_{cr} = [88.37 \quad 88.37]\ kips. \tag{144}$$

4. Shear Capacity of Pier

In the transverse direction, the shear capacity of each pier is calculated using Equation (28). An α_c value of 3 is used based on the height to length ratio and a lambda (λ) value of 1 is used for normal-weight concrete. The reinforcement ratio for each pier is 0.12%. The yield strength of the longitudinal reinforcement is assumed to be 40 *ksi* (27.58 kN/cm^2) because the bridge was built during or after 1945 (*Manual for Bridge Evaluation* Table 6A.5.2.2-1 (AASHTO, 2018)). The shear capacity of each pier in the transverse direction is calculated using Equation (48) is

$$V_n = [3122.3 \quad 3122.3]\ kips. \tag{145}$$

The shear capacity of the piers in the longitudinal direction is calculated using Equations (50) through (53) and is

$$V_n = [1242.0 \quad 1242.0]\ kips. \tag{146}$$

5. Shear Capacity of Connection

As mentioned in Case Study 2, the shear capacity of the connection is conservatively taken as the frictional force between the substructure and the superstructure and it is the same in the transverse and the longitudinal direction. The shear capacity of the connections of Piers 6 and 7 are calculated using Equation (60) is

$$V_{conn} = [457.5 \quad 457.5]\ kips. \tag{147}$$

6. Identify Limiting Capacity

Table D.25 and Table D.26 show the controlling capacity and the corresponding failure mechanism for all the piers in the transverse and longitudinal direction, respectively.

Table D.25 System B: Limiting Capacity of Substructure in Transverse Direction for Bridge NBI 19430

Pier No.	Capacity–Trans.	Mechanism
6	457.5 kips	Shear Connection Failure
7	457.5 kips	Shear Connection Failure

Table D.26 System B: Limiting Capacity of Substructure in Longitudinal Direction for Bridge NBI 19430

Pier No.	Capacity–Long.	Mechanism
6	88.37 kips	Brittle Failure of Pier
7	88.37 kips	Brittle Failure of Pier

6.1. Additional Longitudinal Displacement Capacity

In the longitudinal direction, when expansion shoe bearings are present, we consider the allowable displacement of the expansion shoe bearing as an additional displacement threshold. This threshold is calculated using Equation (63) and is

$$\Delta_{rb} = 5.42 \text{ in.}$$

Demand

7. 2-D Bridge Model

The stiffness in both the transverse and longitudinal direction derives solely from the substructure stiffness. As mentioned previously, the deck is assumed to be rigid enough to allow the intermediate piers to act as springs in parallel.

7.1a Transverse Stiffness

The stiffness of wall piers in the transverse direction is calculated using Equations (32) through (34). The resulting stiffness of each pier in the transverse direction is

$$K_{pier} = [109097.7 \quad 109097.7] \frac{kip}{in}. \tag{148}$$

7.1b Longitudinal Stiffness

As described in Case Study 2, piers with expansion shoes connecting the superstructure to the substructure do not add stiffness in the longitudinal direction. Because of this, Pier 7 is the only pier that contributes to the longitudinal stiffness. The value is calculated using Equation (68) and is

$$K_{pier} = 228.2 \frac{kip}{in}. \tag{149}$$

7.2a Transverse Mass

The activated mass of the bridge in the transverse direction is calculated using the superstructure geometry. Since the superstructure of System B consists of built-up plate girders, the weight per linear foot is calculated using the density of steel and the volume of the plates (as described in Equations (69) through (70)). An elevation view of the plate girder can be seen in Figure D.67.

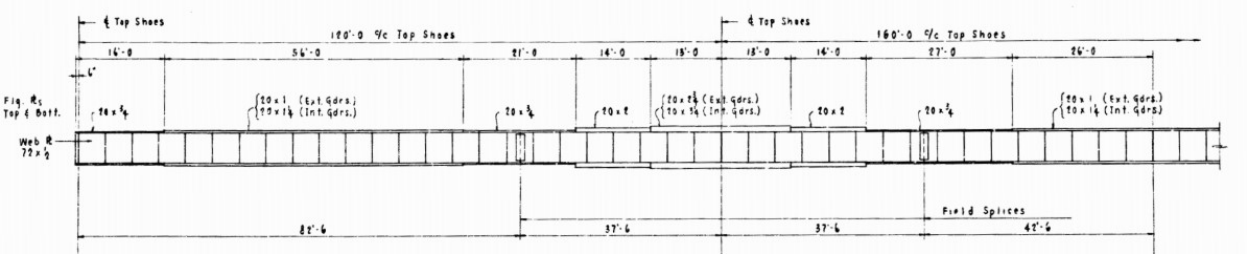

Figure D.67 System B: Typical Plate Girder Elevation for Bridge (NBI 33240)

Using Equation (71) the mass of the superstructure over each pier is calculated as

$$m_{pier} = [2.08 \quad 2.08]\frac{kip}{g}. \tag{150}$$

7.2b Longitudinal Mass

The entire superstructure mass is activated in the longitudinal direction as is

$$m_{sup} = 5.94\frac{kip}{g}. \tag{151}$$

7.3 Equation-of-Motion

The equation-of-motion for the transverse direction is written as

$$4.16\frac{kips}{g}\ddot{x}_s + \left(95.27\frac{kips * s}{in}\right)\dot{x}_s + \left(218195.4\frac{kips}{in}\right)x_s = -4.16\frac{kips}{g}\ddot{x}_g. \tag{152}$$

The equation-of-motion for the longitudinal direction is written as

$$5.94\frac{kips}{g}\ddot{x}_s + \left(3.68\frac{kips * s}{in}\right)\dot{x}_s + \left(228.2\frac{kips}{in}\right)x_s = -5.94\frac{kips}{g}\ddot{x}_g. \tag{153}$$

8. Pushover analysis

As mentioned earlier, because the cracking moment of each pier is larger than the yield moment, the bridge will remain in the linear region until brittle failure. Because of this, no pushover analysis is needed.

9. Apply Ground Motions

The same process for developing and applying ground motions used in Case Study 1 is used to develop 100 stochastically-simulated ground motions using generic site amplification factors.

10. Maximum Force and Displacement Demand

The linear displacement and the linear stiffness are used to calculate the total force applied to the bridge. Since the pushover analysis is not applicable to this bridge, the force is distributed to each pier based on the relative stiffness of the piers. With the force, the corresponding displacement is calculated. As mentioned earlier, because of the moment-curvature relationship, the total displacement is the linear displacement.

11. Compare Force Demand to Capacity

In each direction, the maximum force resulting from the application of each of the seismic ground motions is compared to the capacity to assess if the capacity is exceeded. For Structure Number 052-24-06649 (NBI 19430), the maximum force resulting from 100 ground motions exceeds the capacity in the transverse direction, controlled be the shear connection between the substructure and superstructure, 12% of the time.

In the longitudinal direction, the maximum force resulting from 100 ground motions exceeds the capacity, controlled by brittle failure of the pier, 100% of the time.

System C:

The substructure for System C is a hammerhead wall. For this substructure type, the geometries relevant to the calculations are wall length at the base, wall thickness, and wall height. Each pier has a uniform thickness of 2′–0″ (0.61 *m*), and an equivalent rectangular base length of 21′–6″ (6.55 *m*). The typical pier elevation is shown in Figure D.68. The heights of Piers 9, 10, 11, 12, and 13 are 25′–6″ (7.77 *m*), 25′–6″ (7.77 *m*), 25′–6″ (7.77 *m*), 15′–3″ (4.65 *m*), and 16′–0″ (4.87 *m*), respectively.

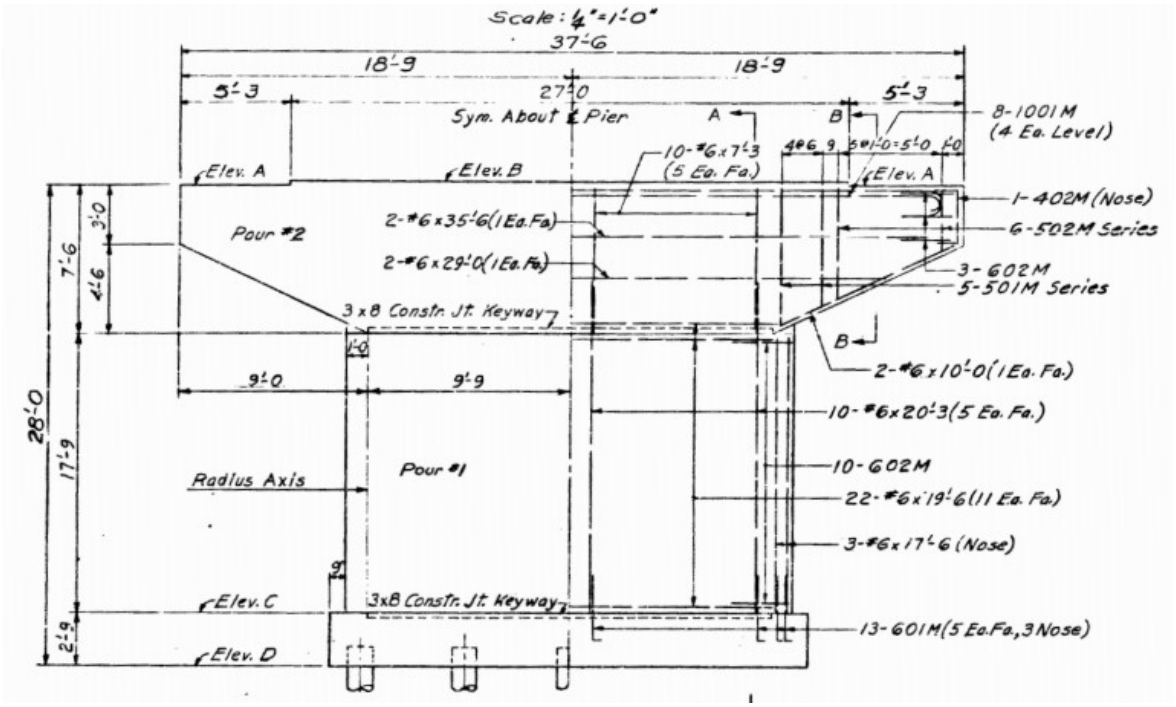

Figure D.68 System C: Transverse Elevation of an Interior Pier the Bridge (NBI 33240) (1978)

Capacity

2. Identify Mechanism of Hinge Formation

As mentioned in Case Study 2, the controlling mechanism of hinge formation for all fixed-free or fixed semi-free hammerheads are identified as the formation of a plastic hinge at the base of the pier.

3. Base Shear

As described in the Case Study 1, walls in the transverse direction with aspect ratios less than 2.5 are controlled by shear. The aspect ratio for this bridge is calculated using Equation (12) and is

$$\lambda_R = \frac{25.5\ ft}{21.5\ ft} = 1.18. \tag{154}$$

This means that the bridge will not develop a hinge in the transverse direction.

In the longitudinal direction, the base shear, controlled by the flexure mechanism, of each pier is calculated using the reinforcement layout shown in Figure D.69 and the procedure described in the detailed calculations for the prestressed concrete bridge (Equations (13) through (25)). The elongated oval shape is modeled as an equivalent rectangular section with a total reinforcement ratio of 0.076% or 0.22 in^2/ft (4.65 cm^2/m). A 12 *in* (30.48 *cm*) section of the wall is used for the longitudinal direction calculations and then multiplied by the total length to get the total base shear. Like in Case Study 2, the cracking moment exceeds the yield moment and the ultimate moment for Piers 9, 10, 11, and 12 and brittle failure may occur unless an alternate load path can be established. This does not occur in Pier 13 due to the increased amount of reinforcement, shown in Figure D.70. Table D.27 shows the results of the moment-curvature analysis of each pier in the longitudinal direction.

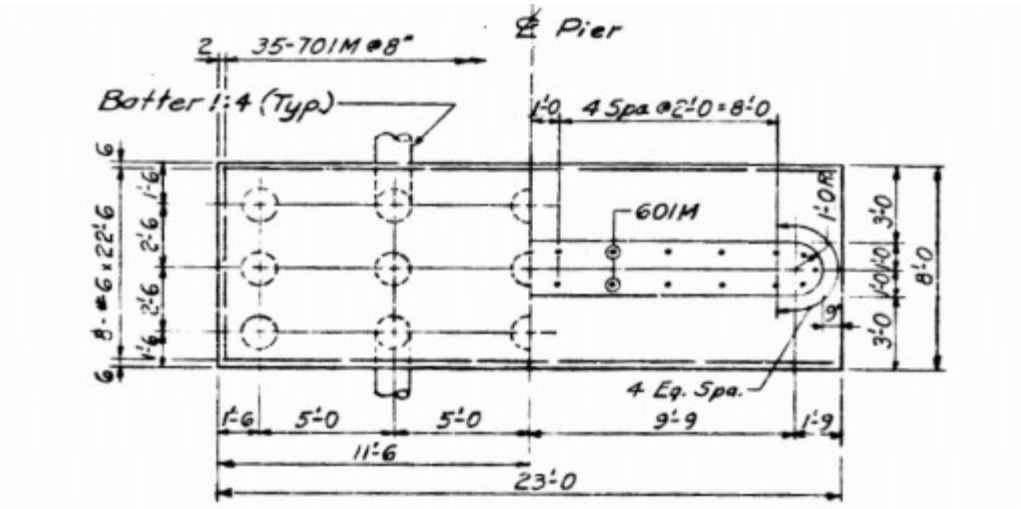

Figure D.69 System C: Cross Section of Typical Interior Pier of the Bridge (NBI 33420) (1986)

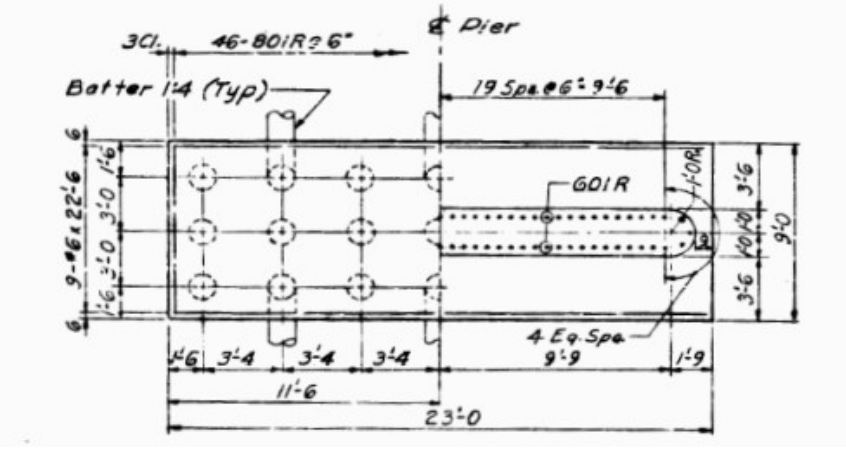

Figure D.70 System C: Cross Section of Pier 13 of the Bridge (NBI 33420) (1986)

Table D.27 System C: Moment-Curvature Results for the Longitudinal Direction for Bridge NBI 19430

	Pier 9, 10, 11 and 12		Pier 13	
	Moment (kip*ft)	**φ**	**Moment (kip*ft)**	**φ**
Cracking	847.87	1.09E-5	847.9	1.09E-5
Yield	319.40	7.13E-5	1196.5	8E-5
Ultimate	340.34	4.79E-4	1300.3	5.04E-4

For Pier 9–12, the cracking moment is therefore conservatively taken as the controlling moment for this bridge and a linear response of the bridge is used in all further calculations. For Pier 13, the resulting base shear, calculated using the ultimate moment, is taken as the capacity. Using Equation (46), the shear force, over the entire length of the wall, that causes cracking or yielding of the three piers in the longitudinal direction is:

$$V_{cr} = [47.76 \quad 47.76 \quad 47.76 \quad 109.40 \quad 152.97]\ kips. \tag{155}$$

4. Shear Capacity of Pier

In the transverse direction, the shear capacity of each pier is calculated using Equation (28). An α_c value of 3 is used based on the height to length ratio and a lambda (λ) value of 1 is used for normal-weight concrete. The reinforcement ratio for Piers 9–12 is 0.20% and for Pier 13 is 0.31%. The yield strength of the longitudinal reinforcement is assumed to be 40 *ksi* (27.58 kN/cm^2) because the bridge was built during or after 1945 (*Manual for Bridge Evaluation* Table 6A.5.2.2-1 (AASHTO, 2018)). The shear capacity of each pier in the transverse direction is calculated using Equation (48) is

$$V_n = [1206.6 \quad 1206.6 \quad 1206.6 \quad 1206.6 \quad 1206.6]\ kips. \tag{156}$$

The shear capacity of the piers in the longitudinal direction is calculated using Equations (50) through (53) and is

$$V_n = [572.1 \quad 572.1 \quad 572.1 \quad 572.1 \quad 535.8]\ kips. \tag{157}$$

5. Shear Capacity of Connection

As mentioned in Case Study 2, the shear capacity of the connection is conservatively taken as the frictional force between the substructure and the superstructure and it is the same in the transverse and the longitudinal direction. The shear capacity of the connections of Piers 9, 10, 11, 12, and 13 are calculated using Equation (60) are

$$V_{conn} = [171.9 \quad 191.0 \quad 191.0 \quad 191.0 \quad 171.9]\ kips. \tag{158}$$

6. Identify Limiting Capacity

Table D.28 and Table D.29 show the controlling capacity and the corresponding failure mechanism for all the piers in the transverse and longitudinal direction, respectively.

Table D.28 Limiting Capacity of Substructure in Transverse Direction for Bridge NBI 19430

Pier No.	Capacity–Trans.	Mechanism
9	171.9 kips	Shear Connection Failure
10	191.0 kips	Shear Connection Failure
11	191.0 kips	Shear Connection Failure
12	191.0 kips	Shear Connection Failure
13	171.9 kips	Shear Connection Failure

Table D.29 Limiting Capacity of Substructure in Longitudinal Direction for Bridge NBI 19430

Pier No.	Capacity–Long.	Mechanism
9	47.76 kips	Brittle Failure of Pier
10	47.76 kips	Brittle Failure of Pier
11	47.76 kips	Brittle Failure of Pier
12	109.40	Brittle Failure of Pier
13	152.97	Base Shear

6.1. Additional Longitudinal Displacement Capacity

In the longitudinal direction, when expansion shoe bearings are present, we consider the allowable displacement of the expansion shoe bearing as an additional displacement threshold. This threshold is calculated using Equation (63) and is

$$\Delta_{rb} = 5.42 \text{ in.}$$

Demand

7. 2-D Bridge Model

The stiffness in both the transverse and longitudinal direction derives solely from the substructure stiffness. As mentioned previously, the deck is assumed to be rigid enough to allow the intermediate piers to act as springs in parallel.

7.1a Transverse Stiffness

The stiffness of hammerhead piers in the transverse direction is calculated using Equations (32) through (34). The resulting stiffness of each pier in the transverse direction is

$$K_{pier} = [35046.7 \quad 35046.7 \quad 35046.7 \quad 91725.0 \quad 82796.5] \frac{kip}{in}. \tag{159}$$

7.1b Longitudinal Stiffness

As described in Case Study 2, piers with expansion shoes connecting the superstructure to the substructure do not add stiffness in the longitudinal direction. Because of this, Pier 2 is the only pier that contributes to the longitudinal stiffness. The value is calculated using Equation (68) and is

$$K_{pier} = 397.5\frac{kip}{in}. \tag{160}$$

7.2a Transverse Mass

The activated mass of the bridge in the transverse direction is calculated using the superstructure geometry. Since the superstructure of System C consists of rolled shapes, the weight per linear foot of each beam, given in the beam designation is used as the weight of the beams. Using Equation (71) the mass of the superstructure over each pier is calculated as

$$m_{pier} = [.78 \quad .87 \quad .87 \quad .87 \quad .78]\frac{kip}{g}. \tag{161}$$

7.2b Longitudinal Mass

The entire superstructure mass is activated in the longitudinal direction as is

$$m_{sup} = 4.86\frac{kip}{g}. \tag{162}$$

7.3 Equation-of-Motion

The equation-of-motion for the transverse direction is written as

$$4.17\frac{kips}{g}\ddot{x} + \left(107.99\frac{kips * s}{in}\right)\dot{x} + \left(279661.6\frac{kips}{in}\right)x = -4.17\frac{kips}{g}\ddot{x}_g. \tag{163}$$

The equation-of-motion for the longitudinal direction is written as

$$4.86\frac{kips}{g}\ddot{x} + \left(4.39\frac{kips * s}{in}\right)\dot{x} + \left(397.5\frac{kips}{in}\right)x = -4.86\frac{kips}{g}\ddot{x}_g. \tag{164}$$

8. Pushover analysis

As mentioned earlier, because the cracking moment of each pier is larger than the yield moment, the bridge will remain in the linear region until brittle failure. Because of this, no pushover analysis is needed.

9. Apply Ground Motions

The same process for developing and applying ground motions used in Case Study 1 is used to develop 100 stochastically-simulated ground motions using generic site amplification factors.

10. Maximum Force and Displacement Demand

The linear displacement and the linear stiffness are used to calculate the total force applied to the bridge. Since the pushover analysis is not applicable to this bridge, the force is distributed to each pier based on the relative stiffness of the piers. With the force, the corresponding displacement is calculated. As mentioned earlier, because of the moment-curvature relationship, the total displacement is the linear displacement.

11. Compare Force Demand to Capacity

In each direction, the maximum force resulting from the application of each of the seismic ground motions is compared to the capacity to assess if the capacity is exceeded. For Structure Number 052-24-06649 (NBI 19430), the maximum force resulting from 100 ground motions exceeds the capacity in the transverse direction, controlled be the shear connection between the substructure and superstructure, 8% of the time. In the longitudinal direction, the maximum force resulting from 100 ground motions exceeds the capacity, controlled by the maximum base shear based on flexural capacity, 100% of the time.

Vulnerability Assessment

In the transverse direction, hammerhead walls supporting steel superstructures is found to be not vulnerable. In the longitudinal direction, hammerhead walls (specifically older walls built before 1990) have the potential for high vulnerability due to the low flexural reinforcement ratio. Given the complexity of the system due to the decoupled behavior of bridge sections, it is recommended that a Level 2 assessment is conducted for bridges with expansion joints. Thus, the Level 1 tool does not accommodate the analysis of bridges that are expected to have one or more expansion joint.

APPENDIX E. APPLICATION OF RECOMMENDED RETROFITS FOR IMPROVED SEISMIC PERFORMANCE OF INDIANA BRIDGE NETWORK

Introduction

A Level 2 assessment of the 100-bridge sample set which form the basis of the Simplified Assessment for the Indiana bridge inventory has identified some specific seismic vulnerabilities present in bridges throughout the state, as summarized in Table E.1. With these deficiencies in mind, common retrofit strategies for the Central and Eastern United States (CEUS) are described herein and their capabilities for improving the performance of bridges to the level of hazard in Indiana is demonstrated. The proposed retrofits will serve to either reduce the seismic demand or to increase the substructure capacity. The necessary adjustments to the modeling techniques leveraged for conducting the Level 2 Assessment (Appendix D) is modified to successfully model each retrofit and verify the improvement in seismic performance of the rehabilitated bridge using a representative vulnerable bridge taken from the 100-bridge sample set.

Table E.1 Summary of Key Vulnerabilities Identified

Vulnerability Case	Substructure Type	Direction	Additional Comments/Criteria (When Applicable)	Level of Vulnerability	Reason for Classification
1	Walls	Longitudinal	Built Before 1990 (Grade 40 ksi steel)*	Highly Vulnerable	Low Flexural Reinforcement Ratio
2	Hammerhead Walls	Longitudinal	Built Before 1990 (Grade 40 ksi steel)*	Highly Vulnerable	Low Flexural Reinforcement Ratio
3	Hammerhead Walls	Longitudinal	Built After 1990 (Grade 60 ksi steel)	Moderately Vulnerable	Formation of Plastic Hinge
4	Hammerhead Walls	Transverse	Prestressed Concrete Superstructure Only	Moderately Vulnerable	Formation of Plastic Hinge
5	Frame Bents	Transverse	All types (H-Pile, CFT, Reinforced Concrete)	Moderately Vulnerable	Formation of Plastic Hinge
6	Frame Bents	Longitudinal	All types (H-Pile, CFT, Reinforced Concrete)	Moderately Vulnerable	Formation of Plastic Hinge
7	-	-	Rocker Bearings	Moderately Vulnerable	Unseating

*In accordance with the *Manual for Bridge Evaluation* (AASHTO, 2018) Table 6A.5.2.2-1, bridges built before 1990 are assumed to have Grade 40 ksi steel. If a given bridge is identified as having Grade 60 ksi steel and was built before 1990, it may instead fall under vulnerability case 3.

Identification of Recommended Retrofits

Figure E.1 provides an overview of several commonly recommended seismic bridge retrofit methods in the Central Southern United States (CSUS) (Timothy et al., 2011). There are similarities between the vulnerabilities identified in past research focused on the CSUS and the vulnerabilities identified through this present study (Choi, 2002; DesRoches et al., 2004a,b; Neilson & DesRoches, 2007). It is therefore reasonable to assume that the retrofits identified for the central US and others recommended by the Federal Highway Administration (FHWA) would also be effective in improving the seismic performance of bridges in INDOT's inventory.

The seismic retrofits discussed herein address previously identified seismic vulnerabilities. Four out of the six approaches shown in Figure E.1 focus on either reducing demand or increasing capacity and will be discussed in the remainder of this report. Of the retrofits shown, shear keys and seat extenders are not explored. According to our examination of Indiana bridges, the shear connection between the superstructure and substructure is not exceeded and most bridges in INDOT's inventory are continuous. As shear keys and seat extenders specifically address vulnerabilities not seen in our evaluation, they are not considered herein.

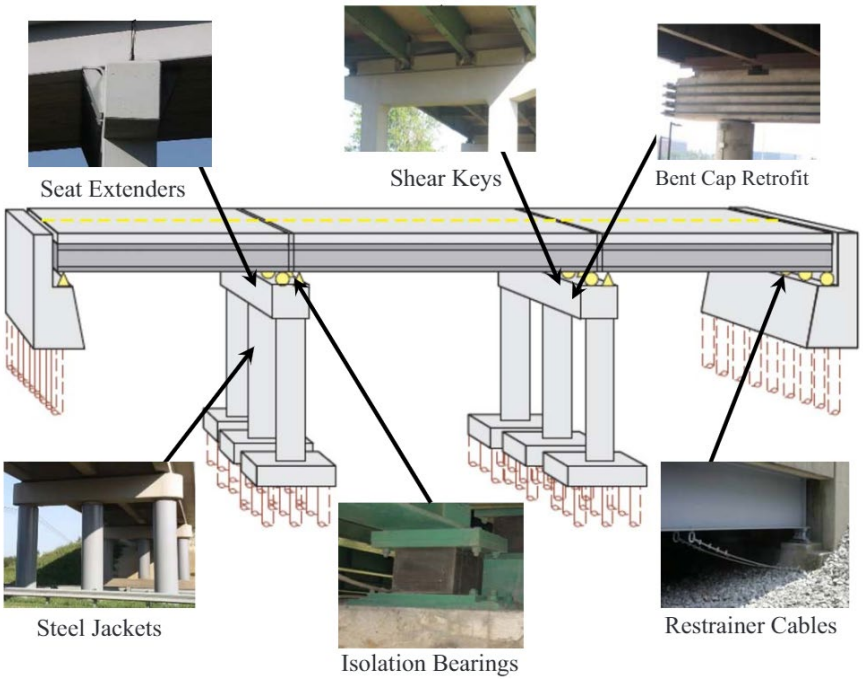

Figure E.1 Common Retrofits in the Central Southern US (Timothy et al., 2011)

Reducing Demand

Retrofit methods focused on reducing demand seek to decrease or eliminate the force transferred between the bridge's superstructure and substructure. This strategy is used, for instance, in methods involving seismic isolation and integral abutments.

Seismic isolation incorporates an energy-dissipation mechanism that, in addition to reducing the seismic demand on the substructure, shifts the natural frequency of the structure to a lower value. Incorporating seismic isolators is a more attractive option than some other quite costly retrofit alternatives that would

instead increase the capacity of the substructure (Timothy et al., 2011). The FHWA retrofit manual refers to seismic isolation and provides guidelines for replacing bridge bearings with isolators. Additionally, it expresses the popularity and success of this retrofit measure (Buckle, Friedland, et al., 2006). The performance of seismic isolation is further emphasized in INDOT's 2013 Bridge Design Manual (2020) and by Timothy et al. (2011).

Previous studies have shown that two types of isolators are particularly effective, elastomeric bearings and friction pendulum devices. Elastomeric bearings normally consist of layered rubber and steel plates, sometimes surrounding a lead core, and often have steel flanges at the top and bottom to facilitate a fully fixed connection. Research has shown that elastomeric bearings reduce substructure damage because they decrease the demand on the substructure (Siqueira et al., 2014). However, standard elastomeric bearings can also significantly increase the displacement of the superstructure, thus creating the need to perform additional checks for abutment pounding. The addition of a lead core to the elastomeric bearing, when applicable, has been shown to mitigate this issue (DesRoches et al., 2004a, b; Wright et al., 2011).

Friction pendulum devices are slider bearings that use low-friction interfaces to decouple the superstructure from the substructure, and sometimes increase the damping in the structure. Several researchers have shown the effectiveness of a friction pendulum to decrease internal forces in substructures, and some states, such as Tennessee, North Carolina, and California, have implemented them (Avossa et al., 2018; Gillich et al., 2018 Timothy et al., 2011). Both elastomeric bearings (with and without a lead core) and friction pendulum device are shown in Figure E.2.

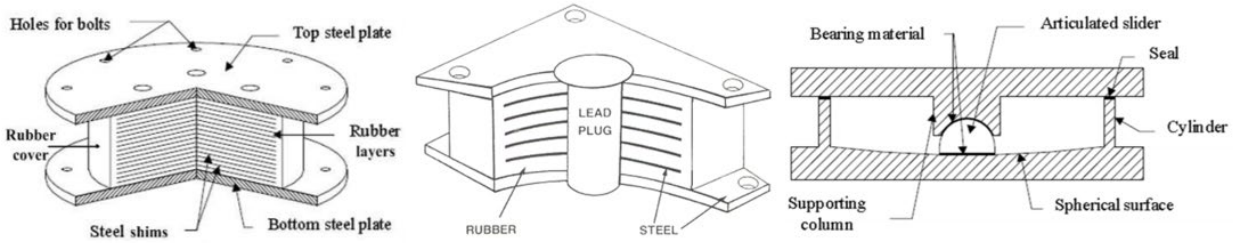

Figure E.2 Seismic Isolators from Left to Right: Elastomeric Bearing, Elastomeric Bearing with Lead-Bearing, Friction Pendulum (Choi, 2002; Ealangi, 2010)

Bridges supported by integral abutments are not vulnerable to seismic hazards in the longitudinal direction, as discussed by Frosch et al. (2009). The reasoning is that the differential displacement and inertial forces generated during seismic loading are negligible, therefore eliminating the demand in the longitudinal direction. Thus, this approach is a suitable seismic retrofit strategy. In cases where construction of integral abutments is not possible, due to bridge length or skew for example, restrainers may instead be added to connect the abutment to the superstructure. Although this retrofit does not result in a monolithic connection like the integral abutment, it can considerably reduce the resulting differential displacement between the structure and adjacent ground, therefore reducing the overall seismic demand.

Two common types of restrainers, cable- and bar-type, are shown in Figure E.3. Restrainers have been shown to effectively prevent excessive longitudinal movement of spans at the abutment or over piers where adjacent simply-supported beams or an internal hinge are present (Timothy et al., 2011). The installation of restrainer bars is relatively inexpensive and recognized by the FHWA for its simplicity and effectiveness. Bar restrainers are less flexible but are more ductile than cable restrainers and are made of galvanized high

strength material. Typically, restrainers are designed using high-strength reinforcement such as carbon-fiber reinforcement because of the increased rigidity and yield stress.

Figure E.3 Restrainer Cables (Left) and Restrainer Bars (Right) (Timothy et al., 2011)

Increasing Capacity

The capacity of each substructure is based on geometry, flexural, and shear reinforcement ratio, concrete strength, and end restraining conditions. Retrofit strategies that are focused on increasing capacity serve to address one or more of these components. One typical strategy is to add exterior reinforcement in the form of a jacket. The addition of a jacket increases the reinforcement ratio therefore increasing flexural capacity and shear strength. It also enhances confinement, which provides an increase in ductility. Common jacketing techniques used in the central US include steel jacketing, concrete overlays, and steel plate encasement, as shown in Figure E.4. These retrofits are usually applied locally at the ends of the substructure member to target the plastic hinge regions, but both steel and concrete jackets can also be applied to the full substructure element height to increase shear strength. For vulnerable walls and hammerheads, the FHWA retrofit manual suggests the use of steel plate encasement with steel anchors, providing active confinement.

Figure E.4 Jackets from Left to Right: Steel Jackets, Concrete Overlays, and Steel Plate Encasement with Steel Anchors (Buckle, Friedland, et al., 2006; Timothy et al., 2011)

Bent caps with a low flexural reinforcement ratio are vulnerable to the mechanism of hinge formation commonly referred to as strong column–weak beam (see Appendix D). This mechanism of hinge formation is rather difficult to rehabilitate after it has formed because the entire superstructure must be lifted so that the hinges in the bent cap may be repaired. Because of these difficulties, the desired mechanism of hinge formation is weak column–strong beam. This mechanism allows a plastic hinge to develop in the column before the beam or bent cap experiences any damage. To ensure that the preferred hinge mechanism forms,

both past research (Timothy et al., 2011) and the Buckle, Friedland, et al., (2006) recommend increasing the strength of the bent cap via external post-tensioning and shear reinforcement, as shown in Figure E.5.

Figure 5 External Post-Tensioning (Left) and Shear Reinforcement (Right) for Bent Cap Strengthening (Timothy et al., 2011)

Application of Recommended Retrofits

The purpose of this appendix is to demonstrate the impact of each retrofit method on the seismic performance of the as-built structure. Each of the recommended retrofit options is demonstrated using a detailed model of its application to a representative bridge. With the outlined procedure and clear evidence of the benefit of each retrofit method, INDOT will have the information to select a suitable retrofit option on a case-by-case basis for bridges identified as moderately to highly vulnerable. Herein, the intention is not to demonstrate a full design for each retrofit method. Rather this report demonstrates the necessary modeling assumptions and methods that should be adopted to successfully demonstrate the impact each retrofit can have on the seismic performance of the retrofitted bridge. All specific retrofit designs should follow applicable codes and standards for the region.

Table E.2 relates each of the identified vulnerabilities (by case) in Table E.1 to the applicable retrofit methods. This table serves as an overarching summary and allows for certain sections of the appendix to be quickly referenced when considering which retrofits apply to a given identified vulnerability. Additionally, the pros and cons for each retrofit are listed at the bottom. As a note, the vulnerability cases for which isolation is identified as a potential retrofit only apply to bridges having a superstructure that is not rigidly connected to the substructure. From the sample set of bridges in Indiana, this has been identified as including primarily steel and prestressed concrete superstructures. It can therefore be assumed that seismic isolation will not typically be a viable retrofit option for bridges having a reinforced concrete slab deck superstructure.

Table E.2 Summary of Recommended Retrofits for Identified Vulnerabilities

Vulnerability Case (Table E.1)	Potential Retrofits					
	Integral Abutments	**Restrainers**	**Isolation**	**Additional Confinement**	**Post-Tension**	**Jacketing**
1	×	×	×			×
2	×	×	×			×
3	×	×	×	×		
4	×	×	×	×		
5	×	×	×	×	×	
6	×	×	×	×		
7	×		×			
Pros	1. Eliminates longitudinal vulnerability entirely	1. Simple design 2. Simple application 3. Common design detail for INDOT bridges	1. Common retrofit 2. Reduce substructure demand significantly	1. Increases ductility 2. Simple design 3. Simple application	1. Changes to preferred failure mechanism (strong column–weak beam)	1. Increases ductility and capacity 2. Identified as most beneficial for highly vulnerable bridges
Cons	1. Transverse direction check still requires vulnerability assessment	1. May require another substructure retrofit (based on design constraints)	1. Potential for pounding unless appropriately designed or additional retrofit exist	1. Negligible increase in structural capacity 2. Not applicable post-damage (per INDOT)	1. Moderate design difficulty 2. May require additional retrofits	1. Jacketing options (steel, reinforced concrete) vary in implementation difficulty

Also, a flowchart that maps each of the vulnerabilities in Table E.1 to the recommended retrofits summarized in Table E.2 is provided in Figure E.6. This flowchart, paired with the flowchart describing the Level 2 assessment procedure and the list of vulnerabilities shown in Table E.1, can used as a design aid. Together they serve as a guide for both conducting a Level 2 assessment and identifying retrofit options to improve the seismic response of bridges. An important note to Figure E.6, is that presently according to INDOT's 2013 Design Manual (Sec. 412-3.05(05)) (2020), improvement in structural capacity and/or confinement is only guaranteed with a jacketing system (concrete or steel) in addition to the fiber wrap.

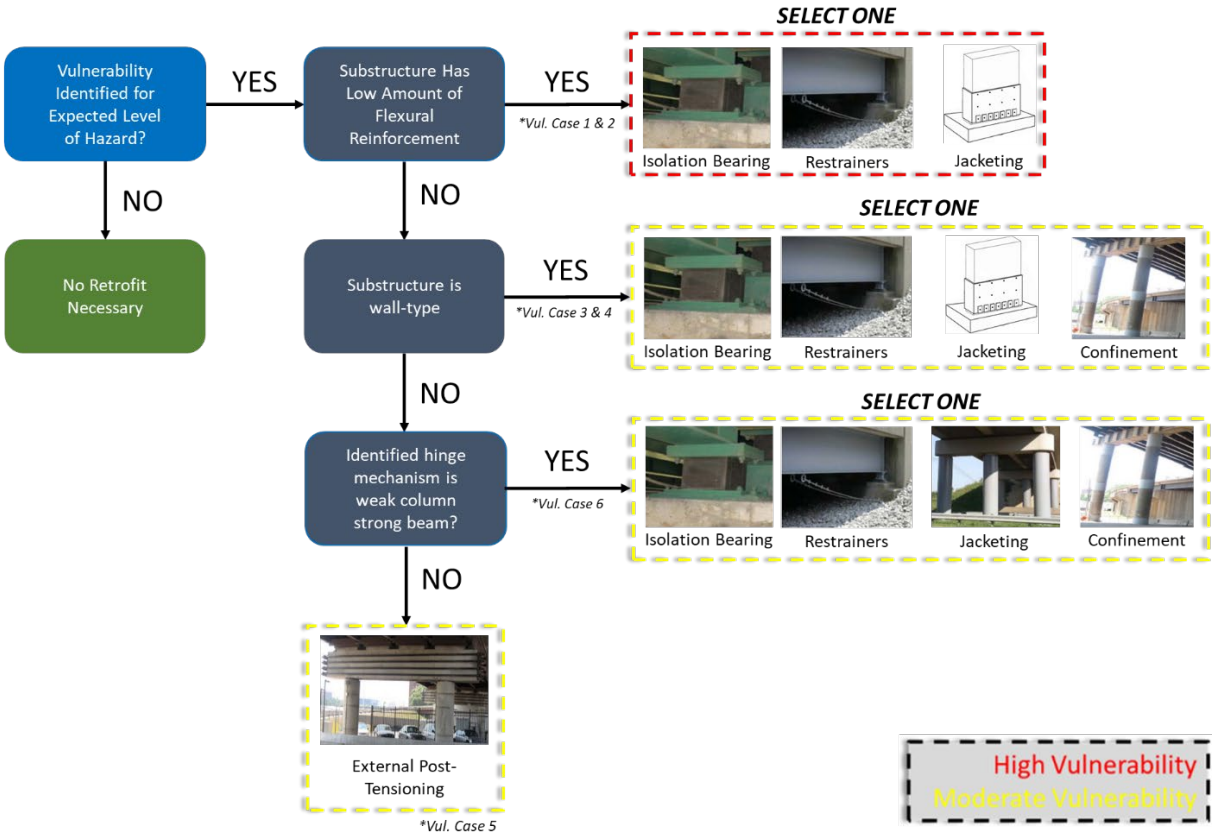

Figure E.6 Retrofit Selection Procedure

The implementation of integral abutments, additional confinement, and post-tensioning do not require modifications to the modeling technique outlined in Appendix D, and thus are only briefly discussed here. These retrofit methods either have the potential to considerably lower the vulnerability level (in the case of integral abutments) or to maintain the same level of vulnerability but facilitate a more desirable response (in the case of additional confinement and post-tensioning). The implementation of restrainers, isolation, and jacketing do require slight modifications to the detailed dynamic modeling technique. The degree of impact of these three retrofit methods on a bridge's vulnerability is dependent on the engineering design decisions. It is feasible through the design process to move a highly vulnerable structure to a lower vulnerability. These retrofit methods are discussed more extensively herein, with the impact of each approach being demonstrated by assessing the change in the seismic response in the longitudinal direction of a representative bridge.

It is possible that the vulnerability of each bridge detail can be improved by more than one of the identified retrofits. Additionally, it is possible that more than one vulnerability case applies to the bridge, such as a combination of one of the vulnerabilities from cases 1–6 and vulnerability case 7 as is the case for a continuous steel superstructure with deficient rocker bearings and substructure.

Structure number 067-18-05459 D (NBI 24210) is a two-span continuous steel girder bridge with 8 beams and a hammerhead wall substructure. The structure was originally constructed in 1973 with rehabilitations in 1996, 1999, 2008 and 2014 focused on the straightening and eventual replacement of a single beam. The substructure has a reinforcement ratio of 0.22% and a 40 ksi yield stress steel. This bridge has been identified as highly vulnerable due to an insufficient amount of longitudinal reinforcement and the potential

for brittle failure. The moment-curvature and displacement response of the as-built structure based on a detailed model is shown in Figure E.7. The retrofit options described in the remainder of this report will be demonstrated with respect to this bridge.

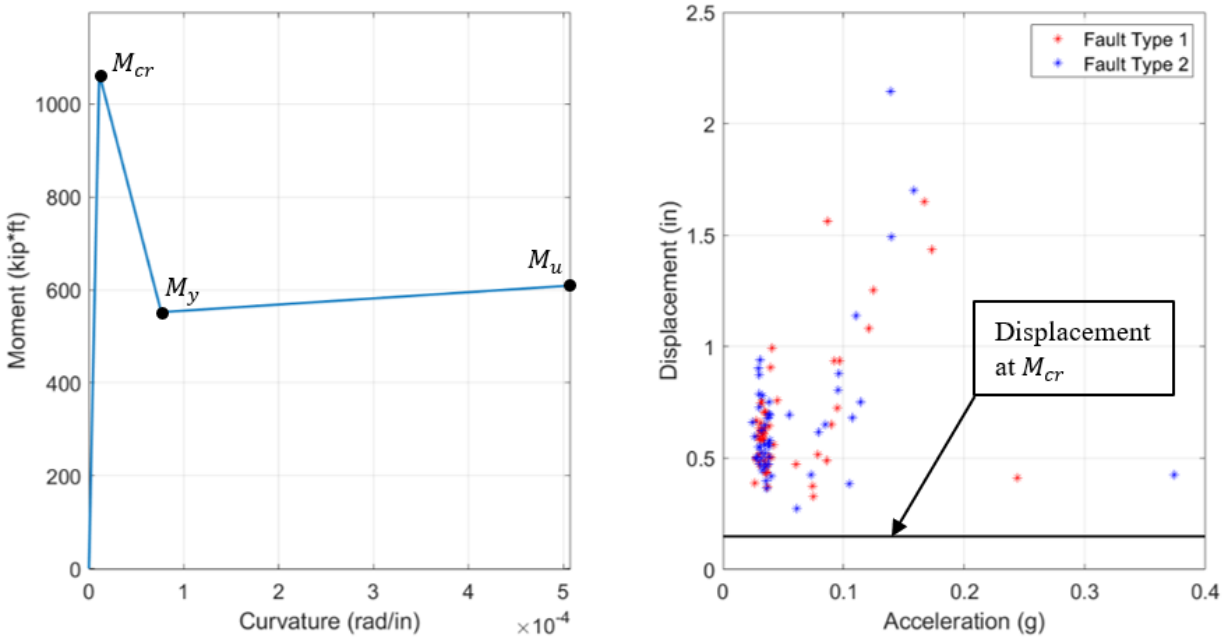

Figure E.7 Moment-Curvature (Left) and Displacement Response (Right) of As-Built Structure (NBI 24210)

Restrainers

The addition of restrainers to bridges with a continuous superstructure, or to bridges with internal hinges, allows for the development of a stiffer system which can lead to decreased displacements and restoring forces. The design of a restrainer system is based on determining the amount of stiffness needed to decrease the overall level of vulnerability to an acceptable level. Figure E.8 shows the response of NBI 24210 with added restrainers considering several different stiffness values. In this figure, the restrainer stiffness (K_{rest}) values correspond to the stiffness associated with one restrainer placed on a single side of one beam. Thus, the overall stiffness of the system is the total stiffness of the restrainers plus the stiffness of the substructure, taken as

$$K_{sys} = K_{pier} + K_{rest} * n_{beams} \quad (1)$$

Typical restrainers do not function well under compression, so the restrainer stiffness is only added to the system when under tension (DesRoches et al., 2004a,b). Therefore, the total stiffness of the restrainers ($K_{rest} * n_{beams}$) must be added at both ends of the superstructure because it is expected that only one end of the bridge will experience tension at a time under normal earthquake excitations.

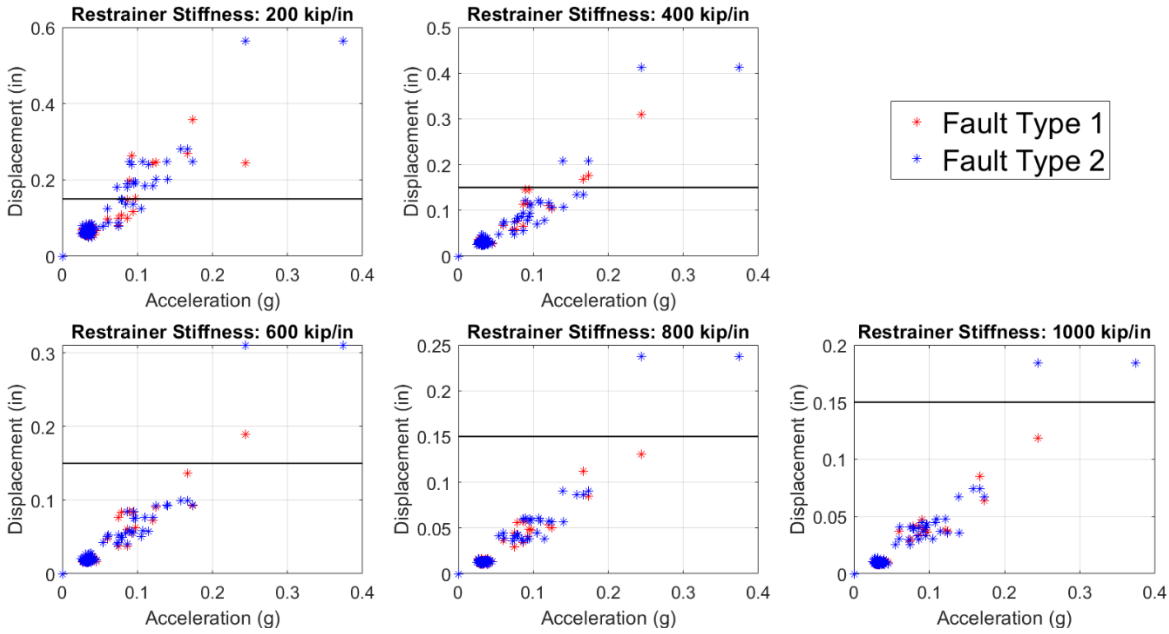

Figure E.8 Displacement Response of Retrofitted Bridge for Several Restrainer Stiffness Values (NBI 24210)

The vulnerability of the bridge is determined here for several restrainer stiffness values. The appropriate amount of stiffness should be selected based on the desired level of performance. Figure E.8 shows the displacement response as a function of base excitation. The impact each restrainer system has on improving the overall vulnerability of the structure is shown in Table E.3, as determined using the suite of site-specific earthquakes for the NBI 24210 bridge. Here the percent exceedance corresponds to the percentage of the total number of earthquakes that results in bridge displacements that exceed the cracking displacement of the substructure.

Once a desired level of performance is identified, the necessary restrainer area can be calculated using a standard approach (Trochalakis et al., 1996). As is common for all materials that function primarily under tension, the stiffness of the restrainer derives from axial stiffness. The cross-sectional area required to achieve a specific axial stiffness can be calculated as

$$n_{bars} * A_{rest} = \frac{k_{rest} * n_{beams} * L_{rest}}{E_{rest}}. \quad (2)$$

Assuming values for length ($L_{rest} = 24\ in$), yield stress of high-strength steel ($f_{y_{rest}} = 150\ ksi$), modulus of elasticity ($E_{rest} = 29000\ ksi$), and a single bar per restrainer (n_{bars}), the minimum area shown in the table is calculated for each scenario. The tensile stress of the restrainer at the design displacement should also be checked to confirm that yielding of the restrainer does not occur, as shown in the last column of Table E.3. A conservative estimate of the stress in the structure is calculated using the maximum allowable displacement of the substructure ($d_{lin} = 0.15\ in$). In practice, the actual displacement corresponding to the level of seismic excitation selected by the designer would be used in this calculation.

Table E.3 Dynamic Parameters and Vulnerability for Several Restrainer Stiffness Values

Restrainer Stiffness (kips/in)	Period (s)	Percent Exceedance (%)	Minimum Area per Restrainer (in^2)	Stress (ksi) at $d_{lin} = 0.15\ in$
200	0.28	18	0.17	30
400	0.2	5	0.33	60
600	0.17	2	0.50	90
800	0.15	1	0.66	120
1000	0.13	1	0.83	150

As shown in Table E.3, most of these restrainers can physically and realistically be applied. However, choosing a restrainer stiffness of $1{,}000\ kips/in$ stiffness is not recommended, as the minimum area invokes yielding of the steel. An alternative in this case would be to either use multiple restrainer bars per beam or to ensure a lower maximum displacement of the structure.

Designers should also be aware of the impact that bridge specific boundary conditions and allowable substructure displacement requirements have on the necessary length of the restrainer. Even for systems with the same amount of restrainer stiffness, the necessary area to reduce seismic vulnerability may differ due to this required length.

Seismic Isolation

The decoupling of the superstructure mass from the substructure via an isolation mechanism has been shown to significantly reduce the amount of displacement and restoring force drawn to the substructure without significantly impacting the displacement of the superstructure (when compared to a non-isolated model). The implementation of seismic isolation primarily requires three modifications to the modeling technique outlined in Appendix D. Specifically, the model is changed from a single-degree-of-freedom (SDOF) system to a multi-degree-of-freedom (MDOF) system, the model incorporates the stiffness of the isolation system, and the model uses non-classical damping to account for the large difference between the damping ratio inherent in the substructure and that introduced by the isolator. In this section, the adjustment made to the model is discussed for each of these factors.

First, the original model assumes a uniform displacement of the superstructure and substructure. With the introduction of a seismic isolator, this assumption is no longer valid. To account for the differential displacement of the isolator, the structure is modeled as a MDOF, as shown in Figure E.9.

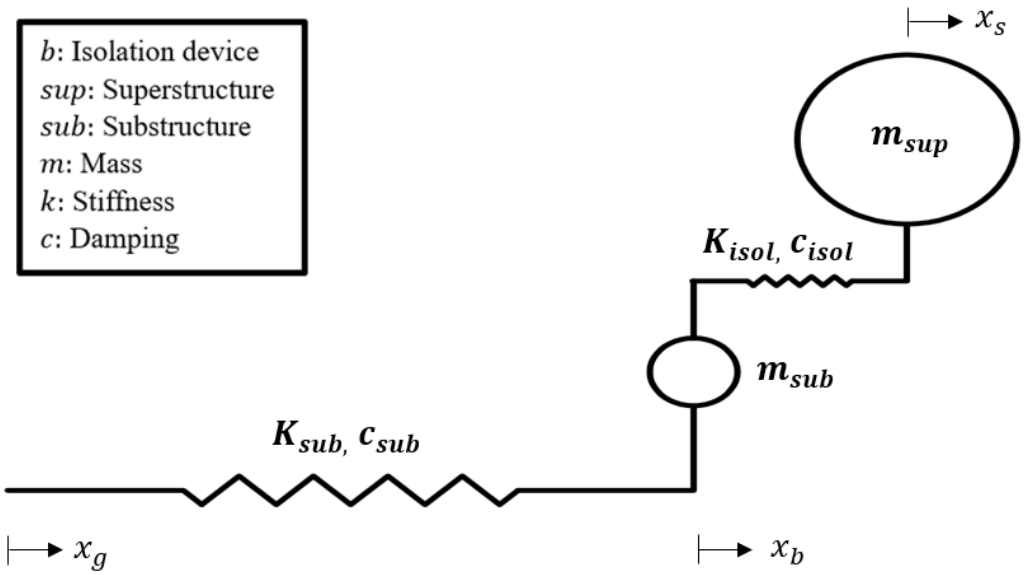

Figure E.9 MDOF Model of the Bridge with Seismic Isolation

Substituting absolute displacement parameters (x_s, x_b, x_g) for relative displacement parameters ($u_s = x_s - x_g;\ u_b = x_b - x_g$), the equation of motion, without initially considering damping, for the model is written as

$$\begin{bmatrix} m_{sub} & 0 \\ 0 & m_{sup} \end{bmatrix} \begin{bmatrix} \ddot{u}_b \\ \ddot{u}_s \end{bmatrix} + \begin{bmatrix} K_{sub} + K_{isol} & -K_{isol} \\ -K_{isol} & K_{isol} \end{bmatrix} \begin{bmatrix} u_b \\ u_s \end{bmatrix} = -\begin{bmatrix} m_{sub} & 0 \\ 0 & m_{sup} \end{bmatrix} \begin{bmatrix} \ddot{x}_g \\ \ddot{x}_g \end{bmatrix}. \quad (3)$$

Next, because isolators such as elastomeric bearings are highly non-linear as shown in Figure E.10, it is common practice to model these elements using an effective linear stiffness (Buckle, Consantinou, et al., 2006). Significant experimental research has been conducted to characterize the basic properties of elastomeric bearings, such as quantifying the shear modulus (AASHTO, 2018; Roeder et al., 1987). This research shows the impact that elastomeric bearing dimensions have on their overall stiffness, which is primarily developed as shear stiffness. Using a common elastomeric bearing pad with dimensions of 20 *in* × 13 *in* × 3 *in* (50.8 *cm* × 33 *cm* × 7.6 *cm*) (INDOT, 2012), the stiffness of the isolator can be calculated as

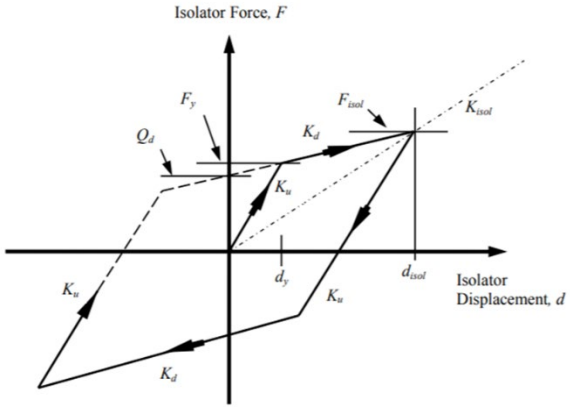

Figure E.10 Force-Displacement Response of Typical Elastomeric Isolator (Buckle et al., 2011)

$$K_{isol} = \frac{G_{isol} A_{isol}}{h_{isol}} = \frac{(100\ psi) * (20in * 13\ in)}{3in} = 8.6ksi. \quad (4)$$

Finally, non-classical damping is used to account for the large difference between the damping coefficients introduced by the substructure ($\zeta_{pier} = 0.05$) and the isolator (Chopra, 2012). Here the presence of the elastomeric bearing pads is captured using a damping ratio in the second mode of 0.10 (Choi, 2002). Using

the same force-equilibrium technique previously used to write the equation of motion, the damping matrix is constructed as

$$\begin{bmatrix} c_{sub} + c_{isol} & -c_{isol} \\ -c_{isol} & c_{isol} \end{bmatrix} \begin{bmatrix} \dot{u}_b \\ \dot{u}_s \end{bmatrix}. \tag{5}$$

Thus, the viscous damping rate for the pier and the isolator, respectively, are calculated as

$$c_{sub} = 2\zeta_{sub}\sqrt{K_{sub} * m_{sub}}\,, \tag{6}$$

$$c_{isol} = 2\zeta_{isol}\sqrt{K_{isol} * m_{sup}}\,. \tag{7}$$

With these modifications applied to the modeling technique, the impact of the retrofit is explored and compared to the non-isolated (or as-built) response shown in Figure E.7. While the capacity of the substructure does not change with the introduction of an isolation system, the substructure displacement is significantly reduced. Furthermore, the superstructure displacement response has the same magnitude as that of the non-isolated structure. The responses of the retrofitted bridge, for the same set of site-specific earthquakes, is shown in Figure E.11.

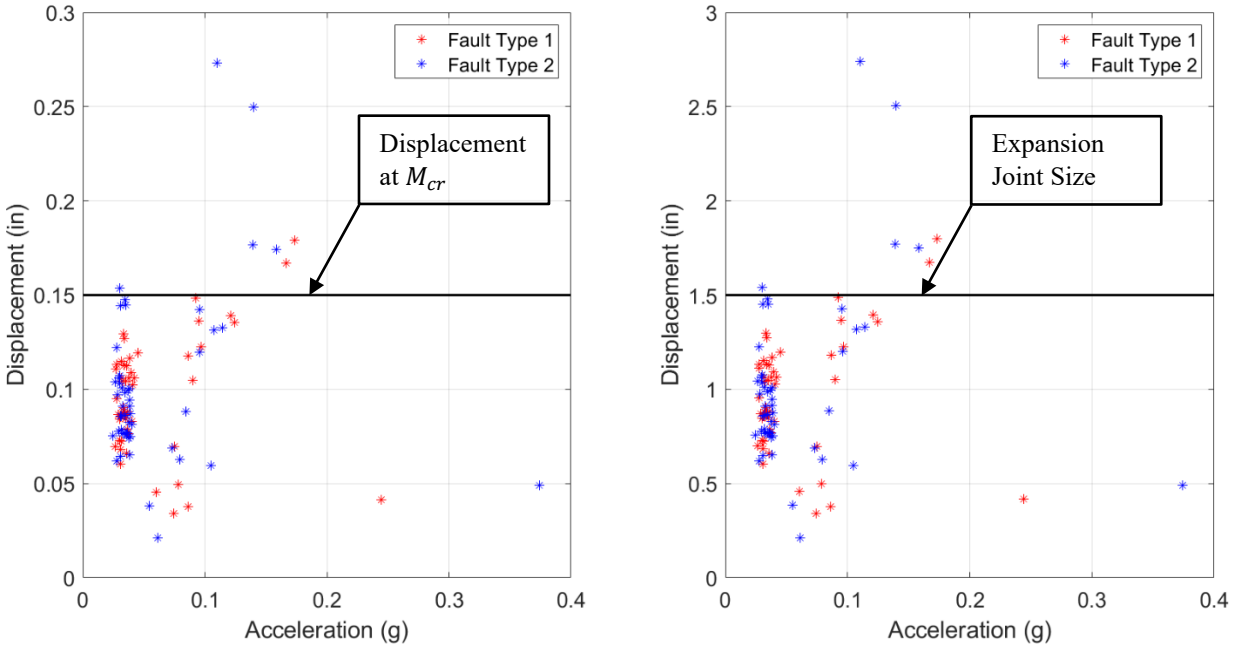

Figure E.11 Displacement Response of Substructure (Left) and Superstructure (Right) of Isolated Bridge for 100 Site-specific Earthquakes (NBI 24210)

As shown in Figure E.11, introducing the isolator reduces the displacement responses for more than 90% of the simulated earthquakes to an acceptable level, moving the structure from a high vulnerability to low vulnerability classification. Seismic isolators for this bridge could feasibly be designed for an identified level of base excitation such that the bridge would achieve a low level of seismic vulnerability.

Jacketing

An alternate approach to improving the seismic performance of the structure is to increase the overall flexural capacity and improve confinement of the vulnerable detail. The addition of a steel jacket to the outside of the substructure has the capability to significantly improve the base shear of the substructure. As a reminder, the base shear is the shear capacity which corresponds to the development of the identified hinge formation (see Appendix D). This retrofit has been identified as most beneficial for the highly vulnerable cases where the mechanism of failure is brittle. To capture this in the model, the implementation of steel jacketing requires a small update to the assumptions made for the moment-curvature calculations presented in Appendix D, specifically the cracking moment. The cracking stress of concrete remains the same ($7.5\sqrt{f_c'}$) and the cracking moment is achieved when this stress occurs at the interface between the original concrete section and the steel jacket. Using a linear strain profile, the corresponding strain is calculated in the steel jacket and the total cracking moment is calculated. The updated moment-curvature response for NBI 24210 and a steel plate thickness (t_{steel}) of $0.25\ in$ is shown in Figure E.12.

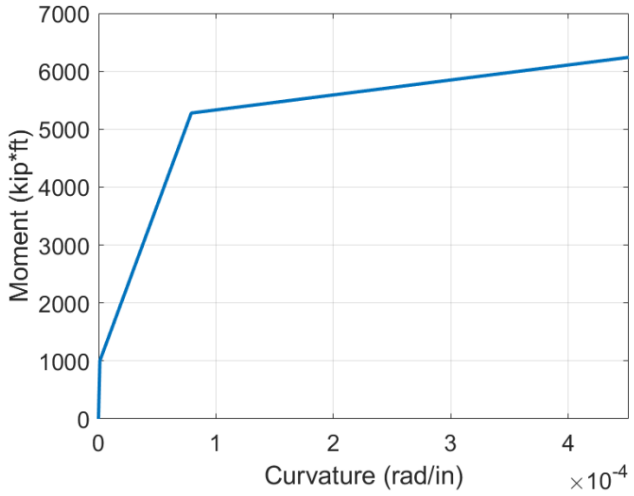

Figure E.12 Moment-Curvature Response for Retrofitted Bridge with Steel Jacketing (NBI 24210)

Next, the overall vulnerability of the bridge can be determined for various potential plate thicknesses. One can select the appropriate plate thickness based on the desired level of performance. Table E.4 shows the impact of the thickness of the jacket on the overall vulnerability of the structure when subjected to the site-specific earthquakes for this bridge. Here, the percent exceedance is the percent of the total number of simulated earthquakes in which the displacement response obtained with the corresponding retrofit exceeds the displacement. As a reminder, a linear model is used for substructures that are expected to exhibit a brittle mode of failure.

Table E.4 Likelihood of EQ Displacement Exceeding Retrofit Capacity for Given Plate Thickness

Plate Thickness (in)	Percent Exceedance (%)
0.25	48
0.38	10
0.50	6
0.63	4
0.75	1
1.00	0

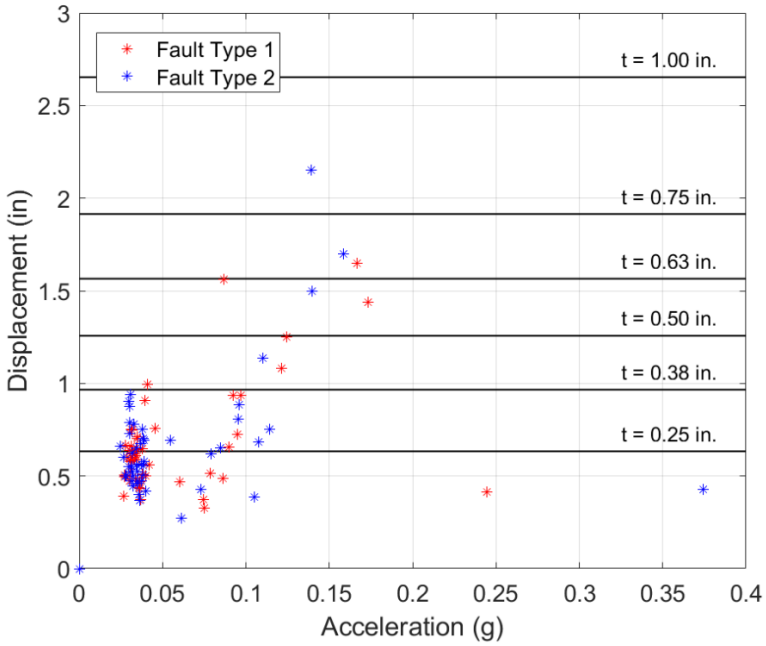

Figure E.13 Impact of Steel Plate Thickness for Retrofitted Bridge (NBI 24210)

As shown in Figure E.13, the response of NBI 24210 improves as the thickness of the steel is increased. While the additional steel allows for a more ductile response of the substructure, as shown in Figure E.12, it is still recommended to design the retrofit such that the structure remains linear. This recommendation is carried out in the modeling approach and in the corresponding results presented. Lastly, since the base shear of the substructure has increased, the mechanism of shear failure must be checked again to determine the controlling mechanism of failure (see Appendix D). It is recommended that the retrofit be designed so that the base shear of the structure controls rather than the shear capacity.

Integral Abutments

The use of integral abutments eliminates the inertial effects of the structure in the longitudinal direction thereby removing any vulnerabilities in this direction (the transverse direction would still have to be checked). Furthermore, Frosch et al. (2009) have shown that INDOT integral abutment details have enough capacity to resist the forces transferred to the abutment by earthquakes. It is recommended to continue with the implementation of integral abutments using INDOT's standard drawing.

Added Confinement

Additional confinement is recommended to increase the rotational capacity of the identified hinge mechanism once it has formed in the structure (Alkhrdaji & Silva, 2008). This retrofit does not reduce the overall vulnerability of the structure, rather it ensures a more ductile performance of the structure at the same moderate level of vulnerability. This retrofit option does not significantly increase the structural capacity of the section. Furthermore, it is recommended that any additional capacity that might be added to the substructure due to the added confinement, e.g., a fiber-reinforced polymer wrap be considered negligible. As Table E.2 shows, this retrofit has the potential to apply to every case in which the identified level of vulnerability is moderate, but a couple of other factors must first be considered when determining whether the retrofit is necessary for the given case. For the vulnerability cases in which the development of the identified hinge formation is expected, the two primary concerns are excessive spalling of concrete and

the occurrence of bar buckling in the longitudinal bars after the formation of the hinge and the corresponding concrete spalling.

Determining whether the section will experience buckling of the longitudinal bars after the formation of the identified hinge mechanism requires a Level 2 assessment of the transverse reinforcement spacing. In accordance with AASHTO section 5.10.11.4, the transverse reinforcement ratio must meet specific criteria depending on the type of substructure. Table E.5 shows a summary of these design requirements.

Table E.5 Transverse Reinforcement Criteria in Region(s) of Plastic Hinge

Substructure Type	Code Requirement	Code Reference
Wall-Type	Weak direction (primary direction of concern) designed using column requirements	5.10.11.4.2
Circular Column	$\rho_s \geq 0.12\frac{f_c'}{f_y}$	5.10.11.4.1d-1
Rectangular Column	$A_{sh} \geq 0.30sh_c\frac{f_c'}{f_y}(\frac{A_g}{A_c}-1)$	5.10.11.4.1d-2
	$A_{sh} \geq 0.12sh_c\frac{f_c'}{f_y}$	5.10.11.4.1d-3

For substructures with an adequate reinforcement ratio, additional confinement is not necessary as the plastic hinge has adequate confinement and stability to prevent the buckling of longitudinal reinforcing bars. For substructures with an inadequate reinforcement ratio, additional confinement is recommended to achieve adequate ductility and improved energy dissipation. Fiber-reinforced polymer, such as carbon-reinforced polymer (Alkhrdaji & Silva, 2008) is typically a recommended material for wrapping vulnerable details. Currently, INDOT does not permit the use of external FRP jacketing to restore the structural ductility of the substructure once damage has occurred. In such a case where the retrofit is applied retroactively to a seismic event on a bridge that experienced damage, jacketing can be implemented to provide the required confinement. Though the purpose of jacketing in this case is not to increase capacity, but rather to improve ductility, the section will also gain some capacity from the jacketing, thereby obtaining improved flexural strength and structural response. According to INDOT's 2013 Design Manual (Sec. 412-3.05(05)) (2020), this improvement in structural capacity and/or confinement is only guaranteed with the addition of a jacketing system (steel or concrete). Of the vulnerability cases identified in Table E.1, the requirements in Table E.5 apply to wall-type substructures and reinforced-concrete frame bents. For pile-type substructures, specifically H-Piles with an outer cage of reinforcement such as typical RC columns, the parameters shown in Table E.5 do apply. For H-Pile columns where an outer cage of reinforcement is not present, additional confinement is generally recommended. Bridges with concrete-filled tubes (CFT) as columns do not require additional confinement as this substructure type is rather ductile due to the presence of the steel jacket and is not prone to local buckling failure as the column is braced along its entire length with the in-fill concrete.

Post-Tensioning

The Level 2 assessment presented in Appendix D suggested that a small percentage of the frame bents have a strong column–weak beam failure mechanism which means that under strong ground motions plastic hinges will form at the base of each column and the ends of every beam element. This mechanism, when formed, is not ideal for rehabilitation as it requires extensive effort to lift the entire superstructure and make

repairs to concrete and steel in the hinge region. Therefore, it is recommended to use post-tensioning to change the failure mechanism from strong column–weak beam to weak column–strong beam (see Appendix D for more details regarding mechanism of hinge formation). The required amount of added post-tensioning should be calculated by first determining the amount of additional energy required for the weak column–strong beam mechanism of hinge formation to occur.

Replacement of Rocker Bearings

While the allowable displacement of the rocker bearing (see Appendix D) often exceeds the displacement associated with the substructure vulnerability or the displacement that would cause abutment pounding, the replacement of rocker bearings is still recommended. The allowable displacement of the rocker bearing is calculated assuming a perfect, upright initial position with the ability to freely rotate. Therefore, it is recommended that any rocker bearings having either an initial angle greater than 30 degrees or a significant amount of corrosion that would limit rotation, be replaced. In addition, rocker bearings should be replaced whenever a bridge is scheduled for rehabilitation. It is recommended to continue with INDOT's current practice of converting bridges with rocker bearings and expansion joints to semi-integral abutments.

Conclusion

The application of seismic retrofit methods has the potential to significantly increase the seismic performance of those bridges throughout Indiana that are found to be vulnerable. As shown in this appendix, a variety of retrofit methods are available for level of hazard and bridges in Indiana. As we demonstrate herein, several of these methods could be applied to the same bridge to achieve a similar level of performance. Based on the vulnerability present in each bridge, the information in this appendix can be used to select an approach that will improve the seismic performance of INDOT's bridge inventory.

APPENDIX F. IDENTIFICATION OF BIAS DATABASE ENHANCEMENTS TO ENABLE SIMPLIFIED (LEVEL 1) SEISMIC VULNERABILITY ASSESSMENT

Introduction

The Recording and Coding Guide for the Structure Inventory and Appraisal of the Nation's Bridges (Guide), compiled by the Federal Highway Administration (FHWA), outlines the requirements for utilizing, recording, and coding bridge information consistently on a national level. Based on the Guide, the National Bridge Inventory (NBI) database retains a homogeneous record of critical information for all bridges and tunnels in the United States which carry or intersect roadways. Although the collection of these NBI data items is required across all states, the collection of additional data items for maintenance and assessment purposes varies from state to state. The Indiana Department of Transportation (INDOT) currently maintains the Indiana Bridge Inspection Application System (BIAS) database, an asset management system that is leveraged for prioritizing repair, retrofit, and rehabilitation of the Indiana bridge inventory.

The purpose of this study is to leverage the available information in the BIAS database toward a simplified seismic assessment procedure, herein referred to as Simplified Assessment, and when necessary, to recommend additional data items to support a robust dynamic analysis. This deliverable specifically identifies and discusses eight data items that we recommend be added to BIAS to support a Simplified Assessment of Indiana's bridge network. We also discuss potential methods for gathering the data items. In this study, the detailed assessment of a specific bridge in the inventory using design drawings and specific ground motions will be referred to as a Level 2 assessment.

Summary of Data Role in Simplified Assessment

To fully appreciate the significance of the data items in the Simplified Assessment, it is important to have a clear understanding of the procedure, which is shown in Figure F.1.

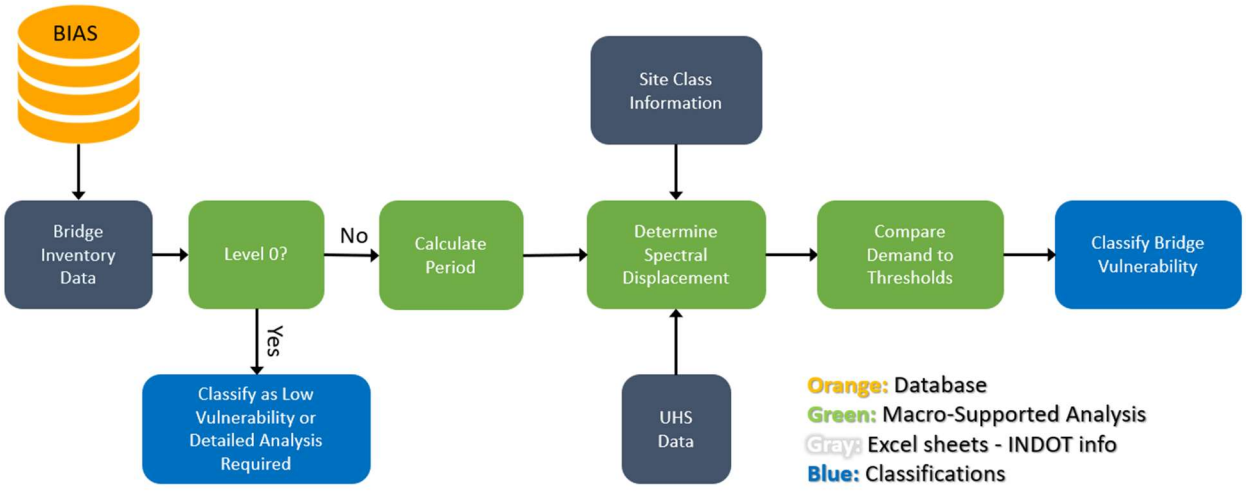

Figure F.1 Simplified Assessment Procedure

As shown, the Simplified Assessment is established on bridge inventory data, which demonstrates the importance of data accuracy and data richness. While BIAS provides part of the necessary bridge inventory data, more data information is recommended to be added to conduct a comprehensive Level 1 assessment.

Recommended Data Items and their Benefits

Eight data items are recommended as additions to BIAS to both enable the execution of the Simplified Assessment and influence its robustness. Before we explain the impact that the data item will have on vulnerability assessment results, we define each as follows:

- **Substructure Type:** The most appropriate substructure type should be identified from these five: rectangular column frame bent, circular column frame bent, hammerhead wall, wall and other. Note that a vulnerability assessment is not possible without this data item, other than the Level 0 of the Simplified Assessment (see Appendix G), is not possible without this data item.
- **Abutment Type:** The most appropriate abutment type should be added from these two: integral-type (including semi-integral) or non-integral-type.
- **Deck Thickness:** The thickness of the reinforced concrete deck (*in*).
- **Number of Elements:** Typical number of columns in a single bent.
- **Element Length:** Out-to-out dimension in the transverse direction for a single substructure element (*ft*). For example, this is the longer dimension for walls and hammerheads.
- **Element Width:** Out-to-out dimension in the longitudinal direction for a single substructure element (*ft*).
- **Element Height:** Clear height of the substructure/unsupported length of the substructure(*ft*). For frame bents, this is measured from the top of the footing or the crash wall to the base of the bent cap. For walls, this is measured from the top of the footing to the top of the wall (including the bent cap if there is one).
- **Height Ratio Flag:** "Yes" or "No" flag to identify if any piers in the bridge have a height ratio (H_{ratio}) between the taller pier (H_{tall}) and shorter pier (H_{short}) greater than 1.1.

To demonstrate the impact of each data item, two kinds of pie charts are generated based on the analysis of the 100-bridge sample set developed for this project. The first type of pie chart is included to demonstrate the number of bridges that can actually be assessed using a Simplified Assessment when certain data items are not available. The charts in Figure F.2 show this impact of estimating the eight vital data items. The basis of comparison here is the case in which all critical information (all data items listed above) is available in BIAS, as shown in Figure F.1(a). Similarly, the charts in Figure F.3 show the impact of these estimates on the accuracy of the assessment results. The basis of comparison is the case is when all critical information is available in BIAS, as shown in Figure F.2(a). Figures 1(b)–(g) and Figures 2(b)–(g) should each be compared to these base cases, respectively, as a measure of their relative quality. The importance of each data item for the Level 1 assessment, as demonstrated in Figures 1 and 2, is further explained in the subsequent sections.

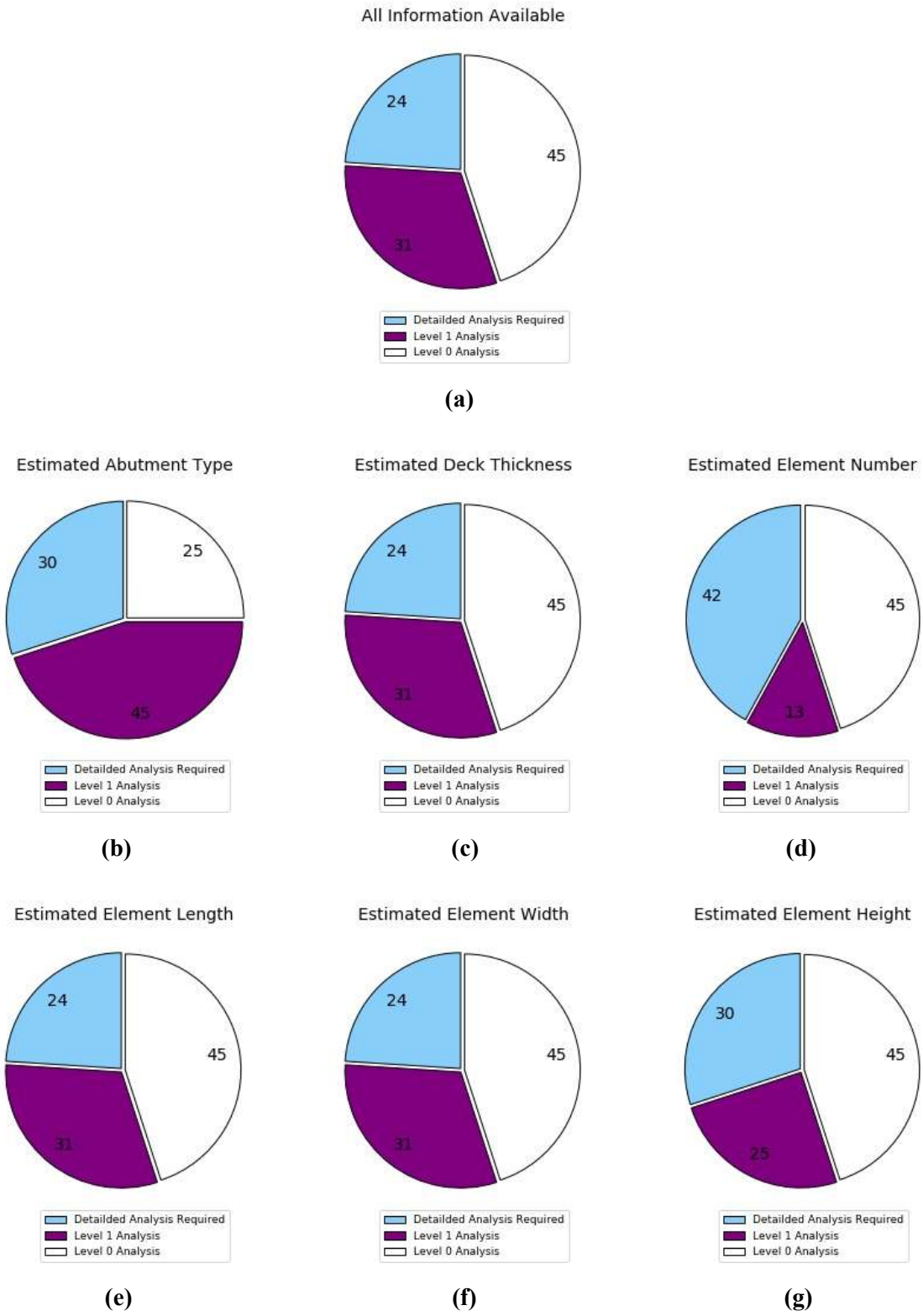

Figure F.2 Number of Assessment Type with Different Estimated Information: (a) All Information Available; (b) Estimated Abutment Type; (c) Estimated Deck Thickness; (d) Estimated Element Number; (e) Estimated Element Length; (f) Estimated Element Width; and (g) Estimated Element Height.

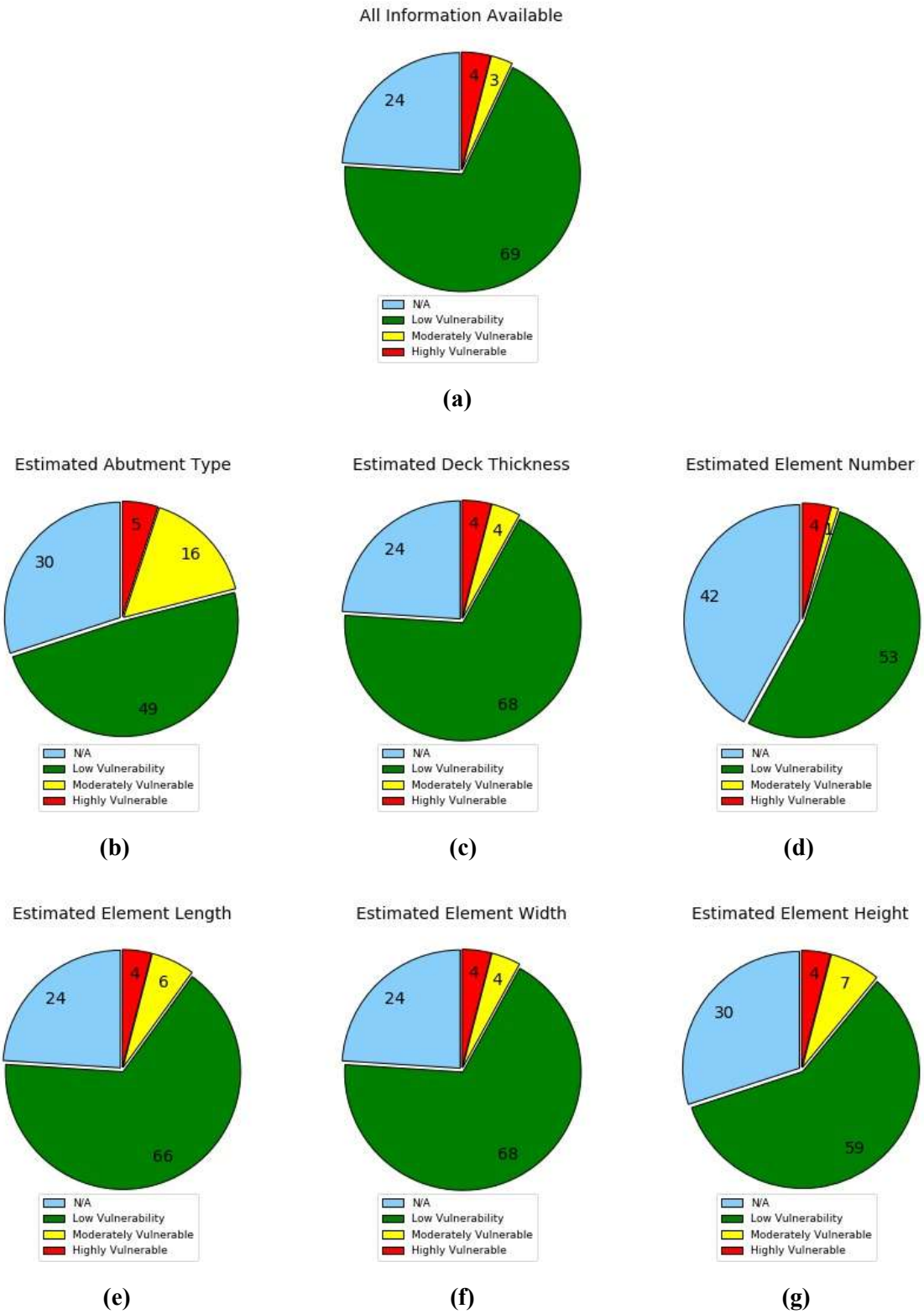

Figure F.3 Level 1 Analysis Results with Different Estimated Information: (a) All Information Available; (b) Estimated Abutment Type; (c) Estimated Deck Thickness; (d) Estimated Element Number; (e) Estimated Element Length; (f) Estimated Element Width; and (g) Estimated Element Height.

Substructure Type

Substructure Type is essential to perform any Simplified Assessment Without this information, the stiffness of the bridge cannot be determined, and all multi-span bridges would require a Level 2 assessment

Abutment Type

During the Level 2 assessment, two types of abutments are identified: integral and non-integral. Bridges with integral abutments are not vulnerable in the longitudinal direction because there is no differential displacement between the bridge and the ground. By including the abutment type in BIAS, the accuracy of the Simplified Assessment improves considerably. Without this information, all abutments are assumed to be non-integral. In that case, the vulnerability of the integral bridges will be misclassified. As shown in Figure F.2(b), when this data item is not available, the number of bridges that are classified as "Level 0 Analysis" assessment type decreases and the number of bridges that are classified as moderately vulnerable in the Level 1 assessment increases, as shown in Figure F.3(b).

Deck Thickness

Deck Thickness is needed to calculate the mass of all superstructure types and its contributing stiffness to reinforced-concrete slab deck superstructures. Thus, this information is critical for reinforced-concrete slab deck bridges. The current BIAS database does not include deck thickness information. Without this information, the number of bridges that are classified as moderately vulnerable during the Level 1 assessment decreases, as shown in Figure F.3(c).

Number of Elements

The *Number of Elements* corresponds to the number of columns in a single pier. For wall and hammerhead substructures this value is 1. While this value is not necessary for walls and hammerheads, it is critical for bridges with frame bent substructures. There is no way to estimate the number of elements in a frame bent, so if this data item is not included, all frame bents in the sample will require a Level 2 assessment, as shown in Figure F.2(d). Consequently, the number of assessment type classified as "Detailed Analysis Required" will increase.

Element Length

Element Length is required for calculating bridge stiffness. As shown in Figure F.2(e), estimating this information does not influence the assessment type that is performed. However, it causes an increase in the number of moderately vulnerable results, and a decrease in the number of low vulnerability results, as shown in Figure F.3(e). Thus, the accuracy of the Level 1 assessment is influenced.

Element Width

Element Width is required for calculating bridge stiffness. As shown in Figure F.2(f), estimating this item will not influence the type of assessment to be performed, but will increase the number of moderately vulnerable results, as shown in Figure F.3(f). Thus, the accuracy of the Level 1 assessment is influenced.

Element Height

Element Height can be estimated as the recorded minimum vertical clearance for bridges over roadways. However, this data item is not consistently accessible in BIAS. Using an estimated height leads to a smaller number of Level 1 assessments (because there is no data in the two fields) and a misclassification of the

vulnerability due to errors in the estimates, as shown in Figure F.2(g) and Figure F.3(g). Thus, the accuracy of the results is influenced, and it is best to include the actual dynamic height of the substructure.

Height Ratio Flag

The height ratio between adjacent piers influences the response of the structure due to non-linear structural softening and force redistribution. The Level 1 assessment uses a single height to estimate the stiffness of the substructure. Thus, the inclusion of a *Height Ratio Flag* is used in two ways. First, this flag identifies bridges for which a single height is not truly representative of every pier. Second, this flag identifies bridges for which the Level 1 is prone to underestimating the vulnerability due to the inability to completely account for non-linear force redistribution. If the *Height Ratio Flag* is not included, the uncertainty in the vulnerability classification greatly increases.

Methods for Generating and Populating the Recommended Data Items

Considering the items that are suggested, we propose several methods to generate this information. These methods include traditional methods, such as gathering the information from bridge design drawings or during visual inspection, and new methods, such as artificial intelligence.

Design Drawings and Visual Inspection

Bridge design drawings provide the most complete form of details for a bridge, which can be utilized for generating the information INDOT needs to leverage the functionality of the Simplified Assessment tool, INSAT. To perform each Level 2 assessment in this project, bridge details were collected from the bridge drawings. It is possible to gather all recommended data items from the bridge drawings, but this process is very time intensive and is not recommended for large scale data collection.

When using design drawings to extract this information, some challenges do exist.

- There are about 6,000 state-owned bridges in Indiana and thus manually gathering the information via design drawings is a time-consuming task.
- Some bridges do not have complete, clear design drawings, particularly for bridges that were built many years ago (which also may generally have higher vulnerability to earthquakes). This may result in yielding incomplete information when it is gathered from design drawings.
- Because of modifications made to the code at different periods, the information recorded in the drawings is not uniform, e.g., some bridge drawings record the soil elevation while others do not, and such variability makes it difficult to extract complete information.

Rather than combing through structural drawings, the recommended information can more readily be collected via visual inspection. Based on a typical bridge inventory inspection cycle of 2 years, all of the bridge information can be collected during a 2-year period.

Artificial Intelligence

An alternative method to gather critical data items recommended by this study could be using some artificial intelligence techniques. With the development of artificial intelligence (AI), image classification and computer vision techniques have matured to the point where they can provide a fast method for generating certain information. Information that can be readily observed by a human can frequently be extracted from suitable photographs by a computer. This does require knowledge of convolutional neural networks and a labeled image set to use for training and validation of the classifier. For instance, substructure type and abutment type are likely choices for extracting from bridge images. The process of classifying the bridge

substructure type by image classification is shown below to demonstrate the application of AI techniques for bridge information generation.

AI-based bridge substructure information generation work is presented as an example to provide a detailed demonstration of how to apply AI technique on bridge information generation work. The basic idea for this application is to utilize bridge substructure images to train a deep neural network model, and then apply this trained model to classify all other bridge substructures in the inventory. The general process is shown in Figure F.4.

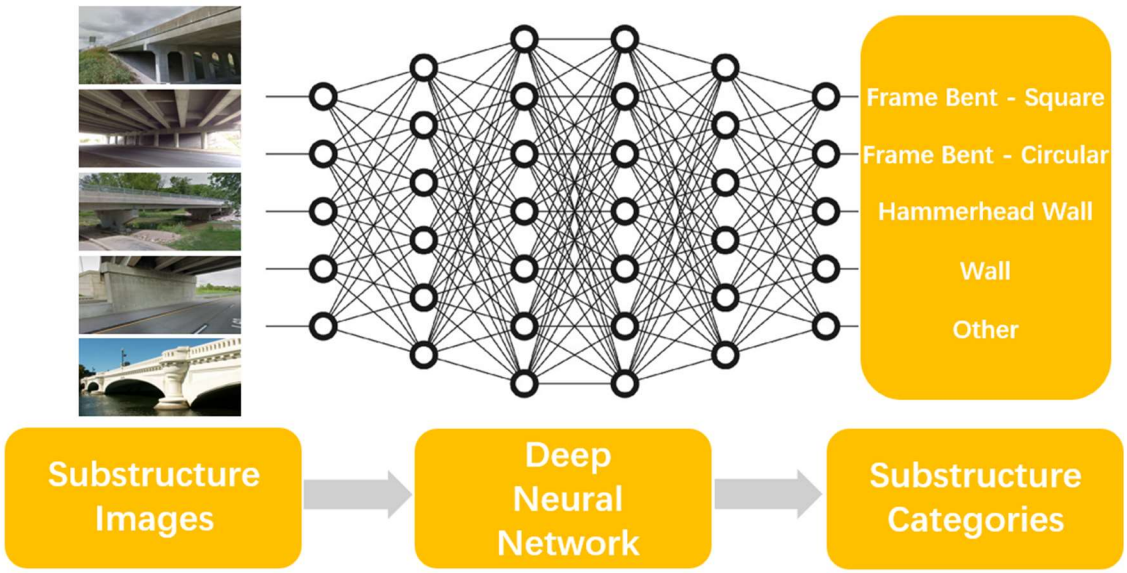

Figure F.4 AI -based Substructure Information Generation Workflow

Recommendations for Improving Database Functionality

During the project, the research team obtained a significant amount of data and drawings from BIAS. Some suggestions surfaced based on facilitating user's convenience. These suggestions include the following:

- Record bridge drawings' name consistently. Inconsistent name of drawings makes the process for finding drawings quite difficult. We recommend posting the bridge NBI number on each drawing document and setting the NBI number as a search term rather than using the structure number.
- Improve the "download image" functionality. At this time, when a large number of images are downloaded at one time, the website stops responding.
- Amend limitations of filtering engine for looking at inspection photos. Refining search terms are required in current usage, which makes it is difficult for engineers and researchers as well as other users to easily get access to the inspection images.

Conclusions

Based on the content above, several key conclusions regarding the current state of BIAS and its capabilities for enhancement can be drawn:

Conclusion 1: As key data items are missing, the number of bridges that can be assessed is greatly reduced and the accuracy of the vulnerability assessments performed is significantly improved.

Conclusion 2: Based on the Simplified Assessment and Level 2 assessments performed, we recommend the following eight data items are added into the database: *Substructure Type, Abutment Type, Deck Thickness, Number of Elements, Element Length, Element Width, Element Height,* and *Height Ratio Flag.*

Conclusion 3: Three methods can be applied to extract the necessary bridge information:

- Design Drawings
- Visual Inspection
- Artificial Intelligence

Conclusion 4: Several database functionalities are recommended for ease of use:

- Modify design drawings name by adding NBI number.
- Improve the "download image" function to match the need of downloading large amount of image.
- Amend search filter engine to enable the searching function to be friendly to less experienced users.

APPENDIX G. DEVELOPMENT OF SIMPLIFIED ASSESSMENT PROCEDURE FOR RAPID IDENTIFICATION OF VULNERABLE BRIDGES

Introduction

The development of the simplified seismic assessment procedure and the identification of critical data items to be added to BIAS is described in detail in this appendix. The process for implementing these two tasks consists of identifying trends from the detailed analysis, applying those trends to develop a simplified SDOF model, and using capacity threshold levels to classify the vulnerability of each bridge. The Level 1 assessment is applicable to 31 of the 100 bridges in the chosen sample set. The rationale for excluding bridges with certain characteristics is described in the initial classification (Level 0) section below.

This appendix first presents the vulnerability analysis results obtained using the best models which use all of the recommended additional data items. Then it discusses potential methods for estimating specific data items when their true values are not readily available and the impact of using these estimates on the results of the Level 1 assessment. The best models for the Level 1 assessment are then used in the associated tool, which is discussed in Appendix H.

Identification of Utilized Data Items

The primary purpose of INDOT's Bridge Inventory Asset Management System (BIAS) is asset management, which includes the storage of inspection reports and information about superstructures that are useful for prioritizing rehabilitations, planning preventative maintenance, and scheduling bridge replacements. In its current state, BIAS does not contain all of the information required to perform an automated simplified assessment of the bridge inventory. However, it does contain some of the information that is needed for the simplified assessment, specifically, the National Bridge Inventory (NBI) data items listed below:

- Asset Name
- Asset Code (NBI Number)
- District
- Latitude
- Longitude
- Number of Spans
- Max Span
- Bridge Length
- Skew
- Year Built
- Superstructure Type
- Minimum Vertical Under Clearance

Required Additional Data items

Detailed rationale for recommendations to add additional data items to BIAS is given in subsequent sections of this appendix. Without these data items, the number of bridges for which a Level 1 assessment can be conducted decreases substantially. If estimates are used for these data items, there is a reduction in the accuracy of the Level 1 assessment results. Throughout the development of the simplified assessment process, eight additional data items were identified as critical. These items, in no particular order, are:

- **Substructure Type** – defined as the structural system supporting the superstructure.
- **Abutment Type** – defined as the connection of the superstructure to the abutments.
- **Number of Elements in Substructure** – defined as the number of elements making up a single pier. For walls and hammerheads, this value is one. For frame bents, this value is the number of columns.
- **Element Height** – defined as the dynamic height of the tallest pier (in feet)
- **Element Length** – defined as the transverse dimension of a substructure element (in feet)
- **Element Width** – defined as the longitudinal dimension of a substructure element (in feet)
- **Deck Thickness** – defined as the thickness of deck (in inches)
- **Height Ratio Flag** – defined as yes or no to signify when two piers in a bridge have a height ratio of 1.10 or greater.
- **Seismic Retrofit Indicator** – defined as a checkbox to signify when a detail seismic retrofit has been applied to the bridge.

Initial Classification (Level 0)

Prior to performing the Level 1 assessment, certain bridges can be identified as having low vulnerability or moderate vulnerability, or as requiring a detailed (Level 2) assessment based on the bridge details. Based on the screening criteria described next, the bridge types that can be automatically identified as *low vulnerability* are:

- **Bridges that have be retrofitted for seismic purposes:** Due to the retrofit having been designed to perform well at the expected level of hazard at the bridge site.
- **Short Single Span Bridges on Rocker Bearings (less than 60′–0″):** Due to the short span, there is a low probability of unseating at abutments
- **Long Single Span Bridges not supported by Rocker Bearings (greater than 60′–0″):** Due to the bearing type, there is a low probability of unseating event at longer lengths
- **Wall Substructures in the Transverse Direction:** Wall type substructures have a large stiffness and capacity in the transverse direction. The large stiffness results in a low period and correspondingly low structural displacement making them less vulnerable to the level of ground motions expected in Indiana.
- **Bridges with Integral Abutments in the Longitudinal Direction:** Bridges with integral abutments are not vulnerable in the longitudinal direction because there is no differential displacement between the substructure and the superstructure. The combination of a wall with integral abutments means there is no potential for vulnerability in the longitudinal and the transverse direction at the level of hazard expected for Indiana.
- **Hammerhead Substructures in the Transverse Direction:** Similar to wall type substructures, hammerhead substructures supporting reinforced concrete and steel superstructures are not vulnerable in the transverse direction due to the large stiffness of intermediate piers. Hammerhead walls supporting prestressed concrete superstructures do not fall into this category.

The bridge details that can be automatically identified as *moderate vulnerability* are:

- **Long, Single Span Bridges on Rocker Bearings (greater than 60′–0′):** Unlike short single span bridges, long single span bridges have the potential for the rocker bearings to overturn. This makes long single span bridges on rocker bearings vulnerable to damage during seismic activity. In order to account for this, single span bridges with a length greater than 60′–0″ are classified as long single span bridges. Steel bridges that are non-integral and long are then marked as moderately vulnerable.

The bridge details that require a Level 2 assessment are:

- **Bridges with Expansion Joints:** These bridges must be modeled as independent elements at each joint. Thus, it is not possible to apply a Level 1 assessment. While there is no NBI data that directly corresponds to the expansion joints, bridges with approach spans, bridges with more than six spans, and bridges that have a total length larger than 1,000 *ft* are assumed herein to have expansion joints based on trends observed in the Level 2 analysis conducted in this study.
- **Bridges with "Other" Substructures:** Unique substructures require additional modeling assumptions to be considered using the detailed assessment procedure presented in Appendix D on a case-by-case basis. Therefore, it is not possible to apply a Level 1 assessment to these bridges.
- **Bridges with piers having a height ratio greater than 1.1:** A height ratio equal to or exceeding 1.1 (between the height of the tallest pier to that of the shortest pier) increases the likelihood of one pier exhibiting a non-linear response while the pier remains linear. It is not possible to capture this complicated response with a single value for the pier height; a detailed analysis must be leveraged to account for the force redistribution due to non-linear behavior.
- **Reinforced concrete superstructures with reinforced concrete column-frame bents:** Reinforced concrete superstructures with reinforced concrete column-frame bents are excluded from the Level 1 assessment because they do not follow the same trends in vulnerability and vulnerability thresholds as the other superstructure materials. In order to accurately assess the vulnerability of these bridges, the reinforcement layout and details are required to model and analyze the bridge (Level 2). The Level 1 assessment does not consider these details.
- **Frame Bent Substructures whose Columns have an Aspect Ratio Less than Three:** An aspect ratio (the ratio of the height of the substructure over the length of the substructure) less than three means that the pier is likely to fail in shear. The Level 1 assessment is unable to accurately estimate the shear capacity without the necessary reinforcement details.

Level 1 Assessment for Applicable Bridges

After the initial screening of the 100 bridges in the sample set, the Level 1 assessment was carried out on 31 bridges. Table G.1 lists these bridges, and each of their superstructure type, substructure type, and abutment type. The number in the first column of Table G.1 corresponds to the bridge identification number and is used in the plots in the following sections.

Table G.1 Bridges for which a Level 1 Assessment is Applicable

Bridge ID #	Asset Name	NBI Number	Superstructure Material	Substructure Type	Abutment Type
1	028-79-07672	7640	Reinforced Concrete	CFT Frame Bent	Integral
2	044-55-06793 A	16310	Reinforced Concrete	CFT Frame Bent	Integral
3	057-14-06739	20690	Reinforced Concrete	CFT Frame Bent	Integral
4	064-19-03723 A	22960	Reinforced Concrete	CFT Frame Bent	Non-integral
5	067-42-07298	23760	Reinforced Concrete	CFT Frame Bent	Integral
6	252-24-06934 A	30780	Reinforced Concrete	CFT Frame Bent	Integral
7	327-17-06419 A	31350	Reinforced Concrete	CFT Frame Bent	Integral
8	I69-334-04590 BNB	40720	Reinforced Concrete	CFT Frame Bent	Non-integral
9	(237)37-13-07277	11840	Reinforced Concrete	H-pile Frame Bent	Integral
10	055-45-07366	19880	Reinforced Concrete	H-pile Frame Bent	Integral
11	056-63-07286 A	19933	Reinforced Concrete	H-pile Frame Bent	Integral
12	067-55-03831 ANBL	24100	Reinforced Concrete	H-pile Frame Bent	Non-integral
13	252-55-08713	30721	Reinforced Concrete	H-pile Frame Bent	Integral
14	018-05-06573 B	4880	Reinforced Concrete	Wall	Non-integral
15	063-86-05970 BNBL	22810	Reinforced Concrete	Wall	Non-integral
16	066-13-05443 A	23670	Reinforced Concrete	Wall	Non-integral
17	I70-112-05137 DEBL	42960	Reinforced Concrete	Wall	Non-integral
18	I69-087-09551 NB	80356	Prestressed Concrete	Frame Bent	Integral
19	064-26-09191	80372	Prestressed Concrete	Frame Bent	Integral
20	(265)I265-11-09604	80482	Prestressed Concrete	Frame Bent	Integral
21	I69-112-09708 SB	51350	Prestressed Concrete	Hammerhead	Integral
22	I69-106-09739 SB	51385	Prestressed Concrete	Hammerhead	Integral
23	024-02-09089 A	76840	Prestressed Concrete	Hammerhead	Integral
24	356-63-09491	80374	Prestressed Concrete	Hammerhead	Integral
25	041-82-05415 CSBL	14280	Steel	Frame Bent	Integral
26	I469-12-06947 AEB	32841	Steel	Frame Bent	Integral
27	038-89-04111 B	13000	Steel	Hammerhead	Non-integral
28	052-24-06649	19430	Steel	Hammerhead	Non-integral
29	062-74-06621	22190	Steel	Hammerhead	Non-integral
30	062-13-07329	22240	Steel	Hammerhead	Non-integral
31	067-18-05459 D	24210	Steel	Hammerhead	Non-integral

Level 1 Assessment Procedure with All Recommended Data Items

A Level 1 assessment is intended to utilize all recommended data items. The Level 2 assessment results obtained with models generated based on accurate dimensions and details will be used as reference points to evaluate the impact of estimating specific data items on the Level 1 vulnerability assessments. Figure G.1 shows the procedure developed to perform the Level 1 Assessment. The steps consists of demand, shown in green; capacity, shown in purple; and the determination of vulnerability, shown in blue. This procedure is described in detail below. Subsequent sections demonstrate and discuss the importance of the additional data items, and if applicable, methods for estimating them.

Figure G.1 Level 1 Assessment Procedure

Estimate Mass

The calculation of the mass used in the Level 1 assessment is based on superstructure dimensions that currently exist in BIAS as well as trends and averages identified in the detailed (Level 2) analysis. The mass calculations are superstructure dependent. The following three sections describe the mass calculations for prestressed, steel, and reinforced concrete superstructures.

Prestressed Superstructure Mass – Longitudinal Direction

For prestressed girder superstructures, the mass calculation is based on estimated values for the number of beams, the average mass per linear foot of the beams, the volume of the deck, and the unit weight of concrete. The average mass of the beams ($m_{avg,PSbeam}$) is 0.0033 *kips/g/lft*, based on the Level 2 assessment calculations. The number of beams is estimated using trends identified during the Level 2 assessment based on the deck width. For deck widths less than 44.4 *ft*, the estimated number of beams is four. Then, for every additional ten feet of deck width, one beam is added. Thus, for deck widths greater than 44.4 *ft*, the number of beams is calculated as

$$N_{beams} = 4 + RoundUp\left(\frac{w_{bridge} - 44.4ft}{10ft}\right). \quad (1)$$

Once the number of beams is estimated, the total mass of a bridge with a prestressed girder superstructure is calculated as

$$m_{PS} = (t_{deck} * L_{bridge} * w_{bridge}) * \gamma_c + N_{beams} * L_{bridge} * m_{avg,PSbeam} \quad (2)$$

Steel Superstructure Mass – Longitudinal Direction

For steel girder superstructures, the mass calculation is based on the deck area and an estimated value of average mass per deck area. The average mass per deck area ($m_{avg,steel}$) is taken as the average over the sample set of bridges and is 3.63×10^{-4} *kips/g/ft*^{2}. Thus, the total mass of a bridge with a steel superstructure is calculated as

$$m_{steel} = m_{avg,steel} * L_{bridge} * w_{bridge}. \quad (3)$$

Reinforced Concrete Slab Deck Superstructure Mass – Longitudinal Direction

For reinforced concrete slab deck superstructures, the mass calculation is based on the volume of the deck, using the actual deck thickness, the estimated value of the average mass per linear foot of railings, and the unit weight of concrete. The total mass of a bridge with a reinforced-concrete superstructure is calculated as

$$m_{RC} = (t_{deck} * L_{bridge} * w_{bridge}) * \gamma_c + 0.002 * L_{bridge}. \quad (4)$$

Transverse Mass Estimate

In the transverse direction, the percent of the mass that is activated is based on the number of spans. This is because the abutments carry a portion of the end-span mass. Table G.2 shows the percentage of mass activated ($\%_{act}$) for different number of spans in the main unit. The Level 1 assessment is not applicable to bridges with more than six spans because of the high likelihood of expansion joints being present.

Table G.2 Percent of Total Mass Activated in the Transverse Direction

Number of Spans	Percent of Mass Activated
2	50%
3	71.5%
4	80%
5	82.5%
6	85%

For prestressed and steel superstructures, this activated mass percentage is all that is needed to calculate the transverse mass. However, because the transverse direction of reinforced concrete slab deck superstructures is modelled as a MDOF system in the Level 2 assessment, the decoupled mass is needed for the Level 1 assessment calculations. This value is calculated as

$$m_{Trans} = \frac{m_{RC} * \%_{act}}{N_{pier}}. \quad (5)$$

Impact of Estimates and Averages on Mass

Figure G.2 shows a comparison between the Level 1 mass and the Level 2 mass for the 31 bridges. The mass used in the Level 1 assessment is calculated using the estimates and averages described above, whereas the mass used in the Level 2 assessment is calculated using information from the bridge drawings. The mass ratio for a majority of the bridges is very close to 1.0, with outliers ranging between 0.8 and 1.2, which indicates that the above equations are suitable for determining a mass to use in the Level 1 vulnerability assessment.

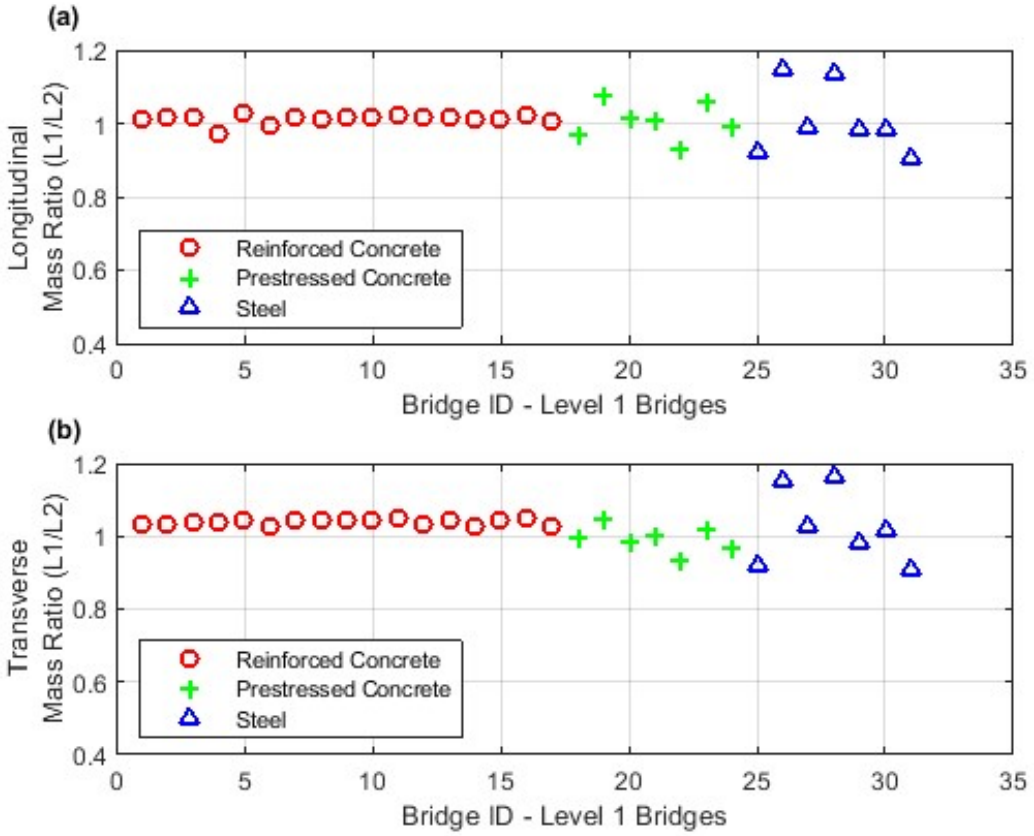

Figure G.2 Comparison of Mass Values Used for the Level 1 Assessment and Level 2 Assessment in the (a) Longitudinal Direction and (b) Transverse Direction

Calculate Stiffness

The stiffness of a bridge is dependent on both the substructure and superstructure types. The substructure type determines the specific modeling procedure and necessary geometric properties to be used. The superstructure type determines which elements contribute stiffness as well as the boundary conditions. The boundary conditions define the constant in the stiffness, F_{con} or connectivity factor, shown in Eq. (6). These are three, six, and twelve for steel, prestressed, and reinforced concrete superstructures, respectively as a function of the type of connection between the substructure and the superstructure type. The required substructure geometry information includes the clear height, the number of elements in one pier, the length of the element (dimension in the transverse direction of the bridge), and the width of the element (dimension in the longitudinal direction).

Wall Stiffness

Longitudinal Direction

The stiffness of a single wall in the longitudinal direction is calculated, using the same equations as the Level 2 assessment, as

$$K_{wall,L} = \frac{F_{con} * E_c * I_L}{H^3}. \quad (6)$$

Transverse Direction

As discussed previously, walls are already found to be not vulnerable in the transverse direction to the level of hazard chosen for this report (a 7% probability of exceedance in 75 years) because of the large stiffness of walls. Thus, the Level 1 assessment need not be applied to any walls in the transverse direction.

Hammerhead Stiffness

Longitudinal Direction

For hammerhead substructures, the stiffness in the longitudinal direction is calculated using the same equations as walls (Equation (6)). The length used in the moment of inertia calculation is the length of the stem of the hammerhead.

Transverse Direction

Hammerhead walls supporting prestressed concrete superstructures have been identified as having the potential for vulnerability due to the combination of the large superstructure mass and the narrowing at the base, corresponding to an increased period. For prestressed bridges with hammerhead substructures, the stiffness of a single pier in the transverse direction is calculated as

$$K_{HH,T} = \frac{F_{con} * E_c * I_T}{H^3} + \frac{G * w_{ele} * L_{ele}}{1.2 * H}, \tag{7}$$

where G is the shear coefficient and is calculated as

$$G = \frac{E_c}{2 * (1 + \nu)}. \tag{8}$$

As noted previously, hammerhead walls supporting steel and reinforced concrete superstructures are found to be not vulnerable in the transverse direction.

Frame Bent Stiffness

For frame bent substructures, it is important to know whether the elements are composite piles [concrete filled tubes (CFT) or H-piles] or reinforced concrete columns. The shape of the element (circular or rectangular) also influences the response. The substructure category identifies the shape of the element but does not differentiate between composite pile and reinforced concrete columns. Rather, this distinction is made using information currently available in BIAS. Pile substructures are only identified in the state for bridges with reinforced concrete superstructures, but not for bridges with steel or prestressed superstructures. Therefore, if a bridge superstructure is prestressed or steel, the frame bent is assumed, for both the Level 1 assessment and tool, herein to be composed of reinforced concrete columns. For reinforced concrete superstructures, the feature intersected is used to differentiate between composite piles and reinforced concrete columns. If the feature intersected is a waterway, like a creek or a river the substructure is assumed to be composed of composite piles, and if the feature intersected is a road or railroad the substructure is assumed to be composed of reinforced concrete columns.

Longitudinal Direction

Calculations for the longitudinal stiffness for frame bents are dependent on superstructure type to determine the connectivity factor. The factors for steel, prestressed, and reinforced concrete superstructures are three, six, and twelve, respectively.

Reinforced Concrete Column

For reinforced concrete column frame bents, the longitudinal stiffness of one bent is based only on the number of columns, the connectivity factor, and the column geometry (length, width, and height). The stiffness of RC frame bents is

$$K_{RCFB,L} = N_c * \frac{F_{con} * E_c * I_L}{H^3}. \quad (9)$$

H-pile Composite Piles

For H-pile composite substructures, the standard shape is an HP 12×53 (Standard Drawing No. E 701-BPIL-01, IN). This standard has been identified as typical in Indiana and the shape properties of the pile have been used to calculate the stiffness as

$$K_{HPFB,L} = N_c * \frac{F_{con} * EI_L}{H^3}. \quad (10)$$

The EI_L component is calculated as

$$EI_L = E_s * I_{HP,L} + c_{HP} * I_c * E_c, \quad (11)$$

where the values for $I_{HP,L}$ c_{HP}, I_c are calculated using the standard shape and are 127 in^4 ,0.3528, 77.06 *kip*ft*, respectively.

Concrete Filled Tube Composite Piles

CFT piles are typically 14-inch diameter piles, which includes a 0.2-inch steel encasement (Standard Drawing No. E 701-BPIL-01, IN). The stiffness of one pier is calculated as

$$K_{CFTFB,L} = N_c * \frac{F_{con} * EI_L}{H^3}. \quad (12)$$

The EI_L term is calculated as

$$EI_L = E_s * I_{CFT,L} + c_{CFT} * I_c * E_c, \quad (13)$$

where the values for $I_{CFT,L}$, c_{CFT}, and I_c are calculated using the standard shape and are 105.47 in^4, 0.5351, and 1780.3 *kip*ft, respectively.*

Transverse Direction

The calculations for the transverse stiffness of reinforced concrete column frame bents are based on a frame bent factor (F_{FB}), determined from trends identified in the detailed analysis, the superstructure type, the number of columns, and the column geometry. The frame bent factor relates the pre-condensed pure translational degree-of-freedom term ($N_c \frac{12A}{H^3}$) of the bent stiffness matrix ri the condensed stiffness of the frame bent. Figure G.3 provides the calculated frame bent factor for all frame bents in the sample set (note that *the bridge number on the x-axis here does not correspond to the bridge ID in Table G.1).* The average frame bent factor is 0.88 with a standard deviation of 0.06 for prestressed and steel superstructures, and the average frame bent factor is 0.96 with a standard deviation of 0.04 for reinforced concrete superstructures. For the Level 1 assessment, these averages are used in the transverse stiffness calculations.

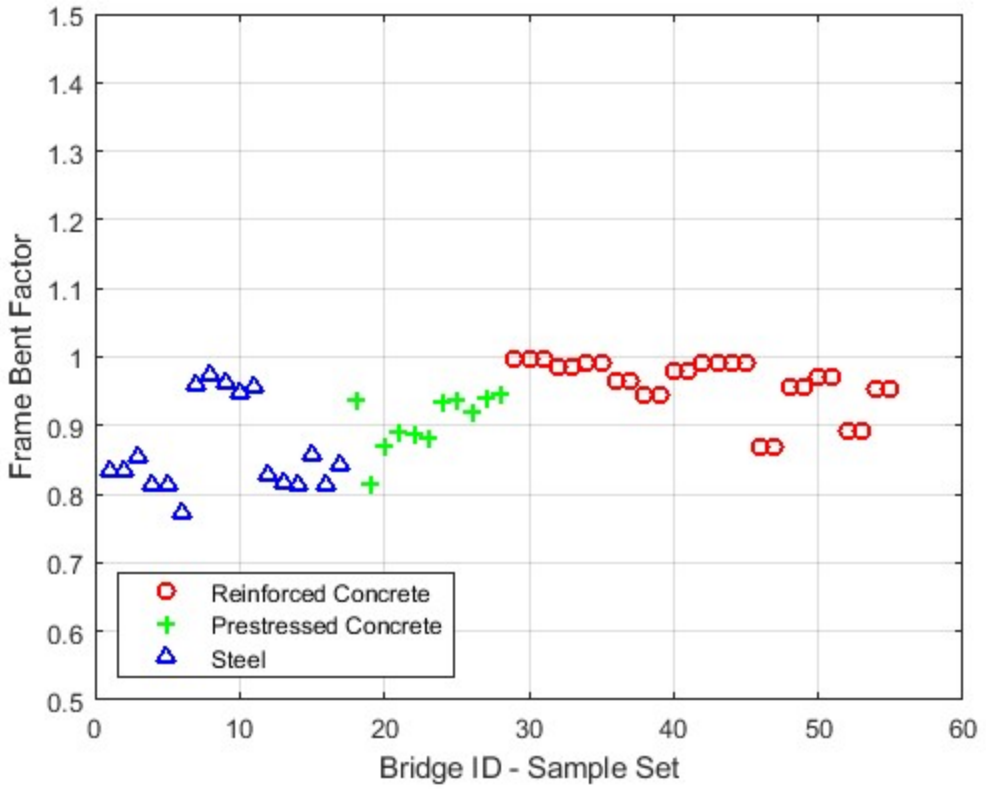

Figure G.3 Frame Bent Factor Spread for All Frame Bents in Sample Set

Reinforced Concrete Columns

The transverse stiffness of a frame bent with reinforced concrete columns, independent of the superstructure type, is calculated as, where F_{FB} is 0.88,

$$K_{RCFB,T} = F_{FB} * N_c * \frac{12 * E_c * I_T}{H^3}. \quad (14)$$

H-pile Composite Piles

Due to the difference in the moment of inertia of the steel shape about the *x*- and *y*-axes, the transverse stiffness of the H-pile substructures is equal to the longitudinal stiffness. The stiffness in the transverse direction of one pier with H-piles is calculated as, where F_{FB} is 0.96,

$$K_{HPFB,T} = F_{FB} * N_c * \frac{12 * EI_T}{H^3}, \quad (15)$$

The EI_T term is calculated as

$$EI_T = E_s * I_{HP,T} + c_{HP} * I_c * E_c, \quad (16)$$

where the values for $I_{HP,T}$ c_{HP}, I_c are calculated using the standard shape and are 393 in^4 ,0.3528, 176.18 *kip*ft*, respectively.

Concrete Filled Tube Composite Piles

The calculation for the transverse stiffness of frame bents with CFT piles is the same as that for the longitudinal direction, Equation (12), because the shape is symmetric about all axes.

Total Stiffness

Equations (6) through (16) are used to calculate the stiffness of one pier in the two fundamental directions. The calculation for the total stiffness of the bridge is dependent on the superstructure type. The following sections detail the calculations of the stiffness in the two fundamental directions for steel girder, prestressed girder, and reinforced concrete slab deck superstructures.

Steel Superstructure Total Stiffness

Longitudinal Direction

Only the piers with fixed bearings (not sliding, expansion, or roller bearings) add to the total stiffness of the bridge, due to their ability to transfer inertial forces from the superstructure to the substructure. In the Level 2 analysis, each bridge typically has one fixed bearing at an intermediate pier and expansion bearings at the other piers and the abutments. The fixed connection means that pier will draw most, if not all of the force, therefore eliminating the softening effects of the expansion bearings. Thus, the piers with expansion bearings are excluded from the stiffness calculation in the longitudinal direction, and the stiffness of steel superstructure bridges in the longitudinal direction is the stiffness of one pier. This stiffness is taken as

$$K_{Long} = K_L, \tag{17}$$

where K_L is the longitudinal stiffness of one pier, calculated based on the substructure type.

Transverse Direction

Steel bridges in the transverse direction are modelled as SDOF systems, thus the intermediate piers behave as springs in parallel. Therefore, the total stiffness in the transverse direction is the sum of the stiffness of each pier. The Level 1 assessment assumes identical piers, in cross-sectional geometry and height. The stiffness of bridges with steel superstructures in the transverse direction is taken as

$$K_{Trans} = N_{pier} * K_T. \tag{18}$$

Prestressed Superstructure Total Stiffness

Longitudinal Direction

Unlike bridges with steel superstructures, the connection between the substructure and the superstructure for prestressed bridges is adequate to transfer forces in the longitudinal direction. Therefore, the stiffness of bridges with prestressed superstructures in the longitudinal direction is calculated as

$$K_{Long} = N_{pier} * K_L. \tag{19}$$

Transverse Direction

Following the same logic as the calculation for the transverse stiffness of bridges with steel superstructures, the transverse stiffness of bridges with prestressed superstructures is calculated using Equation (18).

Reinforced Concrete Slab Deck Superstructures

Longitudinal Direction

Because the longitudinal bars extend from the substructure into the superstructure in reinforced concrete slab deck bridges, each pier adds stiffness in the longitudinal direction, and the stiffness is calculated using Equation (19).

Transverse Direction

Unlike bridges with prestressed and steel superstructures, bridges with reinforced concrete slab deck superstructures are modelled as MDOF systems in the detailed analysis. However, the Level 1 assessment is unable to handle MDOF systems, so an equivalent SDOF system is developed. As discussed in Appendix D, the deck is modelled as a deep beam with the stiffness of each pier added to the pure translation degrees-of-freedom in the deck stiffness matrix.

The Level 1 assessment assumes that the contributions from the fundamental mode of the MDOF system control and all other modes do not affect the results significantly. As with the calculation for frame bent stiffness in the transverse direction, the stiffness calculation for reinforced concrete slab deck bridges uses a deck stiffness factor (F_{RCDS}). This deck stiffness factor relates the pure translational degree-of-freedom term, $\frac{12*E_c*I_d}{(1+\mu_1)l_1^3} + \frac{12*E_c*I_d}{(1+\mu_2)l_2^3} + K_{RCFB,T}$, for the pier that supports the maximum mass to the first modal stiffness in the decoupled stiffness matrix.

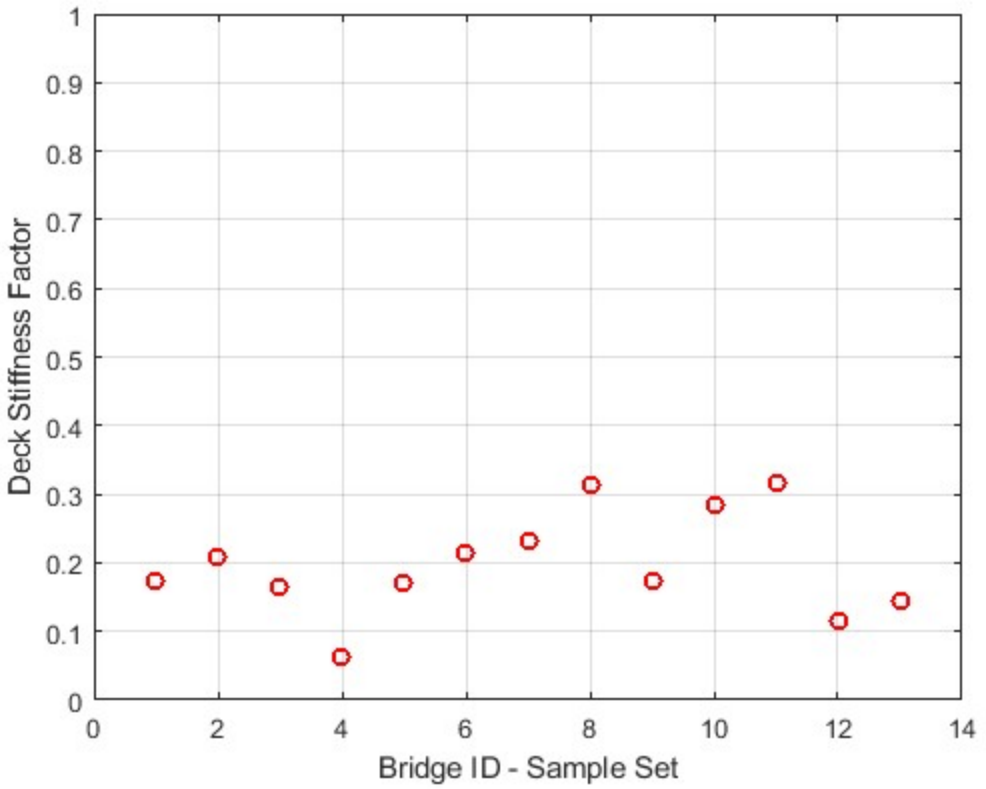

Figure G.4 Deck Stiffness Factor for RC Bridges with Pile Substructures

The entire suite of three-span reinforced concrete slab deck bridges with pile substructures is used to determine an appropriate value for the deck stiffness factor. *The outlier, bridge 4, is a four-span bridge that does not follow these trends and is excluded from the average calculations*. The average deck stiffness factor (F_{RCDS}) of these results is 0.217 with a standard deviation of 0.07, as shown in Figure G.4. The average value is used to calculate the stiffness of these bridges for the Level 1 assessment as

$$K_{Trans} = F_{RCFB} * \left(\frac{12 * E_c * I_d}{(1+\mu_1) l_1^3} + \frac{12 * E_c * I_d}{(1+\mu_2) l_2^3} + K_{RCFB,T} \right), \tag{20}$$

where

$$\mu_1 = \frac{12 * E_c * I_d}{G * t_{deck} * L_{bridge} * w_{bridge} * l_1^2}, \tag{21}$$

and

$$\mu_2 = \frac{12 * E_c * I_d}{G * t_{deck} * L_{bridge} * w_{bridge} * l_2^2}. \tag{22}$$

Because reinforced concrete solid slab bridges are the only superstructure type in which the deck is considered to add stiffness, they are the only type of bridge that require knowledge of the adjacent span lengths (l_1 and l_2). Span lengths other than the maximum span are not given in BIAS and must be estimated based on trends seen during the Level 2 assessment. Since the pier supporting the maximum mass will be one that is adjacent to the maximum span, l_1, is always taken as the maximum span. The other span length

used in the calculations is determined based on the number of spans, the bridge length, and the maximum span length. For two-span bridges, the remaining length, l_2, is calculated as

$$l_2 = L_{bridge} - l_1. \tag{23}$$

For three-span bridges, the Level 1 assessment procedure assumes symmetry about the middle of the bridge. Therefore, l_2 is calculated as

$$l_2 = \frac{L_{bridge} - l_1}{2}. \tag{24}$$

For bridges with four or more spans, the Level 1 assessment conservatively assumes that there are two adjacent spans of the maximum span length and therefore $l_2 = l_1$.

Impact of Estimates and Averages on Stiffness

Figure G.5 shows the comparison of the stiffness used in the Level 1 assessment with that used in the Level 2 assessment for all 31 bridges. The stiffness used for the Level 1 assessment is calculated using the estimates and averages described in the previous paragraphs, whereas the stiffness used for the Level 2 assessment is calculated using information from the bridge drawings. If a particular bridge does not have a data point shown in Figure G.5, the Level 1 assessment is not performed in that direction for that bridge (e.g., bridges 13–17 in the transverse direction because they are reinforced concrete superstructures with wall substructures). The bridge ID on the *x*-axis corresponds to the bridge ID found in Table G.1.

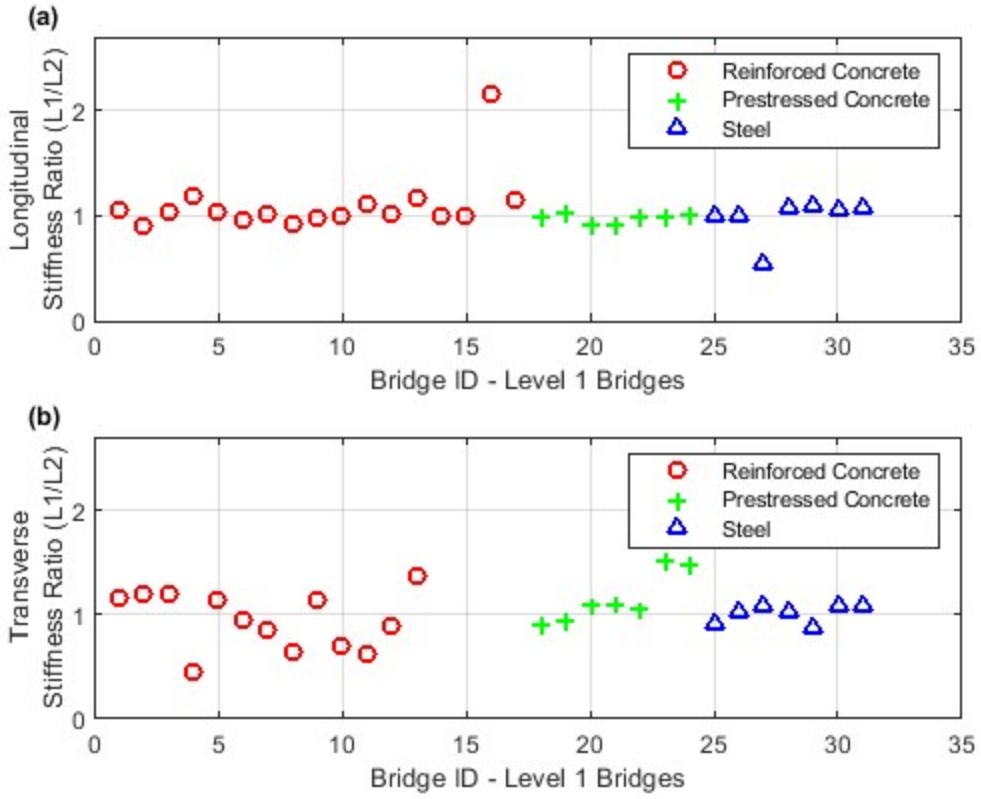

Figure G.5 Comparison of Level 1 Assessment and Level 2 Assessment Stiffness in the (a) Longitudinal Direction and (b) Transverse Direction

While most of the stiffness ratios are approximately 1, there are a few outliers. *In the longitudinal direction, the Level 1 stiffness for bridge 16 is approximately double the Level 2 stiffness.* This outcome occurs because in that bridge one of the two intermediate piers is not rigidly connected to the deck. Therefore, the Level 1 assessment assumption that both intermediate piers add stiffness is not suitable for this specific case. *In the longitudinal direction, the Level 1 stiffness for bridge 27 is approximately 50% of the Level 2 longitudinal stiffness because this bridge does not follow the "one fixed bearing per bridge"* assumption that is made in the Level 1 assessment. Each of the two intermediate piers on this bridge is connected to the superstructure with a fixed bearing, and thus, the Level 2 analysis considers the fact that both piers add stiffness. *In the transverse direction, the Level 1 stiffness of bridge 4 is approximately 50% of the Level 2 stiffness. This result is because this bridge is the only example of a four-span reinforced concrete superstructure with pile substructures in the sample set, and it does not follow the same stiffness trends those identified for three-span bridges.*

Calculate Period

The period of the structure, which is used to determine the demand, is calculated as

$$T = 2\pi\sqrt{\frac{m}{K}}. \tag{25}$$

Figure G.6 compares the actual period obtained in the Level 2 assessment to the estimated period from the Level 1 assessment. The bridge ID on the *x*-axis corresponds to the bridge ID found in Table G.1. As in Figure G.5, bridge IDs that do not have a period calculated represent bridges that do not require a Level 1 assessment in that direction. From these results, the methods described above appear to provide a practical approach to estimate the period of each bridge for the superstructure and substructure combinations identified in the sample set. Recall that the sample set was carefully selected to be representative of the Indiana bridge inventory. The outliers shown in Figure G.6 are a result of carrying forward the outlying cases described earlier for the mass and stiffness estimates.

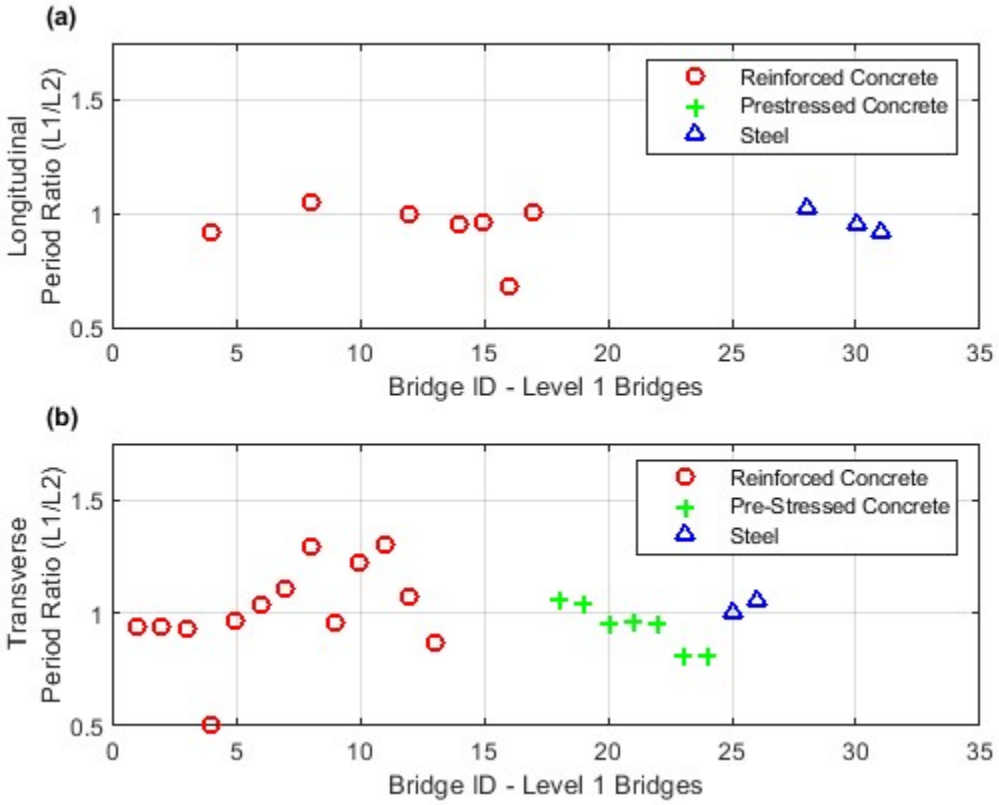

Figure G.6 Comparison of Level 1 Assessment and Level 2 Assessment Period in the (a) Longitudinal Direction and (b) Transverse Direction

Demand Estimation

Demand in the Level 1 assessment procedure includes both a displacement demand and a force demand. The controlling demand depends on the substructure/superstructure combination because a force capacity, due to lack of information on details in BIAS, cannot be determined using a Level 1 assessment for some combinations.

Because all bridges are modelled as SDOF systems in the Level 1 assessment, the spectral acceleration and displacement can easily be determined using a response spectrum. For purposes of validating the Level 1 assessment process, the response spectra for the 100 simulated time-histories used in the Level 2 assessment

are used to determine the spectral acceleration. An example of the 100 acceleration response spectra, from the simulated time-histories is shown in Figure G.7.

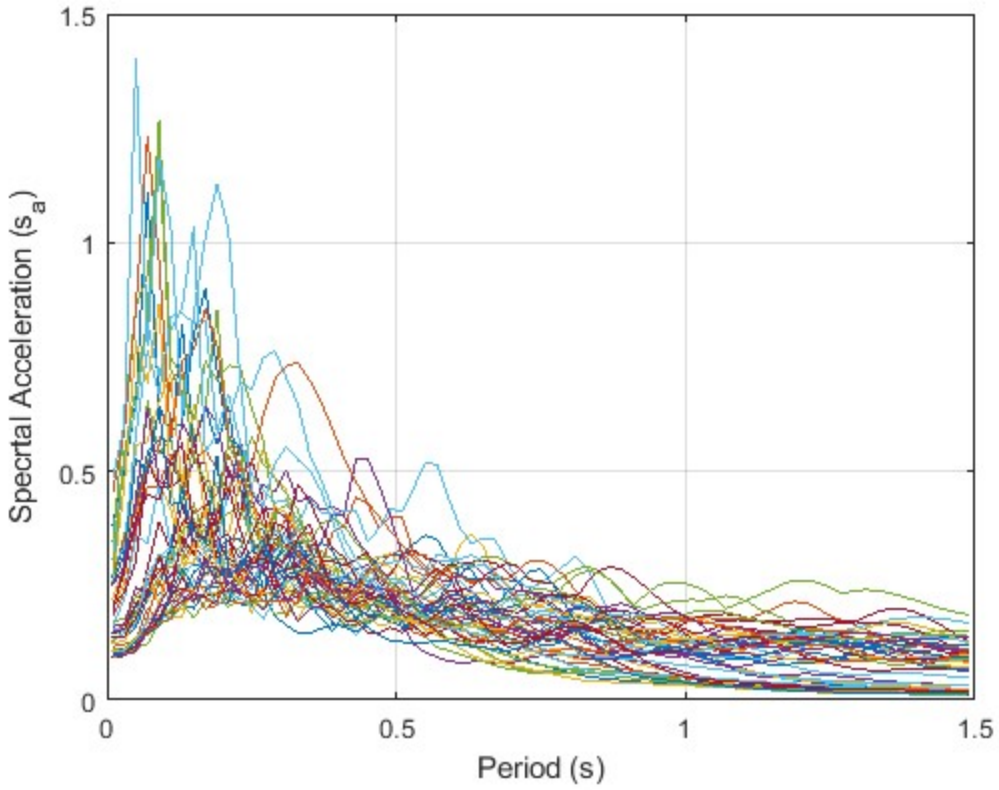

Figure G.7 Acceleration Response Spectra for a Sample Site

Each response spectrum is used to obtain the spectral acceleration (s_a) value associated with the period of the bridge, which is then used to calculate, Δ_l, the equivalent linear spectral displacement.

$$\Delta_l = \frac{s_a}{(\frac{2\pi}{T})^2}. \tag{26}$$

This spectral displacement assumes that the substructure remains in the linear region. However, as is shown in Appendix D, this assumption is not valid for the reinforced concrete substructures that have adequate reinforcement ratios. For these bridges, a multiplier of $\sqrt{2}$ is used to calculate an expected nonlinear displacement (Δ_{NL}) (Sozen, 2003).

$$\Delta_{NL} = \sqrt{2} * \Delta_l. \tag{27}$$

Using force-displacement relationships, the force on the bridge is calculated as

$$F_{dem} = K * \Delta_l. \tag{28}$$

Frame bents use a comparison of a drift demand to a drift capacity to determine the vulnerability. The drift demand for frame bents in the transverse direction is calculated as

$$drift = \frac{2 * \Delta_{NL}}{H}. \quad (29)$$

Determine Capacity Thresholds

Displacement

Table G.3 shows the predetermined capacity thresholds for the substructure/superstructure combinations typical in Indiana. These thresholds were identified from trends seen in the Level 2 assessment of the 100-bridge sample set. When no threshold is given, the bridge is considered to have low vulnerability in that direction. For brides that have a displacement capacity threshold, the limits found in Table G.3 are compared to the displacement demand, calculated using Equations (26) and (27).

Drift

For bridges that have a drift capacity threshold, the limits found in Table G.3 are directly compared to the drift demand based on the type of substructure and the direction being considered, calculated using Equation (29). Drift corresponds to the lateral displacement divided by the height of substructure between the fixed end(s) and point of zero moment, or contraflexure. For walls in the transverse direction this corresponds to the Element Height whereas for frame bents this typically corresponds to half the Element Height.

Force

The force demand is calculated using Equation (28). For bridges that require a force demand to capacity comparison, *the force capacity is calculated using trends and averages seen in the Level 2 assessment*. The force capacity is dependent on the substructure/superstructure columns. For prestressed hammerhead substructures, the force capacity in the transverse direction is calculated as

$$F_{cap} = m_T * g * \left(1.9 - 0.4 * \frac{H}{L_{ele}}\right). \quad (30)$$

For pile substructure types, the force capacity in the transverse direction is a base shear capacity and is calculated as

$$F_{cap} = \frac{2 * N_c * N_{pier} * M_u}{H} \quad (31)$$

where M_u is the ultimate moment for the typical piles used by INDOT. For concrete filled tubes, this moment is 63.21 *kip*ft* and for H-piles, this value is 176.18 *kip*ft*.

Table G.3 Vulnerability Thresholds by Superstructure Material

		Steel Superstructures				
		Walls		**Hammerheads**		**Frame Bents**
		Year Built < 1990	**Year Built > 1990**	**Year Built < 1990**	**Year Built > 1990**	**RC Columns**
Low Vulnerability	Longitudinal	Δ_{lin} < 0.1"	Δ_{NL} < 1"	Δ_{lin} < 0.1"	Δ_{NL} < 1"	Δ_{NL} < 1"
	Transverse					Drift < 0.5%
Moderate Vulnerability	Longitudinal		1" < Δ_{NL}< 6"		1" < Δ_{NL}< 6"	1" < Δ_{NL} < 6"
	Transverse					0.5% < Drift < 1.5%
High Vulnerability	Longitudinal	Δ_{lin} > 0.1"	Δ_{NL} > 6"	Δ_{lin}> 0.1"	Δ_{NL} > 6"	Δ_{NL} > 6"
	Transverse					Drift > 1.5%
		Prestressed Superstructures				
		Walls		**Hammerheads**		**Frame Bents**
		Year Built < 1990	**Year Built > 1990**	**Year Built < 1990**	**Year Built > 1990**	**Columns**
Low Vulnerability	Longitudinal	Δ_{lin} < 0.1"	Δ_{NL} < 1"	Δ_{lin} < 0.1"	Δ_{NL}< 1"	Δ_{NL} < 1"
	Transverse			F_{cap}> F_{dem}	F_{cap}> F_{dem}	Drift < 0.5%
Moderate Vulnerability	Longitudinal		1" < Δ_{NL}< < 6"		1" < Δ_{NL} < 6"	1" < Δ_{NL} < 6"
	Transverse			F_{cap}< F_{dem}	F_{cap}< F_{dem}	0.5% < Drift < 1.5%
High Vulnerability	Longitudinal	Δ_{lin} > 0.1"	Δ_{NL}<> 6"	Δ_{lin} > 0.2"	Δ_{NL} > 6"	Δ_{NL}> 6"
	Transverse				N/A	Drift > 1.5%
		Reinforced Concrete Superstructures				
		Walls		**Hammerheads**		**Frame Bents**
		Year Built < 1990	**Year Built > 1990**	**Year Built < 1990**	**Year Built > 1990**	**Composite Piles**
Low Vulnerability	Longitudinal	Δ_{lin} < 0.1"	Δ_{NL} < 1"	Δ_{lin} < 0.1"	Δ_{NL}< 1"	F_{cap}> F_{dem}
	Transverse					F_{cap}> F_{dem}
Moderate Vulnerability	Longitudinal		1" < Δ_{NL} < 6"		1" < Δ_{NL}< 6"	F_{cap}< F_{dem}
	Transverse					F_{cap}< F_{dem}
High Vulnerability	Longitudinal	Δ_{lin} > 0.1"	Δ_{NL}> 6"	Δ_{lin} > 0.1"	Δ_{NL} > 6"	
	Transverse					

Comparison of Vulnerability Classifications Level 2 with those from Level 1

For each bridge location and period, 100 synthetic time-histories were generated in each direction. The demand obtained from the Level 1 assessment must be compared to the capacity thresholds to classify the vulnerability of the bridge. The capacity thresholds for steel, prestressed, and reinforced concrete superstructures are shown in Table G.3.

For each of the 100 time-histories, the classification obtained with the Level 1 assessment is compared to that obtained with the Level 2 assessment to show the robustness of the Level 1 assessment. If the Level 1 assessment classification matches the Level 2 assessment classification, then the Level 1 assessment results are considered correct. If the Level 1 assessment classifies the bridge as having a higher level of vulnerability than the Level 2 assessment, the Level 1 assessment results *overestimate* the level of vulnerability of the bridge. If the Level 1 assessment classifies the bridge as having a lower level of vulnerability than the Level 2 assessment, the Level 1 assessment results are deemed to *underestimate* the vulnerability of the bridge.

The results for all 3,400 time-histories are shown in Figure G.8, respectively. The results show that the Level 1 assessment results either matches or overestimates the vulnerability of the bridge for the majority of bridges and time-histories. This shows that the Level 1 assessment, given all of the requested data items, is robust enough to assess the potential vulnerability of bridges across the state.

There are a few instances in which the Level 1 assessment procedure underestimates the bridge vulnerability, i.e., the bridge vulnerability is less than that estimated by Level 2, even when all of the recommended information is used. This outcome occurs in a small portion of the bridges because some of the assumptions or estimates are not applicable.

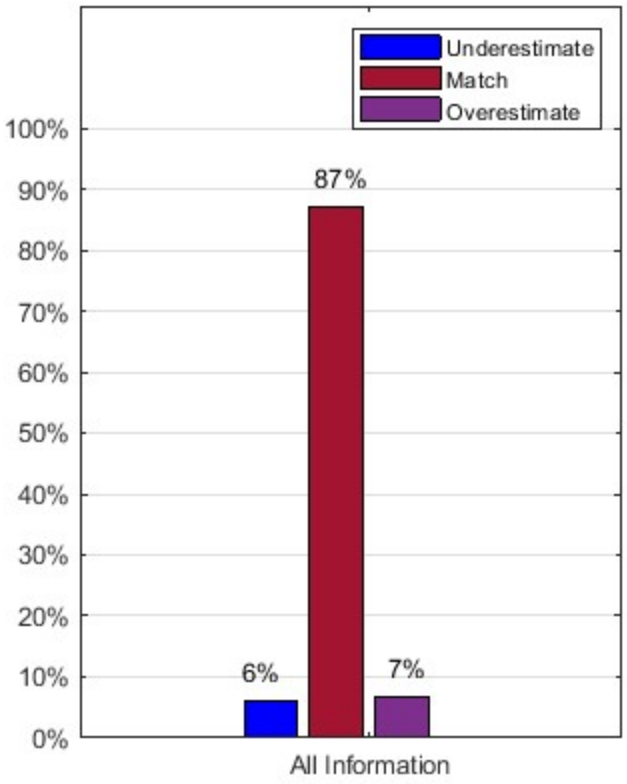

Figure G.8 Comparison of Classification Results for a Level 2 Assessment and a Level 1 Assessment when All Information is Known

Estimating the Impact on Assessment of Requested Data Items

The calculations and results discussed above assume that all the recommended data items have been added for all of the bridges. However, there is some potential to run a Level 1 assessment without all of the recommended data items, provided that a less robust vulnerability assessment can be accepted. The following sections discuss each data item, the methods for estimating the values, and the impact of these estimates on the accuracy of the results.

1. Substructure Type

Substructure type is a critical data item for the simplified seismic assessment. At this time, there is no way to determine the substructure type of a bridge given only the information that is currently in BIAS. While BIAS does contain images of the substructure in the inspection reports, this information is not in a format that is currently minable. Without knowing the substructure type there is no way to estimate the stiffness of a bridge to apply the Level 1 assessment procedure. *Therefore, without the substructure type, all 31 bridges that were previously eligible for analysis with the Level 1 assessment methodology would require a Level 2 assessment in order to establish vulnerabilities*.

2. Abutment Type

The abutment type is used in the Level 0 assessment to determine if the longitudinal direction of the bridge needs to be checked. As with the substructure type, the abutment type is not currently in BIAS and there is no way to infer the abutment type based on what is currently in BIAS. However, unlike the substructure type, if the abutment type is not given, the Level 1 assessment can still be applied to a bridge. This approach will classify more bridges as moderately or highly vulnerable when they might be classified as low vulnerability if the abutment type were available.

3. Seismic Retrofit Indicator

The seismic retrofit indicator is used in the Level 0 assessment to determine if the bridge needs to be checked. This data item identifies if an engineer has done detailed calculations to design the bridge to perform well under the expected level of hazard at the bridge site. Like the previously discussed data items, there is no way to infer if a seismic retrofit has been completed based on what is currently in BIAS. However, if the seismic retrofit checkbox is not marked, the Level 1 assessment is still applicable to the bridge, but none of the retrofit actions will be considered in the assessment, therefore classifying more bridges as moderately or highly vulnerable, when they might be classified as low vulnerability if a detailed seismic retrofit was performed on the bridge.

4. Height Ratio Flag

The height ratio flag is used in the Level 1 assessment to determine which bridges the Level 1 assessment applies to. The height ratio is calculated as

$$H_{ratio} = \frac{H_{tall}}{H_{short}}. \tag{32}$$

The Level 2 assessment procedure requires a nonlinear pushover analysis for bridges with piers of varying heights to consider the potential for non-simultaneous nonlinear response due to plastic hinge formation or potential for shear failure in the shorter ones. The Level 1 assessment procedure is unable to capture this response and therefore cannot assess bridges with significantly different pier heights.

This can be illustrated using a representative hypothetical three-span bridge model with two piers of varying heights. As the structure is exposed to ground motions, the shorter, stiffer pier will initially take the most force, causing it to yield first if it has sufficient shear capacity. At this point, it will start to soften and redistribute the force to the adjacent pier, which has yet to yield. The Level 1 assessment procedure is incapable of capturing this region of non-simultaneous yielding. The hypothetical model, with height ratios ranging from 1 to 1.2, was passed through a nonlinear pushover analysis to determine the height ratio that corresponds to this region. The results for a height ratio of 1.15 are shown in Figure G.9. The green box shows the region where non-simultaneous yielding occurs.

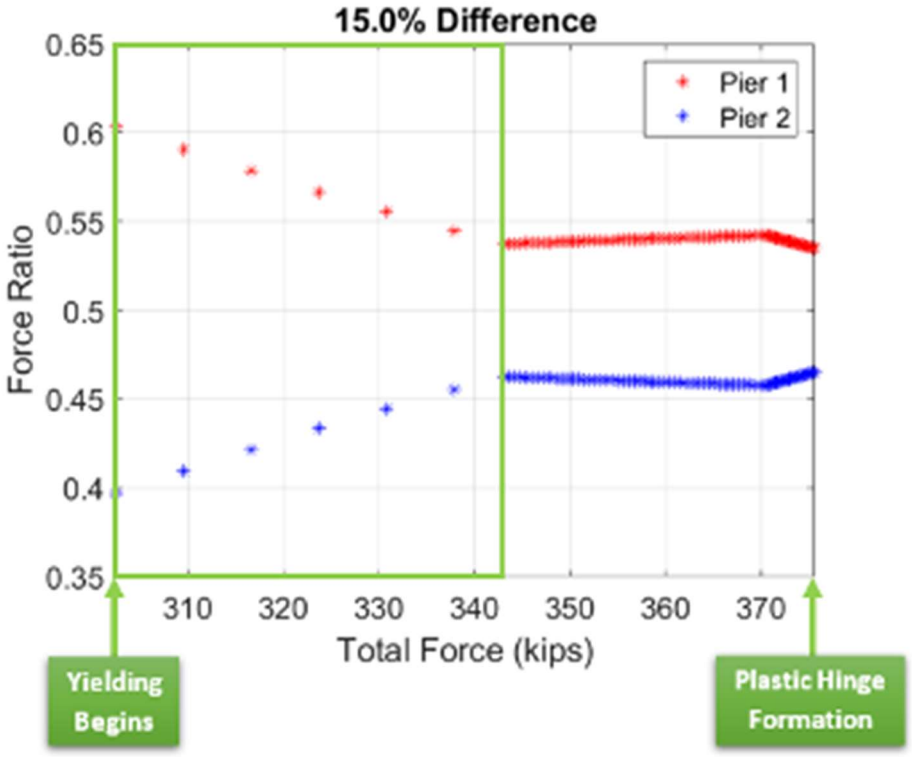

Figure G.9 Nonlinear Pushover Analysis of Adjacent Piers with a Height Ratio of 1.15

Table G.4 shows the percentage of the bridge responses to all 100 ground motions which land in the region of non-simultaneous yielding as a function of the height ratio and resulting stiffness ratio of the two piers. It is clear that once the height ratio exceeds 1.10, the percent of responses that land in the non-simultaneous yielding region increases substantially. This analysis is further confirmed after a review of California Department of Transportation (CalTrans) Seismic Design Criteria (CalTrans, 2019) stating that stiffness for adjacent frames be between 0.75 and 1.33.

Table G.4 Results of Nonlinear Pushover Analysis for Varying Pier Heights

Height Ratio (H2/H1)	EQ in Green Zone	Stiffness Ratio (H2/H1)
1	0	1
1.025	0	0.93
1.05	0	0.86
1.075	2	0.81
1.1	1	0.75
1.125	6	0.70
1.15	6	0.65
1.175	6	0.62
1.2	7	0.58

Because the Level 1 assessment procedure only considers a single height (the maximum dynamic height of all of the piers), bridges with piers of varying heights must be excluded from the Level 1 assessment. When using BIAS, there is no way to estimate whether or not piers have a height ratio greater than 1.1 with current data items. Not having this information does not prohibit the use of the Level 1 assessment, but the likelihood for unfavorable misclassification (e.g., underestimating the vulnerability) is increased considerably.

5. Element Height

While the actual dynamic height of the substructure is important for the accuracy of a Level 1 assessment, there are a few data items currently stored in BIAS that can be used to estimate the relevant height. For bridges over roadways or railroads, the minimum vertical under clearance (NBI Data Item 054B) gives the minimum clear height from the road or railroad to the bottom of the beam. For bridges over waterways, there are no minable data items currently in BIAS. However, the scour channel profile is recorded during inspections. This value includes the depth to the top and the bottom of fixed items, like piers, in the channel. If these data were to be made minable, they could be used to estimate the height of bridges over waterways. Figure G.10 shows the comparison of the dynamic height determined from the bridge drawings and the height determined using the minimum vertical under clearance or the scour channel profile. The bridge ID on the x-axis corresponds to the bridge ID found in Table G.1. The height from the scour channel profile was manually obtained to show the effects of using this data. If there is no scour channel profile or minimum vertical under clearance in BIAS, the height is zero and no Level 1 assessment can be performed on those bridges. Figure G.10 shows that these approaches for estimating the dynamic height result in significant variability, suggesting the importance of adding the height of the structure as a data item in BIAS.

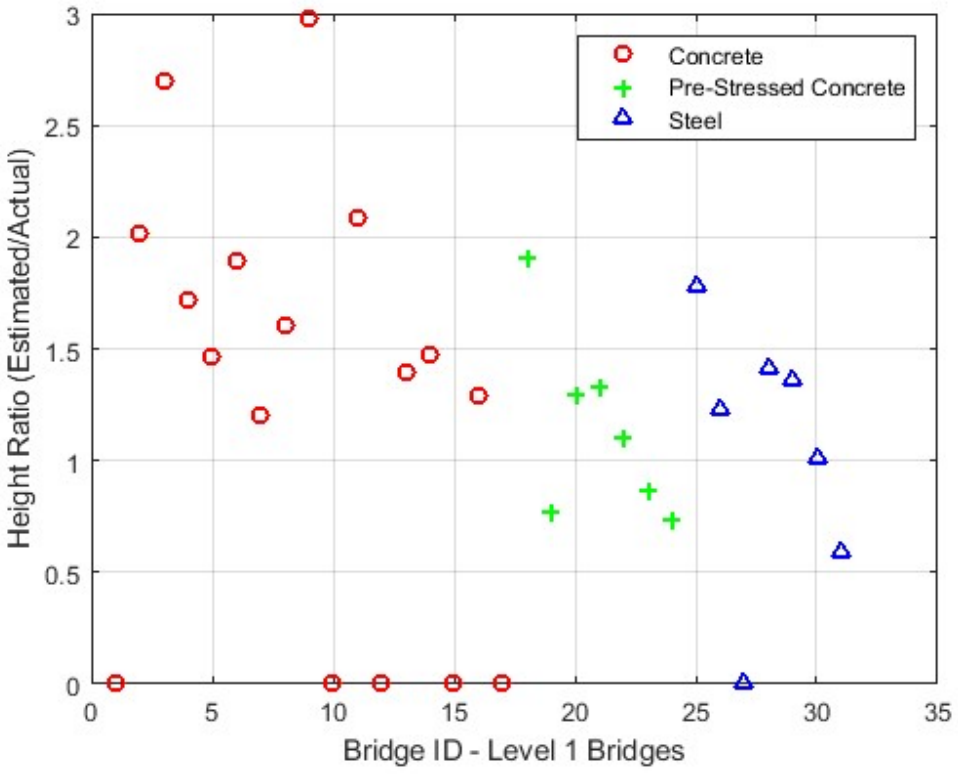

Figure G.10 Comparison of Estimated Height and Actual Dynamic Height

Figure G.11 shows the new comparison between the Level 2 analysis and the Level 1 analysis when the element height is not given, for all 3,400 ground motions. It is important to note that six bridges did not have a value for the minimum vertical under clearance and did not have any information in the scour channel profile. These gaps in the data items result in 21% of results classified as "No Data." Without adding the dynamic height, a Level 1 assessment is not possible on these six bridges.

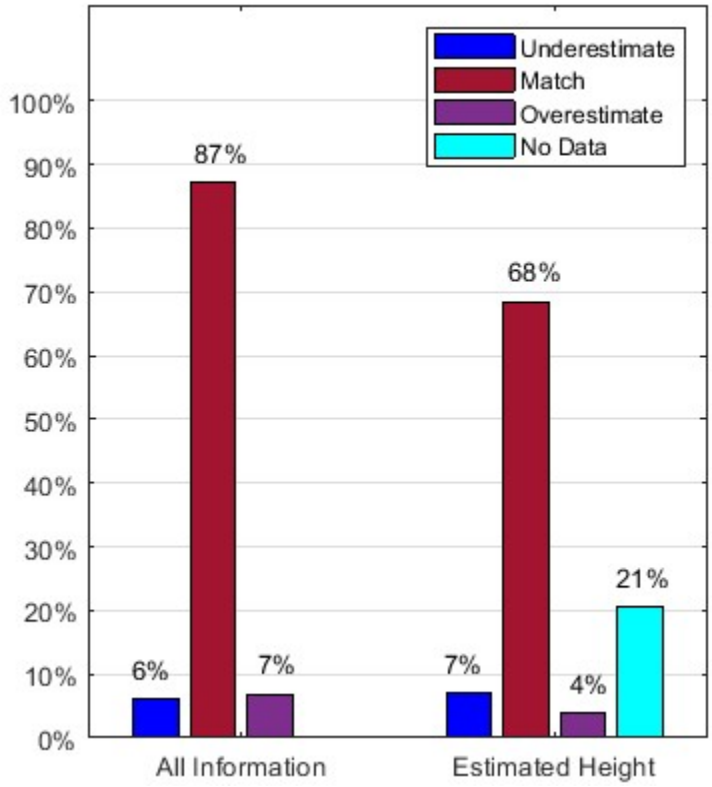

Figure G.11 Comparison of Detailed and Simplified Classification using a Height Estimate

Comparing the "All Information" results with the "Estimated Height" results in Figure G.11, the total percent of matching results between the Level 2 assessment and the Level 1 assessment decreases considerably when the height is estimated. It also shows a decrease in the number of bridges for which a Level 1 assessment applies due to a lack of consistent data in BIAS. This outcome shows the importance of including an accurate element height to perform the Level 1 assessment.

6. Number of Elements in Substructure

The number of elements in the substructure refers to the number of columns in a single pier. For walls and hammerhead substructures, this value is one. For frame bent substructures the number of elements in the substructure is critical for the stiffness calculations. Without this information, a Level 1 assessment for frame bent substructures is not possible. Figure G.12 relates the number of columns to the tributary area that a given pier supports for our sample set of bridges. It is clear that there is no definitive correlation between the number of columns in a pier and the tributary area supported by the pier. *Therefore, the number of elements in the substructure is a critical data item. Without it, the Level 1 assessment cannot be applied to frame bent substructures with any confidence.*

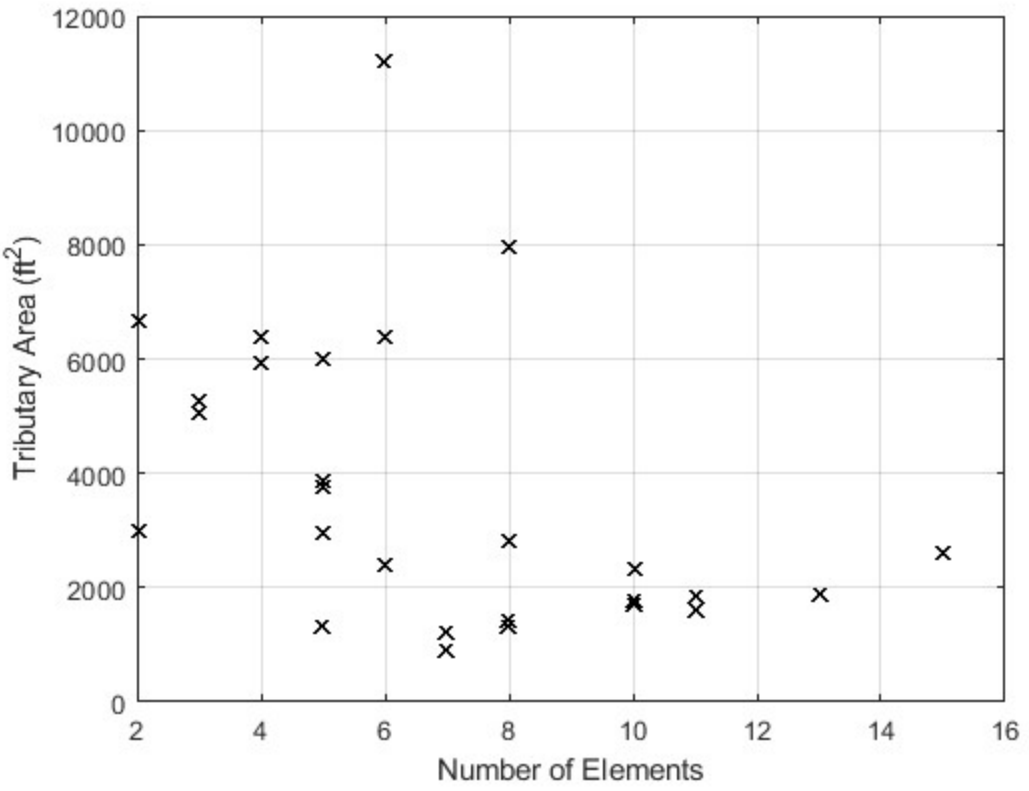

Figure G.12 Tributary Area vs. Number of Elements for all Frame Bents in Sample Set

7. Element Length

Element length is defined as the dimension in the transverse direction of one substructure element. For walls and hammerheads, this value corresponds to the long dimension of the substructure at the base and for frame bents, this value corresponds to the dimension in the transverse direction of a single column. This data item can be roughly estimated using information that is currently available in BIAS along with the critical information discussed in the sections above. However, estimating this data item will decrease the confidence in the Level 1 assessment results, as shown in Figure G.13. The following three sections describe how the element length can be estimated for walls, hammerheads, and frame bents.

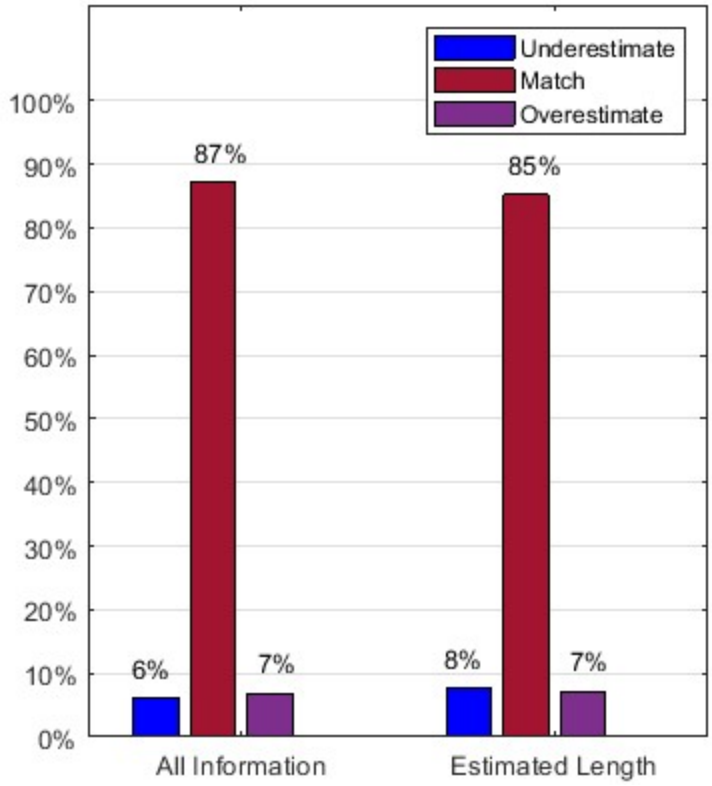

Figure G.13 Comparison of Classification Results for the Level 2 and the Level 1 Assessments using a Length Estimate

6.1 Walls

BIAS currently contains information on the deck out-to-out width and the skew of the bridge. Some bridges in the inventory maintain a skew entry of 99 which indicates a major variation in skews of substructure units (FHWA, 1995). Therefore, if the skew is listed as 99 for a given bridge in BIAS, the Level 1 assessment is not applicable to the bridge and a Level 2 assessment is required. For bridges with a skew less than 90-degrees, the length of the pier is estimated as

$$L_{ele} = \frac{w_{bridge}}{cos(skew)}. \tag{33}$$

Figure G.14 shows the ratio of the estimated length to the actual length for all the wall substructures in the original sample set of 100 bridges. *The bridge ID on the x-axis does not correspond to the bridge ID in Table G.1.*

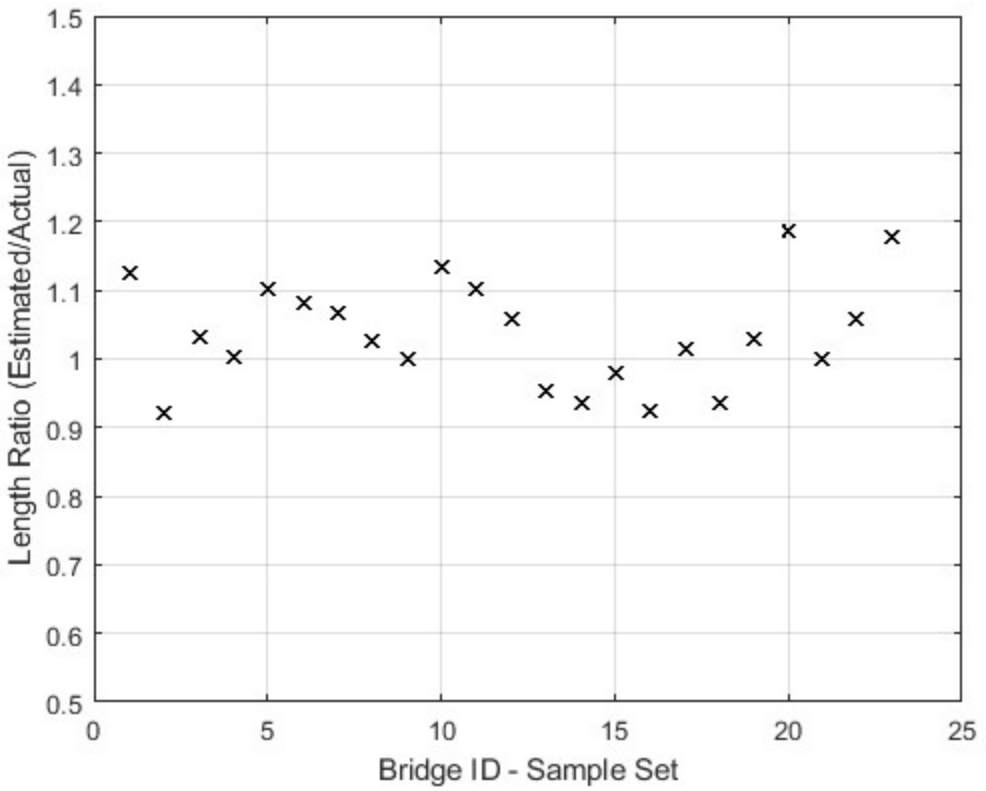

Figure G.14 Comparison of Estimated Length to Actual Length for all Walls in the Sample Set

6.2 Hammerheads

Hammerheads are very similar to walls except for the narrowing of the cross-section in the stem. Thus, the dimension at the base of the hammerhead is the value used in all the calculations. The dimension at the top of the hammerhead can be estimated using Equation (33). Additionally, a ratio between the stem length and the length at the top of the sample can be calculated. Only one reinforced-concrete superstructure bridge is supported by a hammerhead substructure in the sample set. It is difficult to identify trends for the ratio depicted in Figure G.15 for this class of bridges, thus if the stem length is unknown they are excluded from the Level 1 assessment. For prestressed concrete and steel superstructures, Figure G.15 shows the ratio of the length at the base to the length at the top. *The bridge ID on the x-axis does not correspond to the bridge ID in Table G.1.*

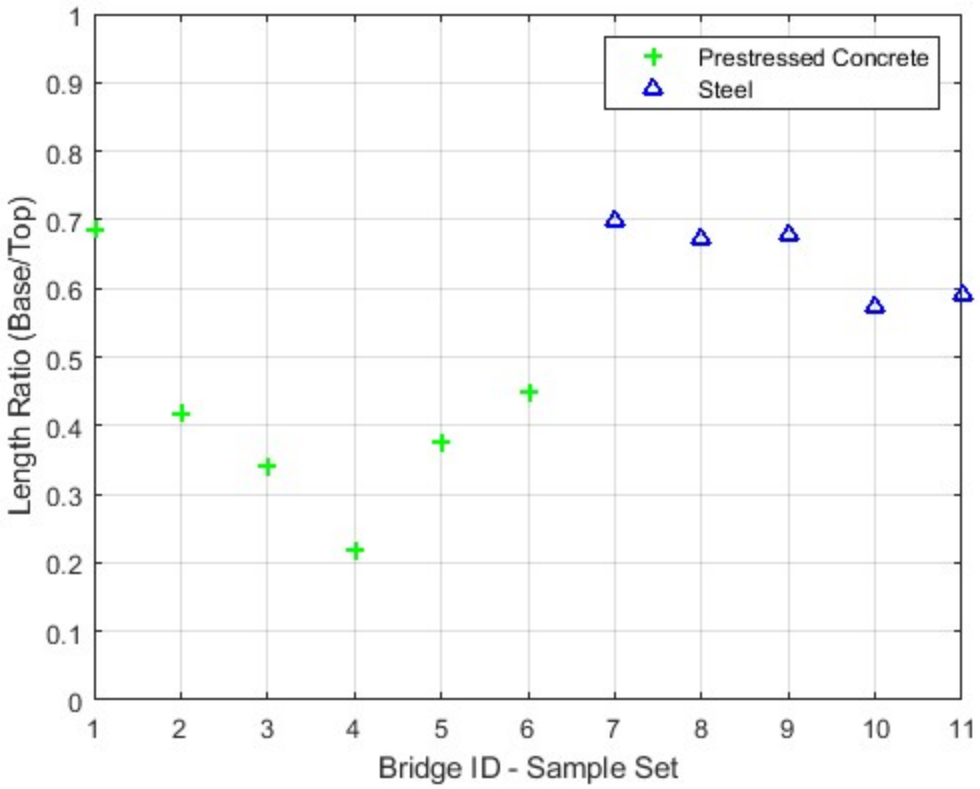

Figure G.15 Base Length to Top Length Comparison for All Steel and Prestressed Hammerhead Bridges in Sample Set

The average ratio for steel superstructures is 0.64 with a standard deviation of 0.05. The average ratio for prestressed superstructures is 0.36 with a standard deviation of 0.15. Due to the small number of samples and the large spread in the results, the average ratio minus one standard deviation is conservatively used to estimate the length at the base of the hammerhead pier (F_{Len}). Underestimating the length leads to an underestimate in the stiffness and an overestimate in the period, which will give results that slightly overestimate the vulnerability. An overestimate in the vulnerability is more desirable than an underestimate in the vulnerability. The length at the base of hammerhead piers is calculated as

$$L_{ele} = F_{Leng} \quad \frac{w_{bridge}}{cos(skew)}. \tag{34}$$

Figure G.16 shows the ratio of the estimated length to the actual length at the base of the hammerhead substructures in the sample set. However, there is error due to the large standard deviation in the prestressed sample set. This outcome shows that while the length of the hammerhead piers can be estimated, the estimate will considerably affect the confidence in the Level 1 assessment results.

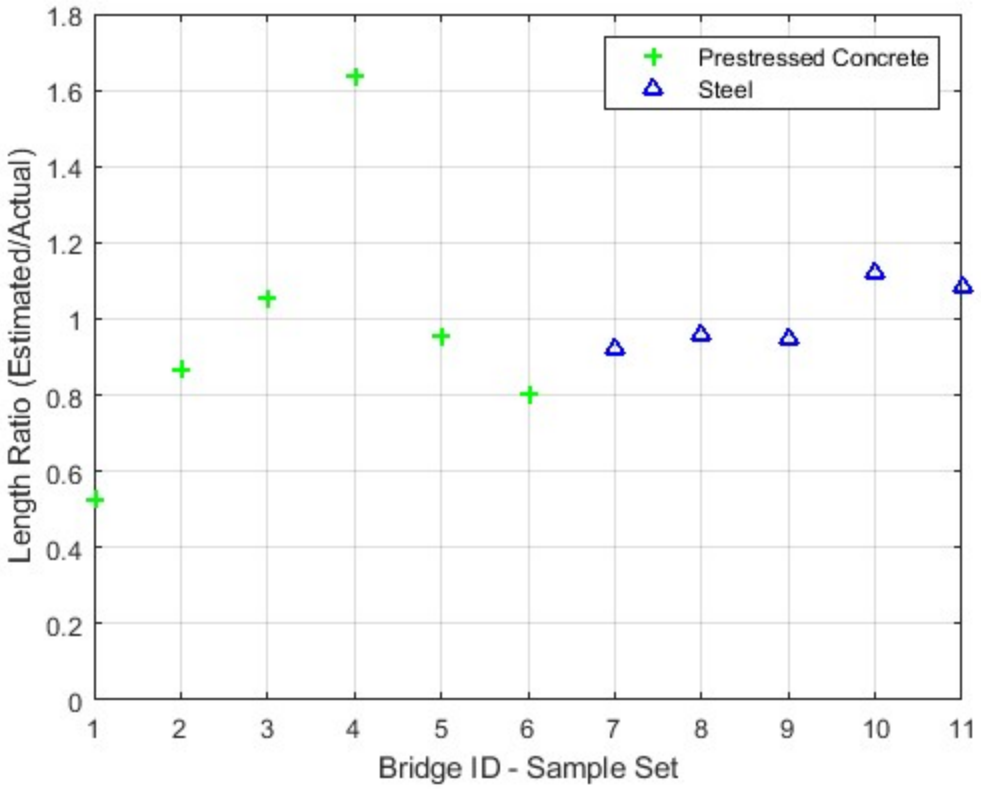

Figure G.16 Comparison of Estimated Length to Actual Length at the Base of Steel and Prestressed Hammerheads in the Sample Set

6.3 Frame Bents

Estimating the length of multiple elements (columns) for frame bents is more difficult than estimating the length of a single element for walls and hammerheads. Given the number of elements in a pier, the deck out-to-out, and the skew, the total length of all columns at the base of the pier is calculated as a ratio of the total substructure out-to-out. For frame bents, this ratio (F_{Length}) is calculated as

$$F_{Leng} = \frac{N_c * L_{ele,act}}{L_{pier}}, \quad (35)$$

where $L_{ele,act}$ is the actual length of the element and L_{pier} is the length of the pier calculated using Equation (33). This ratio for each frame bent in the sample set is shown in Figure G.17. *The bridge ID on the x-axis does not correspond to the bridge ID in Table G.1.*

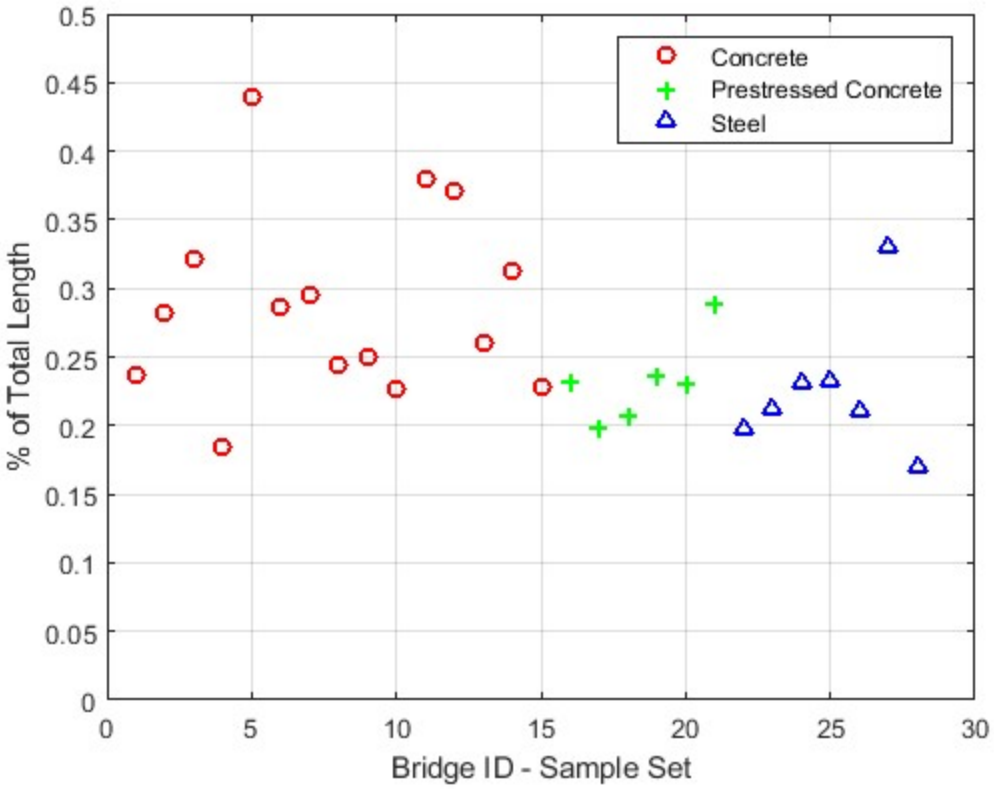

Figure G.17 Percent of Total Length of Frame that is the Length of Elements

The values are primarily concentrated around an average value of 0.26. The standard deviation of F_{Lengt} for this sample set is 0.06. The average minus a standard deviation (0.2) is again used to estimate the ratio in the Level 1 assessment if the length is not given. This approach aims to account for the variability in the results. The ratio of the estimated length to the actual length of the element is shown in Figure G.18.

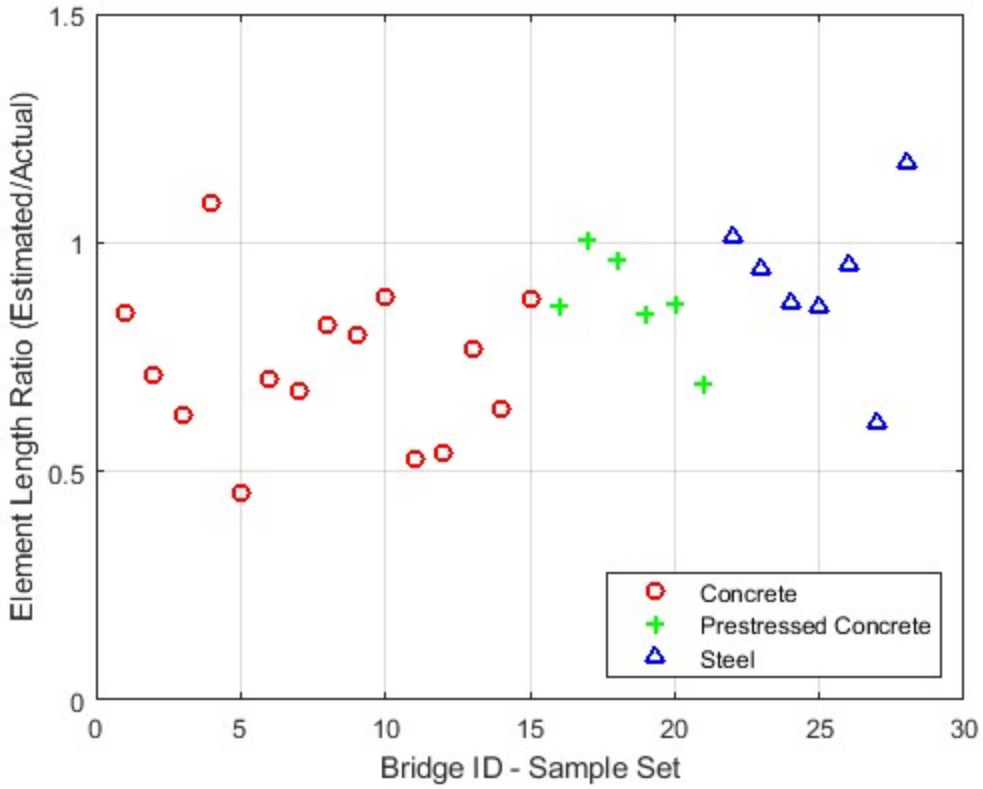

Figure G.18 Ratio of Estimated Length of a Column to the Actual Length for All Frame Bents in the Sample Set

8. Element Width

Element width is defined as the dimension in the longitudinal direction of one substructure element. As with element length, this dimension can be approximated using an average of the values seen in the Level 2 assessment. If the substructure has circular elements, the element length is also the element width. For all other substructures, a width of two-feet is used as a lower-bound estimate for the width. Figure G.19 shows the distribution of width of the non-circular substructures for all bridges in the sample set. A lower-bound estimate is used because it leads to an underestimate in the stiffness which corresponds to an overestimate in the vulnerability of the bridges. The comparison between the vulnerability classifications obtained from the Level 2 and the Level 1 assessments, when estimating the width of the elements, is shown in Figure G.20. Note that estimating this parameter does not have a significant influence on the classification results.

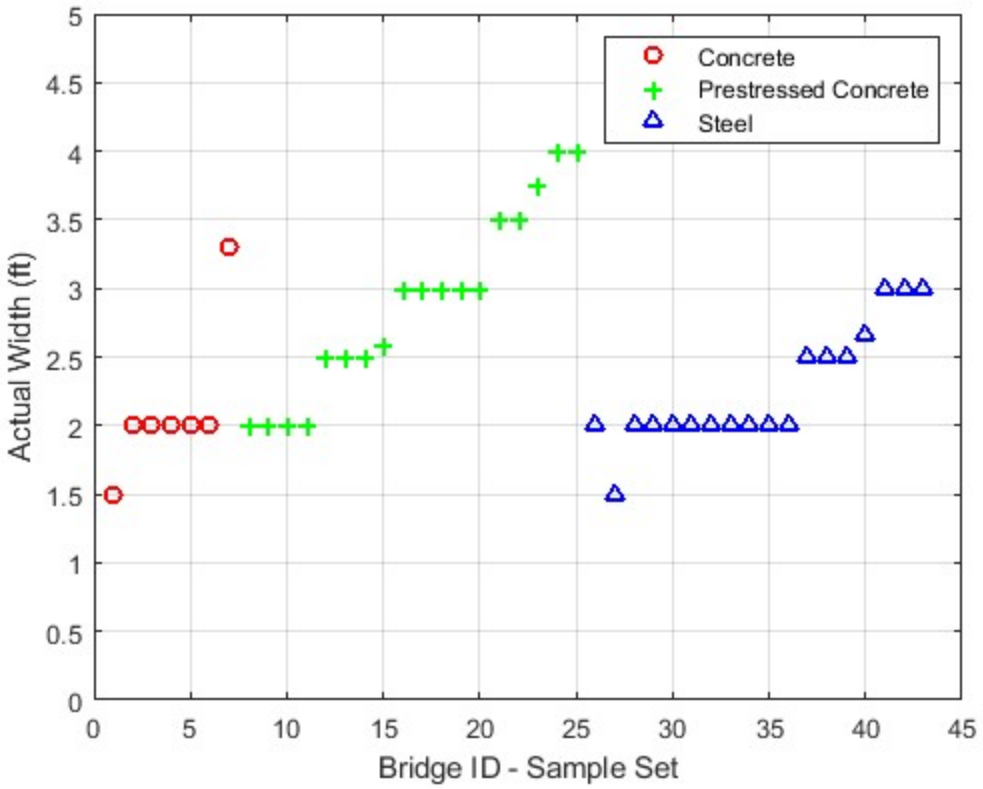

Figure G.19 Width of Non-Circular Substructure Elements of Entire Sample Set

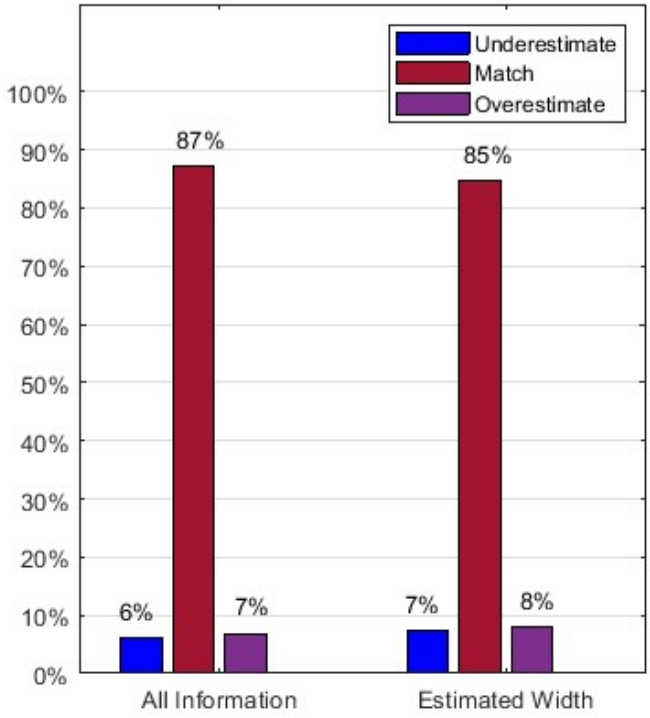

Figure G.20 Comparison of Detailed and Simplified Classification using a Width Estimate

9. Deck Thickness

Knowing the thickness of the deck is important for the mass and stiffness calculations for reinforced concrete superstructures. For prestressed and steel superstructures, an average deck thickness of 8 inches is typical and is assumed in all Level 1 assessment calculations.

For reinforced concrete bridges, the thickness of the deck is needed for both mass and the stiffness calculations. As shown in Figure G.21, there is a large spread in the thickness of the deck for reinforced concrete slab deck bridges, which supports the need to know the actual deck thickness.

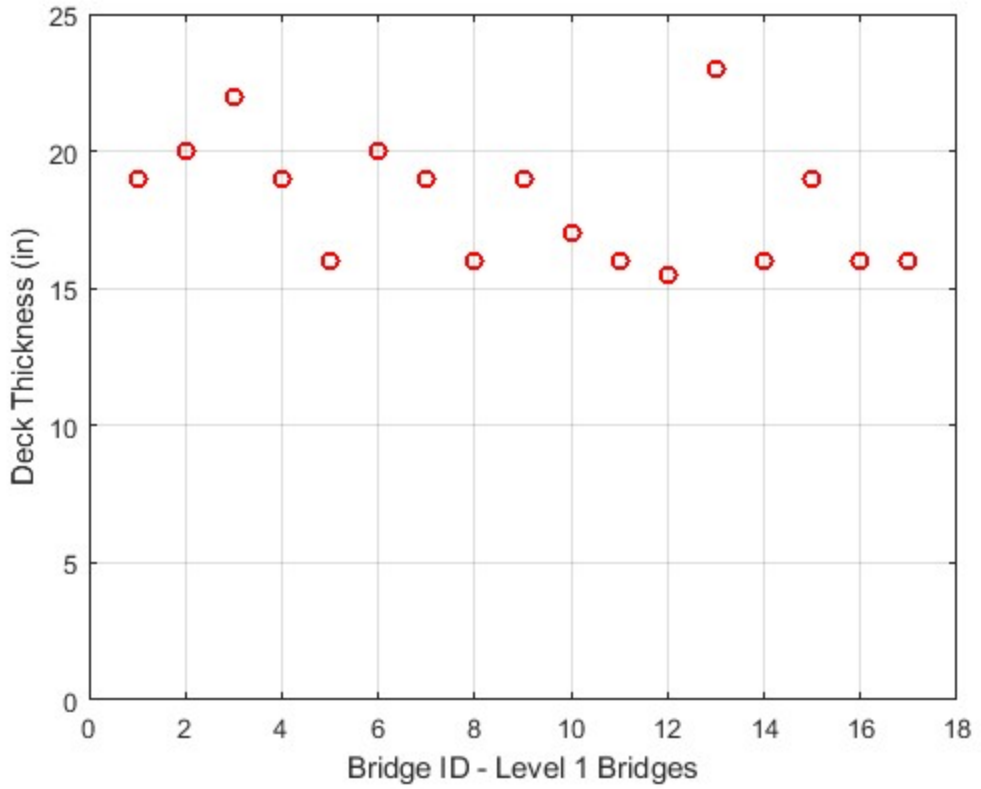

Figure G.21 Reinforced Concrete Slab Deck Superstructure Deck Thickness Spread of Entire Sample Set

However, if the deck thickness is not given, it is assumed to be the average from the sample, 18.6 inches. Figure G.22 and Figure G.23 show the ratio of the calculated mass and stiffness using the estimated deck thickness to the calculated mass and stiffness using the actual deck thickness. The results for the stiffness results in the longitudinal direction, shown in Figure G.23(a), is one because deck thickness does not have an impact on the stiffness calculations in the longitudinal direction. *The bridge number on the x-axis corresponds to the bridge ID number in Table G.1.*

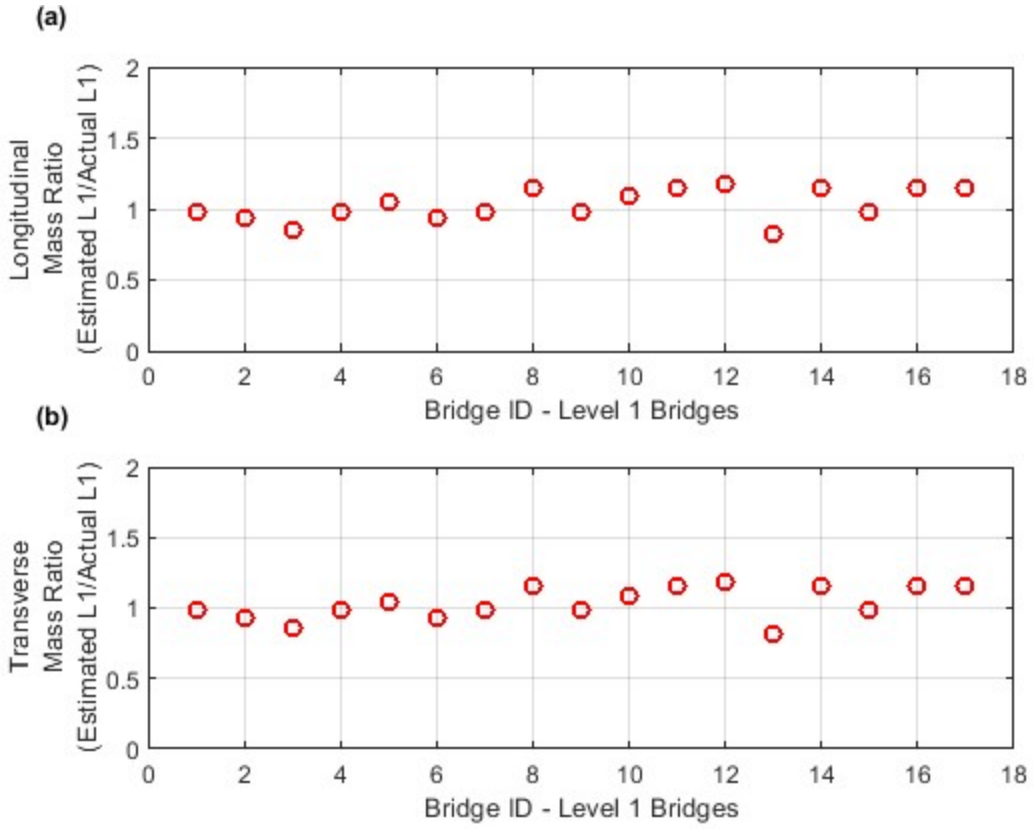

Figure G.22 Mass Ratios (Estimated/Actual) Using an Estimated Deck Thickness for RC Slab Deck Bridges in the (a) Longitudinal Direction and (b) Transverse Direction

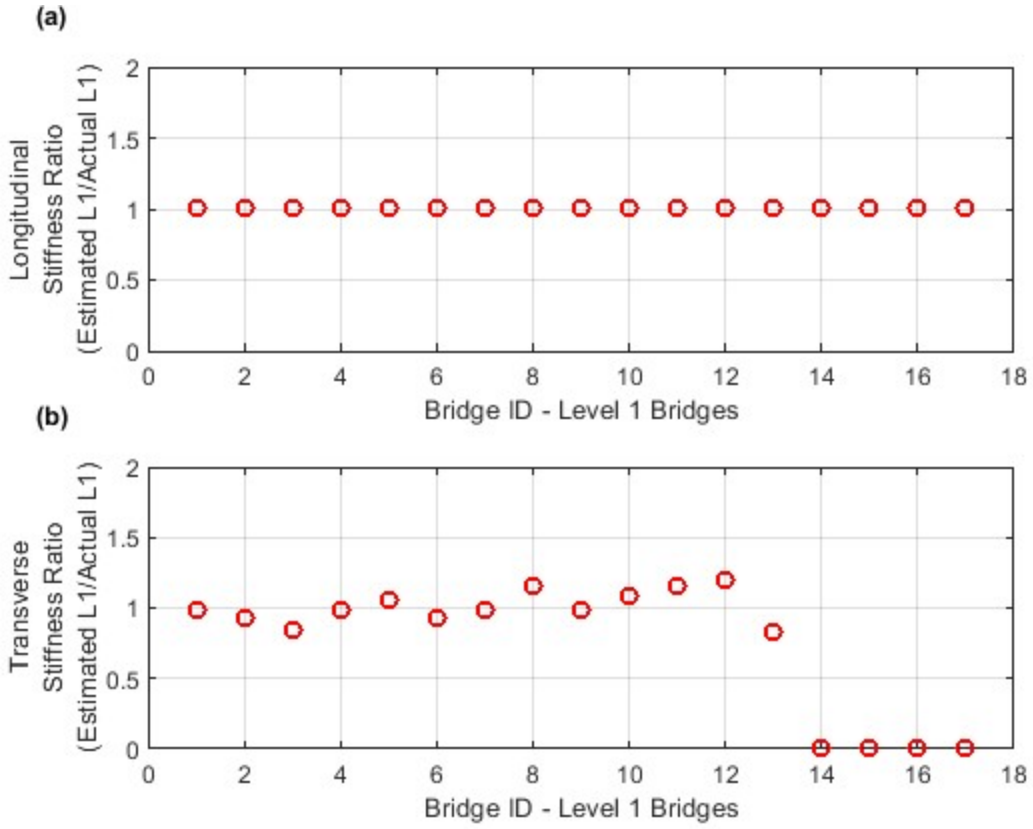

Figure G.23 Stiffness Ratios (Estimated/Actual) Using an Estimated Deck Thickness for RC Slab Deck Bridges in the (a) Longitudinal Direction and (b) Transverse Direction

The results obtained using the average compared to those obtained using the actual deck thickness are shown in Figure G.24. For reinforced concrete slab deck bridges, using the average deck thickness for our sample set of bridges does not change the comparison of the Level 1 and Level 2 vulnerability classifications. However, as shown in Figure G.22 and Figure G.23, the mass and stiffness values are impacted, potentially affecting the vulnerability classification for other bridges, even though it did not for the bridges in our sample set.

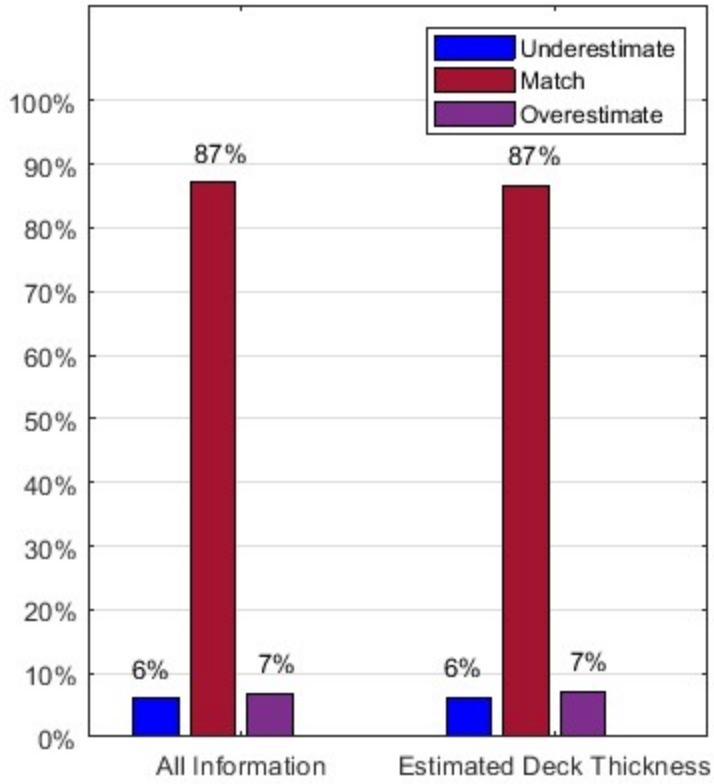

Figure G.24 Comparison of Detailed and Simplified Classification using a Deck Thickness Estimate

Conclusions

The methodology and the results presented in this appendix show the importance of adding the requested information to BIAS. The conclusions that can be made based on the findings in this appendix are as follows:

- The Level 1 assessment is not applicable to all bridges. There are certain bridge details and types that restrict the use of the Level 1 assessment procedure, even if all the recommended information is provided. A Level 2 assessment may be used to determine their vulnerability. These are the following:
    - Bridges with expansion joints
    - Bridges whose superstructure combination is not reinforced concrete slab deck bridges, steel girder bridges, or prestressed beam or girders (both box and tee)
    - Bridges with a substructure type classified as "other"
    - Frame bents with an aspect ratio less than three

- **Data items needed in BIAS** to run the Level 1 assessment are the following:
    - Substructure Type
    - Number of Elements
    - Element Height
    - Deck Thickness
    - Element Length

- Element Width
- Height Ratio Flag
- Abutment Type
- Seismic Retrofit Checkbox

- While the additional information we are recommending for addition in BIAS is critical, it is possible to estimate some of the information needed based on the data items that are already available in BIAS. These data items that might be estimated or assumed without excessively affecting the vulnerability assessment are the following:
  - Element Height
  - Element Length
  - Element Width
  - Deck Thickness

- If all the recommended information is not added, more bridges will require a detailed analysis and the accuracy of the vulnerability classifications from the Level 1 assessments will be affected.

Summary

In this appendix, the critical additional information needed to perform the simplified assessment is introduced and the procedure to perform the Simplified Assessment using all of the information, is described in detail. The importance of each additional data item is also discussed, and if there is a way to estimate the value of the data item based on information that is currently available in BIAS, that method for estimating is proposed. The impact of that estimate on the vulnerability classification is evaluated through a comparison of the classification results obtained with the Level 1 assessment and the Level 2 assessment. The procedure developed in this appendix as well as the methods for estimating certain data items are implemented in the simplified assessment tool presented in the following appendix.

APPENDIX H. DEVELOPMENT OF INDIANA SEISMIC ASSESSMENT TOOL (INSAT) TOOL

Introduction

The Indiana Seismic Assessment Tool (INSAT) is intended to be used by INDOT to conduct a simplified seismic assessment of its bridge network. The MS-Excel-based, macro-driven desktop application implements and automates the simplified seismic assessment methodology presented in Appendix G. INSAT screens the bridges to a Level 0, 1, or 2 assessment and classifies the vulnerability of these bridges. This vulnerability assessment is conducted based entirely on information found in BIAS and the recommended data items discussed in Appendix F. INSAT was developed by combining various modules, and this appendix discusses the logic used within each module and the connectivity between each module.

Discussion of Static Sheets within INSAT

INSAT contains six static sheets, each of which contain information needed for INSAT's functionality. These six sheets are locked to ensure the integrity of the data and of INSAT as a whole. Changes to these sheets, specifically the addition of new bridges, will require the use of the *password: JTRP4222* to unlock the cells so that data can be manipulated. Once such changes have been made, each sheet should be locked again using the same password. The intended use of and data requirements for each sheet are described in detail in the following sections.

Instructions Sheet

The *Instructions Sheet* is the main sheet in INSAT. This sheet contains general instructions for executing INSAT as well as the button that begins an assessment. More detailed instructions for executing the tool can be found in the *Simplified Seismic Evaluation Tool User Guide* provided with the INSAT tool (Bonthron et al., 2020).

General Information Sheet

The *General Information Sheet* contains information regarding data requirements, the format for input files, and the main assumptions used in INSAT.

Routes Sheet

The *Routes Sheet* contains two columns. The first column is a list of all the roads in Indiana. This list is used if the user chooses to assess the bridges along a specific road. The second column is a list of critical routes in the state, as defined by the INDOT Primary Disaster Routes Map (CETRP Attachment No. 4). If the state updates the routes defined as critical routes or primary disaster routes, this column should be updated to reflect those changes. The list of identified disaster routes can be found in the user guide.

"Site Class" Sheet

The *Site Class Sheet* contains the predetermined site class for each of the 5,902 state owned bridges, as of January 24, 2020. The site class is determined by extracting the metadata from Indiana Geological Survey's 2011 Seismic Shaking Materials Response Map using the latitude and longitude coordinates of each structure. The first three columns contain the NBI number for each bridge, a number extracted from the map that corresponds to the site classification, and the site class classification extracted from the map, respectively. Table H.1 shows the number and the corresponding site class classification. If additional bridges are added to BIAS, their site class should be included on the *Site Class Sheet*. If no site class is provided to the tool, site class D is assumed.

Table H.1 Site Class Classification and Corresponding Number

Site Class Number	Site Class Classification
0	–
1	B
2	C
3	C through D
4	D
5	D or F
6	D through E
7	D through F

UHS Information Sheet

The *UHS Information Sheet* contains the predetermined Uniform Hazard Spectra (UHS) data for a return period of 1,000 years. The development of the UHS data is not compatible with INSAT, so the data must be predetermined. To change the return period or to get the data for additional bridges, the latest version of USGS's nshmp-haz platform and the appropriate version of the national seismic hazard map should be used. Instructions for using the nshmp-haz platform can be found on the nshmp-haz wiki (nshmp-haz, n.d.). To deliver INSAT to INDOT, nshmp-haz version 1.1.9 and the 2014 National Seismic Hazard Map were used to prepare the UHS data. The *UHS Information Sheet* has two heading rows and eight columns. The first column contains the NBI number for each structure in INDOT's bridge inventory (based on the assets at the time INSAT was developed). The other seven columns contain the acceleration values, in terms of *g*, for seven spectral periods, ranging from 0.0 s to 2.0 s.

"Site Factors" Sheet

The *Site Factors Sheet* contains the factors used to convert the UHS from site class B/C to the site class at the bridge location since the program used to generate the UHS data for the bridges in the state only provides results for a single site class, which is site class B/C boundary. The site factors found in AASHTO Section 3.10.3.2 (2017) are used to amplify or reduce the acceleration to account for the soil conditions at the site. This sheet contains these tables, converted to have B/C boundary reference site class. There are three tables in this sheet. Each table corresponds to a specific structural period. For short period, i.e., less than 0.1 s, the first table is used. For periods between 0.1 s and 0.5 s, the second table is used; and for long periods, greater than 0.5 s, the third table is used. This sheet only needs to be updated if AASHTO updates their site factors.

Module Description and Logic

SeismicEvaluation(--) – Module 1

This module is the primary module performing the seismic evaluation. All other modules are called from this one. This module initializes all public variables as well as those variables used only in this module. After the initialization, this module deletes the previous analysis results, and if requested by the user, the previous *BIAS Information Sheet* and the previous *Additional Information Sheet*. If there is no sheet named "BIAS Information" after the initial deletion of the extra sheets, INSAT prompts the user to select the file that contains the BIAS data, using the **BIASFile(OS) Module** (Module 3). If the file selected contains the required data items in the correct format, INSAT moves on. If not, a descriptive error message is sent to the user and they are prompted to rerun the seismic evaluation with the correct inputs.

INSAT is programmed to work with various levels of added information. INSAT first searches the BIAS data input file to determine if all recommended data items are present. If all of the recommended data items, with the correct headings, are found in the BIAS data input file, then INSAT moves forward. If some, but not all data items are in the BIAS data input file, INSAT notifies the user which data items are missing and asks if the user would like to load in an additional data input file. If the user selects "yes," INSAT prompts the user to select the file that contains the additional data items using the **AddInfoFile(OS) Module** (Module 4). If the BIAS data input file does not contain any of the additional data items, INSAT prompts the user to select the file that contains the recommended data items, using the **AddInfoFile(OS*)* Module** (Module 4).

After the required data has been entered into INSAT, the module asks the user if they have a file containing the reinforcement checks for bridges with old wall and hammerhead substructures. If the user selects "Yes," they are prompted to select the file containing this check using the **ReinforcementCheckFile(OS) Module** (Module 13). If a file is not selected or the selected file does not contain the correct headings, the user is alerted and INSAT move onto the next part. However, if the information is correct, the data from this file is saved to a *Reinforcement Check Sheet* so that it can be used during the seismic assessment to inform INSAT of the engineer's findings from the bridge drawings. If the user selects "No," INSAT moves forward to the next portion. A variable `ReinforcementRatioFile` is used to inform INSAT across the different modules if this file has been correctly loaded. If `ReinforcementRatioFile` is one, then a file was loaded and if it is zero, then no file was loaded.

The module then prompts the user to select the subset of bridges to assess. The user has several options to choose from: the entire bridge database, a specific list of user-provided NBI numbers, all critical routes, specific set of districts, or a specific route. Each option, except for the option that includes the entire bridge database (largest), corresponds to and calls a separate module in which the NBI numbers corresponding to the specific option selected are defined. Table H.2 shows the options available and the module corresponding to each.

Table H.2 Assessment Options and Corresponding Module

Selection Option	Module
Entire Bridge Database	-
User Inputted NBI List	**NBIFile()** - Module 5
Critical Routes	**CriticalRoute()** - Module 6
District(s)	**SelectedDistrict()** - Module 7
Specific Route	**SpecificRoute()** - Module 8

If the entire database is selected, INSAT copies all NBI numbers from the created *BIAS Data Sheet* and stores them on a new *NBI List Sheet*. If any of the other options are selected, the logic described in the corresponding module description (shown in subsequent sections) is followed to determine which NBI numbers to analyze. These NBIs are stored on the *NBI List Sheet*.

Once the list of NBI numbers to analyze has been compiled, this module creates a temporary *Database Information Sheet* which stores the BIAS data and Additional Information data for every bridge. The data stored in this sheet is used in all future classifications and calculations and is stored in the tool until these data sheets are reloaded in some subsequent call of **SeismicEvaluation(--)**.

INSAT then prompts the user to determine whether or not to customize the output information, using the **FormattingOutput(--) Module** (Module 9). Certain data items are automatically provided as outputs, including: Asset Name, NBI Number, District, Superstructure Type, Substructure Type, and any classifications and warnings identified by INSAT. The user has the option to select any or all of the follow

addition data items to output, such as: Latitude and Longitude, Feature Intersected, Facility Carried, Number of Main Spans, Skew, and Abutment Type.

After the outputs have been selected, INSAT calls the **SeismicEvaluationCalcs(TotalNBIs) Module** (Module 2) to perform the simplified seismic evaluation on the selected set of bridges.

INSAT includes the option to have the user apply a user-defined priority factor to each of the bridges based on its relative importance for a given run. After the simplified assessment is complete, the user is asked if they'd like to add a factor to prioritize the results. If the user selects "yes," the **PriorityFactor(OS) Module** (Module 10) is called to load the priority factors and to sort the results by both priority and by vulnerability classification. The bridges with the highest priority factor are shown first within each vulnerability class (high, moderate, and low). If the user selects "no," the **SortAllResults(--) Module** (Module 12) is called to sort the results such that the bridges with the highest vulnerability class are at the top.

The module then removes the added sheets, except for the *All Results Sheet*, the *BIAS Data Sheet,* and the *Add'l Information Sheet.*

Throughout the process, if an error occurs or the user inputs do not match the required format, an error message is shown to the user and the tool implementation must be reinitiated.

SeismicEvaluationCalcs(TotalNBIs) – Module 2

This module contains the calculations for the simplified assessment portion of INSAT. It is called from the **SeismicEvaluation() Module** (Module 1) along with the variable `TotalNBIs`. `TotalNBIs` is an integer that captures the number of bridges that INSAT will assess. It is defined within the *NBI List Sheet* discussed in the **SeismicEvaluation() Module** (Module 1) above. The calculation module begins with defining material properties, constants identified from the Level 2 assessment, factors used in the mass and stiffness calculations, and the vulnerability thresholds. The determination of these values and thresholds can be found in Appendix G. Table H.3 shows these variables, their values, and their usage.

Table H.3 **SeismicEvaluationCalcs() Module** Constants and Factors

Variables	Value	Description
fc_psi	3500 *psi*	Compressive strength of concrete
Ec_ksi	3410 *ksi*	Young's Modulus of concrete
E_Steel	29000 *ksi*	Young's Modulus of Steel
poisson	0.15	Poisson's Ratio for Concrete
FrameBentFactor	0.88	Average factor relating the pure translational degree of freedom to the condensed, decoupled stiffness of frame bents with **steel and prestressed superstructures**
FrameBentFactorRC	0.96	Average factor relating the pure translational degree of freedom to the condensed, decoupled stiffness of frame bents with **reinforced concrete superstructures**
DeckStiffnessFactor	0.217	Average factor relating the pure translational degree of freedom to the condensed, decoupled **stiffness of the reinforced concrete slab deck**

Hpile_IL	127 in^4	The longitudinal moment of inertia for assumed h-pile section (12x53)
Hpile_IT	393 in^4	The transverse moment of inertia of the assumed h-pile (12x53)
H_SteelHpile	15.5 in^2	The total area of steel of the assumed h-pile steel shape (12x53)
c_hpile	0.35	H-pile coefficient
Filled_IL	105.5 in^4	Moment of inertia of steel for the assumed CFT pile
Filled_IC	1780.3 in^4	Moment of inertia of the concrete for the assumed CFT pile
c_filled	0.53	CFT coefficient
CFTMom	63.2 kip*ft	Ultimate moment capacity (M_u) for the typical CFT pile
HPileMomT	176.2 kip*ft	Ultimate moment capacity (M_u) in transverse direction for the typical h-pile (12x53)
HPileMomL	77.1 kip*ft	Longitudinal moment capacity at ultimate for the typical h-pile (12x53)
SteelAvgMass	$3.6*10^{-4}$ kips/g/ft^2	The average mass per deck area for steel girder bridges
PrestressedAvgMass	0.0033 kips/g/lft	Average deck mass per linear foot
SteelHHFactor	0.58	The ratio relating the length at the top to the length at the steam of hammerhead substructures with steel superstructures
PSHHFactor	0.21	The ratio relating the length at the top to the length at the steam of hammerhead substructures with prestressed superstructures
FrameBentLengthFactor	0.2	The ratio relating the length of the columns to the total length of the pier for frame bent substructures
NLFactor	1.414	The multiplier used to estimate the nonlinear displacement using the linear displacement
TransDriftLimita	0.50%	The moderately vulnerable lower drift limit in the transverse direction
TransDriftLimitb	1.50%	the highly vulnerable lower drift limit in the transverse direction

LongDispLimita	1 in	The moderately vulnerable lower displacement limit in the longitudinal directions
LongDispLimitb	6 in	The highly vulnerable lower drift limit in the longitudinal direction
OldWallDispimit	0.1 in	The highly vulnerable lower displacement limit for old walls in the longitudinal direction

Once these constants and factors are initialized, the module proceeds to the simplified seismic assessment. INSAT moves through the following logic and calculations, if applicable, for each bridge in the *NBI List Sheet*. First, the BIAS data and the Additional data for the bridge is saved to working variables for use in the calculations. Then, the site class for the bridge is determined using the NBI number and the *Site Class Sheet*.

With all of these variables assigned, the next step is the Level 0 assessment. This series of If-Else-If statements determines the following: whether the bridge can automatically be classified as "low vulnerability" or "moderate vulnerability"; and then, whether the bridge requires a detailed analysis, or if the simplified assessment procedure is applicable. Figure H.1 shows a flow chart for the logic involved in performing the Level 0 classification, assuming that all of the recommended information has been added for every bridge. There are additional If-Else operators built into INSAT to handle different levels of added information, although they are not shown in Figure H.1. The simplified assessment is bypassed either when a given bridge can automatically be classified as "low vulnerability" or "moderately vulnerable," or, when a detailed analysis is required, and the results and bridge properties are sent to the *All Results Sheet*.

If the simplified assessment is deemed applicable, one more Level 0 check is performed based on the superstructure type. The purpose of this check is to make sure that the superstructure combination, main material type and the type of structure, is applicable to the simplified assessment. The logic for this check can be found in Figure H.2.

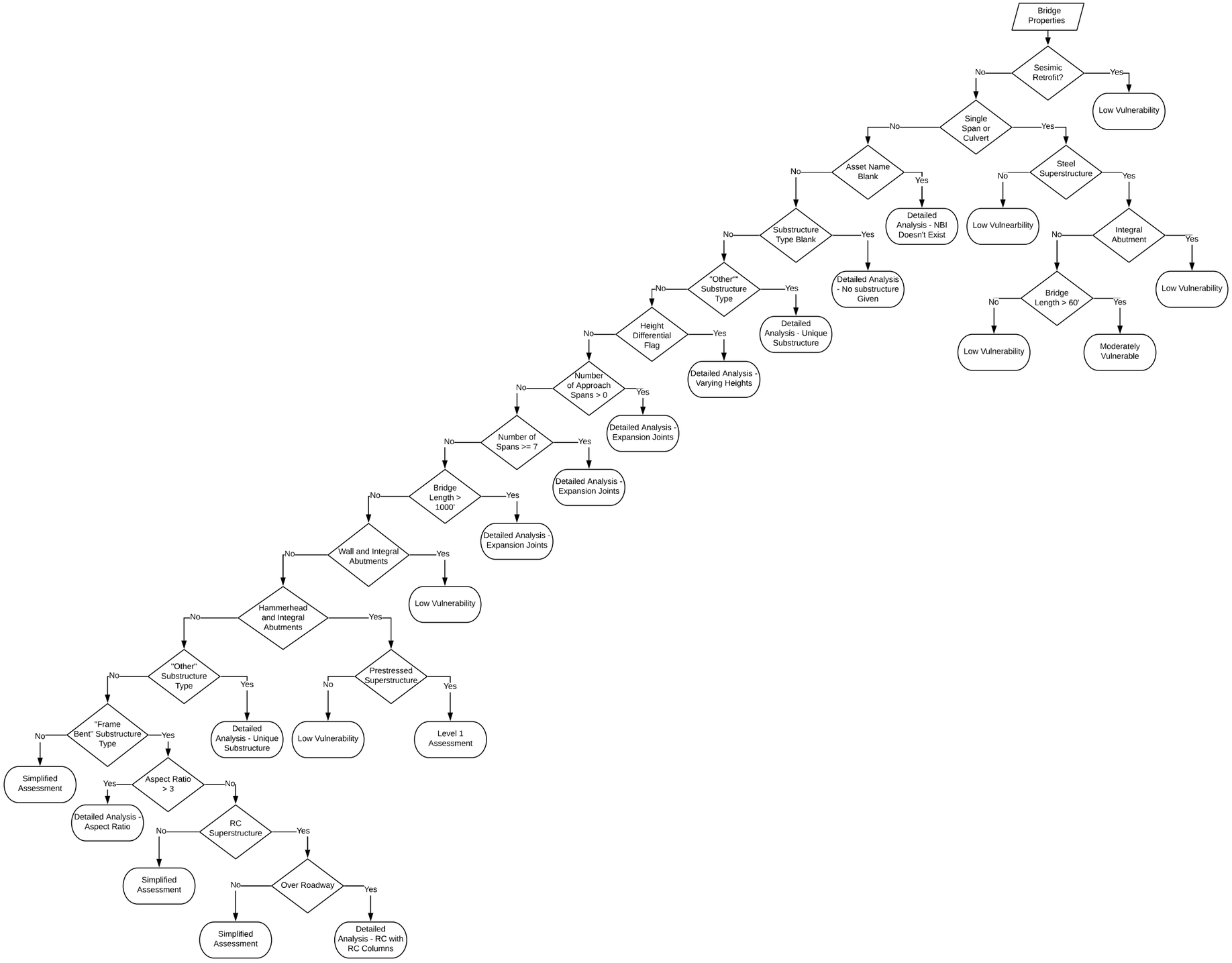

Figure H.1 Initial Classification Logic Flow

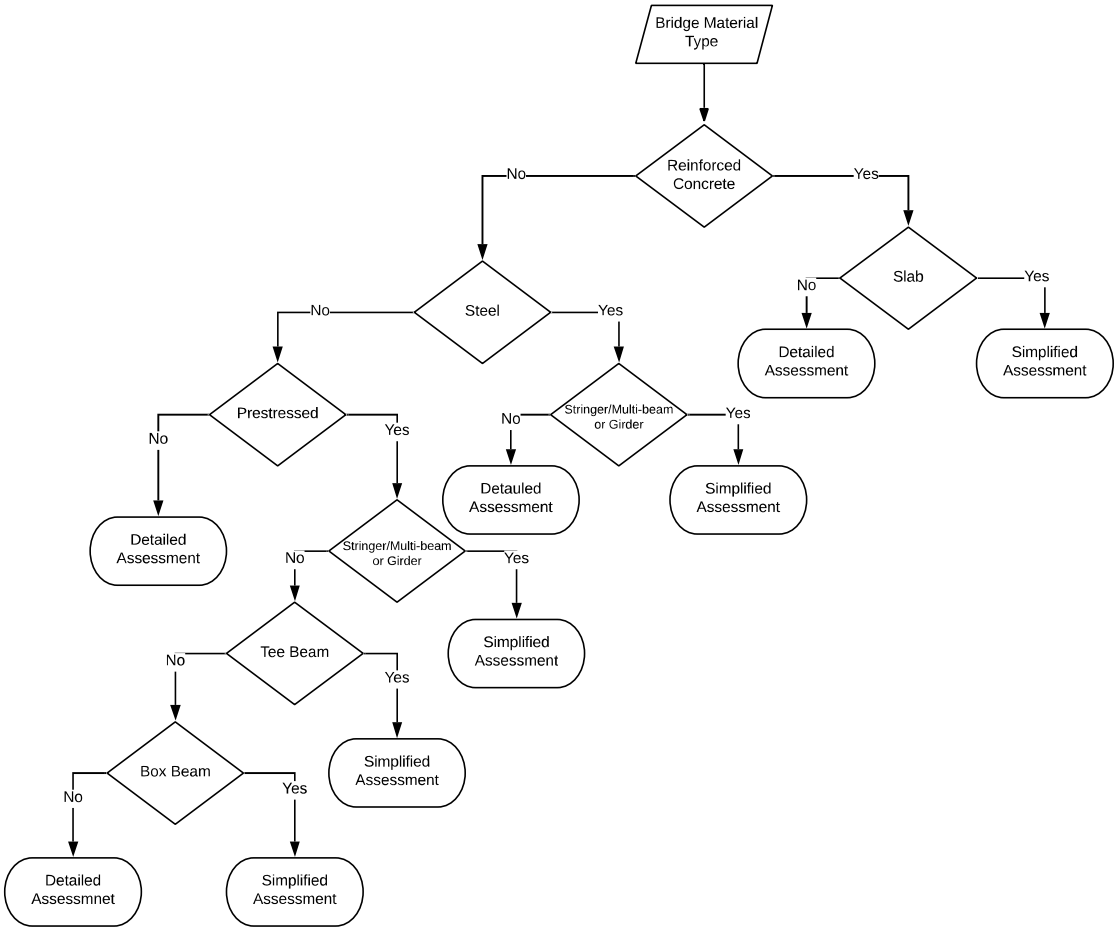

Figure H.2 Material Type Initial Classification Logic Flow

The next step, if deemed applicable, is to estimate bridge geometries that are not provided. The methodology and equations used in the estimates are discussed in Appendix G. The variable `EstimatedProp` is used to keep track of these estimates and is displayed on the *All Results Sheet* to alert the user that the values and assumptions should be verified before making any decisions related to retrofits or rehabilitations.

This module then calculates the dynamic properties (mass, stiffness, and period) of the bridge for both applicable directions, using the methodology and equations found in Appendix G. Only directions identified as having potential vulnerabilities are assessed. For example, if a given bridge has integral abutments, only the transverse direction is assessed. Similarly, if the transverse direction of the substructure is identified as not vulnerable due to its substructure type (e.g., wall substructure), only the longitudinal direction is assessed.

Using the calculated period(s) and the data found on the *UHS Information Sheet*, the spectral acceleration(s) expected at that site, for site class B/C soil, is determined. If the calculated period falls in between the periods for which the acceleration value was determined using USGS's nshmp-haz platform, the acceleration value to use for the corresponding structure period is determined using interpolation (nashmp-haz, n.d.).

The calculated acceleration value is amplified or reduced based on the soil conditions at the specific bridge location, using: the site class, the determined spectral acceleration, the period of the structure, and the table found on the *Site Factors Sheet*. The period of the structure determines which table to use. The spectral acceleration for site class B/C determines which columns to interpolate between to get the correct factor and the site class determines which row in the table to use. The amplification/de-amplification factor is multiplied by the spectral acceleration determined for site class B/C and the results in the expected spectral acceleration at the site, accounting for site soil conditions. The linear and nonlinear displacements are calculated using the equations presented in the simplified assessment appendix—Appendix G.

The final step of the simplified assessment procedure is to determine the vulnerability based on spectral acceleration, linear and nonlinear displacements, bridge properties, and applicable capacity thresholds, shown in Appendix H. Figure H.3 and Figure H.4 show the logic used to determine the vulnerability of the bridge in the transverse and the longitudinal directions, respectively. The most severe vulnerability classification obtained for the bridge governs the process and is thus taken as the overall vulnerability classification of the bridge.

When INSAT is determining the vulnerability, and the bridge is identified as having either old wall or hammerhead substructures, and if the variable `ReinforcementRatioFile` equals one, INSAT searches the *Reinforcement Check Sheet* and determines if the current bridge's NBI is included. If it is included and if the "Reinforcement Ratio > 0.25%" column has an "X," then the capacity thresholds for the old wall do not apply, and the vulnerability is based on the new wall capacity thresholds The warning in the warning column will then be the confirmation of the reinforcement ratio as well as the engineer's initials and the date, found in the file containing this information. If the column is left blank, the old wall capacity thresholds still apply, and the warning now lists the engineer's initials and the corresponding date this detail was confirmed in the third and fourth column of the file containing the reinforcement ratio checks. If there is no file loaded, then the tool makes the typical assumptions and warns the user about these assumptions using warning (a).

Once the vulnerability classification of the bridge is complete, the results and bridge properties are sent to the *All Results Sheet* and the process is repeated for each of the remaining NBIs in the *NBI List Sheet*.

The dynamic properties, including the mass, stiffness, and period, for each of the bridges for which a Level 1 assessment is applicable are written to the *Dynamic Properties Sheet*.

When all of the bridges have been assessed, INSAT returns to Module 1.

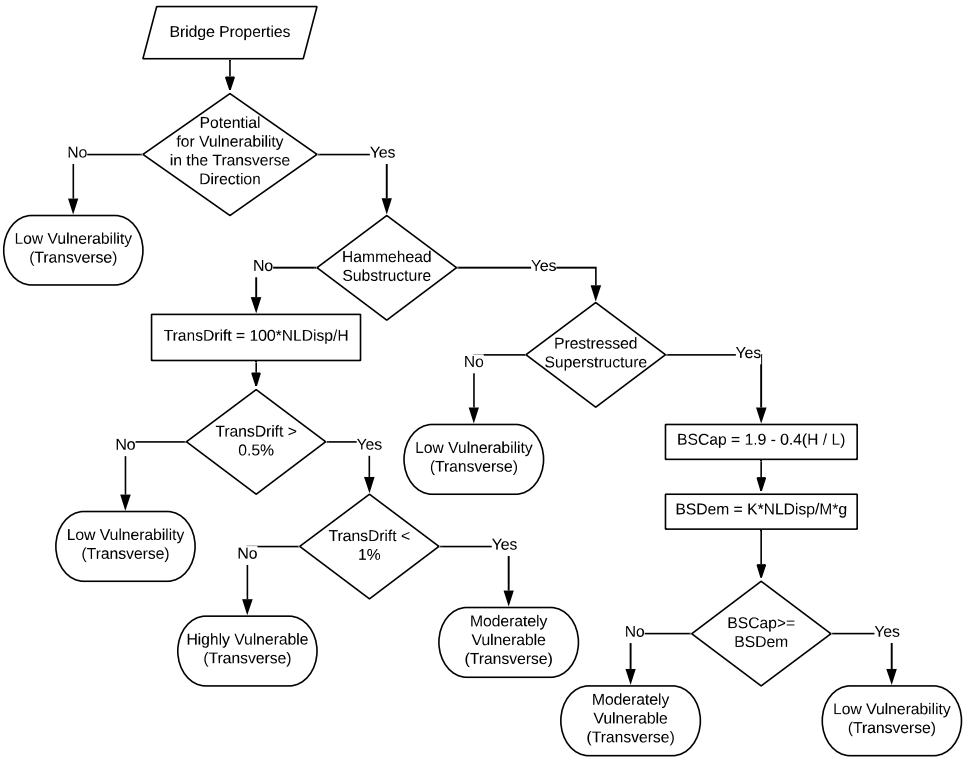

Figure H.3 Logic for Transverse Vulnerability Classification

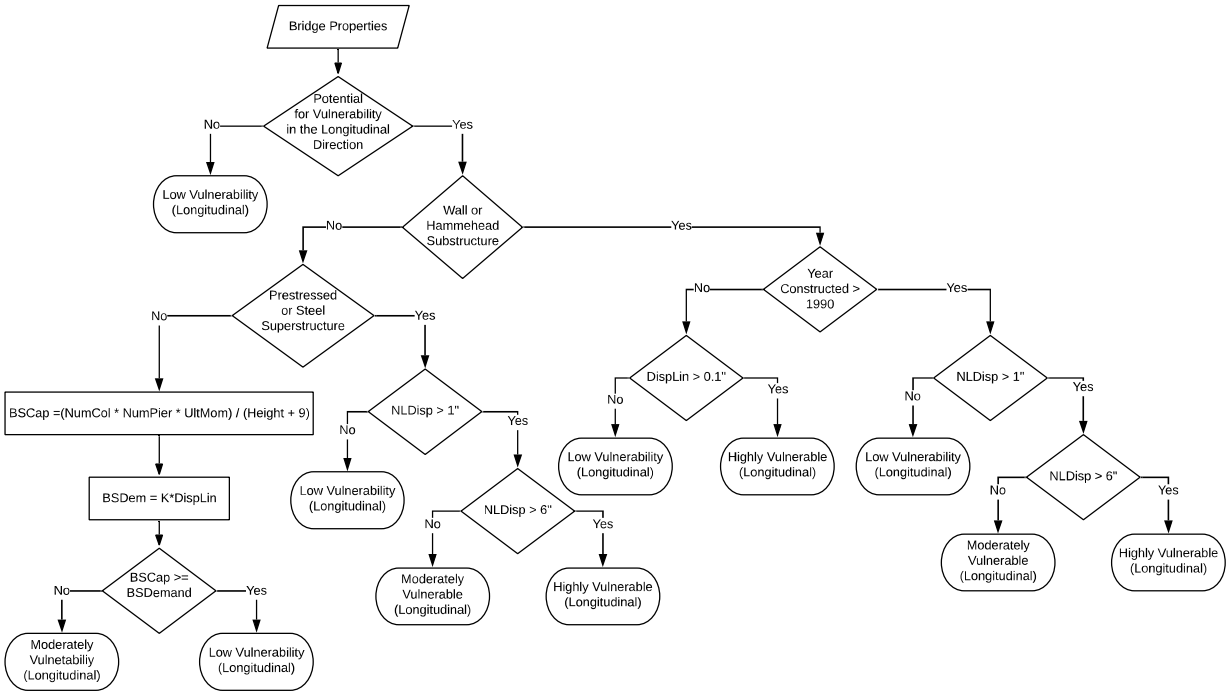

Figure H.4 Logic for Longitudinal Vulnerability Classification

BiasFile(OS) – Module 3

This module is used for loading the file that contains the BIAS data. It requires the variable `OS`, which identifies the operating system. It prompts the user to choose the file containing the BIAS data, and then opens the file explorer. The script is dependent on the operating system since mac OS file paths function differently than Windows OS file paths. Regardless which operating system is in use, it allows .xlsx or .xls files to be selected. If the file containing the BIAS data is open when INSAT is running, this module will copy the information from the open file and leave the file open. Otherwise, the BIAS data file is closed after being loaded into INSAT. There is an error catch if the user does not select a file which alerts the user that no file was selected. In this case the implementation of INSAT is halted and the assessment must be restarted.

AddInfoFile(OS) – Module 4

The same logic used in the **BiasFile(OS) Module** (Module 3) is used in this module. The module prompts the user to choose the file containing the additional recommended data for all bridges and opens the file explorer to allow the user to choose the .xlsx or .xls file containing this information. There is an error catch if the user does not select a file, like in the **BiasFile(OS) Module**, which alerts the user that no file was selected and to rerun the seismic evaluation.

NBIFile(OS) – Module 5

The same logic used in the **BiasFile(OS)** and the **AddInfoFile(OS)** is used in this module, however it requires the user to select a .csv file. Like the previous two modules, there is a built-in alert if the user does not select a file that tells the user that no file was selected and to rerun the seismic evaluation.

CriticalRoute(DistrictColumn, NBIColumn, FeatCarriedColumn, FeatInterColumn, TotalDataBaseRows) – Module 6

If the user chooses to run the assessment for bridges on or over the critical routes, this module is called. It requires the following variables to be passed from Module 1: `DistrictColumn, NBIColumn, FeatCarriedColumn, FeatInterColumn, TotalDataBaseRows`. These variables identify the location where specific information is stored on the *BIAS Data Sheet* and the number of bridges contained on that sheet. The user is prompted to choose whether they'd like to run all the bridges on or over a critical route, or if they'd like to specify a certain district(s) to run. If the user chooses to run the critical route bridges in all districts, each bridge in the *BIAS Data Sheet* is checked to determine if it carries or crosses a critical route, defined on the *Routes Sheet*. If the bridge carries or crosses a critical route, the NBI number is stored on the *NBI List Sheet*. If the user chooses to narrow the set of bridges to smaller set of districts or a single district, they are prompted to select the district or districts. Then each bridge in the *BIAS Data Sheet* is checked, first to determine if the bridge carries or crosses a critical route, and then to determine if the bridge is in one of the selected districts. For every bridge where both of those are true, the NBI number is stored to the *NBI List Sheet*. Once every bridge has been checked, this module is exited and INSAT returns to the **SeismicEvaluation() Module** (Module 1).

SelectedDistricts(DistrictColumn, NBIColumn, TotalDataBaseRows) – Module 7

If the user chooses to run a specific district or districts, this module is called. It requires the following variables to be passed from Module 1: `DistrictColumn, NBIColumn,` and `TotalDataBaseRows.` These variables identify the location where specific information is stored on the *BIAS Data Sheet* and the number of bridges contained on that sheet. This module prompts the user to select which districts they'd like to assess. The user-form allows the user to choose any combination of districts but does not allow the user to exit the form until at least one district is selected. Once the user has specified the district(s), each bridge in the *BIAS Data Sheet* is checked to determine whether or not the bridge is in one of the specified districts. If it is, the NBI number is added to the *NBI List Sheet*, and if not, the next

bridge is checked. Once every bridge has been checked, this module is exited and INSAT returns to the **SeismicEvaluation(--) Module** (Module 1).

SpecificRoute(DistrictColumn, NBIColumn, FeatCarriedColumn, FeatInterColumn, TotalDataBaseRows) – Module 8

If the user chooses to run a specific route, this module is called. It requires the following variables to be passed from Module 1: `DistrictColumn`, `NBIColumn`, `FeatCarriedColumn`, `FeatInterColumn`, `TotalDataBaseRows`. It first prompts the user to select the route they'd like to run from the predetermined list of routes stored on the *Routes Sheet*. Like **CriticalRoutes(--)** (Module 6), the user can also decide whether or not to narrow down the analysis to a subset of districts. If the user decides to analyze all the bridges crossing or carrying the selected route, each bridge in the *BIAS Data Sheet* is checked to determine if the bridge carries or crosses the selected route. If it does, the NBI number is added to the *NBI List Sheet*. If not, the next bridge is checked. However, if the user chooses to narrow the analysis down by districts, they are prompted to select the districts they'd like to run. Once they've selected the district(s), each bridge in the *BIAS Data Sheet* is checked to determine first if the bridge crosses or carries the selected route and then to determine if the bridge is in the selected district(s). For every bridge where both of those are true, the NBI is added to the *NBI List Sheet*. If the entire database is checked and there are no bridges crossing or carrying the selected route in the selected district(s), there is an error message which alerts the user that no bridges match the specified constraints and to rerun the seismic evaluation.

FormattingOutput(--) – Module 9

This module contains the script for formatting the *All Results Sheet*. The user is first prompted to choose to customize the data output. The default outputs are the following:

- Asset Name
- NBI Number
- District
- Superstructure Type
- Substructure Type
- Classification Results

If the user chooses to customize the data output, they are prompted to select the data items that they would like to have displayed (in addition to the default options). The additional data items they can choose from are:

- Latitude and Longitude
- Feature Intersected
- Facility Carried
- Number of Main Spans
- Skew
- Abutment Type

Based on the options the user picks, the column headings on the *All Results Sheet* are assigned and the column location for each data item is saved for use in displaying the results in Module 2.

PriorityFactor(OS) – Module 10

This module is called when the user chooses to include user-defined priority factors as an additional sorting feature. The user has three options for adding a priority factors, which can be applied individually or to compound each other. If more than one option is selected, the factor assigned to a bridge is the product of the individual priority factors.

The first option is to apply a priority factor to those bridges carrying or crossing critical routes. The second option is to apply a priority factor to bridges by district, giving each district a distinct factor. The third option is to apply a user-defined priority factor to each individual bridge using a .xlsx file provided by the user. This file must contain the NBI number and the factor to be applied to the bridge. If the user chooses to prioritize by critical route, they are prompted to input the associated priority factor. This value can be any number, positive or negative, including decimals. If the value provided is not acceptable, the user is alerted and prompted to enter a new value. This priority factor is then assigned to any bridge on the *All Results Sheet* that carries or crosses a critical route. If the user chooses to prioritize by district, they are prompted to input a factor for each of the six districts. The default for each district is 1, however, the user has the option to change any/all of the priority factors. Again, the priority factor can be any number, positive or negative, include decimals. As with prioritizing by critical route, if the input value is not acceptable, the user is alerted and prompted to enter a different number. The priority factors are then applied to each bridge based on the district that bridge is in. If the user chooses to prioritize by individual NBI number, they are prompted to select the file that contains the priority factors, using the **PriorityFile(OS) Module** (Module 11). If the file is in the correct form, the NBI's in the input file are matched with the NBI's on the *All Results Sheet* and the correct priority factor is applied to the bridges on the *All Results Sheet*. If the file is not in the correct form, the user is alerted and a priority factor of 1 is assigned to all the bridges.

After the process of computing the priority factors is complete, the module sorts the results from highest vulnerability to lowest vulnerability. Within in each vulnerability classification category, the results are displayed from highest total priority to lowest priority. The program then returns to the main module.

PriorityFactorFile(OS) – Module 11

This module is called when the user chooses to add priority factors by NBI number. It uses the same script as Modules 3–5. The user is prompted to select the file containing the NBI number and the priority factor and opens the file explorer to allow the user to choose an .xlsx file containing this information. There is an error catch if the user does not select a file, as in the **BIASData(OS) Module,** which alerts the user that either no file was selected or the file was not in the correct format, and then informs the user that the priority factor used does not account for prioritization by NBI number.

SortAllResults(--) – Module 12

This module is called if no priority factors are added. This module sorts the *All Results Sheet* so that the highest vulnerability bridges are at the top and the low vulnerability bridges are at the bottom.

ReinforcementCheckFile(OS) – Module 13

This module is called when the user notifies INSAT that there is a file that contains information with engineer-checked reinforcement ratios for bridges with either old wall or hammerhead substructures. It uses the same script as Modules 3–5. The user is prompted to select the file containing the NBI number, the reinforcement ratio check, the engineer's initials and the date and opens the file explorer to allow the user to choose an .xlsx file containing this information. There is an error catch if the user does not select a file, as in the **BIASData(OS) Module,** which alerts the user that either no file was selected or the file was not in the correct format, and then informs the user that the information from this file will not be considered in the vulnerability assessment.

REFERENCES FOR THE APPENDICES

AASHTO. (2017). *AASHTO LRFD bridge design specifications* (8th ed.). American Association of State Highway and Transportation Officials.

AASHTO. (2018). *The manual for bridge evaluation* (3rd ed.). American Association of State Highway and Transportation Officials.

Alkhrdaji, T., & Silva, P. (2008). *Seismic strengthening of concrete buildings using FRP composites.* American Concrete Institute.

Atkinson, G. M., & Boore, D. M. (2006). Earthquake ground-motion prediction equations for eastern North America. *Bulletin of the Seismological Society of America*, *96*(6), 2181–2205. https://doi.org/10.1785/0120050245

Avossa, A. M., Di Giacinto, D., Malangone, P., & Rizzo, F. (2018). Seismic retrofit of a multi-span prestressed concrete girder bridge with friction pendulum devices. *Shock and Vibration*. https://doi.org/10.1155/2018/5679480

Bolisetti, C., Whittaker, A. S., Mason, H. B., Almufti, I., & Willford, M. (2014). Equivalent linear and nonlinear site response analysis for design and risk assessment of safety-related nuclear structures. *Nuclear Engineering and Design*, *275*, 107–121. https://doi.org/10.1016/j.nucengdes.2014.04.033

Bonthron, L., Beck, C., Lund, A., Zhang, X., Cao, Y., Dyke, S. J., Ramirez, J., Mavroeidis, G., Baah, P., & Hunter, J. (2020). *A rapid seismic vulnerability assessment tool for bridges in Indiana–INSAT*. DesignSafe-CI Repository. https://doi.org/10.17603/ds2-b5s1-6686

Boore, D. M. (1983). Stochastic simulation of high-frequency ground motions based on seismological models of the radiated spectra. *Bulletin of the Seismological Society of America*, *73*(6A), 1865–1894.

Boore, D. M. (2013). The uses and limitations of the square-root-impedance method for computing site amplification. *Bulletin of the Seismological Society of America*, *103*(4), 2356–2368. https://doi.org/10.1785/0120120283

Boore, D. M. (2016). Determining generic velocity and density models for crustal amplification calculations, with an update of Boore and Joyner (1997) generic site amplification for $V_S(Z)$ = 760 m/s. *Bulletin of the Seismological Society of America*, *106*(1), 313–317. https://doi.org/10.1785/0120150229

Boore, D. M., & Campbell, K. W. (2017). Adjusting central and eastern North America ground-motion intensity measures between sites with different reference-rock site conditions. *Bulletin of the Seismological Society of America*, *107*(1), 132–148. https://doi.org/10.1785/0120160208

Bouchon, M. (1979). Discrete wave number representation of elastic wave fields in three-space dimensions. *Journal of Geophysical Research: Solid Earth*, *84*(B7), 3609–3614. https://doi.org/10.1029/JB084iB07p03609

Bouchon, M., & Aki, K. (1977). Discrete wave-number representation of seismic-source wave fields. *Bulletin of the Seismological Society of America*, *67*(2), 259–277.

Buckle, I., Friedland, I., Mander, J., Martin, G., Nutt, R., & Power, M. (2006). *Seismic retrofitting manual for highway structures: Part 1—Bridges* (Publication No. FHWA-HRT-06-032). Research, Development, and Technology Turner-Fairbank Highway Research Center.

Buckle, I. G., Al-Ani, M., & Monzon, E. (2011). *Seismic isolation design examples of highway bridges* (Final Report NCHRP 20-7/Task 262(M2)). Transportation Research Board, National Research Council.

Buckle, I. G., Consantinou, M. C., Dicleli, M., & Ghasemi, H. (2006). *Seismic isolation of highway bridges* (Special Report MCEER-06-SP07). Multidisciplinary Center for Earthquake Engineering Research. https://www.eng.buffalo.edu/mceer-reports/06/06-SP07.pdf

California Department of Transportation (CalTrans). (2019, April). *CalTrans seismic design criteria version 2.0.* https://dot.ca.gov/programs/engineering-services/manuals/seismic-design-criteria

Choi, E. (2002). *Seismic analysis and retrofit of mid-America bridges* [Doctoral dissertation, Georgia Institute of Technology]. Georgia Tech Library. http://hdl.handle.net/1853/21538

Chopra, A. K. (2012). *Dynamics of structures: Theory and applications to earthquake engineering* (4th ed). Prentice Hall.

Coppersmith, K. J., Salomone, L. A., Fuller, C. W., Glaser, L. L., Hanson, K. L., Hartleb, R. D., Letiss, W. R., Lindvall, S. C., McDuffie, S. M., McGuire, R. K., Stirewalt, G. L., Toro, G. R., Youngs, R. R., Slayter, D. L., Bozkurt, S. B., Cumbest, R. J., Falero, V. M., Perman, R. C., Shumway, A. M., . . . Tuttle, M. P. (2012). *Central and eastern United States seismic source characterization for nuclear facilities* (NUREG-2115). Electric Power Research Institute, U.S. Department of Energy, and U.S. Nuclear Regulatory Commission. https://www.nrc.gov/reading-rm/doc-collections/nuregs/staff/sr2115/

DesRoches, R., Choi, E., Leon, R. T., Dyke, S. J., & Aschheim, M. (2004a). Seismic response of multiple span steel bridges in central and southeastern United States. I: As built. *Journal of Bridge Engineering, 9*(5)*,* 464–472. https://doi.org/10.1061/(ASCE)1084-0702(2004)9:5(464)

DesRoches, R., Choi, E., Leon, R. T., & Pfeifer, T. A. (2004b). Seismic response of multiple span steel bridges in central and southeastern United States. II: Retrofitted. *Journal of Bridge Engineering*, *9*(5), 473–479. https://doi.org/10.1061/(asce)1084-0702(2004)9:5(473)

Ealangi, I. (2010). *Earthquake protection of buildings by seismic isolation. Devices and concepts.* Technical University of Civil Engineering Bucharest.

Fares, A. M. (2018). Simplified equations for rigidity and lateral deflection for reinforced concrete cantilever shear walls. *International Journal of Civil and Environmental Engineering*, *12*(10), 1051–1055.

FHWA. (1995). *Recording and coding guide for the structure inventory and appraisal of the nation's bridges* (Report No. FHWA-PD-96-001). Federal Highway Administration. https://www.fhwa.dot.gov/bridge/mtguide.pdf

Frosch, R. J., Kreger, M. E., & Talbott, A. M. (2009). *Earthquake resistance of integral abutment bridges* (Joint Transportation Research Report No. FHWA/IN/JTRP-2008/11). West Lafayette, IN: Purdue University. https://doi.org/10.5703/1288284313448

Garcia, L. E. G. (1998). *Dinámica estructural aplicada al diseño sísmico*. Bogotá: Universidad de los Andes, Facultad de Ingeniería, Departamento de Ingeniería Civil.

Gillich, G. R., Iancu, V., Gillich, N., Korka, Z. I., Chioncel, C. P., & Hatiegan, C. (2018). Decoupling the structure from the ground motion during earthquakes by employing friction pendulums. *Materials Science and Engineering*, 294, 012025 https://doi.org/10.1088/1757-899X/294/1/012025

Griffiths, S. C., Cox, B. R., & Rathje, E. M. (2016). Challenges associated with site response analyses for soft soils subjected to high-intensity input ground motions. *Soil Dynamics and Earthquake Engineering*, *85*, 1–10. http://dx.doi.org/10.1016/j.soildyn.2016.03.008

Halldorsson, B., & Papageorgiou, A. S. (2005). Calibration of the specific barrier model to earthquakes of different tectonic regions. *Bulletin of the Seismological Society of America*, *95*(4), 1276–1300. https://doi.org/10.1785/0120040157

Hashash, Y. M. A., Musgrove, M. I., Harmon, J. A., Groholski, D. R., Phillips, C. A., & Park, D. (2016). *DEEPSOIL 6.1, user manual*. University of Illinois at Urbana-Champaign.

Herrmann, R. B., Withers, M., & Benz, H. (2008). The April 18, 2008 Illinois earthquake: An ANSS monitoring success. *Seismological Research Letters*, *79*(6), 830–843. https://doi.org/10.1785/gssrl.79.6.830

INDOT. (2012). *Standard Drawing No. E 726-BEBP-05: Elastomeric bearing pads type S* (Indianapolis, IN). https://www.in.gov/dot/div/contracts/standards/drawings/sep17/e/700e/e700%20combined%20pdfs/E726-BEBP.pdf

INDOT. (2020, January 23). *2013 INDOT design manual: Chapter 412.* Indiana Department of Transportation.

Johnston, A. C., & Schweig, E. S. (1996). The enigma of the New Madrid earthquakes of 1811–1812. *Annual Review of Earth and Planetary Sciences*, *24*(1), 339–384. https://doi.org/10.1146/annurev.earth.24.1.339

Luco, J. E., & Apsel, R. J. (1983). On the Green's functions for a layered half-space. Part I. *Bulletin of the Seismological Society of America*, *73*(4), 909–929.

Mai, P. M., Spudich, P., & Boatwright, J. (2005). Hypocenter locations in finite-source rupture models. *Bulletin of the Seismological Society of America*, *95*(3), 965–980. https://doi.org/10.1785/0120040111

Metzger, L. E. (2004). *Vulnerability of bridges in southern Indiana to earthquakes* [Master's thesis, Purdue University].

Nielson, B. G., & DesRoches, R. (2007). Analytical seismic fragility curves for typical bridges in the central and southeastern United States. *Earthquake Spectra*, *23*(3), 615–633. http://dx.doi.org/10.1193/1.2756815

nshmp-haz. (n.d.). *National seismic hazard mapping project (NSHMP) code*. Retrieved June 20, 2018, from https://github.com/usgs/nshmp-haz

Obermeier, S. F. (1998). Liquefaction evidence for strong earthquakes of Holocene and latest Pleistocene ages in the states of Indiana and Illinois, USA. *Engineering Geology*, *50*(3–4), 227–254. https://doi.org/10.1016/S0013-7952(98)00032-5

Papageorgiou, A. S., & Aki, K. (1983, June 1). A specific barrier model for the quantitative description of inhomogeneous faulting and the prediction of strong ground motion. I. Description of the model. *Bulletin of the Seismological Society of America*, *73*(3), 693–722.

Petersen, M. D., Moschetti, M. P., Powers, P. M., Mueller, C. S., Haller, K. M., Frankel, A. D., Zeng, Y., Rezaeian, S., Harmsen, S. C., Boyd, O. S. Field, E. H., Chen, R., Rukstales, K. S., Luco, N., Wheeler, R. L., Williams, R. A., Olsen, A. H. (2014). *Documentation for the 2014 update of the United States national seismic hazard maps* (USGS Open-File Report 2014–1091). U.S. Geological Survey. https://dx.doi.org/10.3133/ofr20141091

Rabbat, B., & Russell, H. (1985). Friction coefficient of steel on concrete or grout. *Journal of Structural Engineering*, *111*(3), 505–515. https://doi.org/10.1061/(asce)0733-9445(1985)111:3(505)

Ramirez, J. A., Frosch, R. J., Sozen, M. A., & Turk, A. M. (2000). *Handbook for the post-earthquake safety evaluation of bridges and roads* (Joint Transportation Research Program, Publication No. FHWA/IN/JTRP-2000/30). West Lafayette, Indiana: Purdue University. https://doi.org/10.5703/1288284315557

Roeder, C. W., Stanton, J. F., & Taylor, A. W. (1987). *Performance of elastomeric bearings* (NCHRP Report 298). Transportation Research Board, National Research Council.

Silva, W. J., Darragh, R. B., Gregor, N., Martin, G., Abrahamson, N. A., & Kircher, C. (2000). *Reassessment of site coefficients and near-fault factors for building code provisions* (Award No. 98HQGR1010). U.S. Geological Survey.

Siqueira, G. H., Tavares, D. H., Paultre, P., & Padgett, J. E. (2014). Performance evaluation of natural rubber seismic isolators as a retrofit measure for typical multi-span concrete bridges in eastern Canada. *Engineering Structures*, *74*, 300–310. https://doi.org/10.1016/j.engstruct.2014.03.009

Somerville, P., Irikura, K., Graves, R., Sawada, S., Wald, D., Abrahamson, N., Iwasaki, Y., Kagawa, T., Smith N., & Kowada, A. (1999). Characterizing crustal earthquake slip models for the prediction of strong ground motion. *Seismological Research Letters*, *70*(1), 59–80.

Sozen, M. A. (2003). The velocity of displacement. In S. T. Wasti & G. Ozcebe (Eds.), Seismic Assessment and Rehabilitation of Existing Buildings. *NATO Science Series (Series IV: Earth and Environmental Sciences),* vol 29, 11–28. Springer, Dordrecht. https://doi.org/10.1007/978-94-010-0021-5_2

Trochalakis, P., Eberhard, M. O., & Stanton, J. F. (1996). *Design of seismic restrainers for in-span hinges* (Research Report No. WA-RD 387.1). Washington State Transportation Center (TRAC).

Vucetic, M., & Dobry, R. (1991). Effect of soil plasticity on cyclic response. *Journal of Geotechnical Engineering-ASCE*, *117*(1), 89–107. https://doi.org/10.1061/(ASCE)0733-9410(1991)117:1(89)

Wang, C. Y., & Herrmann, R. B. (1980). A numerical study of P-, SV-, and SH-wave generation in a plane layered medium. *Bulletin of the Seismological Society of America*, *70*(4), 1015–1036.

Wells, D. L., & Coppersmith, K. J. (1994). New empirical relationships among magnitude, rupture length, rupture width, rupture area, and surface displacement. *Bulletin of the Seismological Society of America*, *84*(4), 974–1002.

Wright, T., DesRoches, R., & Padgett, J. E. (2011). Bridge seismic retrofitting practices in the central and southeastern United States. *Journal of Bridge Engineering*, *16*(1), 82–92. https://doi.org/10.1061/(ASCE)BE.1943-5592.0000128

About the Joint Transportation Research Program (JTRP)

On March 11, 1937, the Indiana Legislature passed an act which authorized the Indiana State Highway Commission to cooperate with and assist Purdue University in developing the best methods of improving and maintaining the highways of the state and the respective counties thereof. That collaborative effort was called the Joint Highway Research Project (JHRP). In 1997 the collaborative venture was renamed as the Joint Transportation Research Program (JTRP) to reflect the state and national efforts to integrate the management and operation of various transportation modes.

The first studies of JHRP were concerned with Test Road No. 1—evaluation of the weathering characteristics of stabilized materials. After World War II, the JHRP program grew substantially and was regularly producing technical reports. Over 1,600 technical reports are now available, published as part of the JHRP and subsequently JTRP collaborative venture between Purdue University and what is now the Indiana Department of Transportation.

Free online access to all reports is provided through a unique collaboration between JTRP and Purdue Libraries. These are available at http://docs.lib.purdue.edu/jtrp.

Further information about JTRP and its current research program is available at http://www.purdue.edu/jtrp.

About This Report

An open access version of this publication is available online. See the URL in the citation below.

Bonthron, L., Beck, C., Lund, A., Mahmud, F., Zhang, X., Orellana Montano, R., Dyke, S. J., Ramirez, J., Cao, Y., & Mavroeidis, G. (2021). *Empowering the Indiana bridge inventory database toward rapid seismic vulnerability assessment* (Joint Transportation Research Program Publication No. FHWA/IN/JTRP-2021/03). West Lafayette, IN: Purdue University. https://doi.org/10.5703/1288284317282

About the Joint Transportation Research Program (JTRP)

On March 11, 1937, the Indiana Legislature passed an act which authorized the Indiana State Highway Commission to cooperate with and assist Purdue University in developing the best methods of improving and maintaining the highways of the state and the respective counties thereof. That collaborative effort was called the Joint Highway Research Project (JHRP). In 1997 the collaborative venture was renamed as the Joint Transportation Research Program (JTRP) to reflect the state and national efforts to integrate the management and operation of various transportation modes.

The first studies of JHRP were concerned with Test Road No. 1—evaluation of the weathering characteristics of stabilized materials. After World War II, the JHRP program grew substantially and was regularly producing technical reports. Over 1,600 technical reports are now available, published as part of the JHRP and subsequently JTRP collaborative venture between Purdue University and what is now the Indiana Department of Transportation.

Free online access to all reports is provided through a unique collaboration between JTRP and Purdue Libraries. These are available at http://docs.lib.purdue.edu/jtrp.

Further information about JTRP and its current research program is available at http://www.purdue.edu/jtrp.

About This Report

An open access version of this publication is available online. See the URL in the citation below.

Bonthron, L., Beck, C., Lund, A., Mahmud, F., Zhang, X., Orellana Montano, R., Dyke, S. J., Ramirez, J., Cao, Y., & Mavroeidis, G. P. (2021). *Empowering the Indiana bridge inventory database toward rapid seismic vulnerability assessment* (Joint Transportation Research Program Publication No. FHWA/IN/JTRP-2021/03). West Lafayette, IN: Purdue University. https://doi.org/10.5703/1288284317282